FUNCTIONALIZED 2,6-BIS-(2-ANILINOETHYNYL) PYRIDINE: ANION-MEDIATED SELF-ASSEMBLY AND CHEMOSENSING

by

CALDEN NATHANIEL CARROLL STIMPSON

A DISSERTATION

Presented to the Department of Chemistry
and the Graduate School of the University of Oregon
in partial fulfillment of the requirements
for the degree of
Doctor of Philosophy

December 2011

DISSERTATION APPROVAL PAGE

Student: Calden Nathaniel Carroll Stimpson

Title: Functionalized 2,6-Bis-(2-anilinoethynyl) Pyridine: Anion-Mediated Self-Assembly and Chemosensing

This dissertation has been accepted and approved in partial fulfillment of the requirements for the Doctor of Philosophy degree in the Department of Chemistry by:

Victoria DeRose	Chairperson
Michael Haley	Co-Advisor
Darren Johnson	Co-Advisor
Shih-Yuan Liu	Member
David Schmidt	Outside Member

and

Kimberly Andrews Espy	Vice President for Research & Innovation/Dean of the Graduate School

Original approval signatures are on file with the University of Oregon Graduate School.

Degree awarded December 2011

DISSERTATION ABSTRACT

Calden Nathaniel Carroll Stimpson

Doctor of Philosophy

Department of Chemistry

December 2011

Title: Functionalized 2,6-Bis-(anilinoethynyl) Pyridine: Anion-Mediated Self-Assembly and Chemosensing

Mimicking the simplicity and efficiency of Nature in the synthesis and design of non-covalent receptors for ions in solution has piqued the interest of the chemical community since the mid 20th century. Until recently most of that focus has been on the binding, sensing, or remediation of inorganic cations instead of their anionic counterparts. With the realization of the role anions play in biological function or dysfunction, the development of selective probes for these highly solvated and elusive targets has become an important goal in the chemical and biological communities.

Concurrently the optoelectronic properties of planar extended π-systems have been exploited in the development of novel light absorbing and emitting organics and carbon-rich materials with tunable optical outputs. While many of these compounds exhibit desirable sensor properties, their insolubility and non-specificity has hindered the inclusion of these materials in probes for biologically relevant substrates. This body of research seeks to combine our knowledge of supramolecular structure-function relationships with novel extended aromatic topologies to yield highly specific probes for anions in competitive media that exhibit discrete, tunable outputs upon interaction with their target substrates.

Chapter I provides a brief overview of phenylacetylene topologies as they have been used in supramolecular assemblies and sensor design, with an emphasis on their use in anion-directed complexes. Chapter II focuses on our choice of specific arylethynylpyridine architectures upon which we can build a modular synthetic scheme to access working receptors. Chapter III encompasses the synthesis of urea and sulfonamide derivatives of phenylethynylpyridine and binding studies with these receptors and halide salts in organic media . Chapters IV and V focus upon the optoelectronic properties of these receptors, the tunability of their outputs and how we utilized their behavior in aqueous media to develop *in vitro* sensors for halides. This chapter concludes with recent results regarding their self-assembly on the micro-scale.

This dissertation contains my previously published and co-authored work.

CURRICULUM VITAE

NAME OF AUTHOR: Calden Nathaniel Carroll Stimpson

GRADUATE AND UNDERGRADUATE SCHOOLS ATTENDED:

University of Oregon, Eugene, OR
Northern Arizona University, Flagstaff, AZ

DEGREES AWARDED:

Doctor of Philosophy, 2011, University of Oregon
Master of Science, Organic Chemistry, 2008, University of Oregon
Bachelor of Science, Chemistry, 2005, Northern Arizona University

AREAS OF SPECIAL INTEREST:

Organic Synthesis
Supramolecular Self-assembly
Fluorescence Analysis and Microscopy

PROFESSIONAL EXPERIENCE:

Graduate Research Assistant, Department of Chemistry, University of Oregon, Eugene, Oregon, 2006-2011

Graduate Teaching Assistant, Department of Chemistry, University of Oregon, Eugene, Oregon, 2006-2010

Undergraduate Research Assistant, Department of Chemistry and Biochemistry, Northern Arizona University, Flagstaff, Arizona, 2003-2005

GRANTS, AWARDS, AND HONORS:

National Science Foundation IGERT Fellowship, University of Oregon, 2008-2011

Japan Society for the Promotion of Science International Scholarship, Osaka University, 2008

American Chemical Society Division of Inorganic Chemistry Grant for the 235th ACS National Meeting, New Orleans, Louisiana 2007

Northern Arizona Physical Chemistry Award, Northern Arizona University, 2005

PUBLICATIONS:

J. M. Engle, C. N. Carroll, L. N. Zakharov, D. W. Johnson and M. M. Haley, *Chem. Sci.*, submitted for publication.

Y. Yang, X. Su, C. N. Carroll and I. Aprahamian, *Chem. Sci.*, DOI: 10.1039/C1SC00658D.

J. M. Engle, P. Lakshminarayanan, C. N. Carroll, L. N. Zakharov, M. M. Haley and D. W. Johnson, *Cryst. Growth Des.*, 2011, **11**, 5144-5152.

C. N. Carroll, B. A. Coombs, S. P. McClintock, C. A. Johnson, O. B. Berryman, D. W. Johnson, M. M. Haley, *Chem. Commun*, 2011, **47**, 5539-5541.

C. N. Carroll, J. J. Naleway, M. M. Haley and D. W. Johnson, *Chem. Soc. Rev.,* 2010, **39**, 3875-3888.

C. N. Carroll, O. B. Berryman, C. A. Johnson, L. N. Zakharov, D. W. Johnson, M. M. Haley, *Chem. Commun.*, 2009, 2520-2522

R. Helburn, M. Bartoli, K. Pohaku, J. Maxka, D. Compton, B. Creedon and C.Stimpson, *J. Phys. Org. Chem.,* 2007, **20**, 321-331.

ACKNOWLEDGMENTS

This dissertation is dedicated to the Calibri typeface, for all its help in making the contents appear as boring as possible.

TABLE OF CONTENTS

Chapter Page

Chapter Page

Chapter Page

LIST OF FIGURES

Figure Page

CHAPTER I

Figure Page

CHAPTER III

CHAPTER IV

Figure Page

Figure Page

CHAPTER V

Figure Page

LIST OF TABLES

LIST OF SCHEMES

CHAPTER I

ARYLETHYNYL RECEPTORS FOR NEUTRAL AND ANIONIC SPECIES: EMERGING APPLICATIONS

General Introduction

The unifying theme of the work presented herein is the application of shape persistent, semi-rigid arylethynyl compounds for fluorometric or colorimetric sensing (e.g., of anions or redox states) in competitive media, specifically working towards *in vitro* applications. This introduction provides a brief, non-comprehensive overview of previously reported research that has made successful use of the rigidity and extension of molecular conjugation afforded by the inclusion of ethynyl linkages to supramolecular assemblies, and outlines the design elements and benefits imparted by the inclusion of these rigid moieties. My contribution to an invited review article in a special issue of *Chemical Society Reviews* dedicated to anion binding is included (2010, **39**, 3875-3888, © Royal Society of Chemistry). This chapter was co-authored with Dr. John J. Naleway, who provided editorial assistance in the cellular imaging section, and my advisors, Profs. Michael M. Haley and Darren W. Johnson. Chapter II will detail some of the preliminary metal-binding experiments undertaken with the help of Dr. Charles Johnson and Dr. Orion Berryman, who carried out the synthesis of the sulfonamide compounds and their crystallographic analyses, respectively. Daisuke Inokuchi synthesized the dithiols

presented therein. Chapter III will focus on the synthesis and binding studies of the parent scaffold and its phenylurea derivative. This chapter was coauthored with Dr. Charles Johnson, Dr. Orion Berryman and my advisors, all of whom provided editorial assistance. Dr. Sean McClintock performed the molecular modeling reported therein. Chapter IV presents the tunable fluorescence data that was collected on the electron-rich and electron-poor urea receptors. This chapter was coauthored with a number of people: Brian Coombs assisted with the synthesis and analysis of these compounds while Dr. Sean McClintock performed the DFT calculations supporting our experimental observations; Dr. Charles Johnson and Dr. Orion Berryman, as well as my advisors, provided editorial assistance and direction on the submitted manuscript. Finally, Chapter V focuses on the *in vitro* imaging applications and the self-assembly of the urea receptors in both aqueous and organic media. This chapter was coauthored with Dr. John Naleway (Marker Gene, Inc.) who provided epifluorescence images. Dr. Matthew Carnes who assisted in designing the circular dichroism experiments. This chapter is followed by brief concluding remarks.

Impetus for Arylethynyl Receptor Development

Many synthetic receptors rely on some degree of preorganization in their approach to achieving high affinities and selectivities. Flexible receptors can achieve increased size-selectivity and preorganization through macrocyclization, and numerous, in-depth reviews have been written which cover the usefulness of the macrocyclic effect in increasing binding affinities.[1-4] However, macrocyclic receptors

tend to exhibit slow binding kinetics[1,2] and indeed many sensor applications rely more upon kinetic selectivity rather than a large contribution from preorganization of the receptor. In addition it can be the case that the guest bound most strongly is not the guest that gives rise to the largest colorimetric or fluorometric response, which is difficult to predict. This gives rise to a delicate balance in designing probes capable of binding a target selectively, while also exhibiting a response for that specific analyte.

There exist many examples of conformationally rigid receptors,[5-7] most of which exploit the inherent rigidity in conjugated π-systems. Expanded porphyrins,[8,9] calixpyrroles or related calixarenes,[10-12] and innumerable other nitrogen[13,14] or oxygen containing heterocycles[15] have been synthesized and their affinities for both ionic and neutral guests studied. In much the same fashion phenylacetylenes have provided structure and optoelectronic handles to a multitude of coordination and host-guest complexes.[16] Macrocyclic host molecules as well as shape-persistent acyclic ligands for metal ions have benefited from their linear, rigid geometries and relatively simple derivatization.[17-20]

In some cases the acetylenes themselves have served as the binding site for transition metal guests.[21] The synthesis and characterization of a Ni^0 complex of dehydroannulene **1** was reported in 1985 (Figure 1).[22] More often, however, the rigid acetylenic linker serves to reinforce a desired binding conformation. The synthesis and characterization of phenylacetylenic macrocycles capable of differentiating transition metals as well as serving as rudimentary proton sensors has also been achieved.[23-25]

Twistophane **2** was shown to signal Pd^{II} and Hg^{II} by a distinct fluorescence quenching response, and to signal H^+ by bathochromic shifting and quenching of the fluorescence emission.[23]

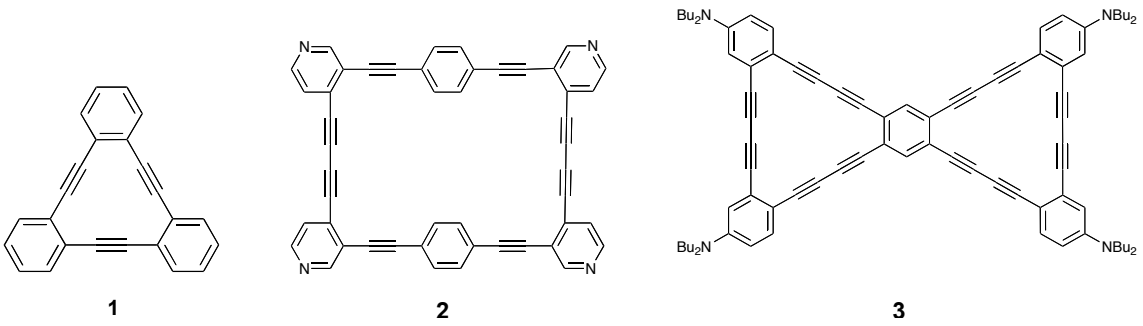

1 **2** **3**

Figure 1. Representative examples of early acetylene (**1**,**2**) and diethynylene (**2,3**) scaffolds.

Phenylacetylenes have well-studied fluorescence emission properties,[26,27] and the optoelectronic response to perturbation of their ground-state conformations can be a useful spectroscopic handle. The conjugation of donor and acceptor groups via alkyne linkages[28] is much studied and this charge transfer process has been used as a fluorescent handle for the visualization of binding events.[29] Dibutylamine-functionalized dehydrobenzoannulene **3** was found to shift fluorescence emission based upon H^+ concentration (as trifluoroacetic acid). Interestingly, it was found that emission shifting was dependent upon stepwise protonation of the dibutylaniline moieties, which indicated independent manipulation of the frontier molecular orbital energies and thus tunable charge transfer pathways.

In 2002 ethynyl-linked pyrrole-naphthyridine compound **4** was found to selectively bind glucopyranoside (Figure 2).[30] The free receptor was found to adopt a

slightly twisted conformation that exhibited a fluorescence emission maximum at 475 nm ($\tau_f \approx 1.25$ ns), which decreased upon addition of octyl β-$_D$-glucopyranoside (OGU). A new emission band at 535 nm ($\tau_f \approx 0.95$ ns) grew in intensity as a 1:1 complex was formed. The association constants for this complex determined by both fluorescence and UV-Vis absorbance measurements were in good agreement (K_a = 5.3 x 10^3 M^{-1} and K_a = 4.8 x 10^3 M^{-1} in CH_2Cl_2, respectively). Interestingly, the association constant for octyl β-$_D$-galactopyranoside was found to be only 1800 M^{-1}, which is impressive considering these saccharides differ only in the orientation of the 4-hydroxyl group. The optoelectronic response in this system was attributed to a rigidification and planarization of the pyrrole-naphthyridine moieties, which served to enhance the charge transfer in this D-π-A-A-π-D system.

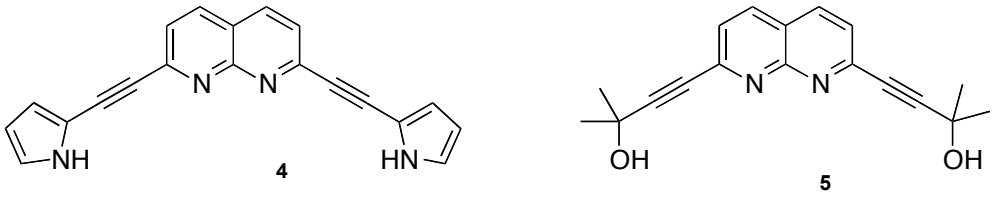

Figure 2. Glucopyranoside receptor **4** and the non-conjugated analog **5** which was used to test the role of rigidification versus electronic perturbation upon binding analytes.

To test this, an analogous receptor **5** was synthesized in which the binding sites were not conjugated through the core. Binding of OGU to this receptor was weaker due to the relative differences in acidity at the binding sites, but fluorescence emission intensity still increased, albeit not bathochromically shifted as could be expected by rigidification in this system. Additionally, modification of the

pyrrolyl moieties of **4** to indolyl units gave the normally CD-silent receptor strong fluorescence-detected CD spectra upon binding, due to chirality transfer from the substrates.[31]

A simple illustration of how flexible macrocyclization of rigid arylethynyl scaffolds can increase binding constants is found in two pyridine based systems **6a** and **6b** (Figure 3).[32] Acyclic **6a** bound ribofuranosides poorly in $CDCl_3$ (K_a = 30 M^{-1}) but macrocyclization of this cleft-like receptor increased binding constants two orders of magnitude (K_a = 2400 M^{-1}). Related poly(ethyleneglycol) linked derivatives of this receptor motif allowed the expanded terpyridine core to adopt a slightly wider conformation while maintaining preorganization.[32a] Due to this longer, more flexible linker these receptors exhibited still higher affinities for larger monosaccharides.

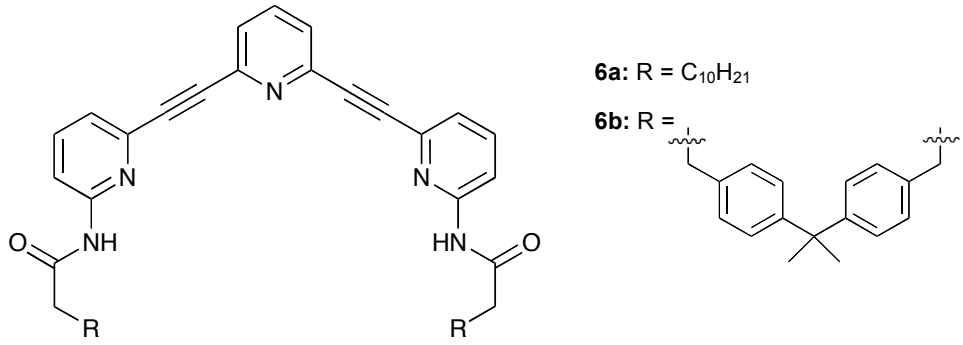

Figure 3. Cleft-receptor **6a** and macrocyclized receptor **6b** used to demonstrate the benefit of macrocyclization, even in receptors with a rigid scaffold.

A number of phosphorylated binol-based macrocycles have been investigated as receptors for neutral guests, such as saccharides.[33-35] The polyanionic cavities in receptors **7a** and **7b** were targeted at the hydroxyl moieties of the sugars, a strategy which proved effective even in slightly competitive media (Figure 4). It was found

that macrocyclization can be a hindrance in these very rigid systems; cyclotrimer **7a** was found to be incapable of binding monosaccharides in the cavity, but was still capable of binding OGU (K_a = 3500 M^{-1} in CD_3CN) ostensibly through a face-to-face interaction.[34] However, cyclotetramer **7b** was large enough to bind pyranose in its cavity, with a corresponding increase in association constant (K_a = 4500 M^{-1} for OGU), while extended cyclotetramer **8** was selective for disaccharides over monosaccharides even in very competitive media (K_a of 10,700 – 12,500 M^{-1} in 88:12 CD_3CN-CD_3OD).[35] The rigidity of the macrocyles in these cases helped to reinforce their size selectivity between guests.

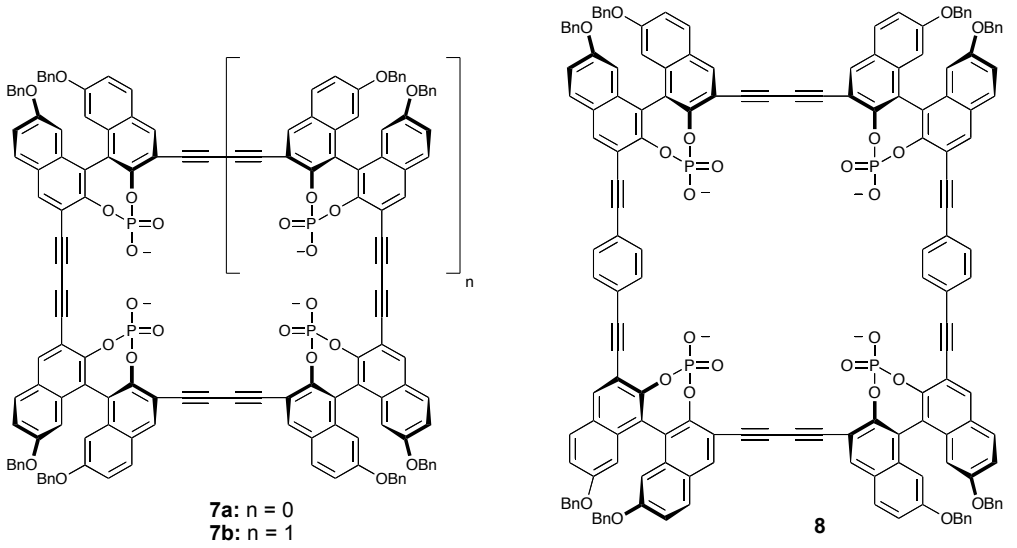

Figure 4. Phosphorylated macrocycles used to illustrate the importance of size regulation in tuning the binding interaction with desired guests.

This size regulation can also be extended to polymers of phenylacetylenic subunits. Polymers of **9** were found to exhibit saccharide-dependent induction of

chirality (Figure 5).[36] Hydrogen bonding with saccharide guests was reinforced by the rigidity and relative angle of the alkyne linkers between pyridine units, which necessarily directed all of the hydrogen-bond accepting lone pairs to the interior of the cavity. This reinforcement also biased the polymer for the 2,3,4,6-OH groups of β-glucoside from other monosaccharides or their derivatives. The above examples, while by no means exhaustive, illustrate a few of the design strategies involved in engineering a selective and sensitive fluorescent probe, and how phenylacetylenes offer one such viable design pathway.

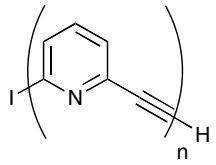

9

Figure 5. Monomer (**9**) of a β-glucoside binding polymer.

Approaches to Receptor Design: Strategies and Methods

A viable non-covalent receptor must strike a balance between selectivity, solubility, robustness and, in the case of sensors, signalling or response.[1-3] There are a few distinct strategies for designing effective non-covalent, fluorionophores. These can be classified simply as either "FSR" (fluorophore-spacer-receptor) or displacement.[37-39]

In the FSR system, an independently tunable binding site is linked covalently to a signalling unit. The role of the signalling unit is simply to transduce the chemical

information upon coordination from the binding site into a specific fluorescent response. This historically has been the most common approach to engineering fluorogenic hosts to complex ionic targets, and many reviews exist.[37,39] There has been considerable success with what could be called a noncovalent version of FSR.[38] This dye-displacement method relies upon careful modulation of a bound fluorophore or chromophore that is designed to have a weaker affinity for the host than the target analyte.

In 1998 there was reported the synthesis of the hexa-substituted benzene-based tripodal receptor **10** that used three guanidinium groups as binding sites (Figure 6).[40] Carboxyfluorescein was found to bind with a K_a = 4.7 x 10^3 M^{-1} in aqueous buffer, while citrate bound with K_a = 2.9 x 10^5 M^{-1}. Modulation of the pK_a of the phenolic proton of carboxyfluorescein was implicated in the decreased fluorescence of free dye versus the host-dye complex.

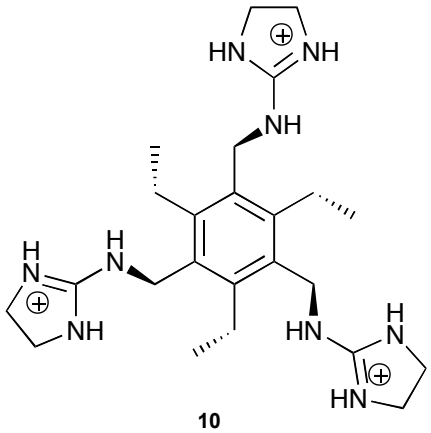

10

Figure 6. Example of a typical tripodal dye-discplacement receptor.

Alternatively, replacement of a non-conjugated spacer with a conjugated linker has proven an interesting approach to recent receptor design. It allows for discrete modulation of the optoelectronic response of a fluorogenic receptor via conformation rather than just electronic effects from guest inclusion, as well as rigidifying the receptor. This provides an element of size-based recognition and can be exploited to modulate the fluorescent response, either through twisting of the π-system[41-43] or extension of excitation/emission into the near-IR for use in biological systems.[44] Regardless of the desired properties, this approach is closely related to traditional FSR receptors, although in this instance the spacer plays a more active role in enforcing receptor conformation. Integration of these components can access smaller molecular sensing systems as well as provide additional information about the binding geometry via modulation of optoelectronic response.

Modularity in Synthesis. Convergent syntheses are a common route in molecule assembly. The well-studied techniques of arene-acetylene cross-coupling can allow the supramolecular chemist to synthesize and derivatize a wide array of functional subunits with spacers that transduce signal themselves, rather than separating these into independent moieties in the receptor.[45] These can then be easily linked together in a convergent fashion through a multitude of cross-coupling reactions, most of which are characterized by their relatively benign reaction conditions.[46] This modular approach to synthesis allows for facile and effective screening of candidates by allowing quick and subtle changes to each building block. Most of the

phenylacetylene work mentioned thus far has made use of sequential cross-couplings of independently synthesized subunits, and the budding field of alkyne metathesis may open up another efficient and modular strategy in the synthesis of ethynyl or butadiynyl-containing small molecules.[47,48] In tuning binding parameters such as cavity size, bite angle or the number or relative position of binding sites, secondary properties (i.e., optoelectronic response, photostability or solubility) of the receptor scaffold can be adjusted as well, and simplicity when modulating all of these parameters is key to quick and efficient discovery of "Goldilocks" candidates for high-performance receptors.

Switchability in Selectivity or Sensitivity. Controlling the affinity of a host for a specific analyte via allosteric modulation (e.g., pH or ionic environment) is an interesting tool for modifying the selectivity of a binding site.[49,50] This allosteric behavior is relatively rare in synthetic receptors, but has particular implications for designing biomimetic receptors that will operate within the diminished pH windows in biological systems, where either "turn-on" or "turn-off" binding may be desired in response to pH changes in cellular compartments. Notably, switchable conformational control has been shown in rotaxanes[51] and in "FSR" type hydrogen-bonding receptors.[52,53] As an example, the switchable complexation of uracil in two amine-triazine-crown ether receptors has been recently reported.[52] Protonation of the amine initiated an intramolecular hydrogen-bonding interaction between the ammonium moiety and the crown ether that sterically blocked the binding site.

Switchability in a sensor can also come from conformational change in induced-fit sensors. In these cases clever design can limit the conformational degrees of freedom such that only a single analyte gives the most intense response. For example, this can be accomplished by appending fluorophores such that conformational change upon binding brings them into proximity for excimer formation (e.g., FRET)[54] or redox active groups can have their environments changed in such a way as to give rise to a known modulation in potential for non-optical sensing.[55,56] Phenylacetylenic systems can be exploited when engineering optically responsive receptors in much the same way, as discussed below.

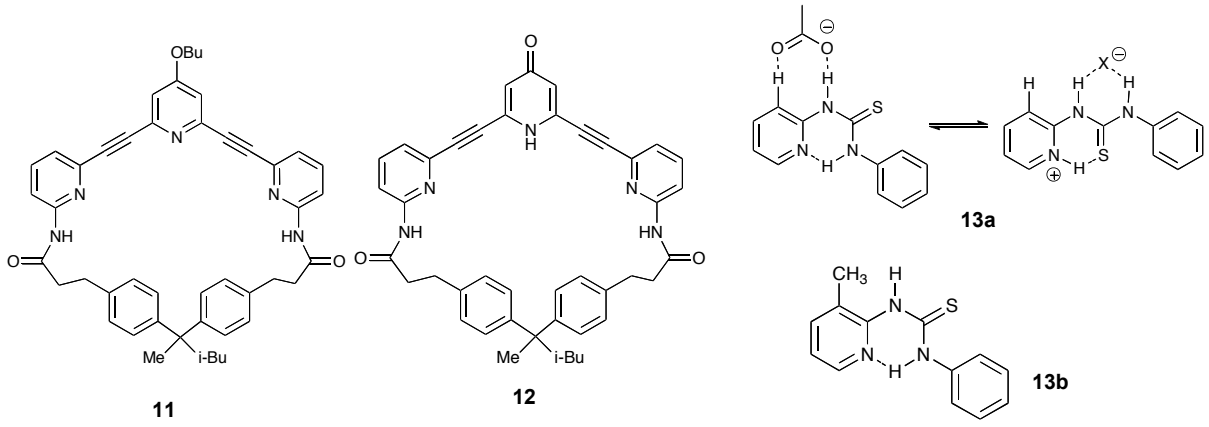

Figure 7. Macrocyclic and acyclic receptors **11-13b** illustrate the influence of small changes to H-bonding character on binding affinities.

Extended bis-ethynylpyridine compounds **11** and **12** were reported to bind deoxyribosides in $CDCl_3$ (K_a = 690 M^{-1} for **11** and K_a = 19000 M^{-1} for **12**, Figure 7).[57] The modification of the hydrogen bond accepting pyridine lone pair to a hydrogen bond donating pyridinone was responsible for this significant increase in affinity.

This switchability, although engineered into the receptor during the synthesis, has interesting implications for the design of receptors capable of binding anionic guests.

As an example, pyridylthiourea **13a** exhibits switchable affinities for either acetate or halide anions.[58] Protonation as a switch in this case provides an additional hydrogen bonding contact which further stabilizes the spherical halides. Treating the protonated receptor with excess acetate led to deprotonation and binding of the residual acetate anion. Replacing the arene C-H with a methyl group yielded **13b**, which had no affinity for acetate or hydrogen halides, thus highlighting the role arene C-H hydrogen bonding can play in designing receptors.

Tuning Receptors for Anionic Targets

As anions have become the focus of more and more research efforts, the modification and application of known cation receptor design criteria for anionic targets has grown as well. For many years the importance of anions in the natural world was overlooked. Relatively benign chloride, carbonate and sulfate, as well as toxic arsenate anions are found naturally in water the world over,[61] or in runoff and acid rain in the case of industrial pollutants.[62] Anthropogenic anions can be expanded to include phosphate and nitrates from agriculture,[63] or pertechnetate and perchlorate from industrial waste streams.[64,65] Their ubiquity in the natural world has lead to an increase of research in this field with modest advances made in the characterization and sequestration of electron-rich wastewater contaminants. This has led to elegant designer nanomaterials that offer selectivity for some of

these myriad problematic anionic pollutants present in both developing and developed countries.[66,67b]

In spite of their prevalence, targeting anionic substrates has its own inherent challenges. Their low charge to radius ratio, high solvation energies, polarizability and the large range of preferred geometries (or lack thereof) make them difficult targets in competitive media.[1-3] Protic solvents tend to form extremely stable hydrogen bonds with most anions, which mandates an extremely strong host-guest interaction if any binding is to be accomplished. On the other hand, relatively nonpolar solvents give rise to ion-pairing, which can have a significant negative influence on binding ability. In addition, many biological anions exist only within narrow pH windows. Nature has many strategies to overcome these difficulties, a fact illustrated beautifully by the complexity of many of the natural receptors whose function depends upon their selectivity for specific anions. A particularly elegant example was the elucidation of the StCIC and EcCIC chloride ion channels via X-ray crystallography in 2002.[68] These CIC ion channels are selective for Cl^- and Br^- through partial positive charges within the channels, rather than a fully electrostatic interaction with the nearby lysine and arginine residues which would bind too strongly and inhibit the function of the channel. Interestingly, the gating mechanism necessary for the channel to function is hypothesized to depend on two chloride binding events, and that even small changes in the anionic substrate, i.e., from chloride to bromide anion, alter the operational efficiency of the channel.[69] In spite of insights such as these into the complexity of Nature's use of anion coordination

chemistry in cell regulation, our understanding of how the properties of specific anions affect changes in these systems is severely limited.

Common Functional Groups for Targeting Anions. This dissertation focuses on receptors with linked sp-carbon atoms to which are appended a variety of functional groups: arenes such as pyrrole, indole, carbazole, or carbonyl-containing amide, urea, thiourea or sulfonamide functionalities.[78] This combination can translate into well-defined binding sites, whether they be based strictly on polycyclic arenes or involve extension via acetylenic linkers, as well as impart distinct optoelectronic properties to these receptors. While the inclusion of metal centers is an important design motif,[59] contributions from organometallic receptors for anions have been recently reviewed[60] and are beyond the scope of this literature review.

An early example of an arene-alkyne based receptor attempted to reinforce face-to-face interactions between the host and guest via multiple butadiyne linkages that were not in conjugation. Investigation of the binding affinities for heterotricyclic receptors **14a-d** found that these bound large, flat substrates well with the highest binding constants observed for the largest substrates (e.g., terephthalate^{2-} > 2,6-naphthalenedicarboxylate^{2-} > 2,6-anthraquinonedisulfonate^{2i}) as these fit the large, reinforced binding pocket better (Figure 8).[70]

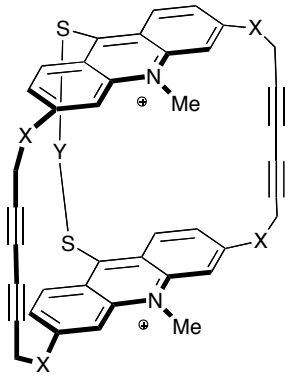

14a: X = O
Y = -$(CH_2)_6$-
14b: X = O
Y = -$(CH_2)_2O(CH_2)_2$-
14c: X = O
Y = -$(CH_2CH_2O)_2CH_2$-
14d: X = NH
Y = -$(CH_2)_2O(CH_2)_2$-

Figure 8. Bicyclic **14** illustrating the effect incremental increases in binding pocket size can have on binding strength.

The binding constants with neutral adenosine were measured in an aqueous buffer (log K_a = 4.00, 3.87, 3.86 and 4.00, **14a-d** respectively) and followed the same trend with doubly charged AMP (log K_a = 4.08, 3.79, 3.92 and 4.08).

Alkyne-linked macrocyclic indole and indolocarbazole receptors **15** and **16** were synthesized and their anion affinities probed in acetonitrile (Figure 9).[71] It was found that further rigidification of receptor **15** to **16** very modestly increased binding constants (e.g. Cl^- K_a = 1.5 x 10^6 M^{-1} to 2.1 x 10^6 M^{-1}, N_3^- K_a = 8.8 x 10^5 M^{-1} to 9.1 x 10^5 M^{-1}, $H_2PO_4^-$ K_a = 2.1 x 10^6 M^{-1} to 3.2 x 10^6 M^{-1}). A crystal structure of the **16**•Cl^- complex revealed that the binding pocket was slightly too small to incorporate the Cl^- anion completely. Both of these receptors exhibited increased affinities over previously studied acyclic receptors **17** and **18**.[72] Rigidification in this system had the same effect as in the macrocyclic versions (**17:** K_a = 5100 M^{-1} to **18:** 110,000 M^{-1} for Cl^-). In more recent work, **19** was used to study the preferred binding geometry of azide, halide and oxoanionic guests.[73]

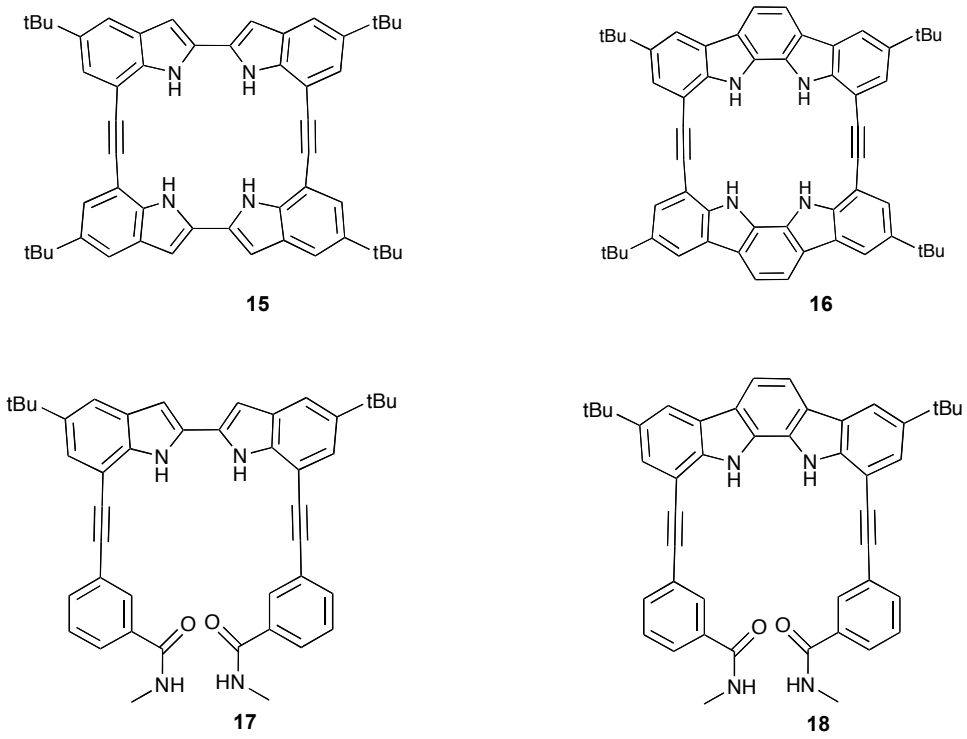

Figure 9. Binding studies performed with **15**-**18** are excellent examples of the consequences of overly restricting the degrees of freedom in a receptor.

Changing the ethynyl linker in **16** to butadiynyl in **19** decreased the affinity for Cl^- anion over four fold, although the affinity for Br^- and I^- anions was greater for the larger cavity of **19** (Figure 10). There was no affinity for acetate, but other polyoxo-anions ($H_2PO_4^-$, NO_3^- and HSO_4^-) exhibited increased affinities of one to two orders of magnitude. Azide bound in an orthogonal fashion (normal to the macrocycle plane) in ethynyl linked **16** with one N atom in the cavity, but butadiynyl **19** had a large enough binding pocket to fully accommodate azide in a linear fashion, with a concomitant increase in binding constant (K_a = 2300 M^{-1} to 81,000 M^{-1}). The binding events in these receptors were followed by UV-Vis or ^{1}H-NMR spectroscopy; the change in their fluorescence emission was not reported. The cleft-like derivative **20**

was studied as well and found to strongly and selectively bind $H_2PO_4^-$ (K_a = 1.1 x 10^5 M^{-1}) due to the inclusion of two additional hydrogen bond acceptors in the ethynyl "arms".[74] Although the binding constant for this system is smaller than for their previously reported macrocyclic receptor **16**, the selectivity increased, highlighting the well-designed binding pocket for the geometry of the desired guest. As expected, when binding guests with hydrogen bond donating capability the pyridine nitrogens were pointed into the cavity (e.g., **20**•$H_2PO_4^-$). The pyridine nitrogens rotated out when binding guests lacking hydrogen bond donating ability (e.g., **20**•Cl^-), and this was accompanied by a downfield shift of the C-H protons at the 3 position in the arene rings indicating C-H···anion hydrogen bonding. This underscores the need for some flexibility in the conformation of the binding site for selective receptors, as well as an increased degree of flexibility in the scaffold.

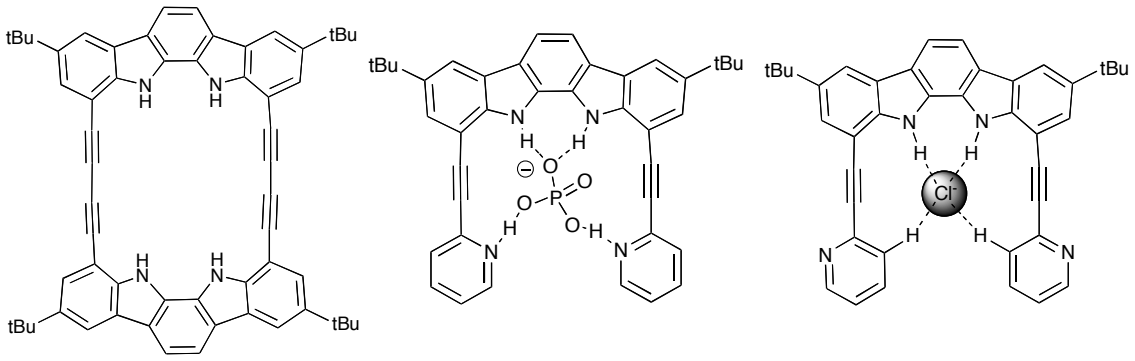

19 **20•$H_2PO_4^-$** **20•Cl^-**

Figure 10. Macrocycle **19**, an enlarged version of **16** and cleft receptor **20** in both the "H-bond accepting" and "H-bond donating" binding modes.

Invariably receptor systems must contain some signalling unit to function as a sensor, as showcased in the phenylacetylene-based tripodal receptor for heparin in serum **21** (Figure 11).[75] In **21** the three ammonium-bearing arms were extended from the fluorophore body by ethynyl linkages, which proved to be the structural criterion necessary for effective binding of anionic heparin. In contrast, **22**, with its closely packed tripodal arms, proved insufficiently sensitive to be viable in biological media such as serum.[76] This was attributed to non-specific binding of proteins in serum which displaced the dye bound in the receptor. Additionally, this provided elegant precedent for the ability of small-molecule synthetic receptors to be viable probes for complex biological substrates in competitive media.

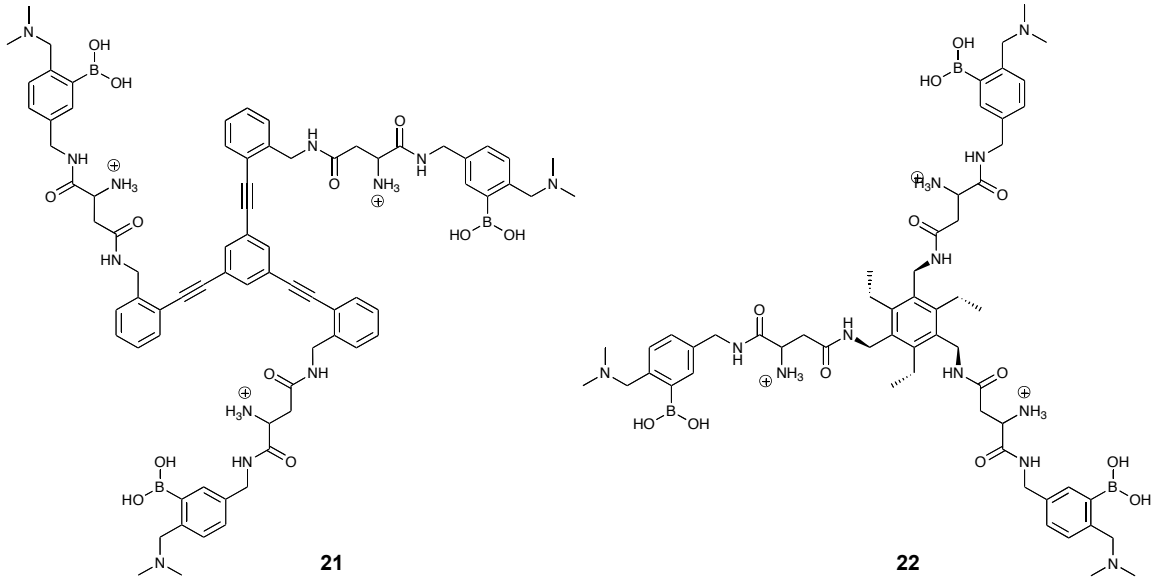

Figure 11. Tripodal alkyne containing receptor **21** was effective in biological media and improved over the smaller cavity of **22** while retaining its desired secondary properties (e.g., solubility).

Recent work has made use of fluorescent "turn-off" anion sensing modes[77] and phenylacetylene subunits for both "turn-on" signalling and binding site size enforcement.[78] The chloride binding properties of diphenylacetylene-based anion receptors **23a,b** exhibited "turn-off" fluorescence in the presence of a suitable guest (Figure 12). Bisurea **23a** exhibited quenched fluorescence emission in its unbound "open" state. The DFT minimized conformation had the typical low fluorescence observed in diphenylacetylenes due to the dark $\pi_y^* \leftarrow \pi_x$ ($^1A_{1u}$) transition being close in energy to the emissive $\pi_x^* \leftarrow \pi_x$ ($^1B_{1u}$) transition. Fitting a suitably sized guest in the receptor cleft (in this case Cl^- anion) induced planarity by rotation around the alkynyl bond. This increased the energy of the $^1A_{1u}$ transition, and the bound receptor thus became emissive. Binding constants for model systems **23b** and **24** were also measured against halide and oxoanions. Receptor **23a** had the highest affinity for Cl^- (log ß = 2.557 versus 1.831 for **23b** and <1 for **24**). The length of the phenylacetylenic linker influenced size selectivity, as Br^- was bound by **23a** and not by **23b**. None of the receptors exhibited any affinity for NO_3^-.

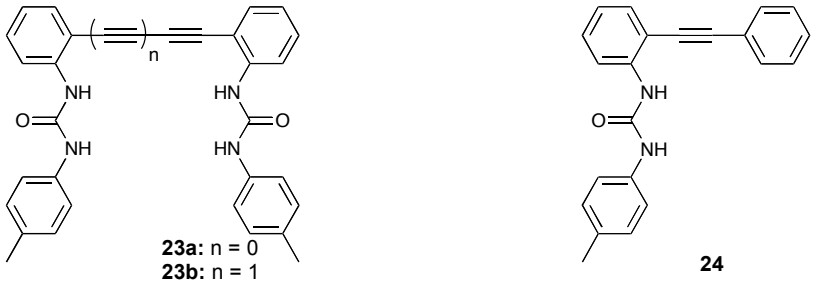

Figure 12. Fluorescent "turn-on" sensors for Cl^- (**23a,b**) and the model compound used to determine the conformational dependence of the fluorescence emission (**24**).

The allosteric binding of **25**, a macrocyclic receptor with a central tetrafluorophenyl "turnstile" suspended in the cavity by ethynyl bridges, was studied by NMR spectroscopy (Figure 13).[79] The turnstile inhibited both amide binding sites in the free receptor. Upon binding one equivalent of a guest the tetrafluorophenyl gate was opened and allowed access to the second binding site. Acetate, Br^-, and phosphate bound cooperatively (Hill coefficients of 1.4, 1.5 and 1.4, respectively). Interestingly, Br^- anion was large enough (1.82Å in an octahedral environment) to exhibit cooperative binding, but Cl^- (1.67Å) ostensibly did not, although chloride had the higher K_{a1} with approximately equivalent second binding constants. This was reflected in the Hill coefficient for Cl^- anion of 1.1.

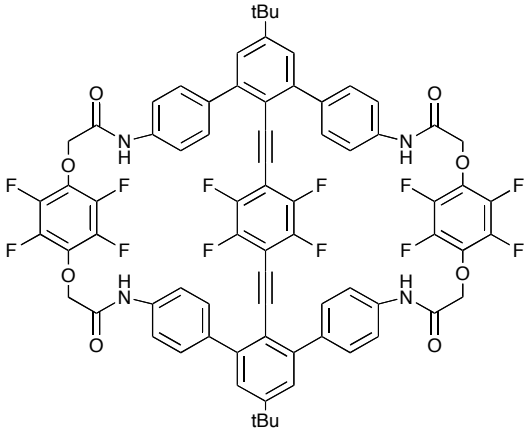

25

Figure 13. Allosteric receptor **25** exhibited no cooperativity with smaller guests, i.e., Cl^-, but cooperative binding for Br^- and larger oxoanions.

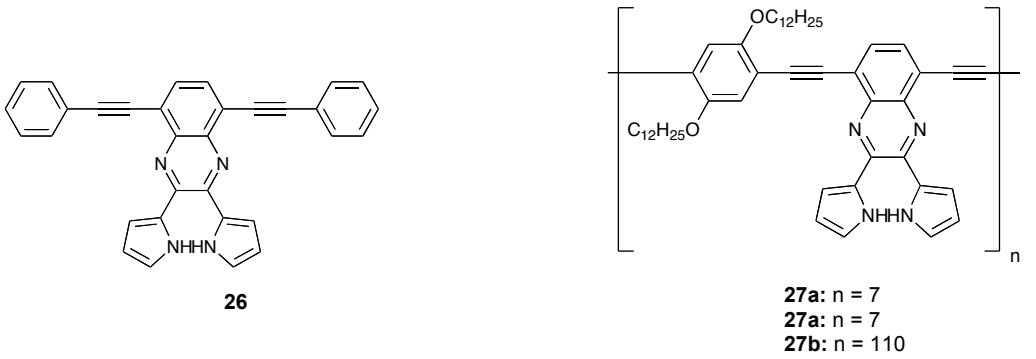

Figure 14. Monomeric **26** and polymeric **27** both bound guests in the typical Hofmeister fashion, but polymerization increased binding 34-fold.

Based on earlier work,[80] dipyrrolylquinoxaline derivative **26** was reported to bind anions with both a chromogenic and fluorogenic response (Figure 14).[81] This monomer exhibited affinity for anions ($F^- > HP_2O_7^{-3} > CN^- > OAc^- > H_2PO_4^- \approx Cl^- \approx Br^- \approx I^- \approx NO^{-3}$) correlating to the relative basicity of the guest, although fluoride and pyrophosphate were found to deprotonate the receptor. Polymerization to **27a** and **27b** was accompanied by a 34-fold increase in optoelectronic response, which translates into increased sensitivity with increased repeat units.

Lastly it is worth noting the two-photon absorption (TPA) properties that the increased conjugation length of some phenylacetylenes can lend to a probe. Cross-conjugated D-π-A-π-D bis(anilinoethynyl)-functionalized pyridine **28** was synthesized and its properties as a two-photon induced polymerization (TPIP) initiator were studied (Figure 15).[82] While free-base **28a** was too poor an acceptor to provide a good TPA cross section, cationic **28b** was assumed to have a much higher value, though this ultimately could not be verified due to the poor solubility of **28b**.

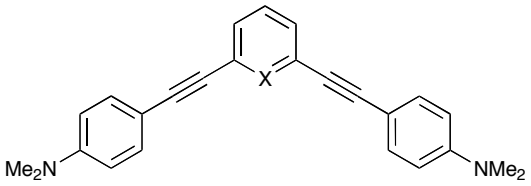

28a: X = N
28b: X = NMe^+

Figure 15. Two-photon absorbing phenylacetylene **28**.

It has also been reported that TPA fluorophores of the A-π-A type can be modulated via their planarity, which has also been a demonstrated handle for supramolecular sensors.[83] A combination of selective targeting and low energy excitation and emission is a promising application for soluble phenylacetylene-based sensors in biological media.

Biological Applications for Phenylacetylene-based Sensors

There are several biochemical factors to consider in the design of new intracellular ion indicators. These include the loading of the indicator(s) into target cells,[84-88] maximizing optimal detection parameters[89] with minimal toxicity[90] and the ability to selectively quantitate the ion concentration in question within the cells or tissues being examined.[91] Within these areas are several additional factors that affect utility including compartmentalization or partitioning within the cell into specific organelles,[92] matching optical excitation/emission wavelengths to match common instrumentation in use[93] and the use of ratiometric determination methods to help quantitate binding and ion levels.[94,95] Finally, factors such as specificity versus other intracellular ions,[96] water solubility,[97] relative binding constants for the

intracellular ion or ions[98] and the effect of pH on binding[89,99] and fluorescence emission[91] are also important factors to be optimized for biochemical probe optimization. Of course, it is impossible to optimize all parameters, but of ultimate importance are ion selectivity and the ability to quantitate intracellular concentration.

Anions in cells are present at roughly 70% of all enzymatic sites and are responsible for everything from the activation of signal transduction pathways to maintaining osmotic pressure and cell volume.[1,100] They are involved in many disease pathways, from cystic fibrosis to osteoporosis.[101-103] In mitochondria, at least 14 different anion transport pathways have been identified[104] and are responsible for the regulation and trafficking of ADP, ATP, citrate, maleate and halide anions, among others.[105,106] The ubiquity of these molecules in living organisms, and their importance in regulating life systems can best be summed up in the realization of the polyanionic character of both DNA and RNA. The acidity of intracellular compartments has been implicated in some disease pathways, notably in the cellular breach of anthrax lethal toxin and edema toxin.[107] This breach has been correlated with decreased endosomal pH, which can be achieved either by concomittant movement of K^+, or an influx of Cl^-.

One recently reported example of a ratioable fluorescent Cl^- probe was dextran-tethered acridinium system **33**, used for charting endosomal Cl^- concentration in tandem with endosomal pH (Figure 16).[99] The biaccridinium subunit of the receptor was found to be quenched by Cl^- anion with a Stern-Volmer constant

of 36 M^{-1}, and to be insensitive to non-halide anions (nitrate, phosphate, bicarbonate and sulfate). By tethering this system to tetramethylrhodamine, which is insensitive to Cl^-, they developed a ratioable sensor for *in vivo* application that allowed them to observe the change in Cl^- concentration in endosomes with decreasing pH. Using this same technique, it was also shown that the intracellular ClC-3 Cl^- channel regulated the vacuolar H^+ pump during endosomal acidification.[108] The ease with which a well designed small molecule sensor can visualize these complex biological responses demonstrates the import role these receptors will play in furthering our understanding of cellular processes.

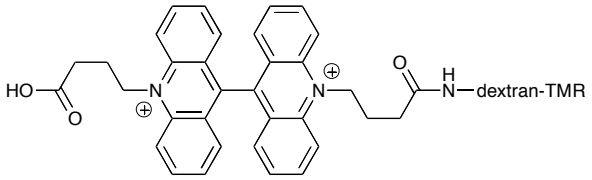

33

Figure 16. The structure of the Cl^- sensitive moiety of the *in vitro* functional fluorogenic probe **33**.

A series of linked pyridylarenes **34** were used as selective antagonists for the metabotropic glutamate receptor subtype 5 (mGlu5)(Figure 17).[109] It was found that phenylethynyl derivative **34c** (MPEP) was the most active antagonist, and bound the receptor much more effectively than the non-ethynylated receptors. This work was continued with radiolabelled derivatives **35a**[110] and **35b-d**.[111] These radiolabelled compounds were thought to be appropriate for binding and following the

distribution of mGluR5 receptors. Radiolabelled **35a** possessed a high affinity (K_d = 2 nM) and was over 90% specific for mGlu5 receptor over the 1-10 nM range.

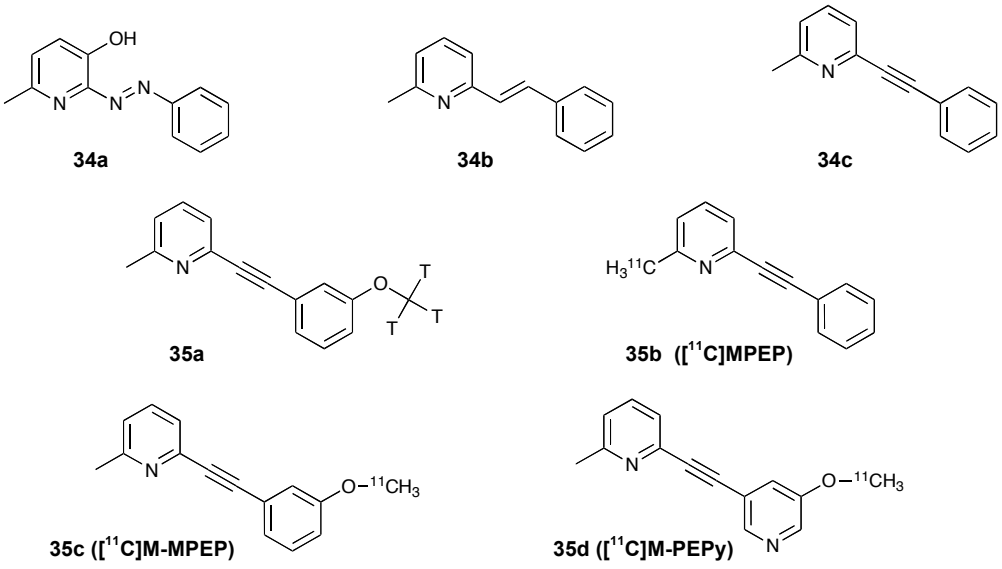

Figure 17. First generation inhibitors **34a,b** were improved by including the ethynyl bridge in **34c**. This receptor was radiolabelled systematically (**35**).

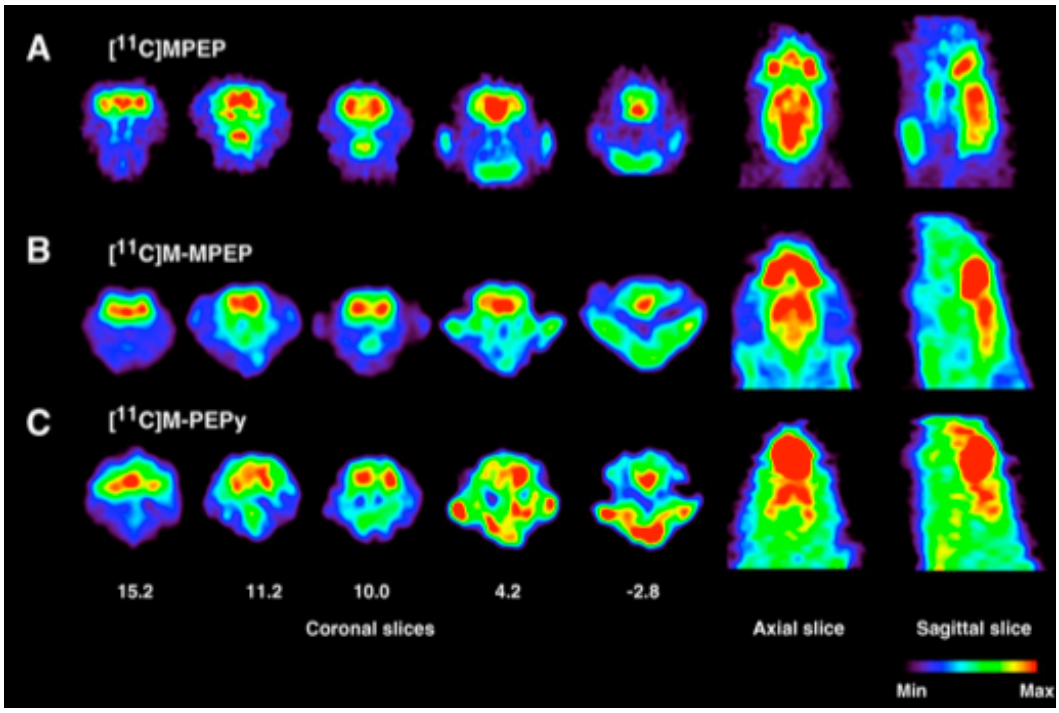

Figure 18. Coronal, axial and sagittal PET images of derivatives of **35** in anesthetized rat brain at 8-10 min after administration of radiolabelled ligand. The coronal level 15.2 corresponds to the olfactory area; 11.2 the cingulate level; 10.0 the striatal level; 4.2 the hippocampal level; and -2.8 the cerebellar level. The axial and sagittal views illustrate the distribution of the radioactivity at the mid-striatal level. (Reprinted from ref. 111 with permission from Elsevier).

Expanding upon **35a**, ligands **35b-d** were also utilized as PET imaging agents in Sprague-Dawley rats.[111] Bioaccumulation of the radiolabelled agents were tracked by *in vivo* microPET imaging (Figure 18), and found to have the highest binding in the olfactory bulb, followed by striatum, hippocampus and cortex localization. It was hypothesized that the glutamate receptor mGluR5 might have major physiological function in the oflactory area as olfactory damage in neurodegenerative diseases is consistent and severe.[112] This would also suggest that early diagnosis of Parkinson's or Alzheimer's could be achieved via the olfactory bulb.

Related work with ß-amyloid plaques (Aß plaques) as pathological features of Alzheimer's onset made use of indolinyl- and indolylphenylacetylenes as PET imaging agents.[113] Both **36a** and **36b** were found to bind Aß plaques, with **36b** being slightly more selective in early trials (via autoradiography, Figure 19). No binding constants were reported, although relative binding was inferred from washout rates.

Figure 19. PET-imaging agents designed to bind Aß plaques

Phenylethynylamides **37a,b** were found to be potent G-quadruplex binders (Figure 20).[114] Binding was studied in this system by FRET melting assays, surface plasmon resonance and CD spectroscopy. Moderate stabilization with G-quadruplexes were observed for both ligands. No discernible duplex DNA stabilization was reported. As there is evidence that small molecules can bind G-quadruplexes and modulate transcription, selectivity like this is promising for future application of these acyclic compounds in this area. Additionally, the ^{1}H-NMR experiments reported were carried out in aqueous buffer, notable due to the low solubility for related analogues (no amide functionality) and water-solubility for many arylethynyl probes is a barrier to their use as bioimaging agents.

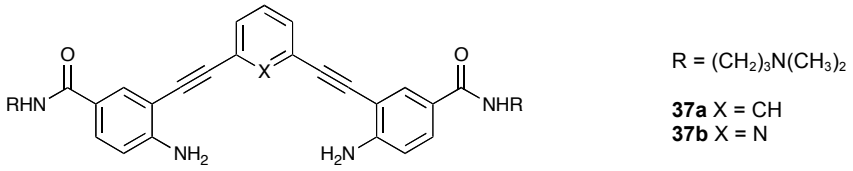

Figure 20. G-quadruplex DNA binding anilinoethynylpyridine **37** made water-soluble by inclusion of the dimethylaminopropyl-appended amides.

Conclusions

This introductory chapter introduces phenylacetylenes as important components in the design of an increasingly diverse array of supramolecular host-guest complexes. Their unique combination of optoelectronic properties, contribution to conjugation and shape persistence has played an important role in the development of many novel coordination compounds, fluorogenic and chromogenic probes and biological imaging agents. In spite of this, non-metal-containing host-guest complexes that make use of only simple organic phenylacetylenes have only recently received attention. Their contribution to the rational and effective design of receptors able to target both neutral and ionic guests with concomitant optoelectronic response upon binding is at the core of this advancement.

Additionally, commonly used synthetic techniques allow for facile and efficient preparation of a variety of novel candidates for study, which further drives innovation in this field, suggesting potential applications in molecular probe

development, nanotechnology, and even recognition of biologically-relevant molecules and ions.

Bridge to Chapter II

Chapter I served as an illustration of the steric and electronic benefits alkyne linkers can bring to a fluorophore, even for use in atypical environments, such as aqueous media or *in vitro/in vivo* application. The second chapter will introduce the first scaffold we chose to build our probes upon. Additionally, the simplest amide derivatives of this scaffold and their basic optoelectronic properties are presented, as well as solution and solid-state assays used to expose their metal cation binding ability. These experiments serve as proof of principle of our design strategy, while allowing us the luxury of using well-known titration experiments to target simple cations as the experimental basis for our ultimate venture into building an effective receptor for anions.

CHAPTER II

SYNTHESIS OF FIRST GENERATION RECEPTORS AND PROOF OF PRINCIPLE

Introduction

This chapter was coauthored with Dr. Orion Berryman and Dr. Charles Johnson, both of whom provided crystallographic support and editorial assistance, and Daisuke Inokuchi who performed the synthesis of **11** and **12**. My advisors Michael M. Haley and Darren W. Johnson conceptualized the project and provided editorial assistance while Dr. Lev N. Zakharov solved the diffraction data for the crystal structures presented herein.

Previous investigation in the Haley lab of novel planar molecular topologies for organic optoelectronics led to the pyridine-containing organic and inorganic heterocycles **1** and **2** (Figure 1).[1]

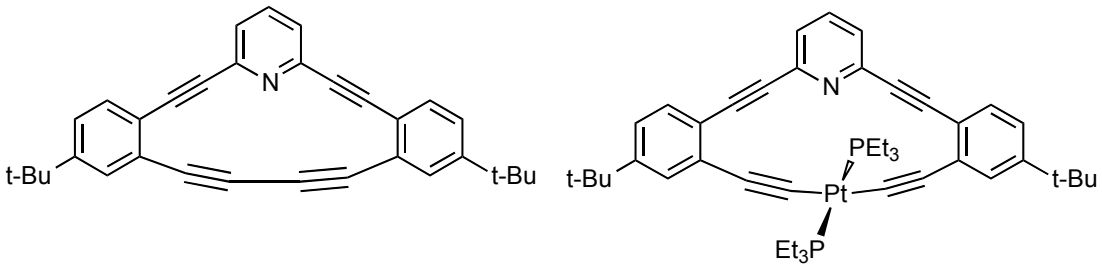

Figure 1. Macrocycle **1** and platinacycle **2**.

Both compound **1** and **2** had well characterized optoelectronic properties that seemed to bode well for their use as scaffolds upon which to build a non-covalent receptor.[1] However, the fully organic macrocycle **1** has only two coordination sites (the diyne bridge and pyridine lone pair) while inclusion of the covalently bound Pt moiety in **2** sterically crowded the cavity.

A key aspect of chemosensor design as opposed to chemodosimeter design is reversibility, and as such the scaffold needed functional handles upon which to append hydrogen-bonding groups. The possibility of using the pyridine nitrogen as a switchable hydrogen bond acceptor/donor upon protonation led us to consider a three-coordinate design that could be achieved by changing the covalent ethynyl linkages to Pt in **2** to easily functionalizable anilines or phenols, depending upon the desired target (Figure 2).

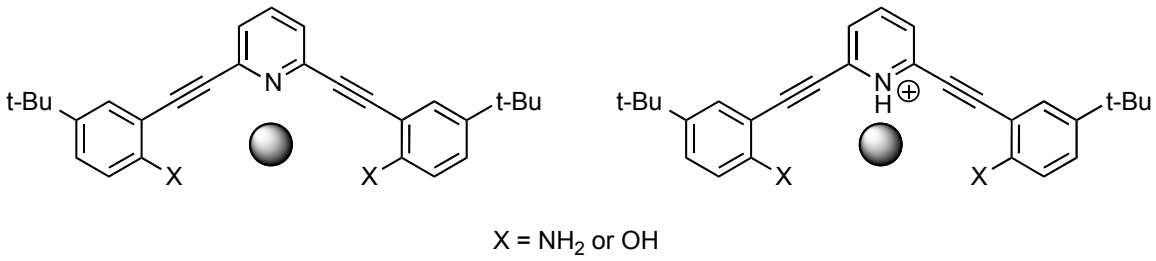

Figure 2. Ethynylarene scaffolds for three-coordinate receptors.

While phenolic substituents would garner us a receptor suitable for cationic species (by lone pair donation) our interest lay in receptors for anions, and thus we designed a simple retrosynthesis of dianiline **3** from previously published or commercially available starting materials (Scheme 1)**.**[2]

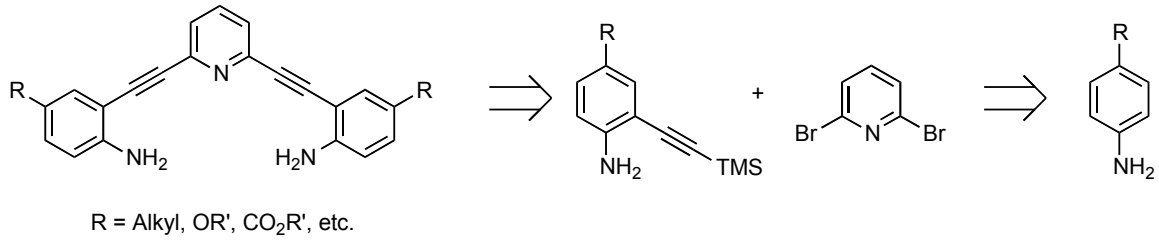

Scheme 1. Retrosynthesis of parent scaffold.

Starting from simple aniline building blocks allows for facile modification of portions of the receptor, thus affording us an efficient route to systematic adjustment of receptor properties. By mixing and matching these modular synthons, large libraries of receptors can be quickly synthesized and screened for desired behavior (e.g., binding strength, fluorescence emission output or solubility). These parent scaffolds can subsequently be functionalized with a variety of hydrogen bond donating or accepting groups depending on the desired optoelectronic output, binding target or application (e.g., fluorometric or electrochemical sensing).

The Parent Dianiline Scaffold

Arylethynylpyridine **3** was the first scaffold synthesized (Scheme 2).[2] The tertiary butyl group was chosen due to its availability, the work done with it previously and the steric bulk, which was expected to decrease the self-association of the receptors in solution.

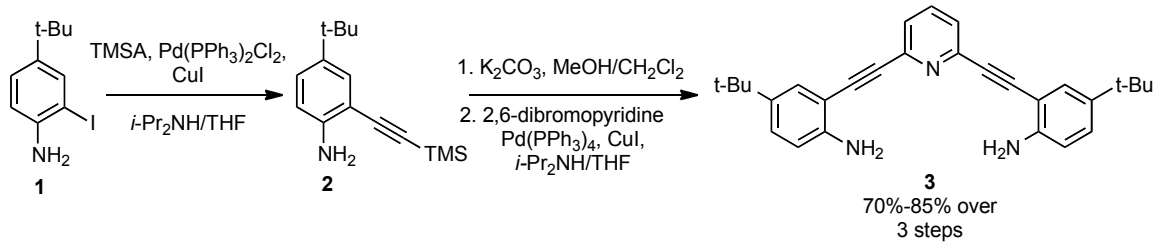

Scheme 2. Synthesis of dianiline **3.**

Readily available **1** was prepared by literature methodology from *para*-*t*-butyl-aniline by iodination with benzyltriethylammonium dichloroiodate.[3] This compound underwent Sonogashira cross-coupling with trimethylsilylacetylene which was subsequently deprotected with potassium carbonate and two-fold crosscoupled to 2,6-dibromopyridine.[4,5]

The absorbance properties of **3** and its salts with trifloroacetic acid (TFA) and HCl in chloroform are summarized below (Figure 3).

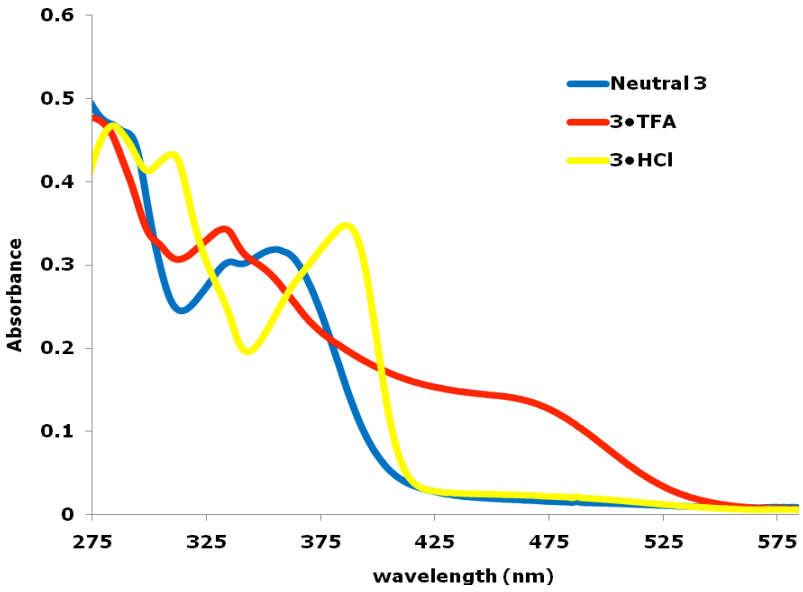

Figure 3. UV-Vis absorbance spectra of **3, 3•TFA**, and **3•HCl** in chloroform.

Neutral **3** shows no absorbance in the visible region of the spectrum, and its π–π* absorbance band overlaps the n–π* band at 355 nm. Upon exposure to TFA the n–π* band is hypsochromically shifted 10 nm, while the π–π* band has an almost negligible hypsochromic shift of 3 nm. The appearance of a charge transfer band at 465 nm gives the solution a yellow tinge.[6] Due to the presence of protonizable anilines in **3**, the stronger acid HCl protonates the anilines as well, and the charge transfer character is no longer observable, while both the π–π* and n–π* bands are bathochromically shifted and can no longer be distinguished between.

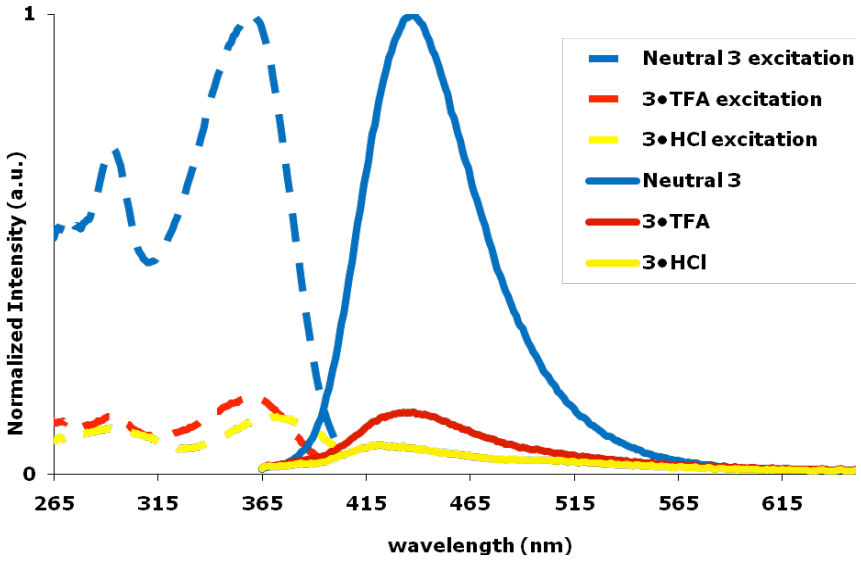

Figure 4. Fluorescence excitation and emission spectra for **3** and its TFA and HCl salts in chloroform. Excitation was at the excitation spectrum λ_{max} (363 nm, 363 nm and 375 nm, respectively).

The fluorescence emission spectra of **3** and its salts differed slightly in photoluminescent quantum yield (PLQY) and in emission λ_{max} values in organic solvents.

The neutral receptor had a PLQY of 2.3%, while protonation with TFA or HCl yielded a salt that had a slightly diminished PLQY (1.8% and 1.6%, respectively). The emission λ_{max} in **3**·TFA was unchanged from the neutral receptor; however, **3·HCl** was hypsochromically shifted 12 nm. The excitation spectra were consistent, indicating no change in excited state conformation between **3** and **3·TFA,** but a slight bathochromic shift in the maximum of excitation in **3·HCl**, indicating a diminished HOMO-LUMO gap in this species. The differences in the protonation with TFA vs. HCl could be attributed to the protonation of the anilines with the stronger acid, and were expected to be unobservable upon further functionalization at this position. The slight differences observed in emission intensity between the neutral and protonated receptors augered well for the application of this compound as a switchable fluorionophore and thus it was chosen as the first candidate for further derivatization.

Functionalized Phenylethynylpyridines: Synthesis and Metal Binding Properties

While the scope of functional groups that could be appended to the dianiline core is broad, initial attempts focused on aniline derivatization due to the preponderance of synthetic routes and literature procedures.[7-9] Amino- or anilino-protecting groups as well as simple substituted acyl halides are available commercially and abundant. Additionally, peptide coupling reagents could be used to modify the aniline moieties with simple carboxylic or benzoic acid derivatives and are attractive due to the ease of isolation of products and functional group tolerance.[10] Metal ions were chosen as the initial targets for proof of principle studies due in part to the expertise in

the Johnson lab with metal cation binding, as well as the stoichiometric predictability and strength of binding in metal-mediated self-assemblies.

Amides: α-Mercaptoamide. The first amide target to be synthesized was α-mercaptoamide **7** (Scheme 3).[11,12] The pendant thiols were chosen due to the Johnson lab's expertise with mercury and arsenic-binding thiol macrocycles.[13,14] It was expected that this binding motif would serve as a good proof of principle for observation of any optoelectronic perturbation of the amide-functionalized core upon binding ions in solution via UV-Vis absorbance or fluorescence emission measurements. Additionally, we considered the possibility of using the thiol-disulfide exchange in this receptor as an electrochemical handle for the development of a single component, small molecule organic redox sensor.

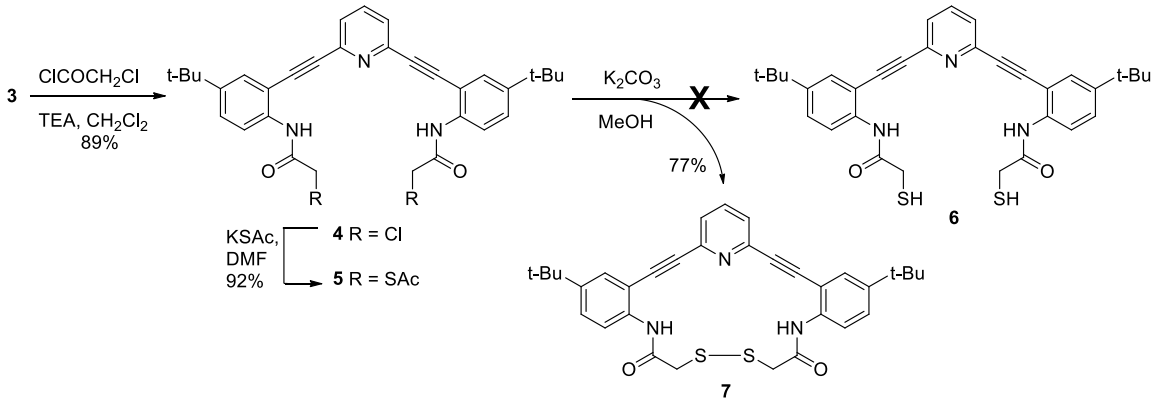

Scheme 3. Synthesis of **7** and first attempted synthesis of **6.**

Synthesis began with dianiline **3** being treated with chloroacetyl chloride and triethylamine as a solution in dichloromethane to yield α-chloroamide **4,** which underwent conversion to the acetyl-protected α-mercaptoamide **5** upon treatment with potassium thioacetate in dimethylformamide in good yield.[15] Attempts to deprotect the thiol with potassium carbonate invariably led to mixtures of the ring-closed disulfide **7** and the free thiol, which proved difficult to separate without oxidizing the thiol to disulfide in the process.

The difficulty in isolating appreciable amounts of the free thiol through simple deprotection led to multiple attempts to reduce the disulfide or to circumvent the deprotection step. Treatment of **7** with dithiothreitol,[16] Mg^0 in methanol,[17] sodium borohydride ($NaBH_4$), and lithium *tert*-butoxyaluminohydride (LTBA) all failed to produce the desired dithiol compound. Additionally, direct synthesis of the free thiol from thioglycolic acid mediated by common peptide coupling reagents (DCC, EDC, and $BOP{\cdot}PF_6$)[10] resulted in intractable mixtures.

Treatment of **4** with sodium thiosulfate ($Na_2S_2O_3$) led to the Bunte salt **8** in almost quantitative yield (Scheme 4).

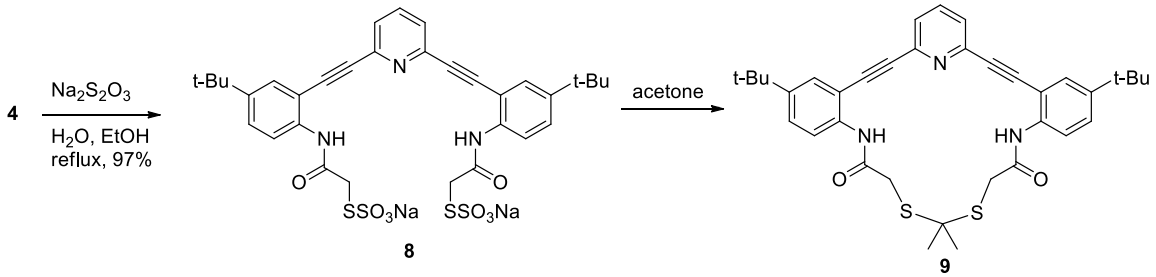

Scheme 4. Synthesis of thioketal **9.**

It was expected that careful treatment of **8** with aqueous acid would yield the free dithiol **6**.[18,19] However, **8** suffered from extremely poor solubility in most water/organic mixtures. Treatment of these suspensions with acid resulted in recovery of starting material or degradation, most likely through intermolecular displacement of the α-substituted sulfur-sulfur bond due to the high local concentration of the compound in poor solvents, resulting in polymeric material. Curiously, this compound was fairly soluble in acetone, but careful inspection of the subsequent ^{1}H-NMR spectra indicated that the dimethyl thioketal **9** was being formed by addition of the compound to this solvent.

Careful consideration of X-ray crystallographic data obtained for **6** and **7** pointed to the possibility of using the α-substitution of these receptors as a point upon which to build steric bulk around the disulfide bond (Appendix A).[20] The first and simplest derivative with which this hypothesis was tested is illustrated below (Scheme 5).

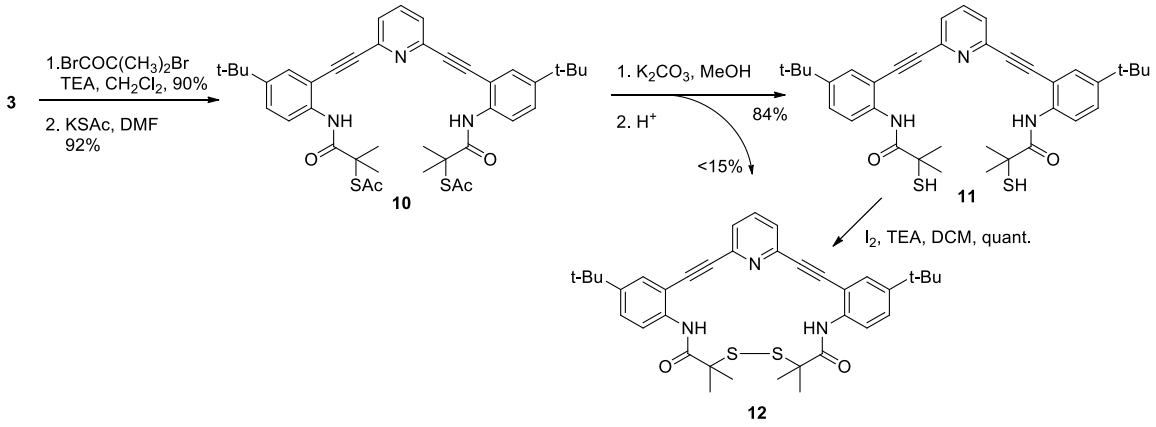

Scheme 5. Synthesis of **11** and **12.**

Parent dianiline **3** was treated with bromoisobutyryl bromide and TEA in dichloromethane to yield the α-bromodimethyl amide in excellent yield. This was treated with potassium thioacetate to efficiently yield **10**. The deprotection of **10** was achieved smoothly under bubbling N_2 in methanol followed by slight basification before stopping the reaction. Dithiol **11** was isolated in moderate yields and proved to be stable to silica in solution and to air when in the solid state. Additionally, a small percent of the disulfide 12 was isolated from the reaction, and **11** could be treated with iodine to convert the dithiol quantitatively to **12**, with matching ^{1}H-NMR spectra. Attempts to recover the thiol from the disulfide formed by iodine oxidation were unsuccessful, hinting at unusual stability of the disulfide bond in this sterically hindered analog, too.

X-ray quality single crystals of the dimethyl-substituted dithiol **11** were obtained from slow evaporation of methanol (Figure 5).

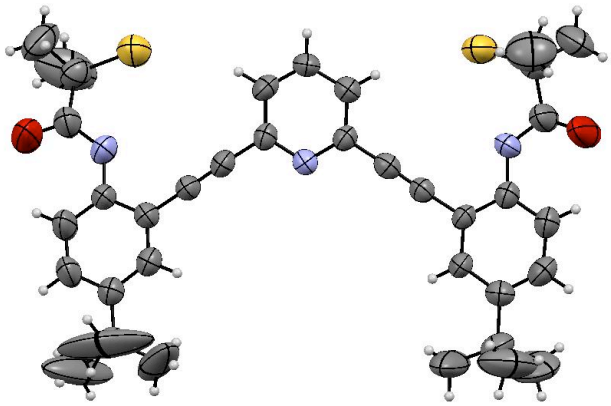

Figure 5. ORTEP representation of **11** with thermal ellipsoids drawn at the 50% probability level. The receptor scaffold is coplanar, deviating by ±1.3^o out of the arene-pyridine-arene plane.

In contrast to the x-ray crystal structure of the unsubstituted disulfide **7** obtained under the same crystal growing conditions, the "arms" of the receptor in all of the isolated single crystals of **11** wrap back into a "W" conformation. This raised questions about whether guest inclusion could compete with intramolecular disulfide formation, since both in the solid-state and in solution this receptor class had been qualitatively observed to form extremely stable S-S bonds. In addition to losing the H-bonding capability of the thiol, the disulfide S-S bond bisected the plane of the ethynylpyridine scaffold, effectively blocking the cleft of the receptor.

After successfully isolating large quantities of **11**, we undertook to use these optimized conditions for the isolation of larger amounts of **6.** The key to the deprotection and work up of that compound turned out to be as simple as a constant stream of bubbling N_2 through the basic deprotection solution, followed by careful acidification while continuing the N_2 bubbling. This slight change in the procedure allowed for the isolation of almost quantitative yields of **6** from **5** on 400-500 mg scale. With the larger amounts now available, analytically pure **6** was prepared and compared to **7** by fluorescence emission, and found to follow the same trend as **11** and **12**: the free thiol exhibited enhanced fluorescence over the disulfide. Solutions of **6** were also found to be relatively stable to oxidation by air during preparation of the fluorescence samples, although they appeared to decompose when left overnight in the cuvet. However, **11** appeared to be more stable than **6,** thus **6** was not chosen as the receptor to use in screening assays for ion binding.

Ion binding. In order to probe the feasibility of our cleft design, as well as offer evidence of the metal ion binding ability of this receptor, many attempts were made to co-crystallize both **11** and **12** with metal cations. Known thiophilic metals (e.g., Hg, Sn and As) were subjected to a variety of crystallization conditions with **11**, of which a mixture of the receptor, $Hg(OAc)_2$ and TEA in MeOH provided large, red single crystals suitable for x-ray analysis.

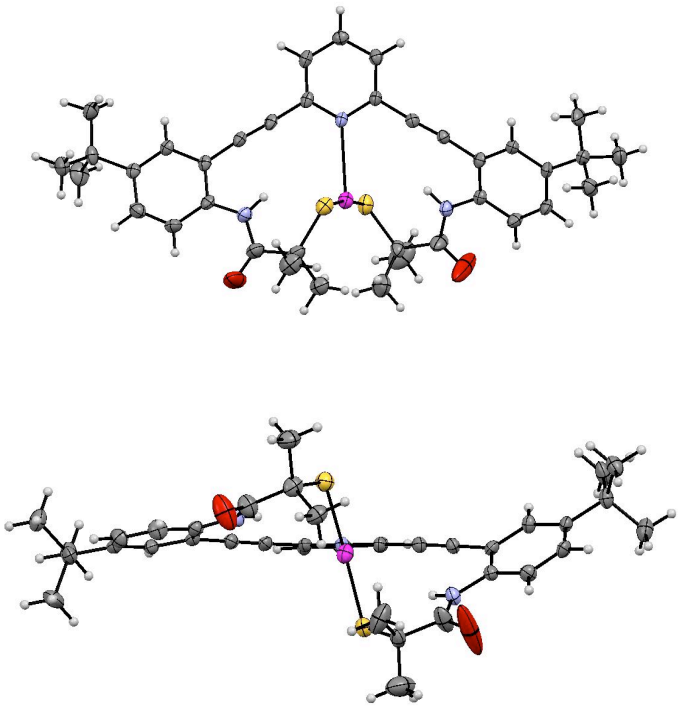

Figure 6. ORTEP representations of **11·Hg(II)** with thermal ellipsoids drawn at the 50% probability level. N—Hg bond distance: 2.743 Å; S-Hg distance: 2.336, 2.341 Å; S-Hg-S bonds deviate from linearity by 8.43°.

From the planarity in the free thiol along with the induced torsion in the Hg-containing and disulfide-linked structures, it could be inferred that the fluorescence emission spectra of these species should be significantly different.

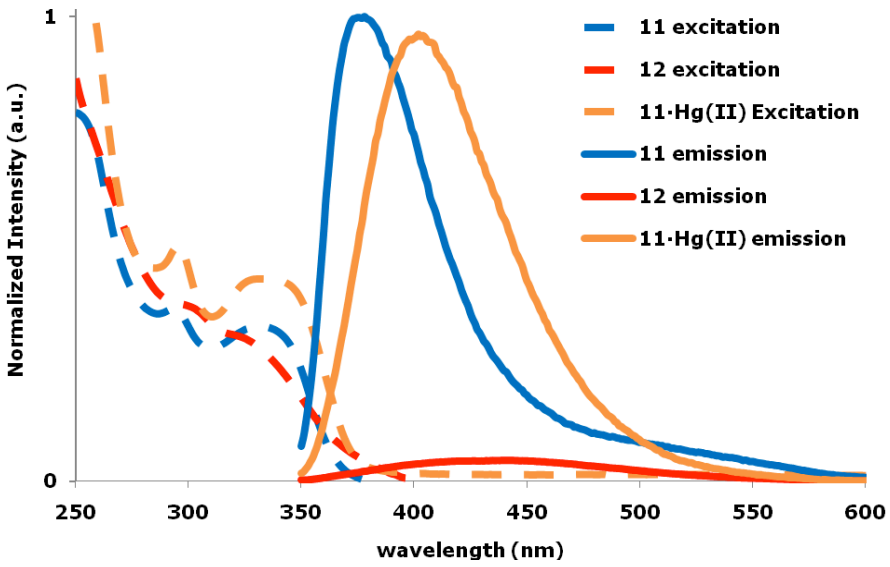

Figure 7. Excitation and emission spectra of **11, 11·Hg(II)** and **12** (excitation at 335 nm) in chloroform.

The excitation spectra of **11** and **12** are similar in the 250-335 nm region, and both match their UV-Vis spectra perfectly, indicating no change in excited state geometry in solution (Figure 7). Intriguingly, the π-π* region of the excitation spectrum (335-360 nm) is significantly different, with both a slight hypsochromic shift in the λ_{max} and a decrease in intensity for the disulfide **12**. This results in quenched emission when exciting at 335 nm, and the receptor exhibits an "ON-OFF" response upon oxidation to the disulfide. Inclusion of the metal ion, however, recovers the fluorescence emission but bathochromically shifts the emission maximum 26 nm. This is unusual in heavy metal ion fluorionophores, which normally experience heavy-atom quenching in the presence of these species due to a lowering of the energy barrier to intersystem crossing and non-radiative decay of the fluorescence.[21,22] This phenomenon is currently being more fully explored in the lab, as these results are extremely promising in both

the development of an “OFF-ON” fluorescent indicator for heavy metals and a redox sensitive small molecule fluorogenic probe.

Amides: Salicylamide. The synthetic pathways to the salicylamide receptor are shown below (Scheme 6).

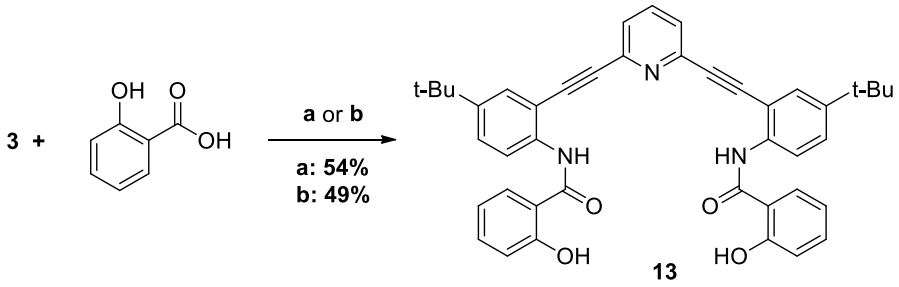

Scheme 6. Reagents and conditions: (a) salicylic acid, DCC, HOSu, DMAP, DIEA, DCM, (b) salicylic acid, BOP•PF_6, TEA, DCM

Synthesis of the salicylamide was accomplished through well known peptide coupling conditions in both cases.[10] In spite of the lowered yields, this methodology avoids the need for protection and subsequent deprotection of the *ortho*-hydroxyl group that would be necessary if synthesis proceeded through the more mundane acyl chloride or mixed anhydride methods. The impetus for the synthesis of **13** was to create a switchable metal cation/inorganic anion sensor based upon the protonation state of the pyridyl nitrogen and the salicylate hydroxyl groups.

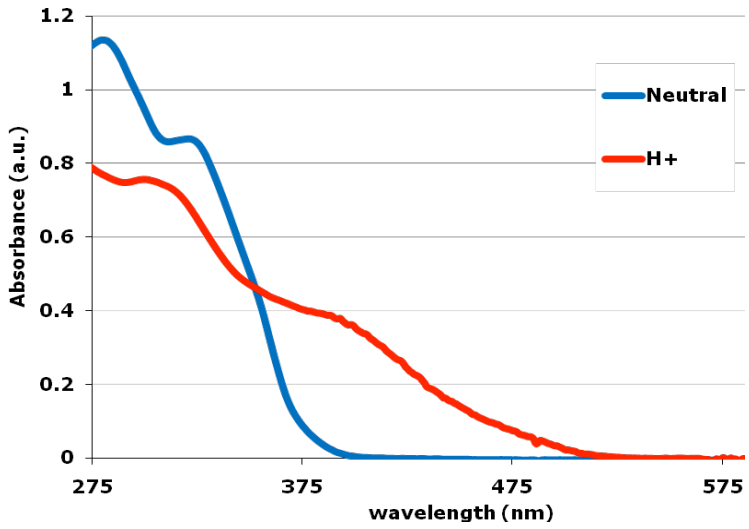

Figure 8. UV-Vis data for **13** and **13·TFA** in acetonitrile**.**

The neutral and protonated state absorption data for **13** correlate well with the parent dianiline **3**. The neutral compound exhibited hypsochromically shifted π-π* and n-π* absorbance bands by almost 30 nm as compared to **3**. Upon exposure to acid a charge transfer band was apparent in the 400 – 450 nm range, accompanied by a hypsochromic shift in the rest of the spectrum. This charge transfer band did not disappear and the solutions remained yellow under visible light even when exposed to excess TFA or stronger acids (HCl), indicating the lack of a secondary protonation event in this receptor.

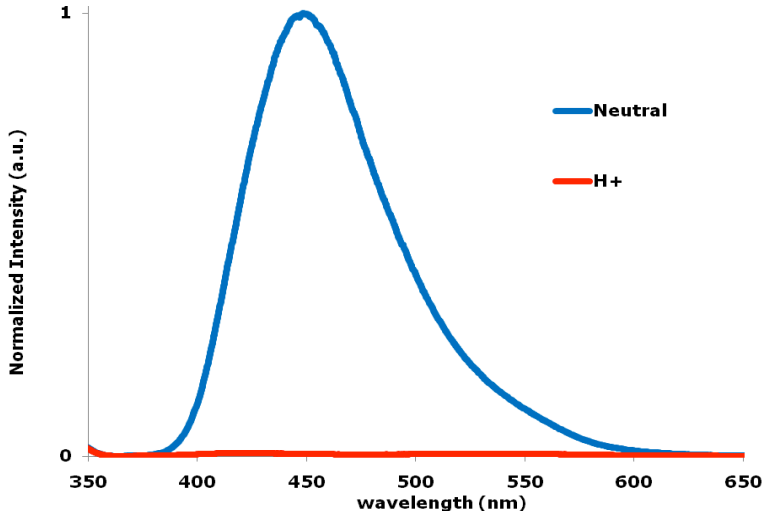

Figure 9. Fluorescence emission of **13** in neutral and TFA-protonated states in acetonitrile.

The fluorescence emission and excitation spectra also follow the trends seen in **3,** with one notable exception. The relative PLQY of freebase **13** was found to be 21% (with L-Tyrosine as the standard), which diminished to >2% upon exposure to TFA. The basis for this drastic difference in quantum yield can be illuminated by inspection of the crystal structure obtained for neutral **13** (Figure 10).

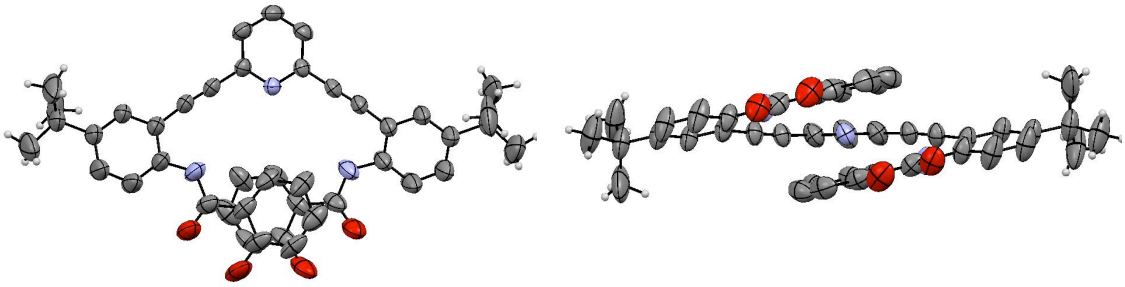

Figure 10. ORTEP representations of **13** with thermal ellipsoids drawn at the 50% probability level. The arene-arene distance is 3.48 Å, with a slip offset of the rings of 1.46 Å.

The high PLQY served as a strong indicator of rigidification of the fluorophore due to π-π stacking interactions present in the arms of the neutral receptor. Disruption of this interaction by protonation of the pyridiyl N and subsequent inclusion of the counteranion in the cleft of the receptor could account for the loss of the emission efficiency in the protonated species, and the return to an approximately 2-3% PLQY, equivalent to the parent dianiline.

Ion binding. Metal cations were chosen as the targets for proof of principle studies due to the large volume of literature upon which to base experiments, and the Johnson group's expertise with metal cation assemblies. In order to ascertain the feasibility of ion binding with **13**, solutions of the neutral species in organic media were added to solutions of $Pb(NO_3)_2$, $Ga_2(SO_4)_3$, $Zn(NO_3)_2$, $ZnCl_2$, and $Zn(BF_4)_2$ salts and either TFA or triethylamine (TEA). No obvious changes in the absorption spectra with both the Ga(III) and Pb(II) salts were observed, while the Zn spectra exhibited some distinct and promising changes (Figure 11). The slightly basic Zn(II) solution exhibits the growth of the same charge transfer band seen upon exposure to acid, which indicated that the receptor was binding Zn(II) by lone pair donation from the pyridine. Thus these conditions were chosen for titration (Figure 12; Appendix A).

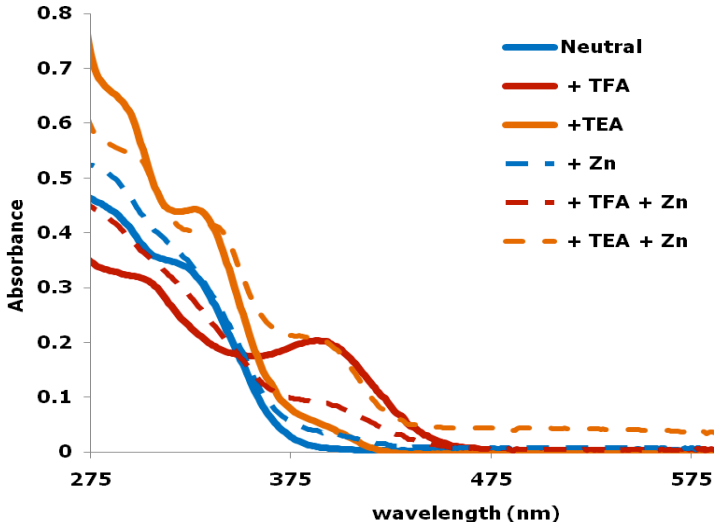

Figure 11. UV-Vis spectra of solutions of **13** at 28 µM (blue trace), with TFA (red trace) and with TEA (orange trace). To these solutions were added a stock solution of 2.5 equivalents $Zn(NO_3)_2$, TEA or TFA and **13** such that the receptor and TFA/TEA concentrations remained constant.

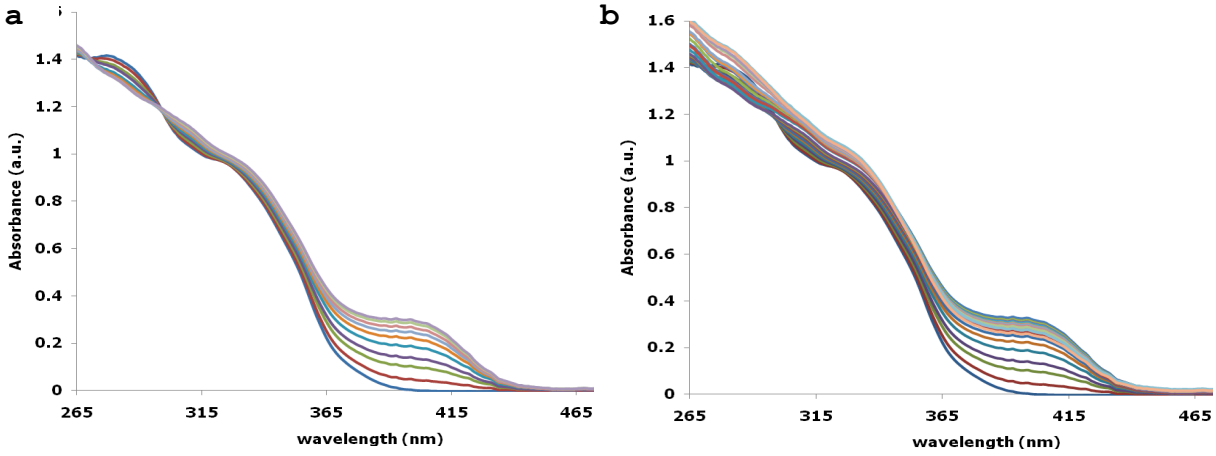

Figure 12. UV-Vis spectra of **13** at 29uM in MeCN titrated with $Zn(NO_3)_2$ in the presence of TEA (a) to 1.5 equivs (b) to 5 equivs.

Titration of **13** in acetonitrile with zinc nitrate results in an increase in the charge transfer band intensity at 370-420 nm, and a decrease in the intensity of the absorbance at 285 nm. This is accompanied by two sharp isosbestic points at 269 nm and 297 nm, indicating a discrete transition between two differently absorbing species in solution. This behavior is observed up to approximately 1.5 equivalents of metal added in all cases. In titrations carried out past 1.5 – 2 equivalents of metal, the charge transfer band stops increasing with each addition, but the isosbestic points are lost due to a steady increase and slight shifts in the absorbance spectra across the high energy range of the spectrum (265-300 nm).

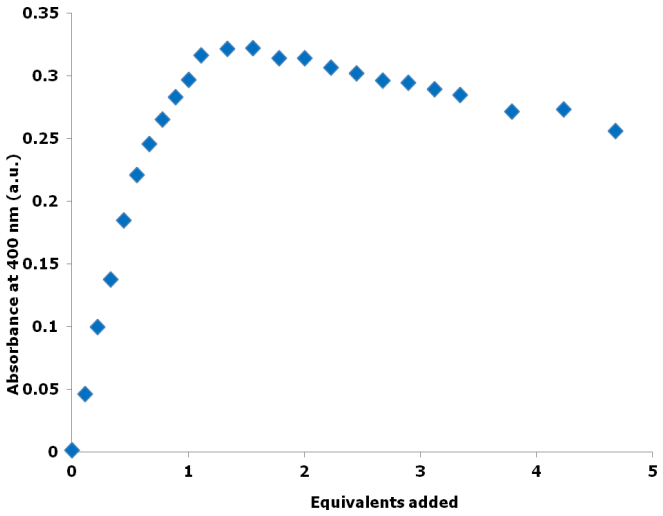

Figure 13. Correlation between equivalents of $Zn(NO_3)_2$ added to **13** in MeCn and the absorbance change in the UV-Vis spectrum monitored at 400 nm.

Plotting an isotherm for the change in absorbance at 400 nm with increasing concentration $Zn(NO_3)_2$ yields a binding isotherm that reaches a maximum at approximately 1 equivalent added, and then steadily decreases as excess metal is

introduced. The abnormal decrease in the isotherm after saturation of the receptor correlates well with the washing out seen in the raw absorbance spectra (i.e., molar absorptivity change), and is indicative of aggregation in solution. Additionally, the baseline increase in the spectra beyond 450 nm is reminiscent of Mie scattering of particulates in solution and supports the notion that this receptor is undergoing some additional, non-stoichiometric process that precludes extraction of a binding constant from the isotherms obtained during these experiments.

Conclusions

Dianiline **3** was found to exhibit slight fluorescence in its neutral state but was quenched upon protonation of the pyridine. The quenching of fluorescence was accompanied by a change in color of solutions of this receptor to a slight yellow due to pyridinium charge transfer absorbance. Protonation of the aniline moieties returned the solution to colorless, but did not result in recovery of the fluorescence emission. This switchability in emission output was well suited for sensor applications, and thus **3** was subsequently functionalized to form simple amide derivatives with which to probe the signaling ability of this scaffold as a fluorionophore. The colorimetric and fluorometric behavior of the parent dianiline **3** was conserved in all of the amide derivatives explored thus far.

Difficulties in isolating the free thiol **6** from deprotection of precursor **5** led us to synthesize the more sterically hindered analog **10**. Deprotection of this system led to almost quantitative yields of free thiol **12** which could be easily oxidized to **11.**

Reduction of this compound back to free thiol **12** remains a challenge. In spite of this, **12** was shown to bind Hg(II) in the predicted fashion, with a concomitant decrease in fluorescence response, which is a strong indicator of the future sensor applications of this family of compounds.

In much the same way, salicylamide **13** was synthesized and its binding ability explored preliminarily. Due to the strong π-π interaction between the pendant phenyl rings in this compound it is highly fluorescent both in solution and the solid-state. Titration of **13** with $Zn(NO_3)_2$ in MeCN indicated strong binding up to a 1:1 stoichiometry, and then non-stoichiometric assemblies forming in solution. This complication precluded the fitting of binding data from the titrations, but holds promise for future cation probe development.

Experimental

General Experimental Data. ^{1}H and ^{13}C NMR spectra were recorded on a Varian Inova 300 (^{1}H 299.95 MHz, ^{13}C 75.43 MHz), Varian Inova 500 (^{1}H 500.10 MHz, ^{13}C 125.75 MHz) or Varian Inova 600 (^{1}H 599.98 MHz, ^{13}C 150.86 MHz) spectrometer. Chemical shifts (δ) are reported in ppm downfield from tetramethylsilane internally referenced to residual non-deuterated solvent present in the sample. UV-Vis spectra were recorded using a Hewlett-Packard 8453 series photodiode array spectrophotometer in 1 cm x 1 cm cuvets. Fluorescence spectra were recorded on a Hitachi F4500 fluorometer equipped with a Hamamatsu R928 photomultiplier tube or a Horiba-Jobin Yvon FluoroMax-4 fluorometer equipped with a Hamamatsu R268P phosphorescence

photomultiplier tube. Quantum yields were obtained by comparison to known standards (quinine sulfate and L-tyrosine). THF was freshly distilled from potassium and dichloromethane from calcium hydride immediately prior to use. All other reagents were purchased commercially and used as received. Column chromatography was performed on Whatman reagent grade silica gel (230-400 mesh).

General Procedure for Cross-coupling. To an Ar purged solution of haloarene in 1:1 freshly distilled THF/*i*-Pr_2NH (50 mM w.r.t. haloarene) is added CuI (0.05 equiv) and $PdCl_2(PPh_3)_2$ or $Pd(PPh_3)_4$ (0.03 equiv). To this solution is added alkyne (1.05 equiv) in minimal THF dropwise with stirring over 4-8 hours. Upon complete addition the reaction is stirred an additional 3-4 hours at which point it is concentrated *in vacuo*, taken up in Et_2O and filtered through a 2.5 cm Celite pad. The remaining salts are washed thrice with Et_2O and the organics combined, concentrated and purified by silica-gel column chromatography.

2,6-Bis-(2-anilinoethynyl)pyridine 3. Iodoaniline **1** is reacted with TMSA according to the General Procedure for Cross-Coupling. After purification by column chromatography, a suspension of TMS-protected ethynylarene **2** (227 mg, 0.92 mmol) and K_2CO_3 (6 equiv) in MeOH (30 mL) and Et_2O (15 mL) was stirred at rt and monitored by TLC until completion (15-20 min). The solution was diluted with Et_2O and washed thrice with water and brine. The organic layer was dried over $MgSO_4$ and concentrated *in vacuo*. Without further purification, the residue was taken up in THF (15 mL) and reacted with 2,6-dibromopyridine (96 mg, 0.40 mmol), $Pd(PPh_3)_4$ (4.7 mg, 0.04 mmol)

and CuI (1.5 mg, 0.08 mmol) according to the General Procedure. The product was purified by column chromatography (3:2 Hex/CH_2Cl_2) or precipitated by the addition of hexanes to a saturated solution of **3** in ethyl acetate to afford **3** (135 mg, 81%) as a pale yellow crystalline solid. Mp: 226 ^{o}C. ^{1}H NMR (300 MHz, $CDCl_3$): ð 7.64 (t, *J* = 8.1 Hz, 1H), 7.45-7.43 (m, 4H), 7.20 (dd, *J* =8.7, 1.8 Hz, 2H), 6.67 (d, *J* = 8.7 Hz, 2H), 4.35 (br s, 4H), 1.27 (s, 18H). ^{13}C NMR ($CDCl_3$): ð 146.31, 143.84, 140.56, 136.36, 129.24, 128.04, 125.73, 114.34, 105.82, 93.11, 87.59, 33.85, 31.31.

Bis-(α-Chloro)amide 4. To a deoxygenated solution of **3** (395 mg, 0.94 mmol) and TEA (379 mg, 3.76 mmol) in CH_2Cl_2 (10 mL)stirring under Ar was added chloroacetyl chloride (571 mg, 5.1 mmol)dropwise. The reaction was stirred for 12 h at rt and monitored by TLC (1:1 Hex/EtOAc). Upon completion the reaction was concentrated *in vacuo* and CH_2Cl_2 (15 mL) was added and the solution transferred to a separatory funnel. This solution was washed with water three times, brine and then the organics were collected and dried over $MgSO_4$ before concentration *in vacuo*. The crude material was purified by column chromatography (1:1 Hex/EtOAc) to yield **4** as a yellow-brown solid (437 mg, 89%). Mp: 193 ^{o}C. ^{1}H-NMR (300 MHz, $CDCl_3$): δ 9.23 (br s, 2H), 8.30 (d, *J* = 8.3 Hz, 2H), 7.72 (t, *J* = 8.3 Hz, 1H), 7.64 (d, *J* = 2.1 Hz, 2H), 7.52 (d, *J* = 8.1 Hz, 2H), 7.43 (dd, *J* = 8.1, 2.1 Hz, 2H), 4.27 (s, 4H), 1.31 (s, 18H). ^{13}C NMR (75 MHz, $CDCl_3$): δ 163.62, 147.46, 143.19, 136.83, 135.83, 129.32, 127.87, 126.20, 119.07, 111.15, 94.78, 84.80, 43.21, 34.41, 31.10. MS (CI pos) *m/z* (%): 578 (M^+ +4, 15), 577 (M^+ +3, 23), 576 (M^+ +2, 75), 575 (MH^+, 38), 574 (M^+, 100); $C_{33}H_{33}Cl_2N_3O_2$ (574.54).

Bis-(α-Thioacetyl)amide 5. Potassium thioacetate (16 mg, 0.14 mmol) was added as a solid to a stirring, deoxygenated solution of **4** (34 mg, 0.06 mmol) in DMF (5 mL). The reaction was monitored by TLC (1:1 Hex/EtOAc) until completion, approximately 12 h at rt. The crude reaction was concentrated *in vacuo* and filtered through a 2.5 cm silica plug (1:1 Hex/EtOAc) and purified by column chromatography to afford **5** as an amorphous yellow solid. Recrystallization by diffusion of heaxanes into EtOAc afforded colorless crystals. Mp: 94 ^{o}C. ^{1}H-NMR (300 MHz, $CDCl_3$): δ 8.75 (br s, 2H), 8.28 (d, *J* = 8.7 Hz, 2H), 7.75 (br s, 3H), 7.58 (d, *J* = 2.4 Hz, 2H), 7.39 (dd, *J* = 8.7, 2.4 Hz, 2H), 3.76 (s, 4H), 2.34 (s, 6H), 1.28 (s, 18H). ^{13}C NMR (75 MHz, $CDCl_3$): δ 195.20, 166.16, 146.18, 143.31, 136.59, 136.54, 129.38, 127.68, 126.57, 119.45, 110.79, 94.31, 85.15, 34.27, 33.99, 31.05, 30.13. MS (CI pos) *m/z* (%): 656 (M^+ +2, 19), 655 (MH^+, 44), 654 (M^+, 100); $C_{37}H_{39}N_3O_4S_2$: (653.85).

Bis-(α-Mercapto)amide 6. A solution of **4** (72 mg, 0.11 mmol) in MeOH (60 mL) was degassed by bubbling N_2 through the solution for 15 min. At this point potassium carbonate (70 mg, 0.5 mmol) was added as a solid and the suspension was stirred for 1 hr at rt with constant N_2 bubbling through the solution. Upon completion degassed dilute aqueous HCl was added until the pH was ~5. This solution was extracted thrice with CH_2Cl_2 and dried over $MgSO_4$. After filtration, the filtrate was concentrated *in vacuo* to yield **6** as a reddish amorphous solid (62 mg, 98%). Mp: 96 ^{o}C, decomp. ^{1}H-NMR (300 MHz, $CDCl_3$): δ 9.73 (br s, 2H), 8.37 (d, *J* = 9.3, 2H), 7.68 (t, *J* = 7.8 Hz, 1H), 7.50 (d, *J* = 2.4 Hz, 2H), 7.47 (d, *J* = 8.1 Hz, 2H), 7.39 (dd, *J* = 2.4 Hz, 8.7 Hz, 2H), 3.49 (d, *J* = 9.3 Hz, 2H), 2.31 (t, *J* = 9.3 Hz, 2H), 1.32 (s, 18H).

Bunte salt 8. To a solution of **4** (240 mg, 0.427 mmol)in 50 mL 20% H_2O in EtOH in a 100 mL 3-neck flask equipped with a stir bar and reflux condenser was added $Na_2S_2O_3$ (530 mg, 2.137 mmol). This solution was refluxed until voluminous precipitate formed, approximately 12 h. Upon completion the reaction was distilled down to 10 mL and the solids collected by suction filtration. The solids were washed with cold EtOH and allowed to dry yielding **8** (320 mg, 97%) as a reddish brown solid. ^{1}H-NMR (300 MHz, d_6-acetone): δ 9.84 (br s, 2H), 8.53 (d, *J* = 8.80 Hz, 2H), 7.97 (t, *J* = 7.88 Hz, 1H), 7.70 (d, *J* = 8.80, 2H), 7.68 (d, 2.99 Hz, 2H), 7.58 (dd, *J* = 2.99, 8.99 Hz, 2H), 3.92 (s, 4H), 1.36 (s, 18H).

Thioketal 9. Obtained from ^{1}H-NMR samples dissolved in d_6-acetone or by heating **8** in acetone. No yield calculated. ^{1}H-NMR (600 MHz, acetone-d_6): δ 9.80 (br s, 2H), 8.48 (d, *J* = 8.9 Hz, 2H), 7.94 (t, *J* = 7.8 Hz, 1H), 7.65 (d, *J* = 7.8 Hz, 2H), 7.48 (d, *J* = 2.5 Hz, 2H), 7.38 (dd, *J* =2.5, 8.9 Hz, 2H), 3.89 (s, 4H), 1.29 (s, 6H), 1.15 (s, 18H). ^{13}C NMR (600 MHz, acetone-d_6): δ 165.35, 144.30, 143.05, 138.02, 137.26, 129.40, 128.91, 125.90, 118.69, 110.65, 95.48, 83.63, 62.05, 40.96, 33.24, 23.22, 14.59.

Bis-(α,α,α-Bromodimethyl)amide. The precursor to **10** was synthesized as **4**, using bromoisobutyryl bromide (0.2 ml, 1.8 mmol). Purification as **4** yields the reddish amorphous solid product (361 mg, 70% yield). ^{1}H-NMR (300 MHz, $CDCl_3$): δ 9.42 (br s, 2H), 8.32 (d, *J* = 8.99 Hz, 2H), 7.76 (t, *J* = 7.20 Hz, 1H), 7.67 (d, *J* = 2.10 Hz, 2H), 7.56 (d, *J* = 7.49 Hz, 2H), 7.46 (dd, *J* = 2.4, 8.99 Hz, 2H), 2.10 (s, 12H), 1.32 (s, 18H). ^{13}C NMR (600 MHz, $CDCl_3$): δ 169.94, 147.18, 143.30, 136.80, 136.74, 129.41, 127.81, 126.15, 118.86, 111.26, 94.82, 85.13, 63.31, 34.46, 32.64, 31.24.

Bis-(α,α,α-Dimethylthioacetyl)amide 10. Synthesized as **5**, from bis-(α,α,α-bromodimethyl)amide above (150 mg, 0.21 mmol) and potassium thioacetate (115 mg, 0.92 mmol). Yields the product (106 mg, 71%) as a yellow amorphous solid. ^{1}H-NMR (300 MHz, $CDCl_3$): δ 9.18 (br s, 2H), 8.35 (d, *J* = 8.99 Hz, 2H), 7.78 (t, *J* = 7.19 Hz, 1H), 7.62 (m, 4H), 7.44 (dd, *J* = 2.39, 8.89 Hz, 2H), 2.26 (s, 12H), 1.31 (s, 18H). ^{13}C NMR (600 MHz, $CDCl_3$): δ 195.20, 166.16, 146.18, 143.31, 136.59, 136.54, 129.38, 127.68, 126.57, 119.45, 110.79, 94.31, 85.15, 34.27, 33.99, 31.05, 30.13.

Bis-(α,α,α-Dimethylmercapto)amide 11. Synthesized in the same manner as **6** from **10** (100 mg, 0.14 mmol) and potassium carbonate (43 mg, 0.31 mmol). Yields **11** (77 mg, 88%) as a yellow amorphous solid. ^{1}H-NMR (300 MHz, $CDCl_3$): δ 9.85 (br s, 2H), 8.34 (d, *J* = 8.69 Hz, 2H), 7.73 (t, *J* = 7.19 Hz, 1H), 7.65 (d, *J* = 2.1 Hz, 2H), 7.56 (d, *J* = 7.80 Hz, 2H), 7.45 (dd, *J* = 2.4, 8.69 Hz, 2H), 1.73 (s, 12H), 1.31 (s, 18H). ^{13}C NMR (600 MHz, $CDCl_3$): δ 173.36, 146.83, 137.15, 129.24, 127.92, 125.98, 118.91, 118.89, 111.05, 94.66, 85.65, 48.90, 34.45, 31.22, 30.47.

Salicylamide 13. Representative synthesis: To 25 mL of dichloromethane in a 50 mL round-bottomed flask was added **3** (100 mg, 0.237 mmol) and BOP (benzotriazolyl oxytris-(dimethylamino) phosphonium hexafluorophosphate) (315 mg, 0.713 mmol). To this solution was added TEA (~6 equiv) and the reaction as stirred for 36 h. Upon completion the crude reaction mixture was concentrated *in vacuo*, filtered through a 2.5 cm silica plug (1:1 EtOAc/hexanes) and concentrated. This crude product was purified by column chromatography, to yield pure **13** as a colorless crystalline solid. ^{1}H-NMR (300 MHz, $CDCl_3$): δ 11.77 (br s, 2H), 9.61 (br s, 1H), 8.47 (d, *J* = 8.9, 2H), 7.84 (t, *J* = 8.9 Hz,

1H), 7.79 (dd, *J* = 1.8, 8.1 Hz, 2H), 7.66 (d, *J* = 2.4 Hz, 2H), 7.61 (d, *J* = 7.8 Hz, 2H), 7.55 (dd, *J* = 2.4, 8.7 Hz, 2H), 7.20 (m, 2H), 6.92 (m, 4H), 1.39 (s, 18H). ^{13}C NMR (600 MHz, $CDCl_3$): δ 207.28, 167.12, 160.57, 146.98, 143.21, 137.35, 134.21, 128.48, 126.85, 119.71, 119.33, 118.74, 115.54, 110.66, 95.03, 86.32, 34.50, 31.23.

Bridge to Chapter III

Chapter III continues with the synthesis and binding analysis of derivatives of the parent dianiline scaffold, specifically sulfonamide and urea functionalized receptors. Focus is shifted from exploratory studies using the more well-known coordination of cationic metals presented in Chapter II to our initial attempts at binding point charge halides and inorganic anions in competitive media. As reported in Chapter I, the binding energies of synthetic receptors with anionic targets can be relatively weak, and thus much attention will be paid to identifying and minimizing competing inter- and intramolecular interactions. Much of the following chapter will be devoted to the parent phenylurea compound, as it was identified as the best foundation upon which to build an understanding of the structure-property relationships that govern self-assembly in this class of molecules.

CHAPTER III

ANION BINDING: SELECTIVITY AND EFFECTS ON SOLID-STATE CONFORMATION

Introduction

This chapter was coauthored with Dr. Orion Berryman and Dr. Charles Johnson, both of whom provided crystallographic support and editorial assistance, and Dr. Sean McClintock who performed the molecular modeling calculations. My advisors Michael M. Haley and Darren W. Johnson conceptualized the project and provided editorial assistance while Dr. Lev N. Zakharov solved the diffraction data for the crystal data presented in the published manuscript (*Chem. Commun.*, 2009, 2520-2522, © The Royal Society of Chemistry).

The synthesis and study of hydrogen bonding receptors for anions is an engaging challenge because of the design difficulties associated with targeting such relatively diffuse, weakly basic and highly solvated analytes.[1] The prevalence of systems in both biological and supramolecular research whose behavior is dictated by their hydrogen bonding ability with simple ions has also generated increased attention in this field.[2] The development of a modular design strategy for the preparation of ion and molecule receptors based off of arylacetylene cores, a well known chromophore and fluorophore, inherently lends itself to facile synthetic modification. The adaptation of phenylacetylene scaffolding to supramolecular chemistry has in the past yielded a surprising array of host-guest and coordination complexes, some of which were covered

in Chapter I.[3] The rigid and linear motif provided by the inclusion of arylethynyl subunits has provided suitable geometric dimensions for both macrocyclic and acyclic ligands and their transition metal complexes, as shown in Chapter II. Among the benefits of such core structures is the degree of preorganization resulting from use of the rigid, conjugated components. Given the other elegant metal cation sensors that have been developed utilizing molecules such as these,[4] a modular receptor class that targets anions based on fluorescent cores may offer a new and improved approach to anion sensing. Both sulfonamides and ureas show well-known affinities for anions in solution,[5] and can easily be coupled to a modular synthetic scaffold built upon the 2,6-bis(2-anilino-ethynyl)pyridine core **1** (Scheme 1). Furthermore, the ethynylpyridine core has the added feature that the protonation state of the pyridine nitrogen can regulate binding geometries and selectivities, and thus receptors that may have been suitable for cationic guests could be switched to select for anionic species through both electrostatic and hydrogen-bond donating interactions.[6]

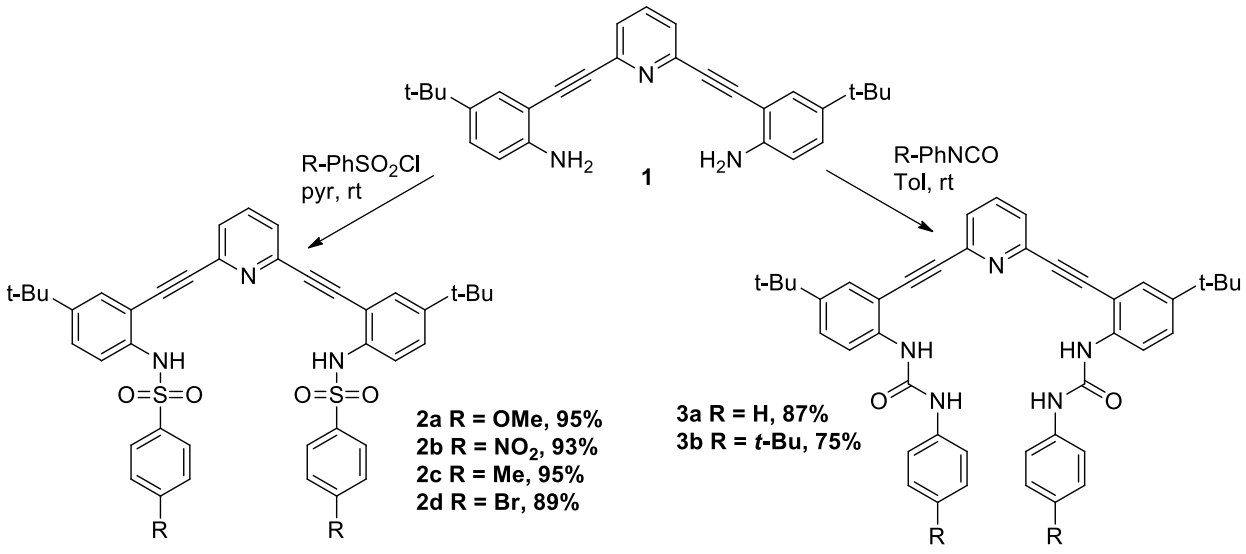

Scheme 1. Sulfonamide and urea synthesis

Scheme 1 illustrates the sulfonamides and ureas first synthesized by the Haley and Johnson groups in 2006.[7] Starting from readily available **1**, sulfonamides can be synthesized in extremely good yield, typically 85-95%, by treatment of the dianiline with commercially available sulfonyl chlorides in pyridine. Ureas can be produced in much the same manner; by simple treatment of **1** with the appropriate isocyanate in toluene the receptor compounds can be isolated in good yield, typically 75-85%. The urea synthesis suffers from some difficult-to-remove byproducts, as the homourea (formed from decomposed isocyanate) hydrogen bonds strongly with the receptors and must be triturated away.

Sulfonamides

Owing to the acidity of the sulfonamide N-H protons, we elected to start our anion binding studies with this class of receptor. We had previously reported two

sulfonamide-based ethynylpyridine compounds that showed promise as rigid receptors for anions and/or water in a [2 + 2] binding mode.[7] Both solid-state and serial dilution experiments revealed that these receptors formed helical, homodimers around two halide or water guests, as well as heterodimers incorporating both a halide and a water guest, depending upon the protonation state of the pyridine nitrogen.

Unfortunately, the complicated equilibria present in solutions of these receptors prevented unambiguous determination of the host-guest stoichiometry outside of the solid-state. It was hoped that larger functional groups appended to the pendant phenyl rings of **2** would serve two purposes: to simplify the binding data by disrupting the dimerization sterically and to provide a more lypophilic tail that would promote the solubility of these receptors, as the dimerization event was blamed for their relatively low solubility in some organic solvents. Additionally, a lypophilic tail on the protonated compound could allow the sulfonamide receptors to serve as membrane transport agents for anions.[5]

a

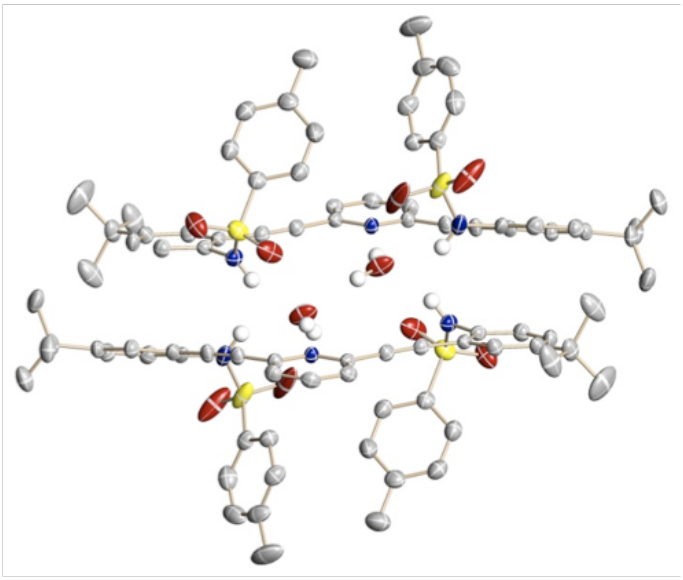

b

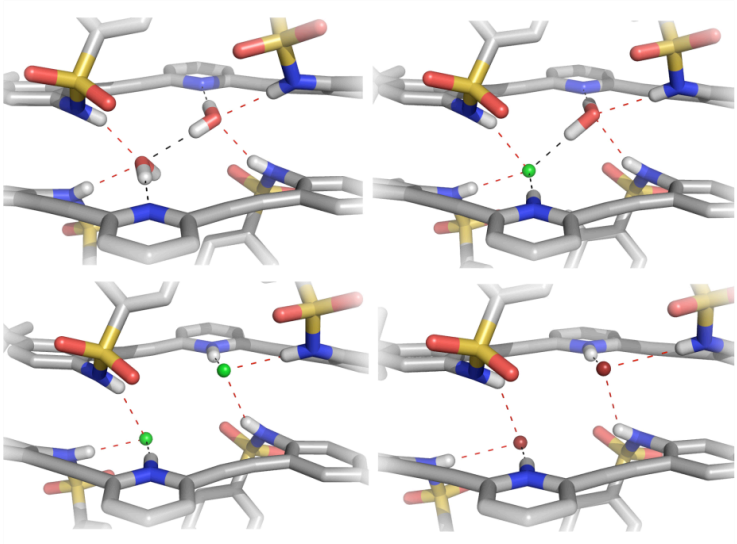

Figure 1. Illustrations of the dimerization of **2c** around (a) two water molecules (ORTEP representation with ellipsoids drawn at the 50% probability level) and (b) a close up of the cavity of **2c** showing (top left) homodimerization around water; (top right)heterodimerization around HCl and water, with Cl^- shown in green; and (bottom panels) homodimerization around HCl and HBr, with Br^- shown in red.[7b]

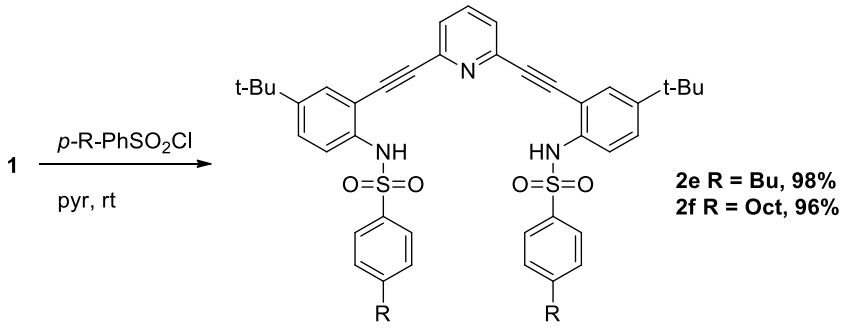

Scheme 2. Synthesis of new sulfonamide receptors **2e**,**f.**

Synthesis of **2e** and **2f** was accomplished under the same conditions as the previous sulfonamides. The starting sulfonyl chloride reagents were each prepared from their respective commercially available benzenesulfonic acid sodium salts treated with 18-crown-6 and cyanuric chloride in acetone.[8] The products of these reactions were used without purification or isolation. Although the solubility in organic solvents such as acetonitrile and chloroform was increased by the long alkyl appendages, preliminary binding studies with these receptors did not result in simplified binding isotherms and still required complicated regressional analysis to fit a correct model to the binding stoichiometry.

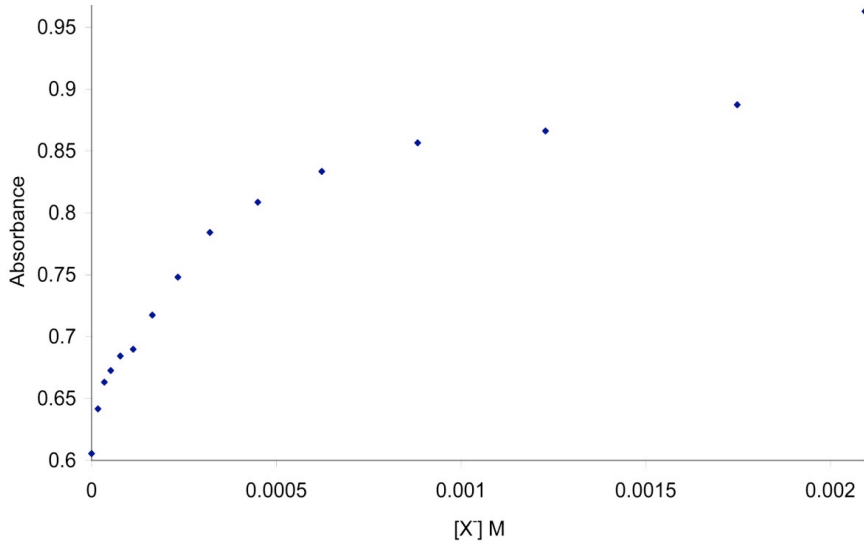

Figure 2. Isotherm generated from plotting the absorbance at 400 nm in a 29.1 µM solution of **2e** with tetrabutylammonium bromide in $CHCl_3$.

As illustrated in Figure 2, the abnormal behavior at the start of the binding isotherm obtained from UV-Vis titration data led to poor fits when fitted by nonlinear regressional analysis to a [1 + 1] binding model because of its position at or near the equivalence point. This "blip" in the isotherm was reproducible in all of the sulfonamide receptors, and may indicate the displacement of tightly bound water and a fluctuating population of **2(2e)·2(H_2O), 2(2e)·(H_2O)(TBACl)** and **2(2e)·2(TBACl)** complexes over the course of the titration. It is possible to fit the binding data to a global [1 + 1] binding model assuming the eventual distribution of host-guest complexes is substantially [1 + 1] in the presence of a vast excess of titrant. Ignoring the stoichiometric difficulties may also have precluded the use of these receptors in competitive media; their tendency to strongly bind water dimers would always compete with their anion binding capability.

Ureas

We reasoned that an increase in the number of hydrogen bonding sites within a convergent receptor binding pocket would likely favor [1 + 1] complexation, and that alkylation of the *para* positions of the pendant phenyl rings could increase the membrane transport potential of the urea receptors. To that end, reported herein is the synthesis of the bisurea analogues **3c,d** derived from **1** and the solution and solid-state data of **3a** that confirm this binding hypothesis (Scheme 3).

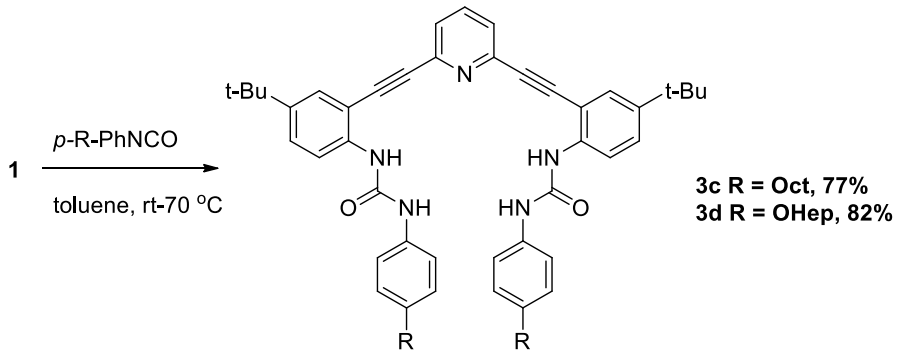

Scheme 3. Synthesis of new urea analogs for ongoing membrane transport studies.

Slow evaporation of a MeOH solution of **3a** yielded crystals suitable for x-ray diffraction (Figure 3). Unlike the sulfonamide [2 + 2] dimers,[7] in which the "arms" wrap around the guest molecules, the solid-state structure revealed that receptor **3a** adopts two different conformations – a "S" and a "W" which stack in an "SWWS" fashion with the bottom "SW" in a centrosymmetrical arrangement with respect to the top "WS". In the W form, a MeOH guest donates a hydrogen bond to the pyridine nitrogen while both urea arms are pointed away from the MeOH. In the S form, a second MeOH donates a hydrogen bond to the pyridine nitrogen and accepts two hydrogen bonds

from the urea N–H of one arm. Intermolecular urea N–H•••O=C contacts make up the remainder of the [4 + 4] "tetrameric" repeat unit. There are no additional H-bonds between these "isolated" units.

As in the case of the neutral sulfonamide receptors,[7] the neutral bisurea receptors show an affinity for neutral guests (e.g., MeOH, Figure 1). Protonation of the central pyridine nitrogen activates strong anion binding in this system as well. To perform binding constant measurements, the trifluoroacetate and tetrafluoroborate salts were prepared under the assumption that these weakly basic, larger anions would not strongly compete for the binding pocket in this receptor. (Preliminary molecular models had indicated halides were appropriately sized guests.) Fortunately, **3a•TFA** proved easy to prepare on large scale as an anhydrous, analytically pure crystalline solid.

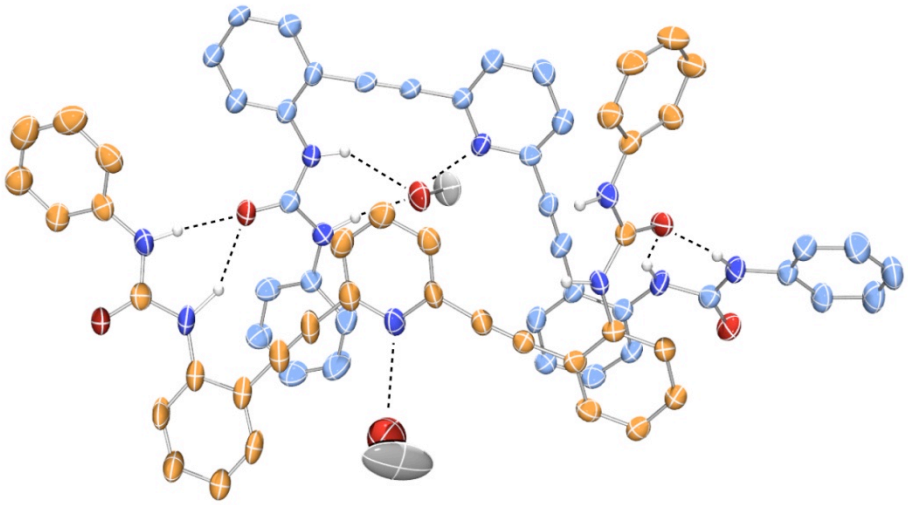

Figure 3. ORTEP representation (50% probability ellipsoids) of the two conformers of **3a**·MeOH with two solven molecules in different H-bonding motifs. The "S" conformer (orange) and the "W" conformer (blue) show half of the "SWWS" tetrameric repeat unit. The *t*-butyl groups have been omitted for clarity. The N···O distances (2.890-3.193 Å) are typical for H-bonds (dashed lines).

While a crystal structure of the TFA-protonated urea has so far proven elusive,[10] DFT modeling of this complex indicated that the urea backbone was flexible enough to partially accommodate the $CF_3CO_2^-$ counterion, with one oxygen stabilized by three hydrogen bonds between the central pyridine, and one urea arm (Figure 4).[11] Nonetheless, the binding pocket in this model is sufficiently compact that the receptor arms must twist significantly from planarity to allow the receptor to accommodate such a large guest. While smaller oxoanions may fit more easily into the binding pocket of protonated **3a**, we reasoned that any competition between the trifluoroacetate and halide guests would favor the guest with the greater number of stabilizing hydrogen bonds, i.e., the halide.

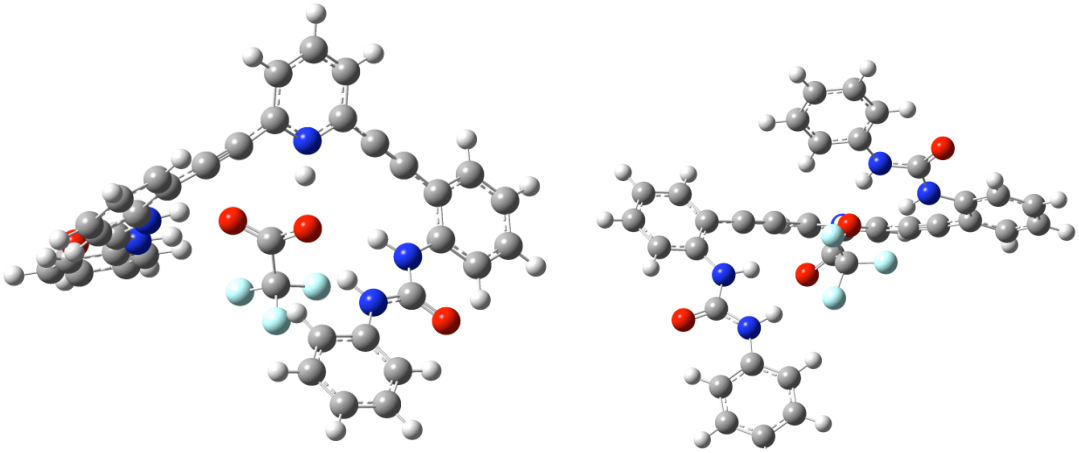

Figure 4. Top (left) and side (right) views of the DFT calculated position of the trifluoroacetate anion in protonated **3a**.

UV-Vis spectrophotometric titrations of protonated **3a•TFA** with Bu_4NCl, Bu_4NBr and Bu_4NI were carried out, and the data individually fit with the HyperQuad 2006 suite

of programs (see ESI).[12] In comparison with the TFA salt, titration with the tetraalkylammonium salts showed a new absorbance band at 422 nm which increased in intensity and shifted bathochromically. Isosbestic behavior was observed when sufficient time was allowed between aliquots for the system to reach equilibrium (less than 3 minutes). Binding constants for **3a** were obtained via titrations using ^{1}H NMR spectroscopy since the UV-Vis spectra of the neutral receptor did not exhibit any significant spectroscopic handle. These latter data were fit to a [1 + 1] model using HypNMR 2006.[12]

As shown in Table 1, protonation of **3a** activates the halide binding ability of this receptor class. Whereas unprotonated **3a** obeys the classic Hofmeister series, protonated **3a** strongly binds all three halides in the range of 42,700–83,200 M^{-1}. In fact, the binding constants for bromide and iodide are two and four orders of magnitude larger in the protonated receptor compared to the neutral receptor. However, these are apparent binding constants and a decrease in the observed binding values from competition with the trifluoroacetate counterion in the **3a•TFA** receptor must be taken into account.

Guest	**3a**[a]	**3a•TFA**[b]
Cl^-	2100	42,700
Br^-	400	61,700
I^-	not measurable	83,200

[a] ^{1}H-NMR data [b] UV-Vis data

Table 1. Calculated K_a (M^{-1}) fit to a [1 + 1] model.[12] Average values from triplicate measurements are shown. Experimental errors are ca. 10%.

Evidence of our target [1 + 1] binding behavior was confirmed in the solid state. X-ray quality crystals of 2a•HCl, were grown by addition of HCl to a solution of **3a** in hexanes/EtOAc. In contrast to the free-base receptor, the two urea arms of **3a•HCl** envelop the chloride ion affording a [1 + 1] host-guest complex with a total of five N-H···Cl hydrogen bonds (N···Cl distances 3.03-3.66 Å, Figure 5).

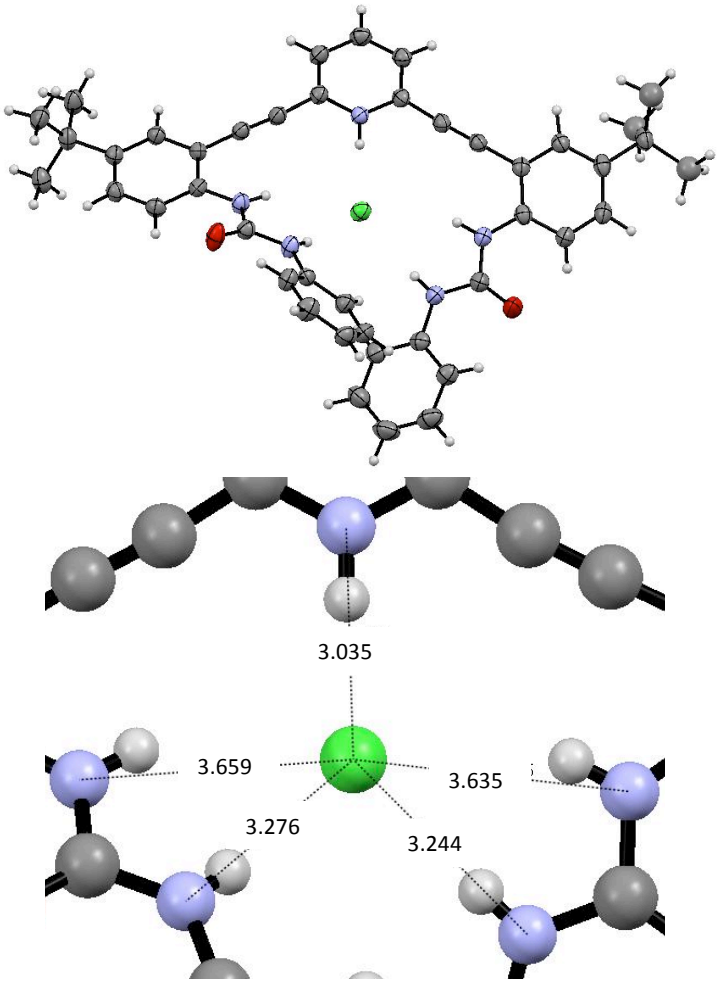

Figure 5. Top: ORTEP representation of the protonated receptor **3a·HCl** with ellipsoids at the 50% probability level. Bottom: the dashed lines indicate N-H···Cl hydrogen bonds with distances in Å.

The neutral receptor relies entirely upon the urea functionality for its hydrogen bonding capabilities, and thus shows preference for the more basic guests. The arms in the neutral receptor seem to be too far apart to participate effectively in cooperatively stabilizing the guest, and exhibit both the S and W forms, while the U-shaped [1 + 1] complex is not observed. In contrast to the neutral receptor, **3a•TFA** has a well-defined binding pocket. The pyridinium hydrogen provides a third point of contact, which anchors the receptor arms in the desired conformation upon guest binding and converges all available hydrogen bonds to the binding pocket. This disrupts the intermolecular hydrogen bond network that held the neutral tetrameric complex intact and yields the [1 + 1] complex while disfavoring our previously observed [2 + 2] dimeric and "SWWS" tetrameric complexes.[7] The slight preference for the less basic Br^- and I^- anions over Cl^- could be attributed to a larger binding pocket in the U-shaped conformation, which mitigates the traditional bias in binding more basic anions to favor the larger halides.

Conclusions

We have synthesized and performed a preliminary analysis on a new class of hydrogen bonding receptors for halide anions, based off of an inherently fluorescent arylacetylene core. Bisurea receptor **3a** binds chloride, bromide and iodide and fit with good agreement to a [1 + 1] model, which significantly simplifies the solution studies of this receptor class relative to the previously reported sulfonamide analogues.

Protonation of the pyridyl nitrogen in the receptor increases the association constant by more than an order of magnitude over the freebase receptor, and alters the selectivity between the larger halides and chloride. The increasing discovery of anionic contaminants in the environment, and the facile mobility of anions in natural systems, makes developing new approaches for anion sensing and binding vitally important. These modular receptors offer potential long-term applications in the design of new materials for remediation and sensing and the development of new molecular probes for anions.

Experimental

General Experimental Data. ^{1}H and ^{13}C NMR spectra were obtained on a Varian 300 MHz spectrometer (^{1}H 299.95 Hz, ^{13}C 75.43 Hz) or Inova 500 MHz spectrometer (^{1}H 500.10 MHz, ^{13}C 125.75 MHz). Chemical shifts (δ) are expressed in ppm downfield from tetramethylsilane (TMS) using non-deuterated solvent present in the bulk deuterated solvent ($CDCl_3$: ^{1}H 7.26 ppm, ^{13}C 77.0 ppm; THF-d_8: ^{1}H 3.58 ppm ^{13}C 67.57 ppm). Unless otherwise specified, solvents were obtained from distillation using published literature procedures directly before use. X-ray crystal data were obtained on a Bruker AXIS CCD diffractometer.

Titration Data. Spectra and the binding isotherms, as well as the conditions for the titration experiments are reported in Appendix B.

***p*-Butylbenzylsulfonamide 2e.** In a flame-dried 25 mL round bottom flask equipped with a nitrogen inlet and magnetic stir bar dianiline **1** (150 mg, 0.356 mmol) was treated with *p*—butylbenzenesulfonyl chloride (414 mg, 1.78 mmol) in 5 mL anhydrous pyridine and allowed to stir for 12 hr at rt. The reaction was concentrated *in vacuo* and run through a short (2.5 cm) silica plug (1:1 hexanes/EtOAc). The eluent was concentrated to yield a yellow oil (284 mg, 98%). ^{1}H NMR (300 MHz, $CDCl_3$): ð 7.75 (d and t, *J* = 7.9 Hz, indistinguishable, 5H), 7.53-7.35 (m, 10H), 7.20 (d, *J* = 7.9 Hz, 4H), 2.58 (t, *J* = 7.5 Hz, 4H), 1.51 (pentet, *J* = 7.5 Hz, 4H), 1.27 (s, 18H), 0.873 (t, *J* = 7.5 Hz, 6H). ^{13}C NMR ($CDCl_3$): ð 149.05, 147.96, 143.32, 136.99, 136.77, 135.91, 129.98, 129.26, 128.18, 127.58, 126.82, 120.78, 113.30, 93.89, 85.60, 35.75, 34.64, 33.27, 31.38, 22.45, 14.12.

***p*-Octylbenzylsulfonamide 2f.** In a flame-dried 25 mL round bottom flask equipped with a nitrogen inlet and magnetic stir bar was added 10 mL anhydrous acetone and cyanuric chloride in small quantities until bubbling stopped (~10 mg, 0.054 mmol). To this was added *p*-octylbenzenesulfonic acid sodium salt (500 mg, 1.71 mmol) and 18-crown-6 (22 mg, 0.09 mmol) before slow addition of the bulk of the cyanuric chloride (346 mg, 1.88 mmol). The flask was equipped with a condenser and allowed to reflux to completion, ~20 hr during which voluminous white solid formed. Upon completion the reaction was concentrated *in vacuo* and taken back up in 5 mL dry pyridine. To this suspension was added dianiline **1** (150 mg, 0.356 mmol) which immediately changed the chalky white suspension to orange. The reaction was monitored by TLC (1:1 hexanes/EtOAc) until complete, ~15 min. The reaction was then concentrated *in vacuo* and run through a 2.5 cm silica plug (100% CH_2Cl_2) and

concentrated to yield **2f** as a white waxy solid (316 mg, 96%) ^{1}H NMR (300 MHz, $CDCl_3$): ð 7.76 (d, *J* = 8.4 Hz, 4H), 7.76 (t, *J* = 7.2 Hz, 1H) 7.53-7.35 (m, 10H), 7.19 (d, *J* = 8.4 Hz, 4H), 2.59 (t, *J* = 7.3 Hz, 4H), 1.53 (br pentet, 4H), 1.28 (s, 18H), 0.872 (t, *J* = 7.3 Hz, 6H). ^{13}C NMR ($CDCl_3$): ð 149.12, 147.88, 143.31, 136.98, 136.79, 135.96, 129.94, 129.26, 128.23, 127.59, 126.74, 120.49, 113.06, 93.80, 85.47, 36.09, 34.64, 32.07, 31.38, 31.20, 29.61, 29.43, 22.89, 14.34.

Phenylurea 3a. All glassware was flame-dried before use. Dianiline **1** (800 mg, 1.9 mmol) was reacted with phenyl isocyanate (3 equiv) in 10 mL toluene with stirring for 3 h under N_2. Following concentration *in vacuo*, the crude product was filtered through a short silica plug (2:1 hexanes/$CHCl_3$). Trituration with Et_2O afforded **3a** (1.15g, 92%) as a fluffy white powder. Mp: 212-215 °C. ^{1}H NMR (300 MHz, $CDCl_3$): δ 8.32 (br s, 2H), 8.07 (d, *J* = 4.8 Hz, 2H), 7.74 (br s, 2H), 7.47-7.28 (m, 11H), 7.15 (t, *J* = 4.5 Hz, 4H), 6.92 (t, *J* = 4.5 Hz, 2H), 1.29 (s, 18H). ^{13}C NMR ($CDCl_3$): δ 152.95, 145.38, 144.62, 141.17, 140.40, 138.15, 10.11, 129.56, 128.78, 127.65, 122.94, 120.33, 114.49, 110.45, 94.38, 87.33, 35.01, 31.75. MS (APCI) *m/e* 660.3 (M^+, 100).

Phenylurea 3a•TFA Freebase phenylurea **3a** (200 mg, 30.3 mmol) was dissolved in $CHCl_3$ (15 mL) and a solution of trifluoroacetic acid in $CHCl_3$ (5 mL, 1.5 M) was added. The bright yellow solution was evaporated to ~10 mL, and pentane was added to precipitate the product as a bright orange, amorphous solid. Recrystallization from $CHCl_3$/pentane yields an orange, crystalline solid. ^{1}H-NMR (600 MHz, $CDCl_3$): δ 9.35 (br s, 1H), 8.47 (br s, 2H), 8.31 (br s, 2H), 8.26 (t, *J* = 8.4 Hz, 1H), 8.15 (br s, 1H), 7.85 (br m,

2H), 7.62 (d, *J* = 8.4 Hz, 2H), 7.56-7.47 (m, 8H), 7.17 (br m, 2H), 6.98 (br s, 1H), 6.91 (br s, 1H), 1.32 (s, 18H).

***p*-Octylphenylurea 3c.** As procedure for **3a**. Dianiline **1** (350 mg, 0.831 mmol) was reacted with *p*-octylphenyl isocyanate (576 mg, 2.49 mmol) in 10 mL of toluene. Upon completion the reaction was concentrated *in vacuo* and filtered through a 2.5 cm silica plug (2:1 hexanes/EtOAc). Following trituration with Et_2O **3c** was obtained (560 mg, 77%) as a waxy solid. ^{1}H NMR (600 MHz, $CDCl_3$): δ 8.26 (br s, 2H), 8.05 (d, *J* = 8.4 Hz, 2H), 7.64 (br s, 2H), 7.35-7.27 (m, 9H), 7.20 (m, 2H), 6.94 (d, *J* = 8.4 Hz, 4H), 2.49 (t, *J* = 8.4 Hz, 4H), 1.50-1.46 (m, 4H), 1.31-1.21 (m, 38H), 0.88 (t, *J* = 7.2 Hz, 6H). ^{13}C NMR (600 MHz, $CDCl_3$): δ 153.19, 144.90, 142.75, 138.36, 138.01, 135.80, 128.73, 128.67, 128.04, 126.01, 120.28, 118.87, 109.52, 93.04, 87.68, 35.27, 34.18, 31.90, 31.23, 29.49, 29.28, 22.66, 14.11.

***p*-Heptyloxyphenylurea 3d.** As procedure for **3a.** Dianiline **1** (120mg, 0.285 mmol) was reacted with *p*-heptyloxyphenyl isocyanate (199 mg, 0.855 mmol) in 10 mL anhydrous toluene. The reaction was monitored by TLC (2:1 hexanes/EtOAc) until completed, ~4 hr at rt. Upon completion the reddish suspension turned to a clear orange solution. The reaction was then concentrated *in vacuo* and filtered through a 2.5 cm silica plug. Concentration of the filtrate and recrystallization from hot EtOH yields **3d** (207 mg, 82%)as a fine white powder. ^{1}H NMR (600 MHz, $CDCl_3$): δ 8.147 (d, *J* = 8.9 Hz, 2H), 7.59 (br s, 2H), 7.45 (t, *J* = 7.8 Hz, 1H), 7.43 (d, *J* = 2.4 Hz, 2H), 7.37 (dd, *J* = 2.4, 6.0 Hz, 2H), 7.28 (d, *J* = 8.6 Hz, 4H), 7.20 (d, *J* = 7.8 Hz, 2H), 6.71 (d, *J* = 8.9 Hz, 4H), 3.78 (t, 7.20 Hz, 4H), 1.70 (pentet, *J* = 7.20 Hz, 4H), 1.40-1.24 (m, 36H), 0.89 (t, *J* = 6.0 Hz, 6H).

^{13}C NMR (600 MHz, $CDCl_3$): δ 155.98, 153.32, 145.09, 142.81, 138.44, 130.61, 126.17, 123.30, 119.00, 114.94, 109.63, 93.28, 87.23, 68.21, 34.22, 31.77, 31.24, 29.09, 25.99, 22.60, 14.08.

Bridge to Chapter IV

This chapter focused on the anion binding ability of the parent phenylurea receptor, while Chapter IV focuses on our work to develop these compounds into fluorogenic probes for anions by examining the optoelectronic properties in their neutral and protonated forms. Functionalization of the sulfonamide receptors with electron donating and withdrawing groups was shown to switch these receptors from "ON-OFF" to "OFF-ON" fluorescence reporters upon protonation of the central pyridine with appropriate acids. The expansion of this trend into the urea compounds by synthesis of analogs of the sulfonamide compounds, examination of their fluorescence by protonation with appropriate acids, probing of their excimer/exciplex emission and solvatochromic effects arising from solvent disruption of receptor complexes will be reported in Chapter IV.

CHAPTER IV

ANION-DEPENDENT, SWITCHABLE ON-OFF AND OFF-ON FLUORESCENCE EMISSION IN BIS(ANILINOETHYNYL)PYRIDINE DERIVATIVES

Introduction

This chapter was coauthored with Brian Coombs, who provided assistance with synthesis, the fluorescence experiments and valuable mechanistic insight; Dr. Sean McClintock, who performed the DFT calculations in support of experimental evidence; Dr. Charles A. Johnson II, who synthesized the sulfonamide compounds and first reported their fluorescence behavior in his dissertation; Dr. Orion B. Berryman, who provided editorial assistance and my advisors, Profs. Darren W. Johnson and Michael M. Haley, both of whom provided editorial assistance and direction on the final manuscript published in *Chemical Communications* (2011, **47**, 5539-5541, © The Royal Society of Chemistry).

A great deal of effort has been devoted to tailoring photoactive switches on the molecular level for use in applications from biological imaging to molecular logic gates and photodynamic therapy.[1,2] In particular, advances in our understanding of intermolecular luminescence processes have led to elegant multicomponent supramolecular switches and probes with nanomolar sensitivity for anions, which have been the subject of many detailed reviews.[3] Fluorescence as a sensing mechanism is desirable due to its inherent sensitivity and relative ease of measurement with common

laboratory equipment. These sensors are often modulated by pH, with the protonation or deprotonation of incorporated heterocycles as a common fluorescence ON–OFF, or more rarely OFF–ON, switching motif.[4,5] Additionally, the tunable luminescence properties of simple organic photoswitches have led to systems capable of responding to multiple inputs or outputs, which has opened the way to entirely organic logic gates.[5] However, these structures are commonly engineered to exploit a single, distinct fluorescence phenomenon (e.g., polarity dependent emission shifting or PET quenching upon binding a guest) or colorimetric changes as their signaling events, and can thus be limited in the flexibility of their application. Consequently, there persists a need for selective, small-molecule organic systems with discrete, easily tunable negative and positive fluorescent responses. Herein we report the development of a compact fluorescent scaffold easily derivatized to yield switchable ON–OFF and OFF–ON responsive compounds.

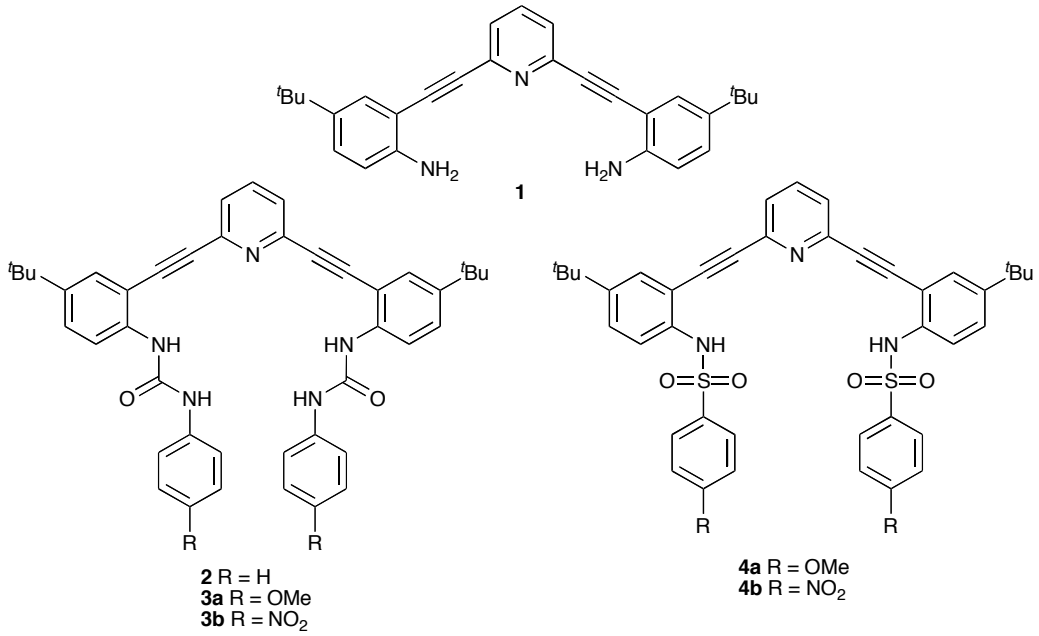

Figure 1. Structures of 2,6-bis(2-anilinoethynyl)pyridine receptor core **1**, urea (**2-3b**) and sulfonamide (**4a,b**) derivatives.

Chapter III reported the synthesis and halide binding studies of the parent phenylurea-substituted receptor **2** (Fig. 1) with a series of tetrabutylammonium halides.[6] During the preparation and characterization of the trifluoroacetic acid (TFA) salts of the protonated receptors, we found that the fluorescence of the arylacetylene core **1** and phenylurea **2** were both quenched upon protonation in $CHCl_3$. This occurred concurrently with a change in the solution from colorless to yellow (Fig. 2). This change in solution color is seen in the UV-visible spectrum as a charge transfer absorbance band from ca. 450–500 nm and is indicative of protonation at the pyridine nitrogen, which has been noted in similar systems.[7]

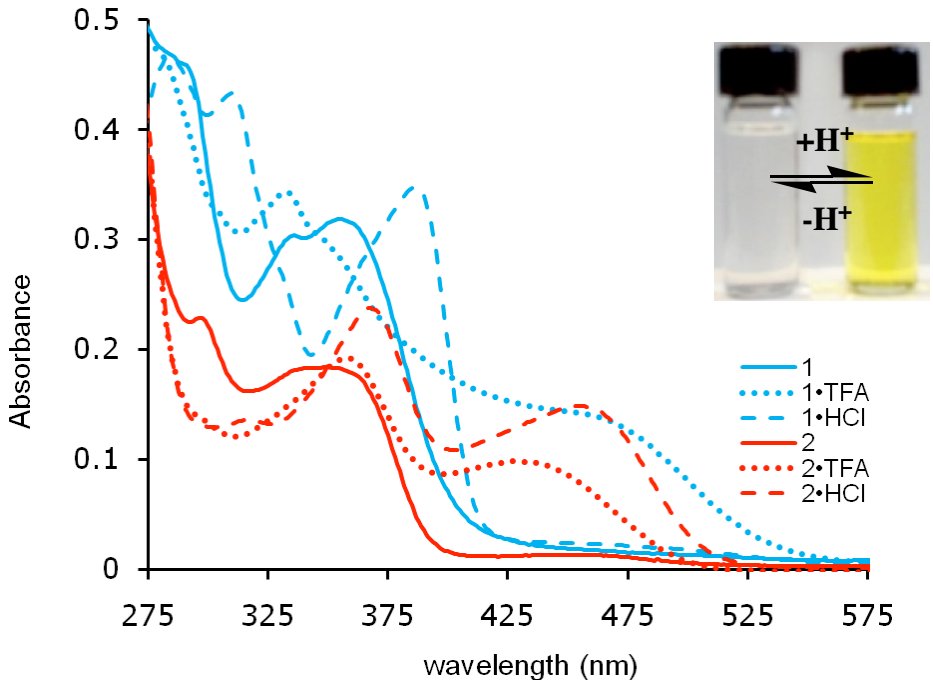

Figure 2. UV-Vis spectra of **1** and **2a** as both protonated and neutral receptors ([H] or [H^+] = 12μM). Inset is a visual depiction of the change in solution colors upon protonation/deprotonation.

Effects of Electronic Modulation on Fluorescence Emission

Due to our interest in fluorescent anion sensors, we have explored how donor/acceptor functionalization could influence the binding strengths and optoelectronic responses of the core dianiline **1**. Consequently, we prepared hydrogen bonding electron-rich and electron-poor ureas **3a,b** and sulfonamides **4a,b** (Fig. 1). We reasoned that electron deficient receptors would possess a higher binding affinity for anionic guests and thus expected changes in fluorescence upon protonation, much like the parent compounds. In electron-rich systems **3a** and **4a**, protonation with TFA gave yellow solutions, and the fluorescence emission was indeed quenched (Fig. 3).

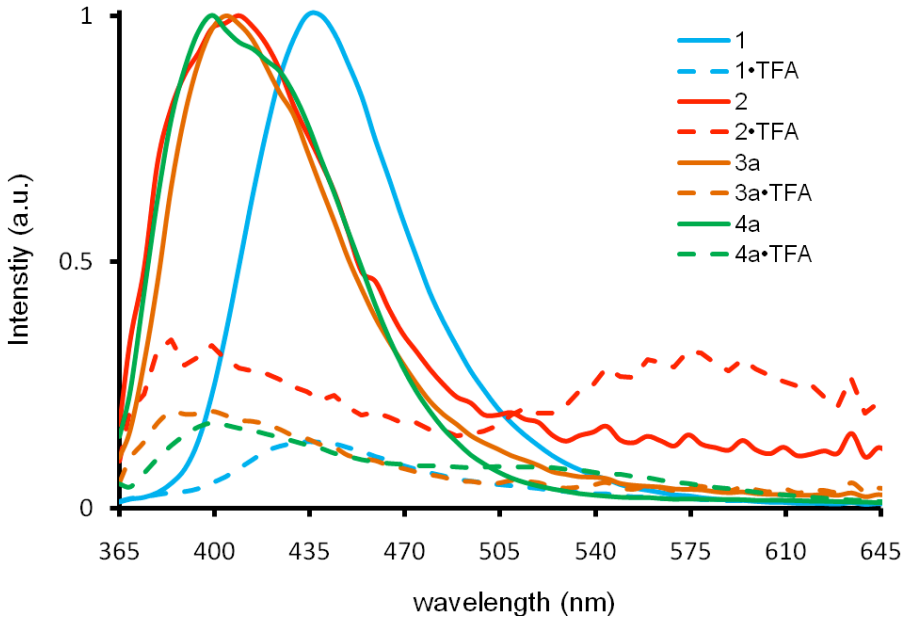

Figure 3. Normalized emission spectra of both the neutral and protonated electron-rich receptors ([H] and [H^+] = 12 µM, excitation **1**: 360 nm; **2, 3a,b:** 343 nm; **4a**: 338 nm).

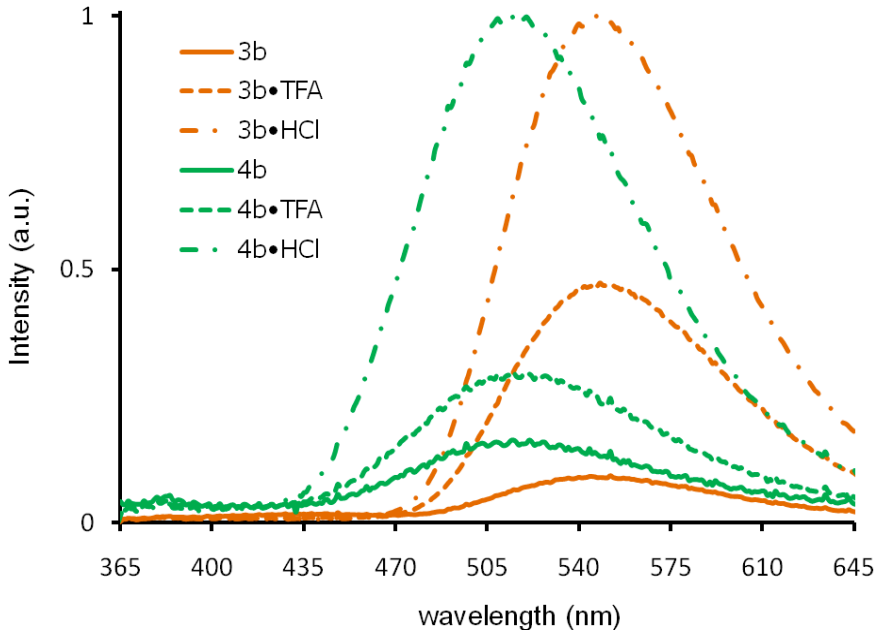

Figure 4. Normalized emission of electron-poor receptors both neutral and protonated with TFA or HCl ([H] and [H^+] = 12 µM, excitation **3b:** 360 nm; **4b**: 365 nm).

In both these and the parent systems, the residual emission peak bathochromically shifted only when Cl^- was present as the counterion (see Appendix C for spectra of **1–3a**, **4a** with Cl^-, as well as UV-visible and excitation spectra). In the case of ureas **2·TFA** and **3a·TFA**, the fluorescence spectra showed a second weak, hypsochromically shifted peak below 400 nm, but this additional feature occurred only when $CF_3CO_2^-$ was present as the counterion.

In contrast to electron-rich **3a** and **4a**, electron-poor analogues **3b** and **4b** were non-fluorescent in the freebase form. Protonation with TFA also resulted in yellow solutions, but significantly increased the fluorescence maxima at ~515–555 nm (Figure 4). To examine the effect of the counterion, receptors **3b and 4b** were then treated with gaseous HCl, as Cl^- is known to bind much more strongly than $CF_3CO_2^-$. The resultant, excimer-like fluorescence (Figure 4, dash-dot lines) occurred at the same wavelength as the residual fluorescence in the quenched **2·TFA**, **2·HCl**, **3a·HCl** and **4a·HCl** receptors. These data were corroborated by the addition of Bu_4NCl to the TFA-protonated receptors, which produced the same emission bands observed upon addition of gaseous HCl to the neutral receptor (i.e., bathochromic shifts in the emission bands).

Figure 5 visually illustrates the very simple trends observed in both the urea and sulfonamide derivatives of **1**: colorless solutions turn yellow upon exposure to acid regardless of the proton source and arene substituent. Electron-donating substituents on the pendant phenyl rings afford compounds that are fluorescent (ON) in the neutral state and quenched (OFF) when protonated. On the other hand, substitution with electron-withdrawing groups furnishes a weakly fluorescent freebase receptor (OFF)

with greatly enhanced fluorescence (ON) and equivalent red shifting in the emission spectra upon exposure to acids with appropriately sized conjugate bases.

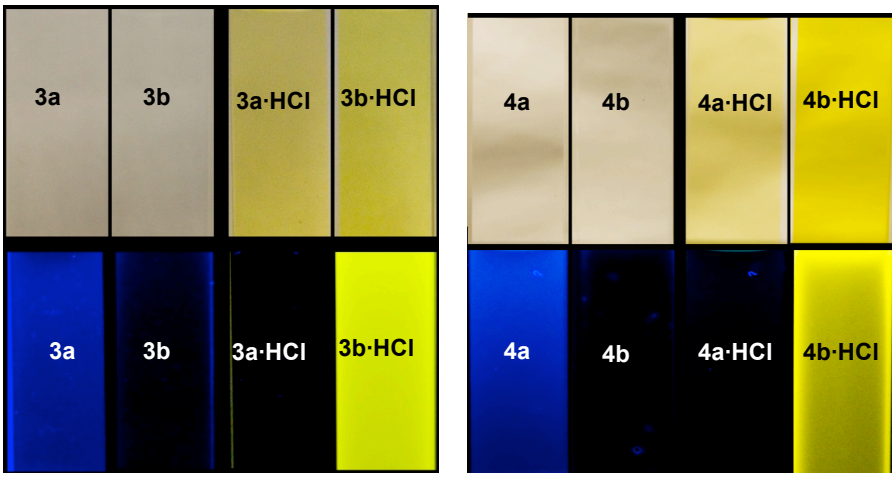

Figure 5. Colorless solutions of neutral compounds in $CHCl_3$ turn yellow upon protonation (top); fluorescence (excitation 365 nm) is quenched in electron-rich systems **3a**, **4a** and "turned on" in electron poor systems **3b**, **4b** (bottom).

	1	**2**	**3a**	**3b**	**4a**	**4b**
Freebase	2.26%	0.3%	8.3%	0.09%	3.04%	0.16%
TFA	1.84%	0.04%	0.05%	2.16%	1.02%	0.36%
HCl	1.65%	0.02%	0.01%	12.6%	0.69%	2.14%

Table 1. Absolute photoluminescent quantum yields of the freebase and protonated receptors obtained with a Horiba-Jobin Yvon integrating sphere in O_2-containing $CHCl_3$.

These trends are also mirrored by the experimentally determined quantum yields in Table 1. For example, receptor **3b** experiences a near full order of magnitude increase in its OFF–ON fluorescence response when Cl^- is the counterion present, even when pre-protonated with TFA.

Calculations. Frontier molecular orbital calculations (B3LYP/6-31G* level of theory) provide insight into the mechanisms behind the behavior of the freebase receptors.[8] Compounds **3a** and **4a** have nearly equivalent lowest-unoccupied molecular orbital (LUMO) maps, while the highest-occupied molecular orbital (HOMO) maps are significantly different, although still overlap with the LUMO on the tri-substituted arene rings (Figure 6). In both, excitation retains electron density near the central alkynyl system, resulting in radiative de-excitation and thus emission. In **3b** and **4b,** however, a charge-transfer fluorescence state is generated, resulting in quenched fluorescence, similar to other known arylacetylene scaffolds.[7] The fluorescence OFF–ON response seems to be intramolecularly excimeric in nature, with this emission having an intriguing dependence on counterion, which warrants further study.

Further Functionalization of Urea Receptors

It could be argued that both the electron-rich and electron-poor sulfonamide and urea derivatives of **1** share the same "OFF-ON" and "ON-OFF" behavior only because of the nature of the functional group used and not the overall electron-rich/poor nature of the receptor (i.e., both classes of receptor have only either the methoxy or nitro functional group). In order to expand upon this trend, receptors **3c-e** were synthesized (Scheme 1).

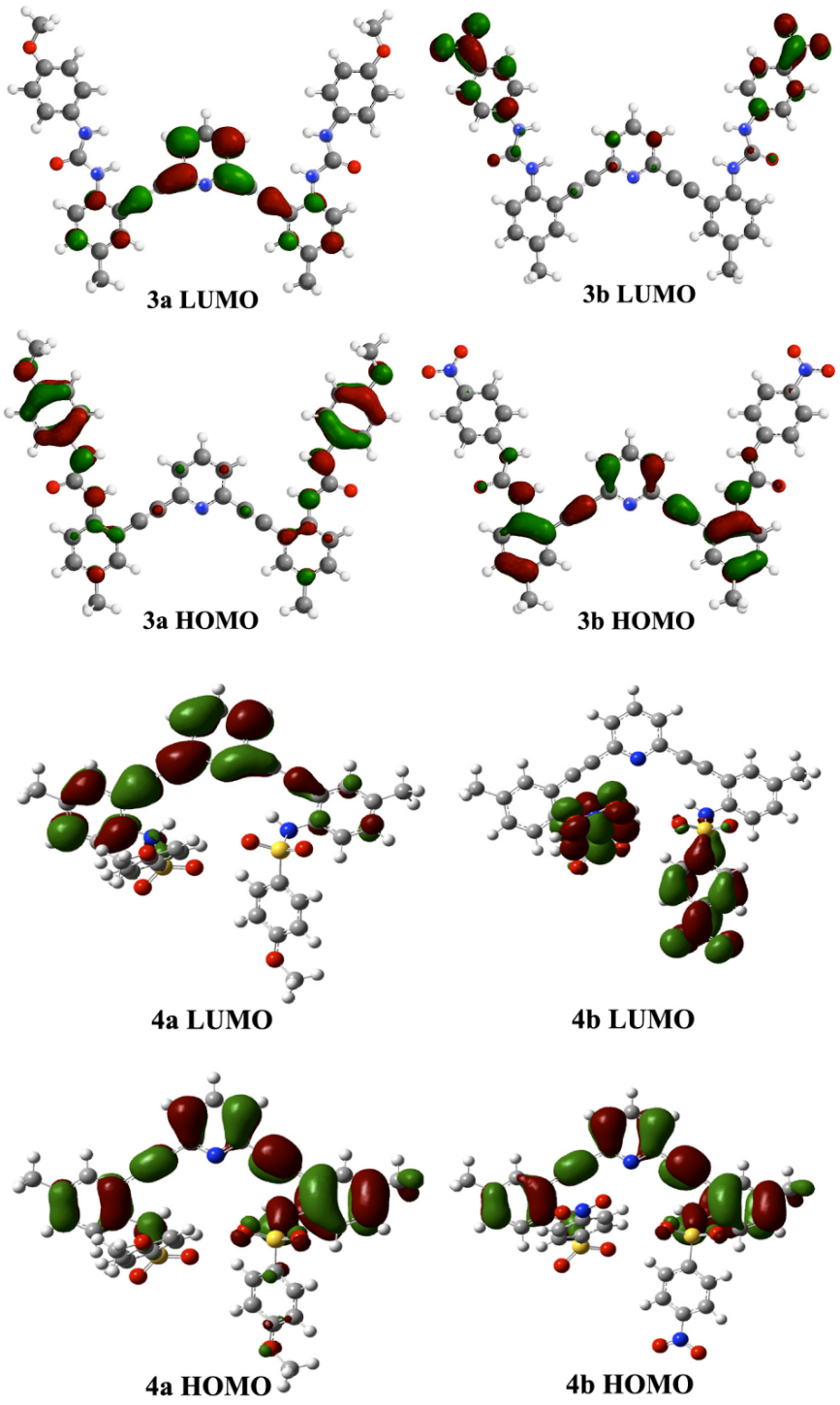

Figure 6. Calculated frontier molecular orbitals for neutral ureas **3a,b** and sulfonamides **4a,b**. Non-overlapping HOMO and LUMO orbitals in the electron-acceptor substituted systems results in charge transfer quenching of the neutral receptors.

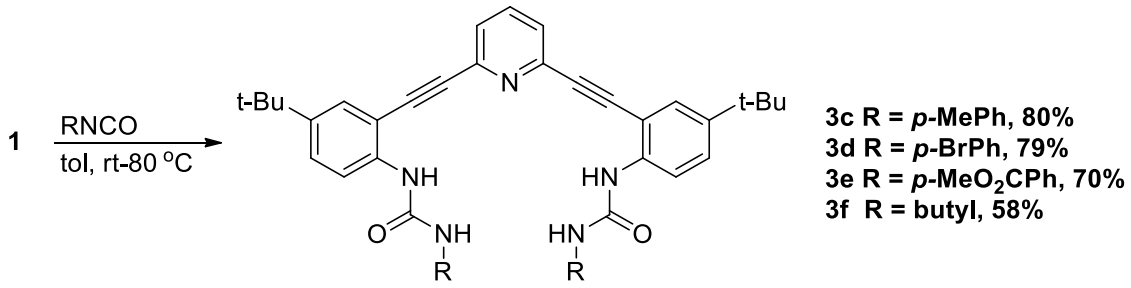

Scheme 1. Synthesis of additional electron-rich and electron-poor receptors.

Investigation of the fluorescence emission dependence upon protonation state in these receptors revealed the expected trend in behavior: regardless of the functional group, electron—rich arenes appended to the urea-substituted scaffold yielded "ON-OFF" responsive receptors while electron-poor arenes were "OFF-ON" responsive (Figure 7).

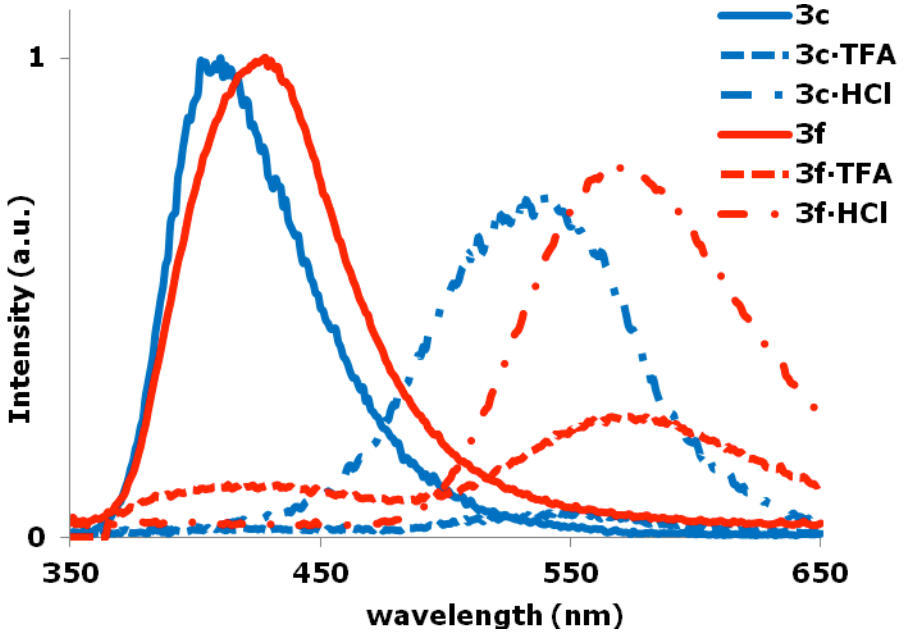

Figure 7. Normalized mission of electron-rich receptor **3c** and its TFA and HCl salts along with the alkylated receptor **3f** and its TFA and HCl salts ([H] and [H^+] = 21 µM, ex = 363 nm).

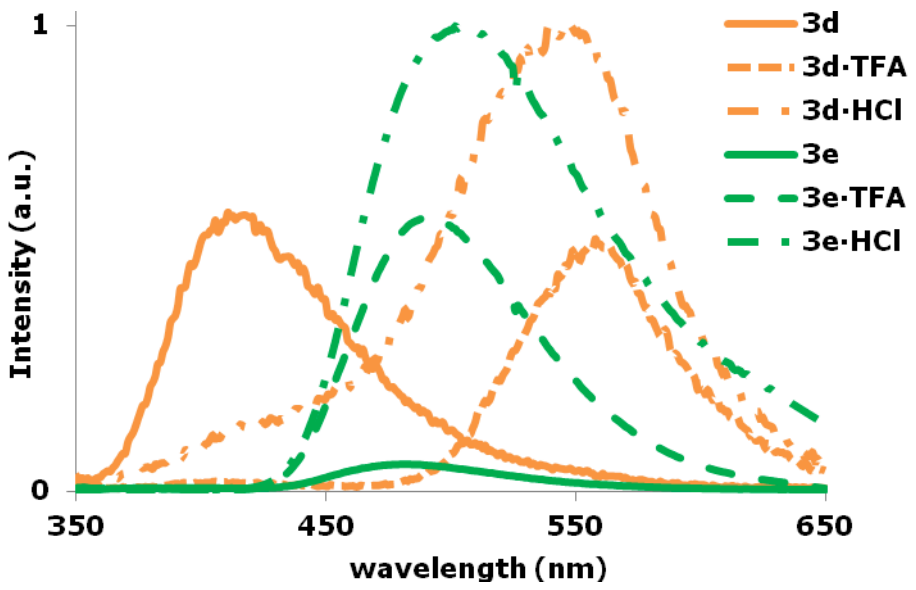

Figure 8. Normalized emission spectra of electron-poor analogs (conditions equivalent to those in Figure 7).

The data presented in Figures 7 and 8 are in good agreement with the observed trend in receptors **3a,b** and **4a,b** with the exception of the magnitude of the quenching event in receptors **3c** and **3f**. In the case of **3c** this can be attributed to very inefficient fluorescence emission in the neutral state, thus upon protonation with either acid the emission intensity changes very little from that of the neutral compound. For **3f**, however, the emission is very intense for **3f** and **3f·HCl**, but significantly quenched in **3f·TFA**. This "ON-OFF-ON" response is promising for the application of this type of receptor to pH-independent sensor applications as it could function as an OFF-ON or ON-OFF sensor across the pH scale. Additionally, it can be seen that all of the receptors experience an increase in intensity when the counterion is Cl^- instead of

trifluoroacetate. This observation raised questions about the mechanisms of both the "ON-OFF" and "OFF-ON" events, and how a full mechanistic understanding could be exploited to increase the Cl^- selectivity.

Mechanistic Investigation of the "OFF-ON" Response

In the majority of pyridine-containing fluorophores, the non-bonding lone-pair located at the pyridine nitrogen offers a low energy n-π* absorbance pathway to the excited state that can be disallowed by protonation of the pyridine.[9] This low-lying n-π* absorbance is characterized by low molar absorptivities, and has the ultimate effect of lowering the fluorescence quantum yield in fluorophores of this type.[9a] Hydrogen bonding to the lone pairs or protonation of the pyridine removes the contribution of the non-bonding electrons of pyridine to the molecular absorbance, and can result in an inversion of the n-π* and π-π* transitions which in general leads to an increase in photoluminescent quantum yield. However, pyridinium groups (either H-protonated or methylated) have the additional effect of being strong fluorescence quenchers due to their highly electron-accepting nature.[10] Intriguingly, pyridinium dimers have been known to exhibit excimeric fluorescence through intermolecular or tethered intramolecular interactions in restricted environments, i.e. solid matrices or covalent polymers.[11]

In many imaging applications, the "OFF-ON" response is desirable due to the low background fluorescence and the inherent increase in resolution when observing the appearance of signal rather than the disappearance.[4] Of importance in this type of

system is the quenching mechanism that dictates the "OFF" phase of a sensor's response, and critical to these quenching events is the possibility of inter- versus intramolecular interactions. Unlike intramolecular charge transfer emission, intermolecular excimeric emission is a diffusion limited process.[9,11] If there is no intermolecular interaction during the lifetime of the excited state, then no emission occurs. In non-excimeric fluorescence, the change in emission must come from interaction with the target analyte and result in changes to the charge transfer or electron transfer processes along the fluorophore's conjugation length, in our case the phenylethynyl core. The absolute concentration of the probe would have only a single effect on the fluorescence output of sensors of this type: affecting the intensity of the sensor emission linearly with concentration.

On the other hand, excimeric fluorescence only arises when the receptor is at a local concentration high enough to undergo excited-state intermolecular interactions, and the concentration of the receptor and its excited-state lifetime then become the dominant considerations in determining emissivity. Both of these factors have direct implications on whether or not the fluorionophore would function as an effective probe; especially large are the implications for *in vitro* or *in vivo* probe design as it is difficult to control quantitatively the concentration of a probe within cellular compartments. Due to the differences in the function of sensors designed upon each of these two types of emission pathway, it became critical for us to ascertain the mechanism of the fluorescence emission event in our receptors in order to intelligently manipulate sensor design.

Our approach was to determine the ground-state association of **3a** and **3b** in solution, which would allow for determination of monomer or oligomer-dependent emission. These data could then be related to the solvatochromic behavior of the receptors, with an eye toward modulation of the receptor design in order to increase quantum efficiency and sensitivity in biologically relevant media.

Self-association in Ureas. The following analysis was carried out primarily on compounds **3a** and **3b**, as they exhibit the greatest responses to anion-induced fluorescence switching. As shown earlier in this chapter, neutral **3a** was found to form [4 + 4] tetrameric stacks of mirror-image dimers. In order to probe the solution behavior of this receptor dilution experiments, ROESY-NMR, DOSY-NMR and mass spectroscopy experiments were undertaken, in all cases using water-saturated solvents in order to limit the number of variables between samples.

Methoxyphenylurea 3a. Attempts to determine dimerization constants from ^{1}H-NMR experiments starting at the limit of solubility of **3a** in $CDCl_3$ were unsuccessful. While small upfield shifts were observed in the spectra during dilution, the low concentrations achieved before the spectra stopped shifting exceeded the sensitivity limits of the instrument (see Appendix C). Dilution experiments by UV-Vis also yielded inconclusive results, making it possible that **3a** was either not self-associating or associating extremely tightly in solution.

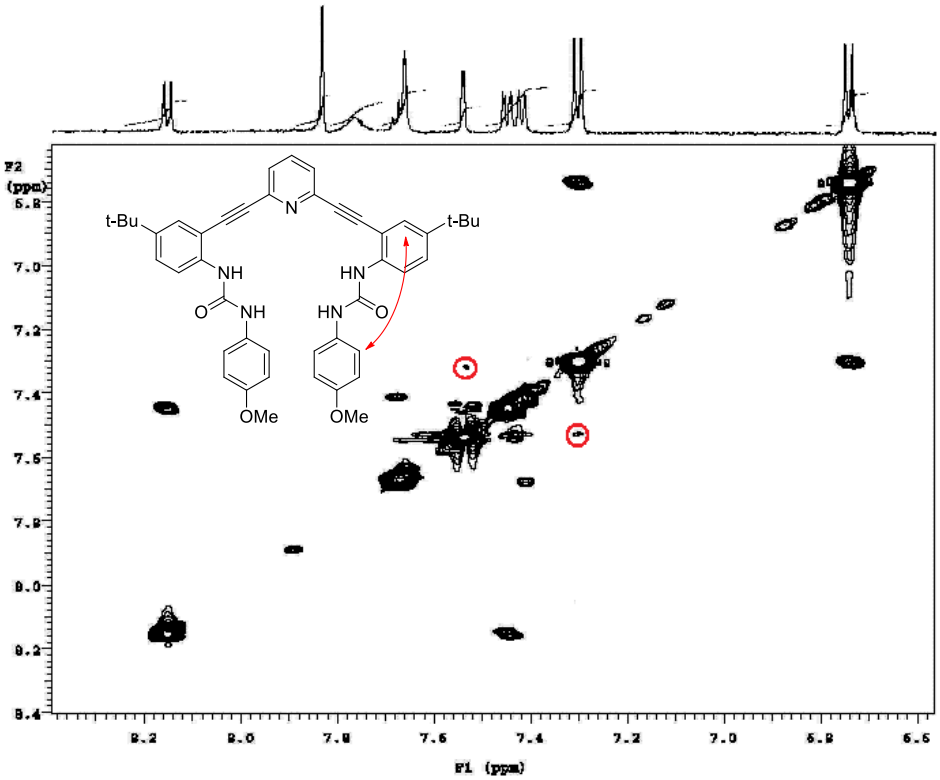

Figure 9. ^{1}H-NMR projection and 2-D ROESY spectrum of **3a** at 3.4 mM, showing the apparently weak NOE that indicated self-association in solution (see Appendix C for additional spectra and assignments).

In place of simple dilution investigations ROESY-NMR and DOSY-NMR experiments were performed. Spectra from ROESY experiments with **3a** in dry CD_2Cl_2 at 3.4 mM concentration showed a small, unexpected NOE between protons on the pendant methoxyphenyl group and the proton between the t-butyl and ethynyl groups which was indicative of self-association in solution (Figure 9). Examination of the crystal structure of **3a** showed the closest contacts to come at the "elbows" of the receptor, where intramolecular NOE could mask the signal arising from additional intermolecular contacts, making this signal the only clue as to whether or not **3a** was a dimer at these

concentrations. Further ROESY data was gathered in water-saturated solvent, and the weak intermolecular NOE was no longer observable (Appendix C).

DOSY-NMR experiments proved much more enlightening (Figure 10). Correlation of the relative diffusivity of the receptor to an internal standard by pulsed field gradient NMR spectrometry allowed the molecular mass in solution to be calculated.[12] Spectra collected on 2.3 mM solutions at 25 ^{o}C of **3a** in water saturated $CDCl_3$ yielded a diffusion coefficient of 5.66 x 10^{-5} cm^2s^{-1}, which corresponds to a molecular mass in solution of 722.06 ± 2.20 g/mol, equivalent to the molecular mass of **3a** within 0.31% error (relative to TMS).

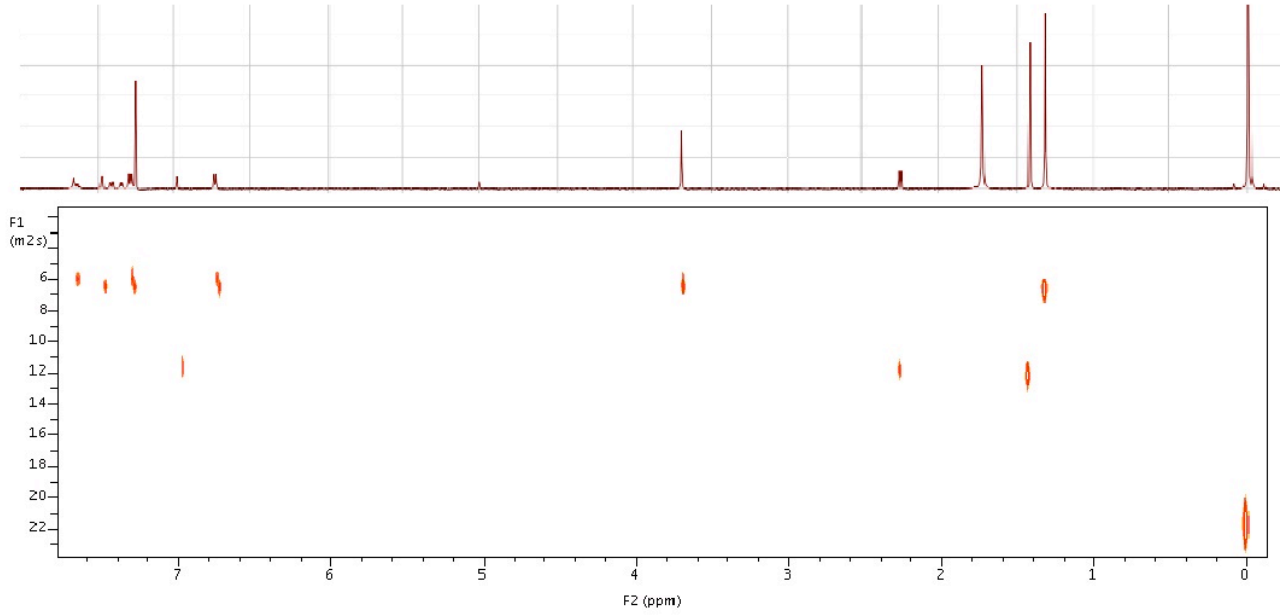

Figure 10. 2D-DOSY spectrum of **3a** showing the average diffusion coefficient used to calculate the molecular mass relative to the internal standard (TMS).

Protonation by introduction of a slight excess of TFA to the same DOSY sample from above resulted in a diffusion coefficient of 5.23 x 10^{-5} cm^2s^{-1}, equivalent to a molecular mass in solution of 895.40 ± 62.06 g/mol, quite close to the mass of **3a·TFA** (833.34 g/mol).

These data were corroborated by ESI-MS experiments on dilute solutions of **3a·TFA** in hexanes**.** Even in the gas-phase, very little dimerization is evident from the spectra, although a mass peak which could be attributed to a singly charged dimer is present at low abundance.

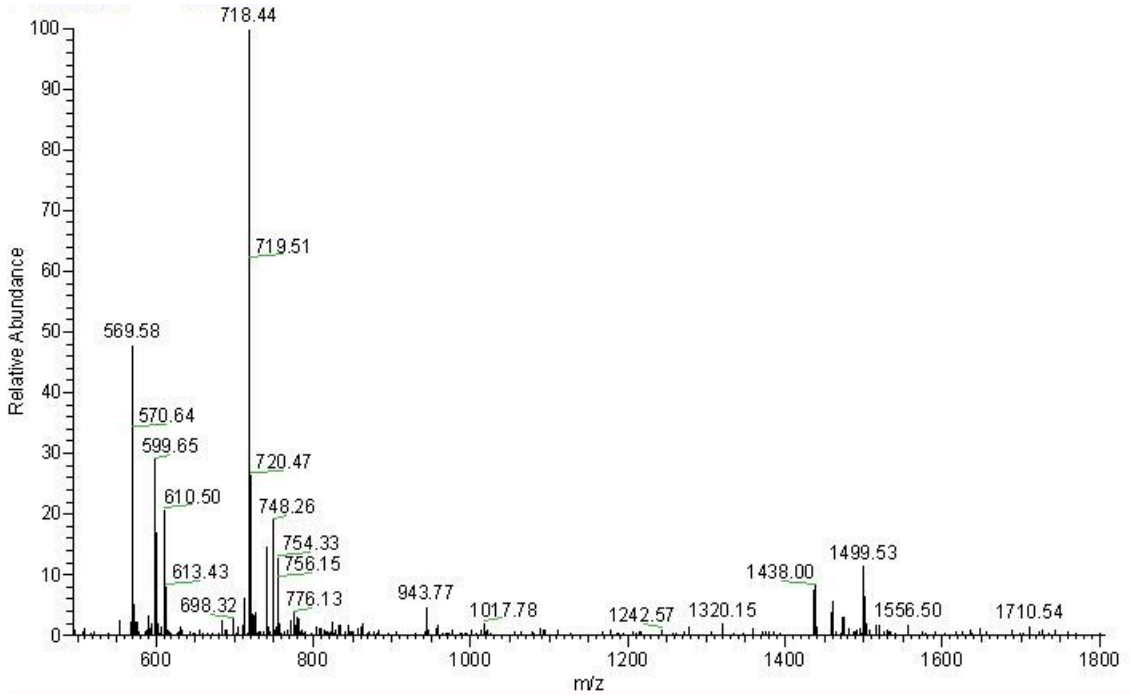

Figure 11. ESI-MS spectrum of **3a·TFA** from hexanes (neg, M^-: 718.44, $C_{45}H_{45}N_5O_4$: 719.87 g/mol). See Appendix C for positive mode spectrum.

Nitrophenylurea 3b. The nitro-substituted receptor **3b** was subjected to the same analysis in order to compare its solution-state aggregation behavior to **3a.** As in the methoxyurea receptor **3a**, dilution experiments seemed to indicate monomer in solution, as no significant shifting of ^{1}H-NMR peaks was observed. ROESY spectra of **3b** exhibited only NOE cross peaks that could be attributed to intramolecular interactions in the neutral form (Appendix C).

Solid-state evidence of monomeric **3b** supported the solution data. Crystals of **3b** grown from MeOH/DMSO were found in the single "U" shape found for protonated **3a,** cocrystallized with one solvent molecule of each type sharing the cavity (Figure 12, Appendix C).

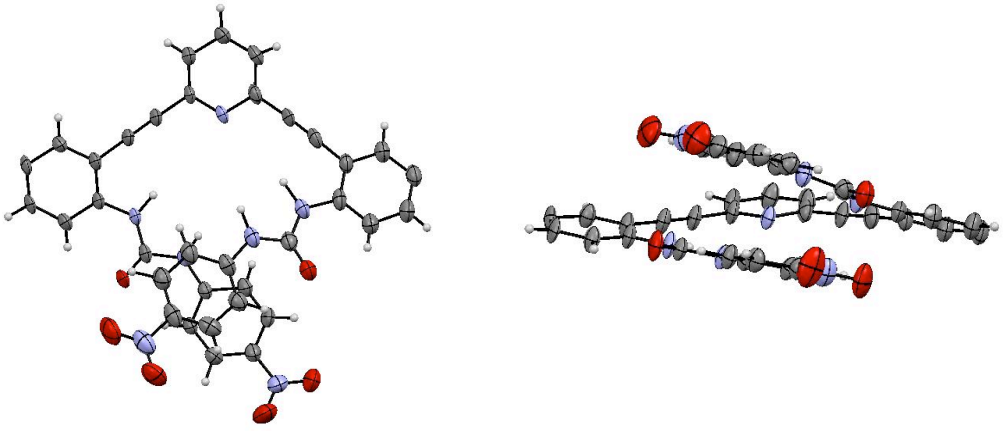

Figure 12. ORTEP representations of **3b** (thermal ellipsoids at 50% probability level, *t*-butyl groups and solvent removed for clarity). Crystal data can be found in Appendix C.

In addition, DOSY spectra of **3b** in $CDCl_3$ clearly indicated monomeric **3b** in solution as the freebase. The diffusion coefficient for this receptor was 5.23 x 10^{-5} cm^2s^{-1}

which produces a molecular mass in solution of 810.44 ± 60.63 g/mol, equivalent to the monomer in solution within error (Appendix C).

Protonation of this receptor with TFA in $CDCl_3$ yielded DOSY spectra that were broad and contained multiple species within single peaks. The mean diffusion coefficient under these conditions could not be calculated with any confidence, but does indicate complex speciation in solution.

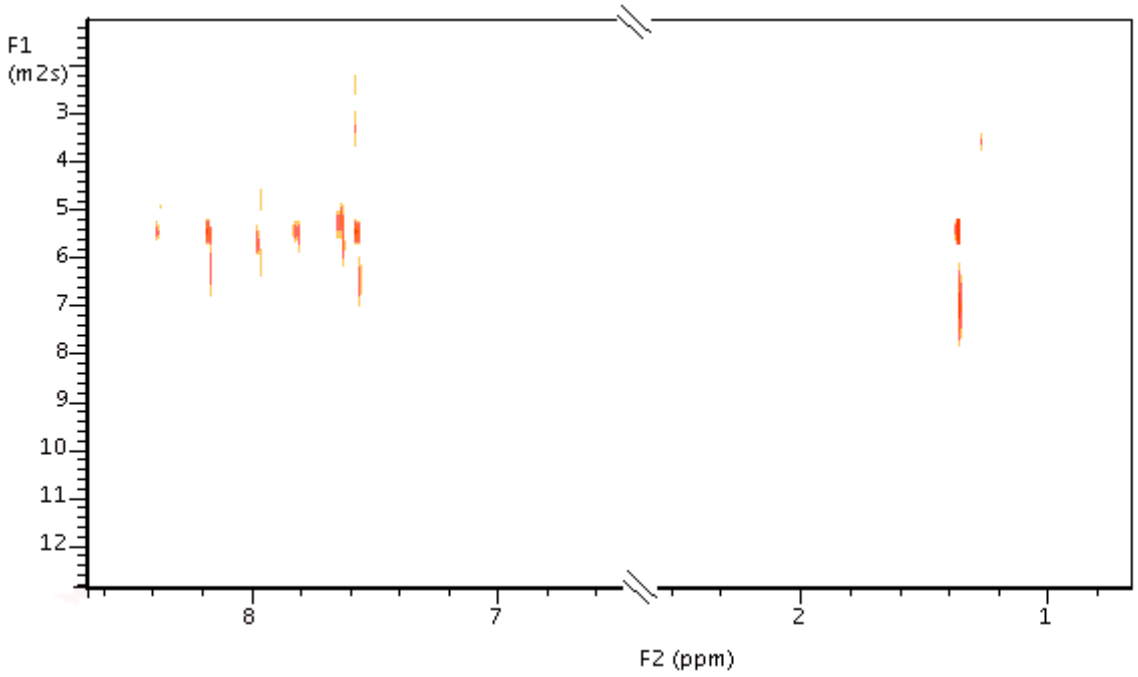

Figure 13. Representative 2D-DOSY spectrum of **3b·TFA** in $CDCl_3$ illustrating the broad, ill-defined diffusion coefficients and speciation in solution.

During initial anion binding studies, ^{1}H-NMR titration data for this receptor had also proven difficult due to a broadening of the signals in the middle of the titration, which we attributed to aggregation in solution (Appendix C). Additionally, ESI-MS

spectra of the protonated receptor in dilute hexanes seemed to indicate dimeric **3b** is present, although the mass peak at 1479.39 *m/z* did not match the expected dimer mass of 1498.59 *m/z*. However, this peak position and its isotopic pattern do correspond to 2[**3b]·Cl⁻,** a dimer around Cl^- that displaced the TFA^- counterion.

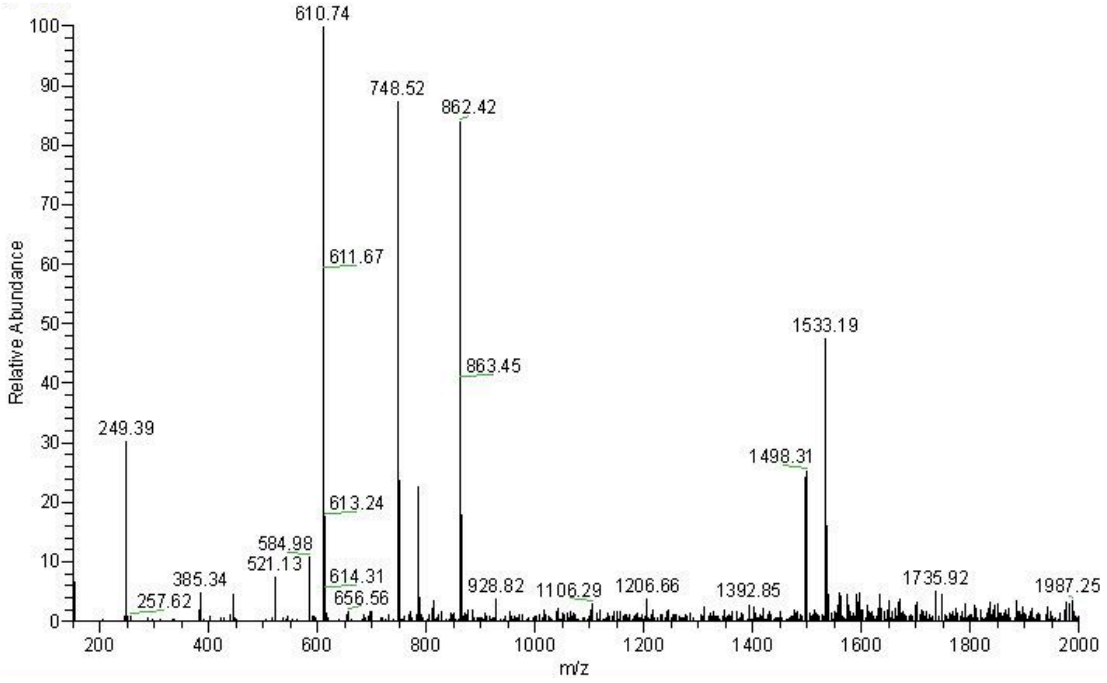

Figure 14. ESI-MS spectrum of **3b·TFA** from hexanes (M^-, 748.52, $C_{43}H_{39}N_7O_6$: 749.81 g/mol; $M{\cdot}TFA^-$: 862.42, $C_{45}H_{39}N_7O_8F_3$: 862.83 g/mol; $M_2{\cdot}Cl^-$, 1533.19, $C_{86}H_{78}N_{14}O_{12}Cl$: 1533.56 g/mol).

Summary. From the above data it is apparent that **3a** weakly self-associates in solution above low millimolar concentration. On the other hand, **3b** exists solely as a monomer in solution and the solid state. Protonation of **3a** does not drastically alter the behavior of this compound in solution and the data for **3a·TFA** corroborate the solid-state

evidence of monomeric species forming. Although there is extremely weak association in the absence of competing guests, mass spectroscopy evidence suggests this is a disfavored occurrence. For electron-withdrawn **3b**, however, protonation with TFA indicates ground-state association of this receptor in solution. Water saturated solvents were used for these experiments in order to both standardize the conditions for each measurement and to more closely mimic the intended aqueous or protic environments found in relevant applications.

	3a	**3b**	**3a·TFA**	**3b·TFA**
Crystal data	Y	N	N	N/A
NMR data	Y	N	N	Y
Mass spec data	Y	N	Y (weak)	Y

Table 2. Evidence of self-association ("Y") or no evidence of self-association ("N") in urea **3a** and **3b.**

Fluorescence Experiments. Knowing the ground-state association of receptors **3a** and **3b** allowed us to elucidate the mechanism of the fluorescence in both systems. The majority of these experiments focused on the origins of the "OFF-ON" response of **3b,** as this result was the most surprising. This section will therefore focus on our efforts to understand the underlying principles governing the response of this receptor.

Methoxyphenylurea 3a. The fluorescence behavior of **3a** was expected due to the observance of this "OFF-ON" phenomenon by a multitude of research groups, although a true mechanism for the quenching of monomeric arylethynyl pyridines has yet to be postulated in the literature.

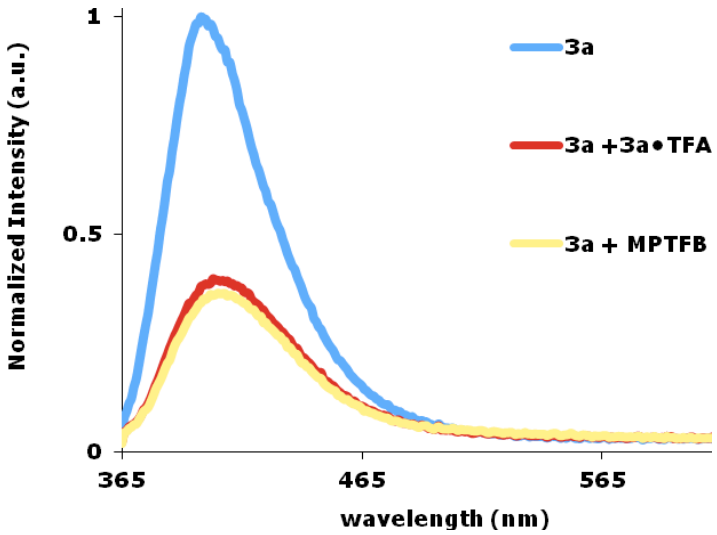

Figure 15. Fluorescence emission of **3a** (16.9 μM, $CHCl_3$) as the freebase, in the presence of 1 equiv of **TFA-**protonated **3a**, and 1 equivalent of *N*-methylpyridinium tetrafluoroborate.

Figure 15 illustrates this phenomenon in our system. Freebase **3a** in $CHCl_3$ fluoresced normally. Upon the addition of 1 equivalent of a concentrated solution of **3a·TFA** such that the overall concentration of **3a** remained constant, the emission was drastically quenched. Repeating this experiment with a concentrated solution of *N*-methylpyridinium tetrafluoroborate with a slight excess of triethylamine resulted in the same quenching, indicating the excited state electron transfer to pyridinium and subsequent quenching of fluorescence is unrelated to the protonation state of the pyridine in **3a.** These data, in tandem with the aforementioned calculations and the literature precedent, served to convince us of the relatively simple fluorescence behavior of this receptor.

Nitrophenylurea 3b. Due to the non-emissive behavior of neutral **3b** which can be understood through examination of the FMO maps presented above, this section will focus on **3b·TFA** and its fluorescent responses.

The evidence of self-association in solutions of **3b·TFA** and the featureless, bathochromically shifted emission both point toward excimer emission. If ground-state association was giving rise to this excimer-like emission, then destabilization of the complex should disfavor emission and decrease the intensity. To probe this, a solution of **3b·TFA** in $CHCl_3$ was systematically solvent switched to MeCN while maintaining a constant receptor concentration.

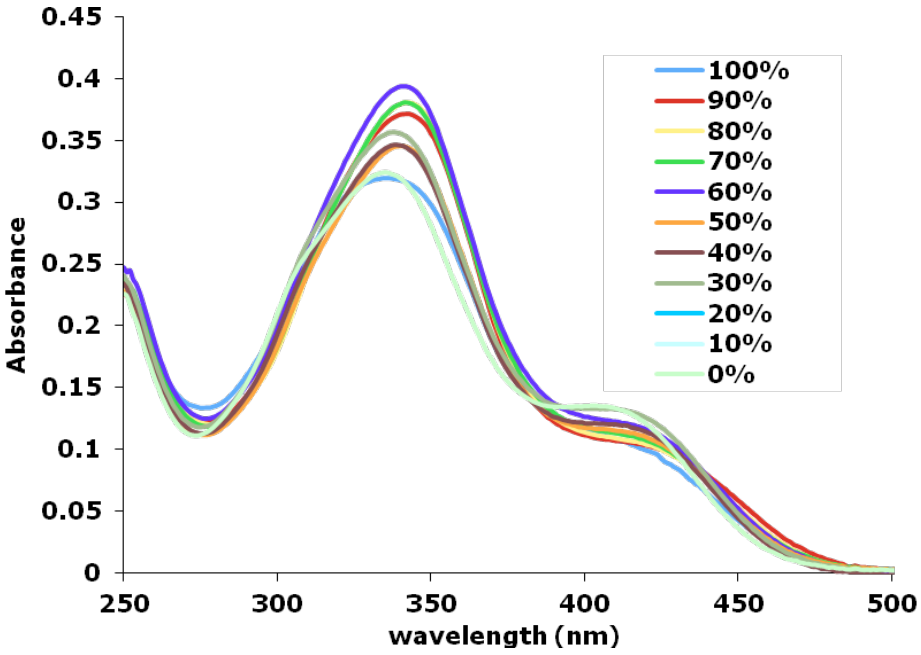

Figure 16. UV-Vis absorbance spectra for the switching of **3b·TFA** in 100% $CHCl_3$ to 0% $CHCl_3$ in MeCN at 7.1 µM.

While the charge transfer band attributable to the formation of the pyridinium-trifluoroacetate salt is still apparent, the shape of the overlapping π-π* and n-π* absorbance bands changes slightly from $CHCl_3$ to MeCN (Figure 16). This separation of the bands by hypsochromically shifting the n-π* absorbance is characteristic of a decrease in electronic density on the pyridine nitrogen. This decrease coupled with the intensification of the charge transfer band absorbance at 405 nm is indicative of a closer contact ion pair in MeCN than $CHCl_3$, which could be attributed to greater localization of the charge upon disruption of the aggregated receptor when switching from $CHCl_3$ to MeCN.

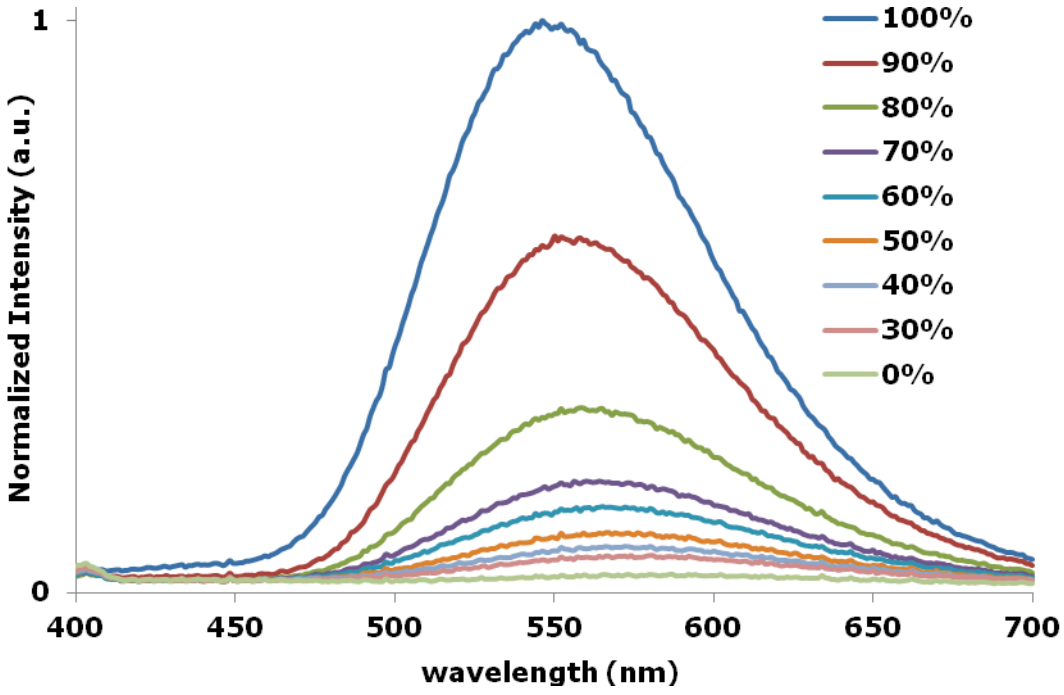

Figure 17. Fluroescence emission spectra of the 7.1 µM solutions of **3b·TFA** from Figure 16 upon solvent switching from 100% $CHCl_3$ to 0% $CHCl_3$ in MeCN.

Upon increasing the MeCN/$CHCl_3$ ratio of the samples, the fluorescence emission is drastically reduced and red-shifted (Figure 17). In fact, by 30% $CHCl_3$ in MeCN the emission is equivalent to the unprotonated receptor in 100% $CHCl_3$ solution. From these data it can be concluded that **3b·TFA** radiatively decays only through excimer interaction with other receptor molecules in solution, which is supported by the bathochromic shift in the emission as de-excitation is in competition with dissociation of the complex in polar media.

Fluorescence lifetimes. An additional piece of evidence for excimer formation can be found in excited state lifetime measurements. Excimeric fluorescence in solution is restricted to short lifetimes, as it is in competition with relaxation by non-radiative intersystem crossing which typically occurs on the order of 10^{-7} to 10^{-9} seconds. This is usually observed as a polyexponential decay due to concomitant fluorescence emission from both monomeric and excimeric species.[13]

Time-correlated single photon counting spectroscopy allows for the measurement of changes in fluorescence emission down to picoseconds time frames without the need for reference compounds. Solutions of **3f**, **3f·HCl** and **3b·HCl** at 8μM were measured using a 360 nm laser diode light source in $CHCl_3$ versus a scattering solution of 15 μM Ludox (Figures 18 and 19). Receptor **3f** was chosen for comparison due to its strong emission at both the longer and shorter wavelengths observed thus far (Figure 7), and HCl was chosen as the proton source due to the increased fluorescence versus protonation with TFA.

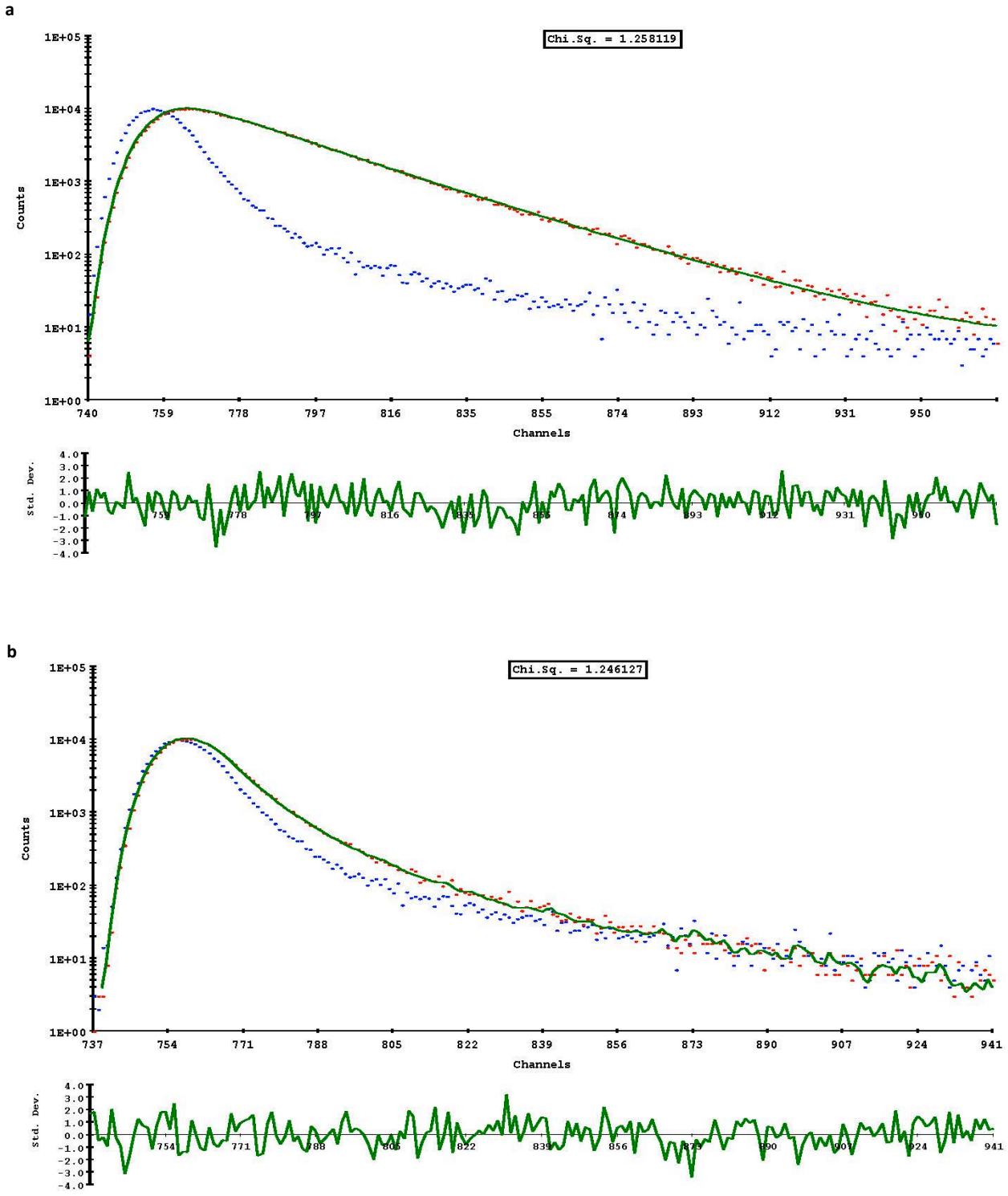

Figure 18. TCSPC fitting of decay data for (a) **3f** in $CHCl_3$ and (b) **3f·HCl** at 8μM ($chi^2 < 2$). The biexponential decay (green line) was fit relative to instrument response (blue scatter plot). Residuals are plotted at bottom of each.

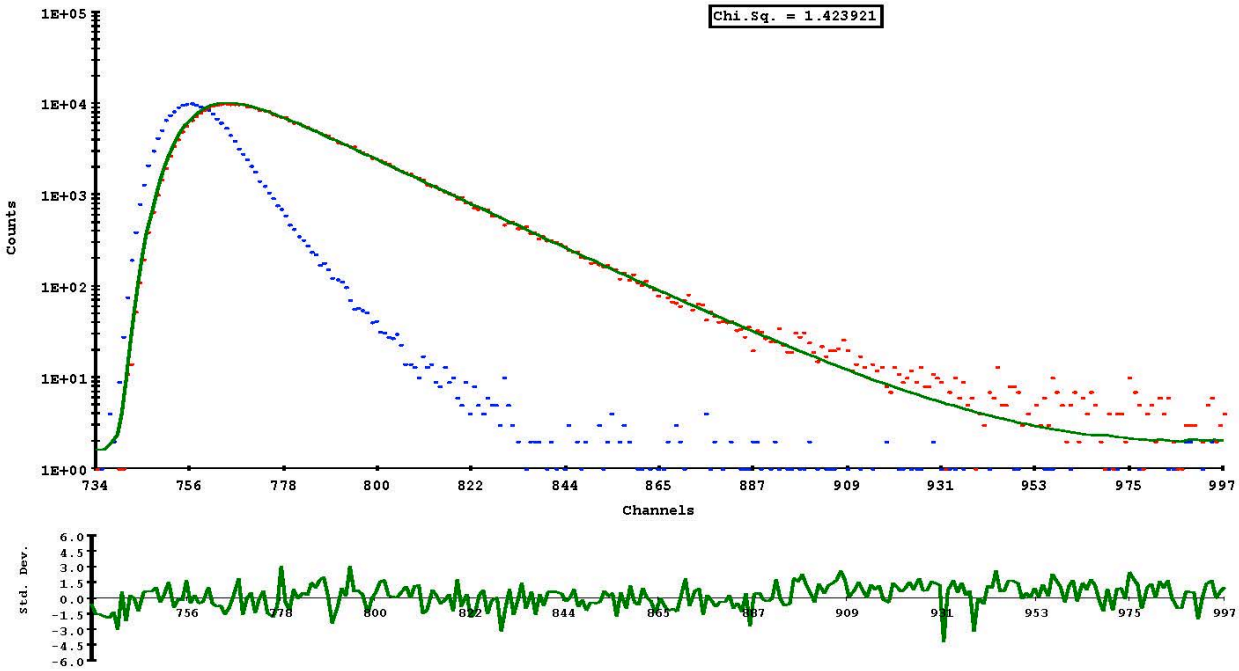

Figure 19. TCSPC fitting of decay data for **3b·HCl** in $CHCl_3$ at 8μM ($chi^2 > 2$). The biexponential decay (green line) was fit relative to instrument response (blue scatter plot). Residuals are plotted at bottom.

From the slope of the fitted curves in Figures 19 and 20 it is apparent that protonation of **3f** significantly shortens the lifetime of the excited state (Table 3).

	3f	**3f·HCl**	**3b·HCl**
Lifetime 1 (ns, ratio)	1.065 ns (82%)	0.121 ns (93%)	0.952 ns (68%)
Lifetime 2 (ns, ratio)	1.707 ns (18%)	0.693 ns (3%)	1.218 ns (32%)

Table 3. Biexponential fitting data for **3f**, **3f·HCl** and **3b·HCl.** The ratios of each lifetime are representative of the relative percent of the population of fluorescing species in solution.

The lifetime data are strong evidence of an excimeric mechanism for the OFF-ON fluorescence response observed in these compounds. In all cases the biexponential fit

can be correlated to the most intense fluorescence band as well as the residual emission band observed in these solutions, and the relative ratio of each correlates well with the relative intensity observed. The lifetimes observed for **3f** are not quite long enough that an excimeric mechanism can be ruled out in the neutral state, but the protonated species in both cases definitively exhibit the short lifetimes characteristic of excimeric fluorescence.

Conclusion

In conclusion, we have disclosed the development of a receptor scaffold with switchable "ON-OFF" or "OFF-ON" fluorescence based upon judicious choice of the pendant phenyl functionalities. While the behavior of ON-OFF responsive receptors was not surprising, the origins of the OFF-ON response of **3b** and its analogs required comparison of fluorescent lifetimes, self-association and stability data in order to determine the origins of this behavior. Remarkably, these results indicate that this class of receptors can function as a positive response (OFF-ON) fluorescent indicator for chloride ion, although it seems to be limited to applications in nonpolar media. Additionally, the occurrence of both a colorimetric and switchable fluorescent ON-OFF or OFF-ON response in a single class of compounds is promising for application in molecular logic systems, where they could conceivably function as complex gates, e.g., INHIBIT or enabled OR operators. Our mechanistic understanding of the process governing the positive OFF-ON response of these receptors should allow for the rational

design of improved receptors capable of exhibiting this response in competitive media for a variety of anionic targets.

Experimental

General Details. ^{1}H and ^{13}C NMR spectra were obtained on a Varian 300 MHz spectrometer (^{1}H 299.95 Hz, ^{13}C 75.43 Hz) or Inova 500 MHz spectrometer (^{1}H 500.10 MHz, ^{13}C 125.75 MHz) or Varian Inova 600 (^{1}H 599.98 MHz, ^{13}C 150.86 MHz) spectrometer. Chemical shifts (∂) are expressed in ppm downfield from tetramethylsilane (TMS) using non-deuterated solvent present in the bulk deuterated solvent ($CDCl_3$: ^{1}H 7.26 ppm, ^{13}C 77.0 ppm; CD_2Cl_2: ^{1}H 5.32 ppm ^{13}C 54.0 ppm). Unless otherwise specified, solvents were obtained from distillation using published literature procedures directly before use.

Mass spectra were acquired on a Thermo Finnigan LCQ Deca XP Plus electrospray ionization spectrometer in positive mode in MeOH solvent.

UV-Vis spectra were acquired with a Hewlett-Packard 8453 UV-Visible spectrophotometer equipped with a 250 nm cutoff filter.

Fluorescence data was acquired with a Horiba Jobin-Yvon FluoroMax-4 fluorescence spectrophotometer equipped with an integrating sphere. All spectra were uncorrected for lamp response unless otherwise specified. Absolute photoluminescence quantum yields were taken in O_2- containing (no inert gas purging) $CHCl_3$. All slit widths (ex/em) were held constant at 5 nm/5 nm, and

quantifiable data was obtained by correction of the spectra to lamp response and integrating sphere reflectivity.

Experimental conditions for fluorescence measurements, excitation spectra, supporting mass spectral and ^{1}H-NMR data can be found in Appendix C.

Methoxyphenyl urea 3a. Dianiline **1** (100 mg, 0.238 mmol) was reacted in a flame dried, 15 ml round-bottomed flask with *p*-methoxyphenyl isocyanate (88.6 mg, 0.594 mmol) in 5 mL freshly distilled toluene. The crude reaction was diluted with pentane, filtered through a sintered glass funnel and the crude solid collected. Trituration with chloroform yields **3a** as an off-white solid (160 mg, 93.4%). Recrystallization by diffusion (pentane/chloroform) yields colorless crystals. Mp: 178-180 ^{o}C. ^{1}H NMR (300 MHz, DMSO-d_6): ð 9.37 (br s, 2H), 8.32 (br s, 2H), 8.12 (d, *J* = 9 Hz, 2H), 8.10 (t, *J* = 7.8 Hz, 1H), 7.91 (d, *J* = 7.8 Hz, 2 H), 7.63 (d, *J* = 2.1 Hz, 2H), 7.57 (dd, *J* = 6.3, 2.1 Hz, 2H), 7.47 (d, *J* = 8.7 Hz, 4H), 6.97 (d, *J* = 8.7 Hz, 4H), 3.82 (s, 6H), 1.40 (s, 18 H). ^{13}C NMR (300 MHz, DMSO-d_6): ð 151.08, 148.83, 140.99, 139.29, 134.93, 133.90, 128.88, 125.49, 124.07. 123.73, 116.63, 116.35, 110.51, 106.44, 89.93, 82.33, 51.61, 30.41, 27.43. MS (ESI pos) *m/z* (%): 744.8 (M+Na^+ +2, 10) 743.8 (M+Na^+ +1, 40), 742.7 (M+Na^+, 100), 741.1 (10), 740.1 (8); $C_{45}H_{45}N_5O_4$ (719.35), $C_{45}H_{45}N_5O_4Na$ (742.34).

Nitrophenyl urea 3b. Dianiline **1** (100 mg, 0.238 mmol) was reacted in a flame dried, 15 ml round-bottomed flask with *p*-nitrophenyl isocyanate (97.5 mg, 0.594 mmol) in 5 mL freshly distilled toluene. The crude reaction was diluted with pentane, filtered through a sintered glass funnel and the crude solid collected. Trituration with chloroform yields **3b** as a pale yellow solid (166 mg, 93%). Recrystallization by diffusion

(pentane/chloroform) yields pale yellow crystals. Mp: 186 ^{o}C – decomp. ^{1}H NMR (300 MHz, DMSO-d_6): ð 10.13 (br s, 2H), 8.54 (br s, 2H), 8.19 (d, *J* = 9 Hz, 4H), 8.02-7.98 (m, 3H), 7.82 (d, *J* = 7.8 Hz, 2H), 7.71 (d, *J* = 9 Hz, 4H), 7.57 (d, *J* = 2.1 Hz, 2H), 7.51 (dd, *J* = 6.6, 2.1 Hz, 2H), 1.30 (s, 18 Hz). ^{13}C NMR (300 MHz, DMSO-d_6): ð 152.49, 146.81, 146.28, 143.45, 141.85, 138.22, 129.94, 128.44, 128.12, 125.92, 121.19, 118.26, 111.68, 94.27, 86.40, 34.77, 31.64. MS (ESI pos) *m/z* (%): 776.6 (M+Na^+ +5, 9), 775.6 (M+Na^+ +4, 14), 774.9 (M+Na^+ +3, 31), 774 (M+Na^+ +2, 65), 773.2 (M+Na^+ +1, 98), 772.4 (M+Na^+, 100); $C_{43}H_{39}N_7O_6$ (749.81), $C_{43}H_{39}N_7O_6Na$ (772.8).

Methoxyphenyl sulfonamide 4a. Dianiline **1** (110 mg, 0.26 mmol) was reacted in a flame-dried 15 mL round-bottomed flask with *p*-methoxybenzenesulfonyl chloride (268 mg, 1.3 mmol) in freshly distilled pyridine under inert atmosphere (N_2). Following concentration *in vacuo*, the crude product was filtered through a 2.5 cm silica plug with 100% EtOAc. Purification by chromatography (20:1 CH_2Cl_2:EtOAc) afforded **4a** (185 mg, 93%) as a white crystalline solid. Recrystallization by diffusion (hexanes:CH_2Cl_2) afforded colorless crystals. Mp: 141-143 ^{o}C. ^{1}H NMR (300 MHz, $CDCl_3$): δ 7.77 (d, *J* = 9 Hz, 4H), 7.72 (t, *J* = 7.7 Hz, 1H), 7.54-7.44 (m, 8H), 7.33 (dd, *J* = 9.2, 2.4 Hz, 2H), 6.81 (d, *J* = 9 Hz, 4H), 3.72 (s, 6H), 1.24 (s, 18H). ^{13}C NMR (75 MHz, $CDCl_3$): ð 163.06, 147.62, 142.93, 136.75, 135.70, 130.85, 129.60, 129.43, 127.85, 126.44, 120.64, 114.09, 113.02, 93.28, 85.33, 55.45, 34.31, 31.03. MS (ESI pos) *m/z* (%): 765.5 (6), 764.5 (18), 763.5 (36), 762.6 (MH^+, 100); $C_{43}H_{43}N_3O_6S_2$ (761.95); 786.3 (M+Na^+ +2, 4), 785.3 (M+Na^+ +1, 9), 784.33 (M+Na^+, 20); $C_{43}H_{43}N_3O_6S_2Na$ (784.85).

Nitrophenyl sulfonamide 4b. Dianiline **1** (150 mg, 0.36 mmol) was reacted in a flame-dried 15mL round-bottomed flask with *p*-nitrobenzenesulfonyl chloride (180 mg, 0.81 mmol) in freshly distilled pyridine under inert atmosphere (N_2). Following concentration *in vacuo*, the crude product was filtered through a 2.5 cm silica plug with 100% EtOAc. Purification by chromatography (20:1 CH_2Cl_2:EtOAc) afforded **4b** (265 mg, 93%) as a yellow solid. Recrystallization by diffusion (hexanes:CH_2Cl_2) afforded pale yellow crystals. Mp: 136-139 ^{o}C. ^{1}H NMR (300 MHz, $CDCl_3$): δ 8.15 (d, *J* = 8.7 Hz, 4H), 8.03 (d, *J* = 8.7 Hz, 4H), 7.74 (t, *J* = 7.8 Hz, 1H), 7.55 (d, *J* = 8.7 Hz, 2H), 7.48-7.38 (m, 6H), 1.29 (s, 18H). ^{13}C NMR (75 MHz, $CDCl_3$): ð 150.10, 149.33, 145.32, 142.68, 137.20, 134.63, 129.82, 128.68, 128.28, 126.31, 124.12, 123.31, 114.59, 92.68, 85.71, 34.51, 31.05 MS (ESI pos) *m/z* (%): 795.5 (M^+ +3, 6) 794.5 (M^+ +2, 16), 793.5 (MH^+, 33), 792.5 (M^+, 59), 608 (18), 607 (46); $C_{41}H_{37}N_5O_8S_2$ (791.89); 817.2 (MNa^+ +3, 6), 816.2 (MNa^+ +2, 20), 815.2 (M+Na^+ +1, 39), 814.2 (M+Na^+, 100); $C_{41}H_{37}N_5O_8S_2Na$ (814.88).

Methylester-phenyl urea 3e. To a flame-dried 50 mL three-neck round-bottomed flask equipped with a stir bar and N_2 inlet was added 25 mL toluene, **3** (100 mg, 0.237 mmol) and *p*-isocyanato-methylbenzoate (88 mg, 0.498 mmol). The reaction was allowed to stir for 3 h, whereupon it was concentrated *in vacuo* and purified by column chromatography (50% EtOAc/hexanes, 5% TEA) to yield **3e** (129 mg, 70.1%) as a yellow amorphous solid. This was taken up in methylene chloride and protonated with trifluoroacetic acid. Precipitation with pentane yielded yellow orange solid suitable for ^{1}H-NMR. ^{1}H-NMR (300 MHz, $CDCl_3$): δ 8.57 (br s, 2H), 8.33

(t, 8.1 Hz, 1H), 8.05 (br s, 2H), 7.91 (m, 6H), 7.62-7.57 (m, 4H), 7.52 (d, 8.7 Hz, 4H), 3.90 (s, 6H), 1.34 (s, 18H).

Butylphenyl urea 3f. To a flame-dried 50 mL three-neck round-bottomed flask equipped with a stir bar, reflux condensor and N_2 inlet was added 25 mL toluene, **3** (250 mg, 0.594 mmol) and butyl isocyanate (235, 2.38 mmol). The reaction was heated to 100 ^{o}C for 12 h. Upon completion the solution was concentrated *in vacuo* and purified by column chromatography (50% EtOAc/hexanes) to yield **3f** as a white amorphous solid upon standing. (265 mg, 58%). ^{1}H-NMR (600 MHz, $CDCl_3$): δ 7.76 (d, *J* = 2.4 Hz, 2H), 7.61 (t, *J* = 7.8 Hz, 1H), 7.48 (dd, 2.4, 8.4 Hz, 2H), 7.38 (d, 7.2 Hz, 2H), 7.27-7.26 (obscured d, 2H), 6.89 (br s, 4H), 3.23 (t, *J* = 7.2 Hz, 4H), 1.45 (*J* =7.2 Hz, 4H), 1.35-1.26 (m, 22H), 0.82 (t, 7.2 Hz, 6H). ^{13}C-NMR (600 MHz, $CDCl_3$): δ 155.64, 152.31, 143.37, 136.44, 131.03, 122.31, 109.99, 92.74, 85.33, 40.27, 34.84, 31.78, 31.16, 31.09, 20.00, 13.70.

Bridge to Chapter V

Chapter IV focused on the switchable fluorescence observed upon protonation of electron-rich and electron-poor urea and sulfonamide-functionalized arylethynylpyridines. The mechanisms dictating the fluorescent responses of the urea receptors were found to be defined by both monomolecular and bimolecular events. In tandem with our knowledge of the binding preferences of the urea receptors, these data serve as a logical bridge to extend our understanding of anion-

mediated self-assembly processes and to develop functional probes for specific anions in biological media.

Chapter V will focus on two major classes of preliminary results: development of these probes for *in* vitro imaging applications and the study of the anion-mediated self-assembly of these receptors. The data presented in this chapter are unfinished, but are included to give an applications context to the mechanistic results presented thus far and to summarize the current state of these ongoing projects. The future directions in which this research is proceeding will also be presented.

CHAPTER V

FUNCTIONALIZED ANILINOETHYNYLPYRIDINE UREAS: *IN VITRO* IMAGING AND ANION MEDIATED SELF-ASSEMBLY

Introduction

This chapter was coauthored with Dr. John J. Naleway of Marker Gene Technologies, who provided the epifluorescence images; and Matthew Carnes, who designed the circular dichroism experiments and synthesized compound **4.** The data presented in this chapter are unfinished and should serve to give the reader an understanding of the current state of the project and the direction in which it will proceed in the near future. It is presented in two parts: cellular assays with **1a·TFA** and current supporting experiments; and anion-mediated assemblies of other urea-functionalized receptors and current supporting experiments.

As the natural ubiquity of ionophores and the importance of the roles they play in the regulation of biological function have been realized chemists have increasingly turned their attention to understanding the structure-function relationships of these compounds.[1] Since many commonly occurring ionophores in biological systems are involved in transmembrane transport or cell signaling pathways, much of the focus has been on the study of single ion or ion-pair channels and cell signaling in these domains.

Chloride and nitrate are commonly occurring and eminently important anions in biological systems. Dysfunction in cAMP-regulated Cl^- ion channels, in particular cystic

fibrosis transmembrane conductance regulatory protein (CFTR) leads to ion misregulation in the epithelial cell lining and results in cystic fibrosis.[1b,2] The choroid plexus inward rectifying channel, which regulates the blood-cerebrospinal fluid ion gradient, supports the neuronal signal cascade via a $K^+/Na^+/Cl^-$ co-transport mechanism.[3] Chloride ion channels (ClC) 1 and 5, regulate ion gradients across many cellular membranes, where dysfunction results in myotonia congenita and renal failure.[4]

Nitrate, on the other hand, was first implicated in gastric cancer via metabolism to nitric oxide and nitrosylation of DNA.[5] In contrast to this, in 2009 it was hypothesized that dietary NO_3^- may serve as the sole regulator of NO/nitroso homeostasis in individuals with inhibited nitric oxide synthase function, i.e., diabetics.[6] Current research on the exact role of nitrate in biological systems demands effective, highly selective and highly resolved probes for this ion in cellular matrices.

For these investigations it is of paramount importance that the chemical species involved be monitored in a quantifiable manner with high temporal and spatial resolution.[7] Under these limiting circumstances, typical cell imaging technologies can fall short. Incorporation of the commonly used fluorescent proteins requires ground-up expression through gene manipulation, which tends to limit the spatial resolution achievable and inevitably leads to slower response times.[8] Probe size can also be detrimental, as large non-natural perturbations to the system can affect the natural function of the pathway or channel under study.[9]

A. Cellular Imaging of Inorganic Anions

Selective, highly responsive small molecule fluorescent indicators are promising entities for use in systems where the typical fluorescent proteins and their analogs may be insufficient. Quantitative and localizable small molecule probes have been developed for biologically relevant inorganic cations, although only a few examples exists for imaging their anionic counterparts *in vitro*.[10] These anion-sensors are invariably "ON-OFF" responsive, thus demonstrating a need for "OFF-ON" responsive indicators for *in vitro* measurement of biologically occurring inorganic anions.

We focused our attention on the fluorescent signaling of Cl^- *in vitro* by our receptors, due to the Cl^- binding ability observed in the parent phenylurea receptor. In collaboration with Marker Gene Technologies, we screened urea and sulfonamide receptor candidates in both the neutral and trifluoroacetic acid-protonated states.

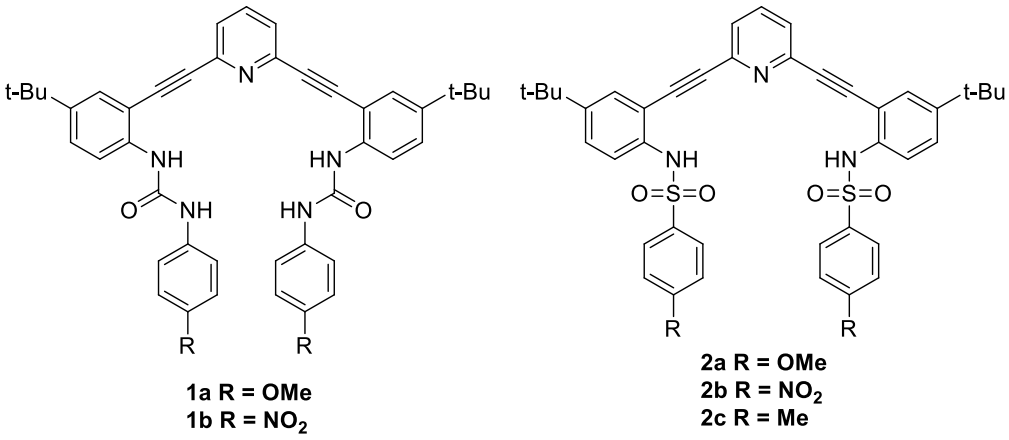

Figure 1. Receptors used in cellular assays.

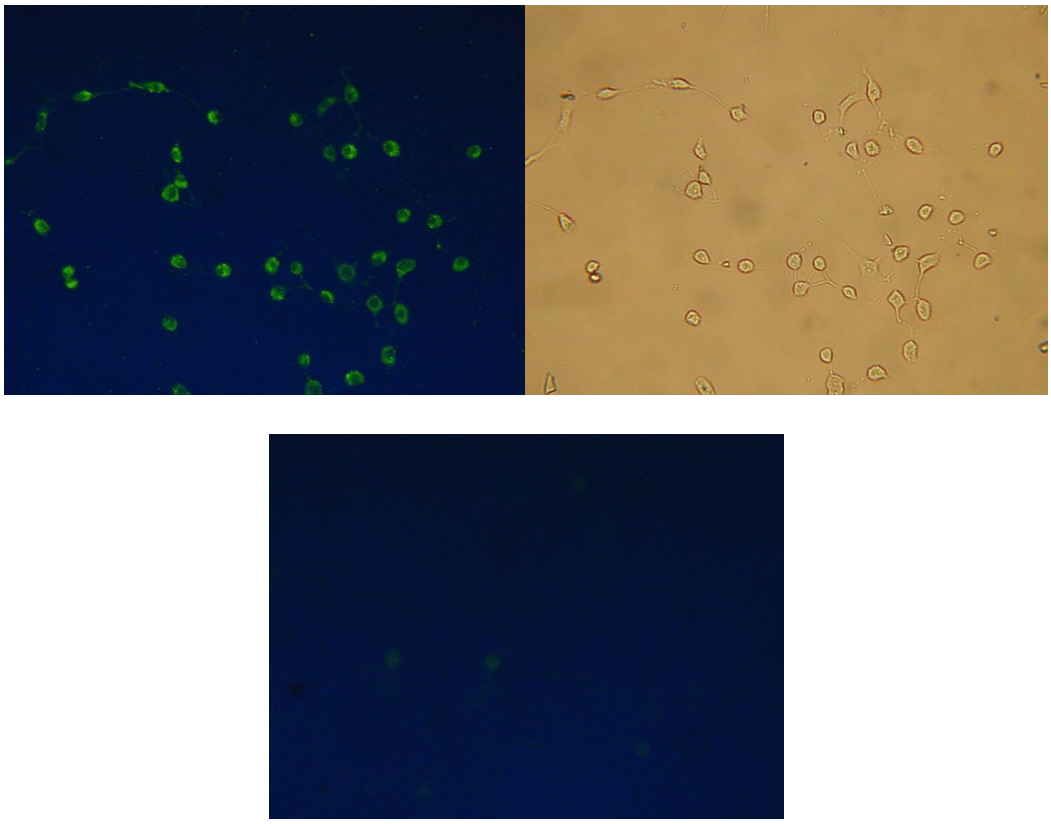

Figure 2. (Top Left) Epifluorescence image of NIH3t3 mouse embryo fibroblasts incubated with a 7.4 pH buffered, high Cl^- solution and stained with **1a·TFA** at 50µM; (top right) Nomarski phase contrast image of same; (bottom) Epifluorescence image of above, incubated in Cl^- free buffer system isotonically balanced by NO_3^- (Appendix D).

The epifluorescence assays were carried out according to literature precedent.[10b] NIH3T3 embryonic mouse fibroblasts were grown in a humidified atmosphere and transferred to 22mm circular sterile glass coverslips in 12-well plates for staining. The cover slips were rinsed and incubated for 20 minutes with a saline solution (120 mM KCl, 20 mM NaCl, 1 mM $MgCl_2$, 1mM $CaCl_2$, 10mM HEPES pH buffer at pH 7.4),

containing high concentration Cl^- ion. For the controls, the saline solution was isotonic with NO_3^- instead of Cl^- (120 mM KNO_3, 20 mM $NaNO_3$, 1 mM $MgCl_2$, 1mM $CaCl_2$, 10mM HEPES pH buffer at pH 7.4) to afford the low Cl^- media. The receptor was dissolved in DMSO and introduced to the well plates such that the DMSO:H_2O ratio was 10%, and the final receptor concentration was 50 µM. This was allowed to stand for 45 minutes, and then rinsed thrice with the saline solution used previously.

Unexpectedly, our initial assays were successful only with **1a·TFA.** We corroborated these results by repetition of the above assays at multiple concentrations of receptor, and by increasing the receptor staining time to one hour (Figure 3).

[1a·TFA]	High Cl^-, 1 hr		Low Cl^-, 1 hour	
50 µM	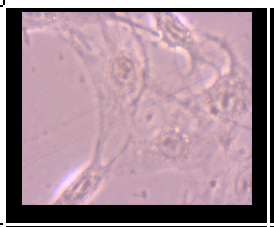	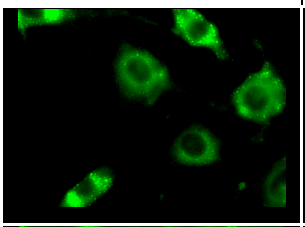	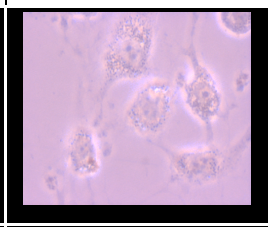	
100 µM	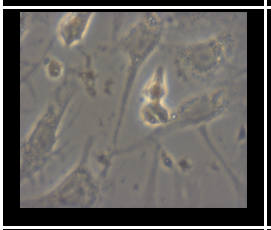	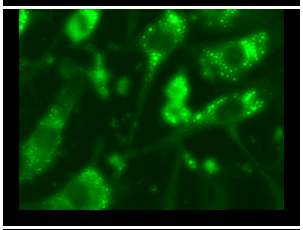	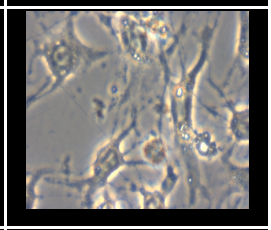	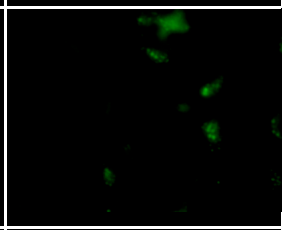
Control	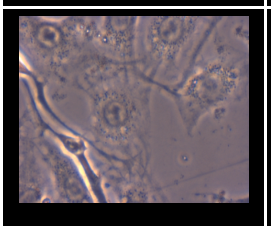	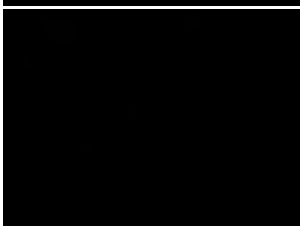	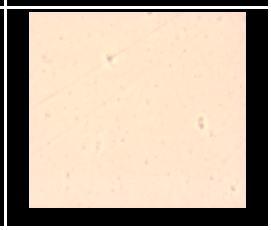	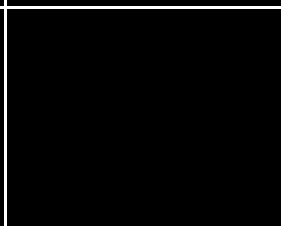

Table 1. Summary of epifluorescence results. The left hand column in each set is the Nomarski phase contrast image, the right hand is epifluorescence (ex: 450-495 nm, 515 nm emission cutoff filter). The controls at bottom are 10% DMSO only (no **1a·TFA**), with and without cells (left and right, respectively). See Appendix D for further details.

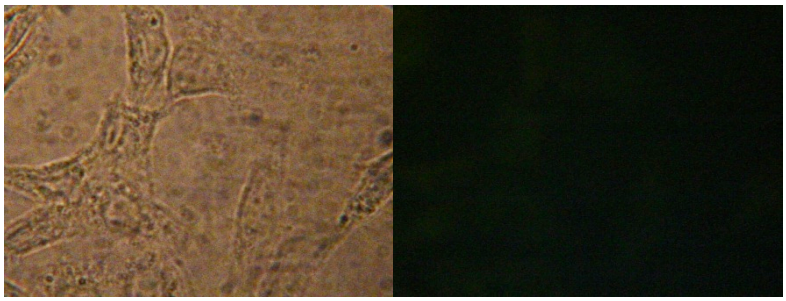

Figure 3. (Left) Nomarski phase contrast image of **1a**, subjected to the same conditions as above; (right) epifluorescence image of same.

From inspection of the epifluorescence results in Table 1 it became apparent that the receptor is localizing in the lipid portions of the cells, most likely due to its low solubility in water. The cells themselves exhibit evidence of hypotonic shock from the multiple washes and distorted membranes, most likely due to the high level of DMSO used to add the receptor.

The binding constants for **1a·TFA** for both chloride and nitrate were determined by UV-Vis titration in $CHCl_3$. In spite of the poor match in solvents, the trend for fluorescence response is conserved, as seen in Table 2.

TBAX	1a[a]	1a·TFA[b]
Cl^-	730 M^{-1}	40,700 M^{-1}
NO_3^-	280 M^{-1}	12,100 M^{-1}

[a] ^{1}H-NMR titration; [b] UV-Vis titration

Table 2. Binding constants for **1a** and **1a·TFA** in water saturated $CHCl_3$ with tetrabutylammonium salts of chloride and nitrate (Appendix D).

Cell viability studies and staining longevity assays indicate that **1a·TFA** is fairly innocuous and that the receptor complex remains highly fluorescent for at least 24 hours (Table 3). With the exception of the entry for the 50 μM receptor under high Cl^- conditions, the cells are no less viable than when treated with 10% DMSO by itself. The 8% viability for 50 μM receptor is attributable to extremely low retention of cells on the slides being examined, a problem that we had to surmount due in part to the addition of DMSO to the cellular media prior to final washes to remove excess **1a·TFA**, and to the presence of semi-amphiphilic **1a·TFA** acting as a surfactant.

Stain concentration	High Cl^-	Low Cl^-
50 uM	8%	95%
100 uM	86%	98%
DMSO	85%	100%

Table 3. Cell viability upon treatment with the receptor and saline solutions, and 10% DMSO.

As reported in Chapter IV, electron-rich receptors in organic media exhibited ON-OFF responses, whereas electron-poor receptors had the same OFF-ON responses as those seen in the cellular assays. Critical examination of both of these results led to the realization that not only are the receptors behaving in direct opposition to what was observed outside of cellular media, but none of the emission bands observed in any of the receptor classes would give rise to the intense green fluorescence seen in cells. The ambiguity of both the results and the media in which we were seeing the occurrence of this fluorescence led us to study this phenomenon in a model cellular system.

Fluorescence in Vesicles. Much of the current research in transmembrane ion transport depends upon model cellular systems consisting of simple vesicles formed by phospholipid bilayers in aqueous media.[11] Using these liposomes as a model for the lipid bilayer of cellular membranes in our system was a logical extension of the cellular studies presented in the previous section and served to explain the unexpected fluorescence behavior.

Phospholipid POPC was used to form vesicles which contained high Cl^- solution (120 mM KCl and 1 mM $CaCl_2$) and low Cl^- solution (120 mM $NaNO_3$ and 1 mM $CaCl_2$). Both vesicle solutions were dialysed, and then split into two equal volumes. Of these aliquots, one was diluted with the same low Cl^- containing aqueous external solution and one with 0 Cl^- content (120 mM KNO_3), both buffered at pH 7.2 (10 mM HEPES). This resulted in four vesicle solutions: high internal Cl^- content and low external Cl^- content (**A**); high internal Cl^- content and no external Cl^- (**B**); low internal Cl^- content and low external Cl^- content (**C**); and low internal Cl^- content and no external Cl^- (**D**). Treatment of these vesicle solutions with **1a·TFA** as a solution in 10% DMSO analogous to the cellular assays led to dual emission spectra in all cases (Figure 4). Solutions of **1b** and **1b·TFA** subjected to the same conditions showed no evidence of fluroescence emission.

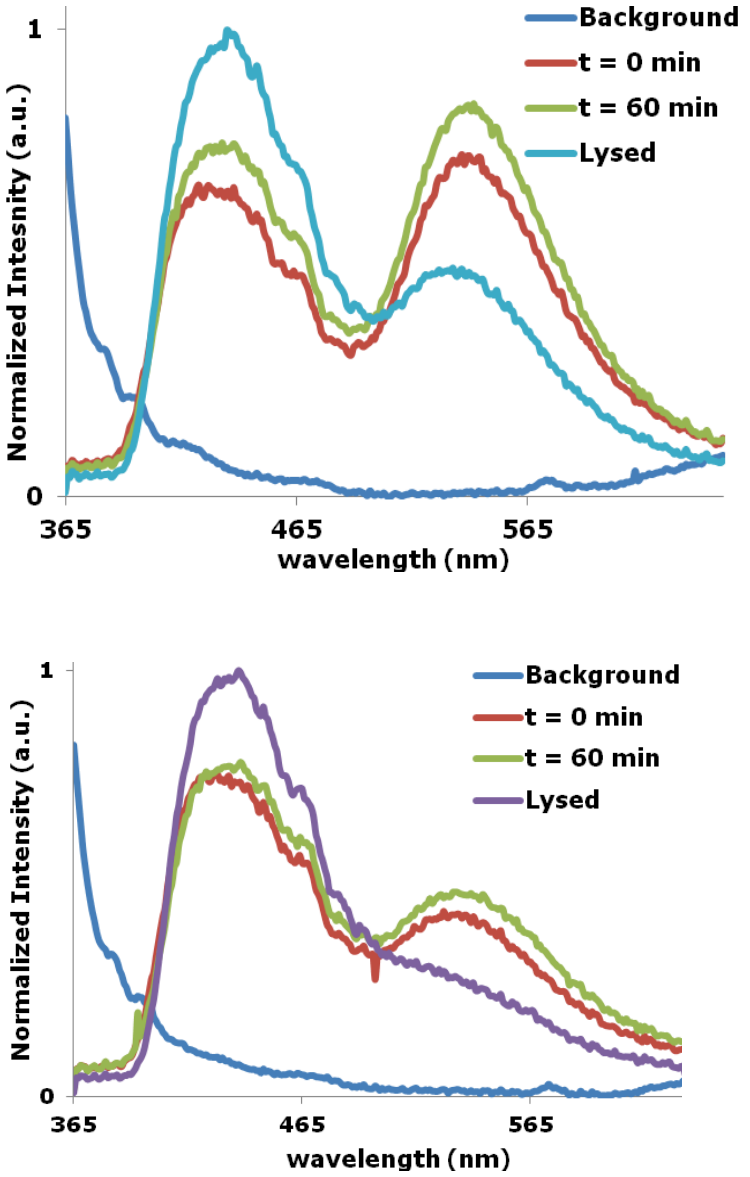

Figure 4. Fluorescence emission spectra of vesicle solutions containing **1a·TFA**: (top) solution **A**; (bottom) solution **C**. Bulk lipid concentration: 4.21 mM; receptor concentration: 2.78 μM.

Figure 4 summarizes the data obtained from the two most balanced solutions, **A** and **C**. The tonic imbalance in solutions **B** and **D** resulted in irreproducible results, most likely from autolysis of the vesicles due to the Cl^- gradient, although *a posteriori* review

of the literature indicates that this could be overcome with judicious choice of balancing ions in the external solution during preparation.[12]

The emission band in the spectra at 530 nm equates to the green emission observed in the epifluorescence assays, and is indicative of the Cl^- concentration as can be seen by the differences in intensities between the two solutions. In the high Cl^- case (solution **A**) it can be seen that lysing the vesicles with the surfactant polyoxyethylene(8)lauryl ether not only diminishes the 530 nm emission band, but that emission is concurrently recovered in the 430 nm band. In fact, this recovery is observed in both solutions and seems to be indicative of the overall concentration of fluorophore in solution. Data from heating solutions of these vesicles to dirupt the vesicle also results in quenching of the 530 nm band, the same as seen upon lysing the vesicles. These data support the hypothesis that there exists a dependence upon complex formation or aggregation for the 530 nm emission to occur. Additionally, the dual emission behavior of **1a·TFA** augers well for the use of this receptor as a self-consistent ratioable sensor in aqueous media.

Aggregation Induced Emission in Aqueous Media. The mechanism for the fluorescence emission of **1a·TFA** is unclear, but seemed to be highly dependent upon solvophobic effects and localization either in cellular or synthetic lipid membranes. Supporting experiments in aqueous media seemed to indicate that it is aggregation induced, which would explain the observed localization of fluorescence emission in lipid-dense areas of the cells. These data are presented herein.

Aggregation induced emission (AIE) arises from restricted intermolecular rotation (RIR) of the fluorophore, which has the effect of destabilizing thermal relaxation and increasing the emission quantum yield.[13b] This process runs counter to the more well understood process of concentration-dependent quenching in photoluminescent systems.[14] Additionally, AIE is rarely seen in aggregates exhibiting large degrees of π-π stacking, as this electronic interaction generally leads to static quenching of the excited-state by electron transfer, with the exception of fluorophores exhibiting excimer or exciplex emission, as in protonated **1b**.[15]

The fluorescence behavior observed in aqueous solutions of Cl^- containing vesicles and **1a·TFA** was not observed for **1a·TFA** in DMSO solution or any aqueous solutions of **1b·TFA**. If aggregation of the receptor was driving fluorescence in **1a·TFA** then it would be expected that a "good" solvent for the receptor, such as DMSO, would result in non-fluorescent, molecularly dissolved receptor solutions. In order to verify aggregation induced emission in this receptor, neutral **1a·TFA** was taken up in DMSO and the resulting solutions slowly switched to a less solubilizing medium. The initial **1a·**TFA/DMSO solutions were orange and non-fluorescent. If AIE was the cause of the observable fluorescence in cell assays and vesicle experiments, then titration of water into the DMSO solutions of **1a·TFA** such that the receptor became poorly solvated would lead to aggregation and fluorescence, while retaining the colorimetric indication of protonation (an orange hue).[13]

To DMSO solutions of **1a·TFA** at 1.96 mM was added HEPES buffered (pH 7.2) aqueous solutions of KNO_3 or KCl such that the final solutions reached 35 - 40% DMSO in

H_2O (see Appendix D for supporting experiments with deionized water and $LiClO_4$ solutions).

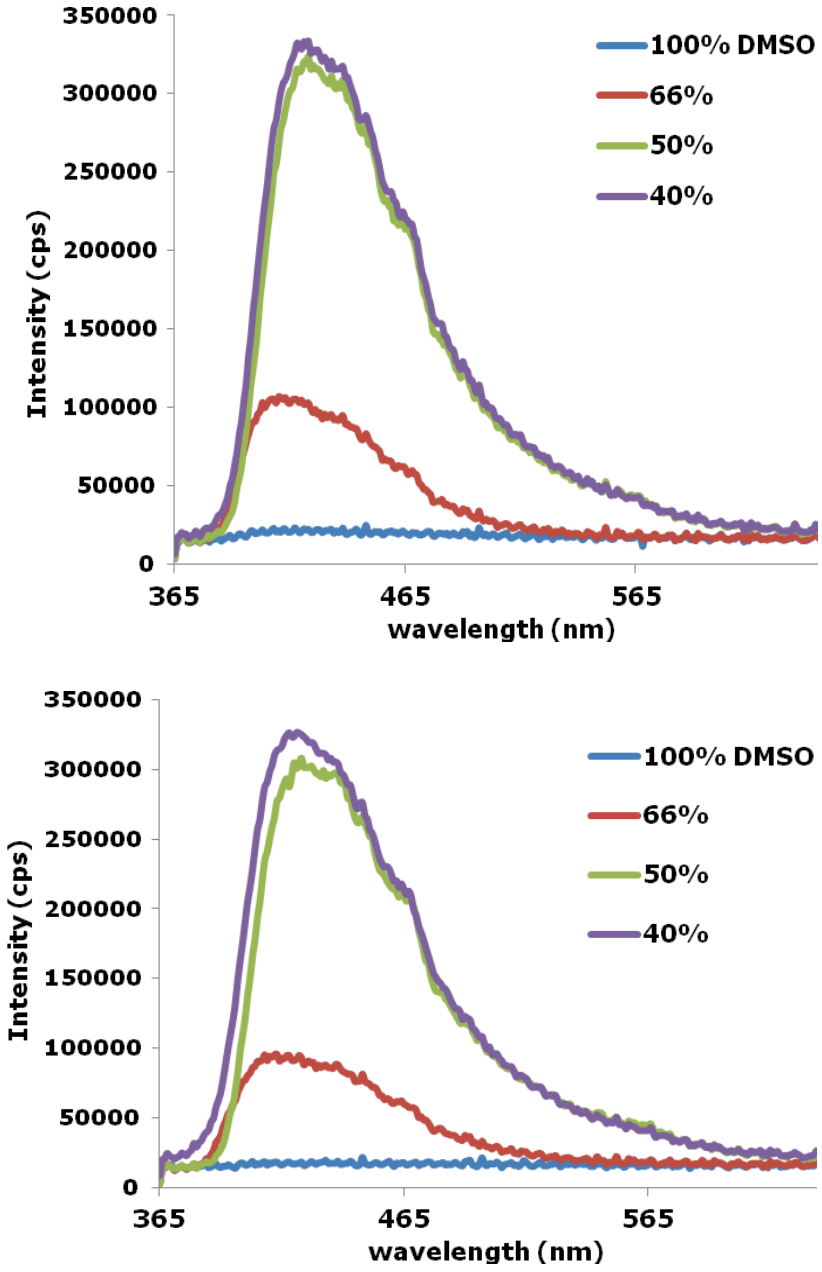

Figure 5. Fluorescence emission data for aggregation experiments. (Top) Titration of KNO_3 in buffered water into DMSO solution of **1a·TFA**; (bottom) titration of KCl in buffered water into DMSO solution of **1a·TFA**.

The results summarized in Figure 5 indicate that solution-phase aggregation is the source of the 430 nm fluorescence emission band. Repeating these experiments with pure water or $LiClO_4$ yielded approximately equivalent spectra, although plain water did not induce aggregation until the solution reached 33% DMSO in H_2O (Appendix D). Of note in the KCl spectra (Figure 5, bottom) is the absence of the 530 nm emission band seen in the vesicle solutions in the presence of Cl^-. The absence of this band could be attributable to the substantial amount of DMSO in these samples disrupting the fluorescent Cl^- complexes, as was seen in the lysed vesicle solutions. Simple injection of **1a·TFA** into buffered Cl^- solution such that the final concentration is 10% DMSO/H_2O yields spectra with strong emission at 530 nm, akin to the vesicle studies (Figure 6).

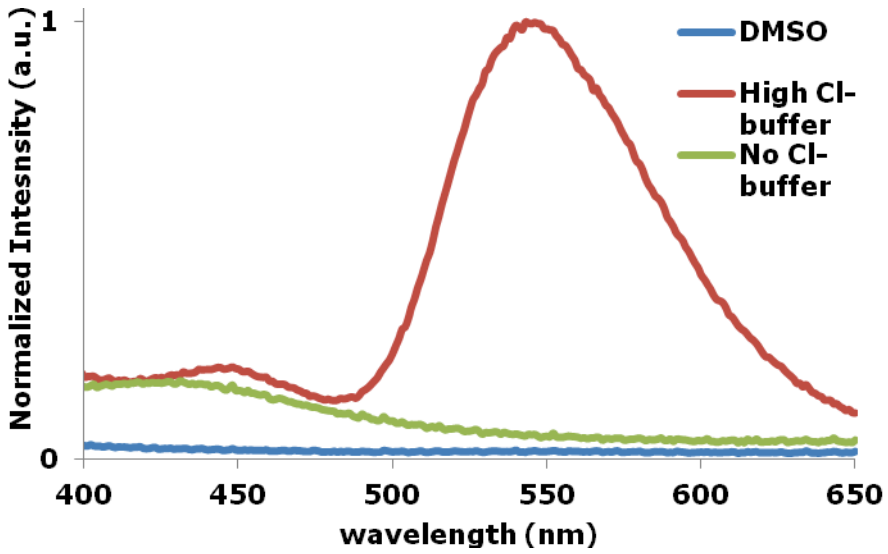

Figure 6. Fluorescence of **1a·TFA** in DMSO injected into DMSO (blue trace), high Cl^- buffered H_2O (red trace) and H_2O buffered with no Cl^- content (green trace).

This longer wavelength emission is indicative of an energy transfer mechanism and may be attributable to a static, ground-state π-stacked complex achievable only with inclusion of a relatively small anion such as Cl^-, which would explain the lower intensity bands and bathochromic shifting of the emission. While the exact mechanism behind the appearance of this emission band in Cl^--containing cells and vesicles remains elusive, the disruption of the emission with high concentrations of molecularly dissolving solvent (e.g., DMSO, lysing surfactants) in solution and the quenching of the 530 nm emission band upon heating are strong indicators of a Cl^- dependent complex and an *inter*molecular energy transfer mechanism.

B. Anion-induced Supramolecular Assemblies of Other Urea Receptors

During the preparation of solutions of **1a·TFA** and **1b·TFA** for the aggregation induced emission studies, a curious dependence upon the order of operations was observed. Protonation of the receptors in apolar organic solvents, followed by collection of the resultant orange solid either by precipitation or concentration yielded yellow to orange solutions upon dissolving in DMSO, indicative of protonation of the pyridyl lone pair. Contrarily, dissolving the neutral receptor in DMSO and adding acid, even in vast excess, would never result in yellow solutions and UV-Vis absorbance spectra indicated that the receptor remained unprotonated in solution.

In an attempt to address this phenomenon, the receptors were taken up in non-hydrogen bonding MeCN instead of DMSO, but this resulted in the same behavior as noted above. Exposure of solutions of the neutral receptors to a slightly stronger acid,

HBF_4, would change the color of the solution slightly at extremely high HBF_4 concentration, but the general trend stayed the same: solutions of **1a** and **1b** in polar organic media would only exhibit the absorbance bands indicative of protonation if they were pre-protonated in an apolar solvent. While it seems apparent that the difference in pK_a of both the protonated receptor and the acid in each of these solvents could account for this observation, the pre-protonated receptors would remain orange and exhibit the UV-Vis absorbance indicative of protonation in solutions of DMSO or MeCN until exposed to base. This instilled in us the idea that there may be an aggregate or ordered stack in solution to account for this apparent incongruity.

Anion-dependent Fluorescent Aggregates. Taking solutions of **1a·HBF$_4$** and **1b·HBF$_4$** in MeCN and exposing them to different anions as TBAX salts yielded unexpected results (Figure 8).

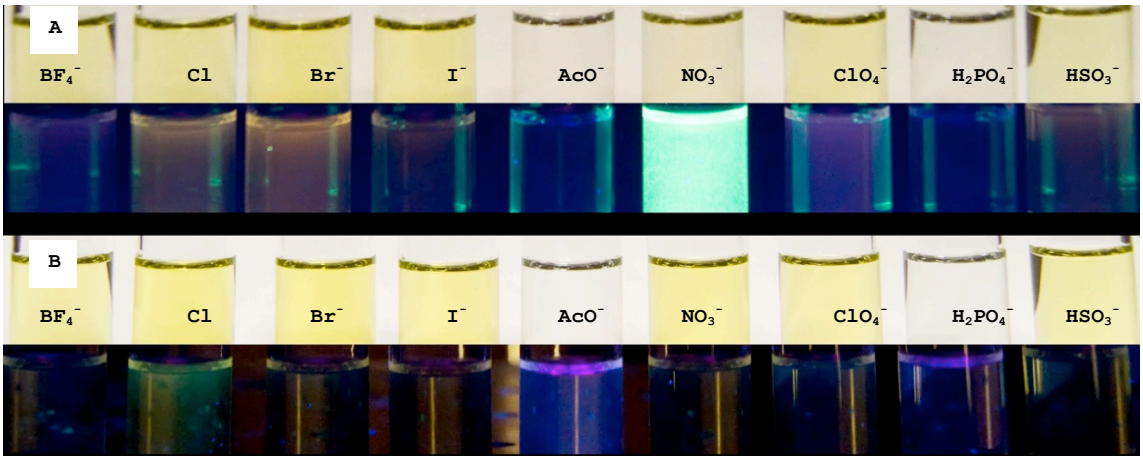

Figure 7. (a) Top: solutions of **1b•HBF$_4$** with TBAX in acetonitrile, bottom: under 365 nm light. (b) Top: **1a•HBF$_4$** with the same anions as (a) in acetonitrile, bottom: under 365 nm light. The clear solutions containing AcO^- and $H_2PO_4^-$ are indicative of deprotonation by these more basic anions.

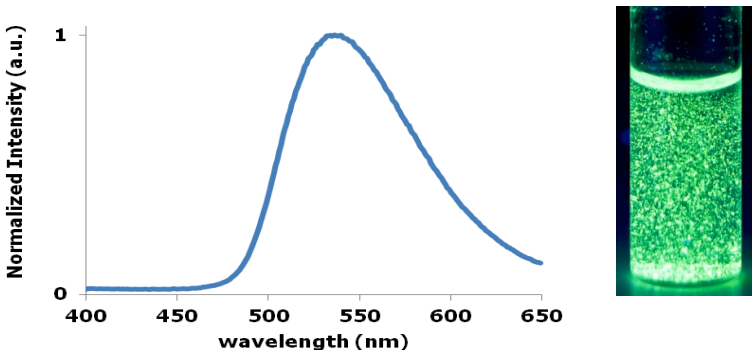

Figure 8. Fluorescence emission of **1b·HBF$_4$** with TBANO$_3$ in the solid state. Inset: the larger precipitate which formed ~10 min after exposure to TBANO$_3$ (under 365 nm light).

In solutions of both **1a·HBF$_4$** and **1b·HBF$_4$** exposure to basic anions (acetate and hydrogen phosphate) resulted in deprotonation of the receptor, and the resultant solution was colorless. With the exception of **1b·HBF$_4$** and tetrabutylammonium nitrate, none of the solutions exhibited noticeable fluorescence emission under 365 nm light. The striking selectivity of **1b·HBF$_4$** for nitrate in MeCN was intriguing, but after letting the solutions sit overnight the fluorescence emission was gone. At the bottom of the vial was a highly green fluorescent precipitate. Repetition of the above experiment showed that the green fluorescence observable in solutions containing NO_3^- was in fact a finely distributed precipitate (Figure 8). These aggregated into larger particles and settled from solution over time, leading to a non-fluorescent supernatant solution and fluorescent, amorphous solids at the bottom. Solid-state fluorescence of the precipitate with 373 nm excitation yielded spectra with a maximum at 530 nm, in agreement with the color of the precipitate in MeCN solution (Figure 8). These fluorescent particles were intriguing, and followed the AIE trend noted above, although the aggregation seemed to be induced by addition of the nitrate anion in this case.

Transmission Electron Microscopy. While TEM and SEM techniques would both be effective probes of the macroscopic topology of the receptor aggregates, only TEM data will be presented here due to its relative completeness. The receptor was deposited onto lacy carbon grids to investigate the nanoscale assembly of **1b·HBF$_4$** aggregates with anions, in particular the nitrate anion. Treatment of MeCN solutions of **1b·HBF$_4$** exposed to MeCN solutions containing high millimolar quantities of tetrabutylammonium salts of the anions used in the aggregation studies reported earlier in this chapter. TEM images were collected on lacy carbon grids by floating the grids upside down on drops of the receptor and salt solutions on glass slides. After 30 seconds the grids were removed and allowed to dry before being introduced to the vacuum chamber of the instrument (Figure 9).

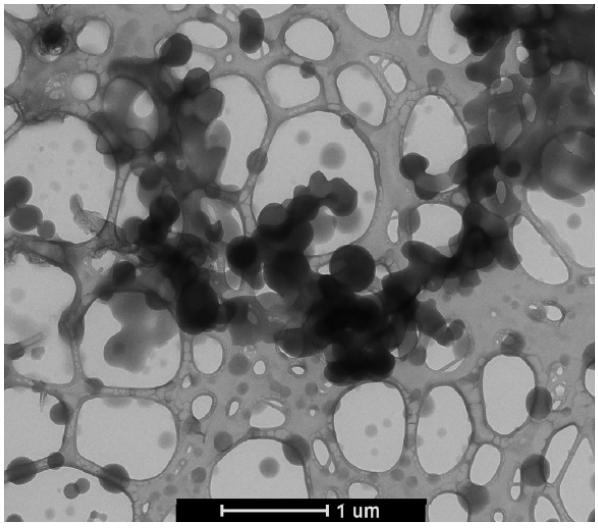

Figure 9. TEM image of **1b·HBF$_4$** on lacy carbon (scale bar inset).

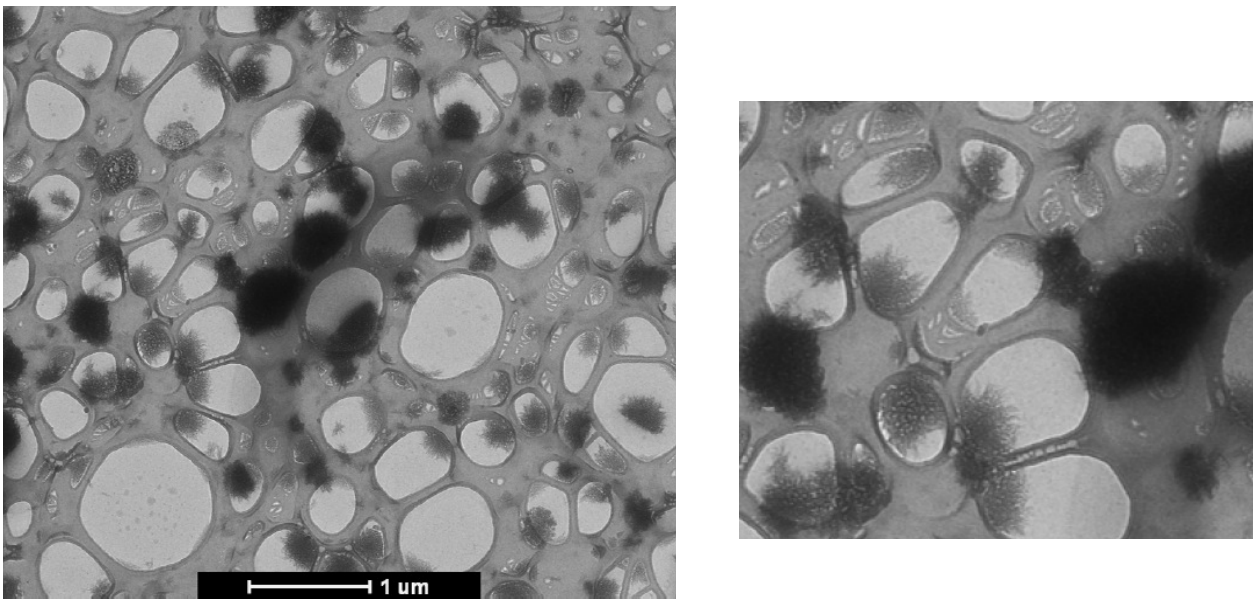

Figure 10. TEM images of **1b·HBF$_4$** after exposure to TBANO$_3$. The globular particles seen in Figure 9 now exhibit finer and more ordered edges. At right is a close-up of these aggregates.

Images of **1b·HBF$_4$** obtained from MeCN are composed strictly of large, amorphous aggregates with no fine structure and soft, globular edges. Addition of a small amount of tetrabutylammonium nitrate to the solution of **1b·HBF$_4$** used in Figure 10 results in sharper, feathered particles which fluoresce green under UV light. Blank images (of just MeCN, and MeCN with TBANO$_3$) have no visible particles present on the lacy carbon, even at high magnification (Appendix D).

The structural change upon introduction of nitrate led us to question the influence of the size of the anion on the mesoscopic topology of the particles. Would smaller anions allow for tighter packing and more ordered structures, or would the particles be uniformly smaller and more monodisperse?

Treatment of the receptor with tetrabutylammonium chloride instead of nitrate led to the formation of long rods, some of which spanned multiple grid windows while

being only 100 – 150 nm wide (Figure 11; blank images of TBACl in Appendix D). This topology was only observed with TBACl, as treatment with TBABr led to disordered clumps of rods; these unordered structures are an apparent midpoint between the particulate seen with nitrate or tetrafluoroborate and the rods formed upon exposure to chloride (Figure 12).

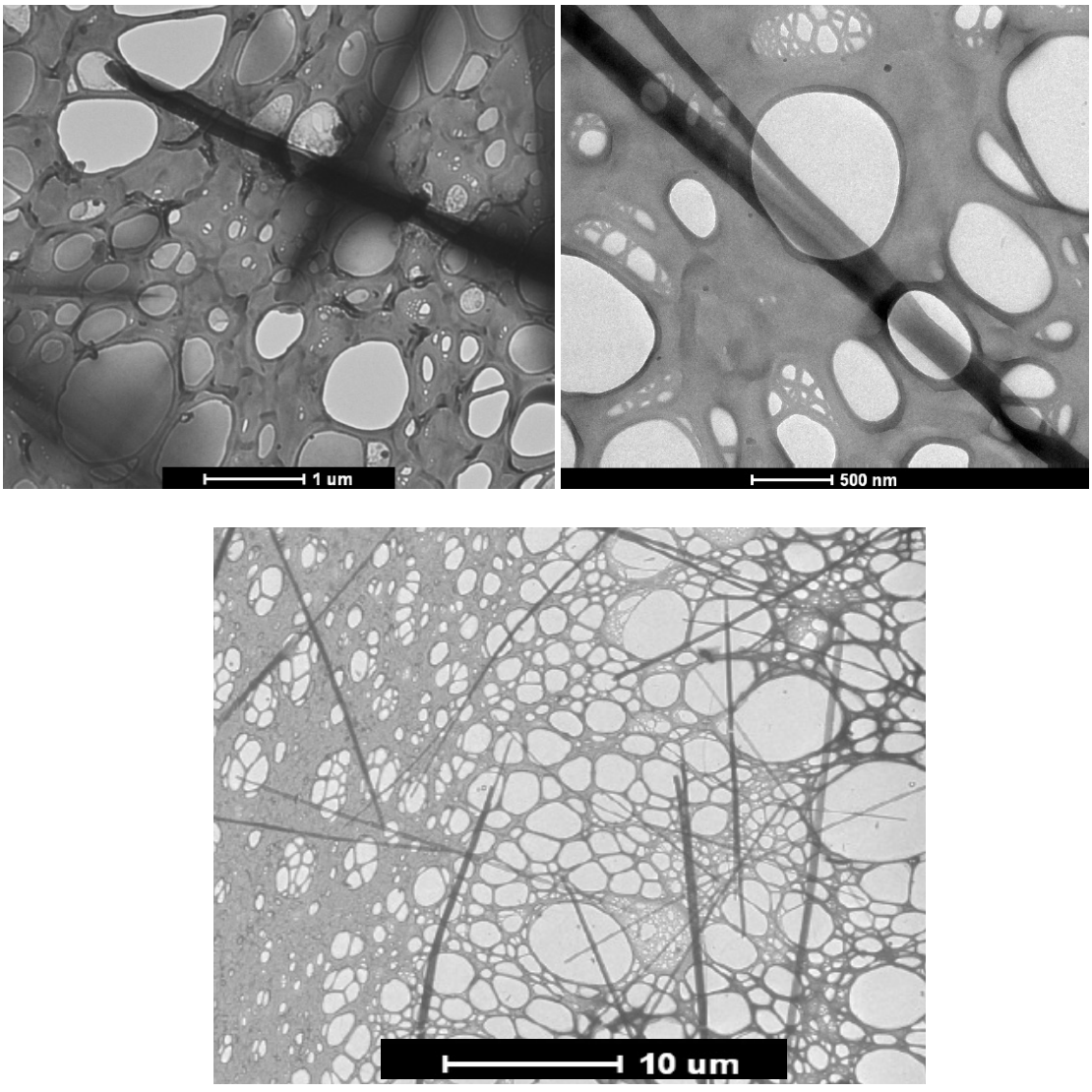

Figure 11. TEM images of **1b·HBF$_4$** exposed to TBACl. The long rods formed under these conditions are 100-200 nm across, and can be up to hundreds of microns long, spanning multiple grid windows with little to no branching.

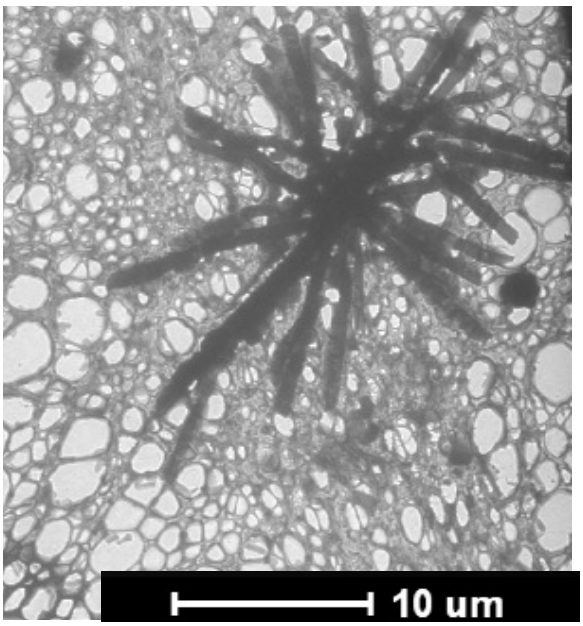

Figure 12. TEM image of **1b·HBF$_4$** after exposure to TBABr.

Upon closer inspection of the rods seen in the Cl^-- containing images we noticed striations in the longitudinal direction of the rod. This pattern is consistent with clumps of smaller rods packed together to form the longer wires, although additional microscopy techniques are still needed to confirm this observation (e.g., SEM topographical images). A good illustration of these rope-like striations observed in all of the TBACl experiments can be seen in Figure 13. We tentatively attribute this to the formation of long, linear molecular aggregates containing Cl^- anions incorporated in the interior cavities along the length of the rod, which subsequently stack together like fibers in a rope to form the wider striated aggregates observable at TEM magnification.

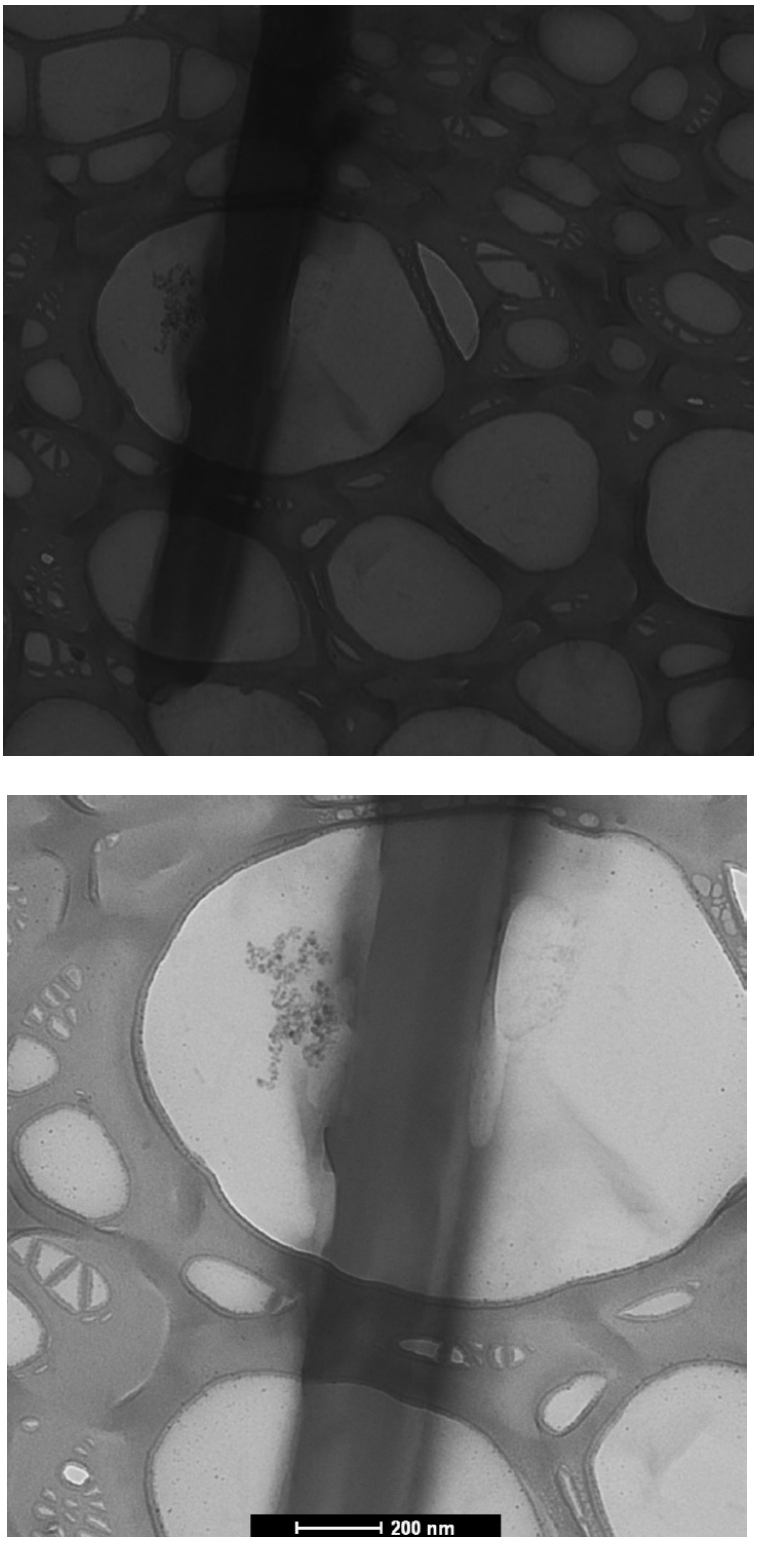

Figure 13. TEM images illustrating the striated pattern in the rods. The image at top is approximately 2 µm wide.

Crystal structures of **1b** offer some support for the columnar stacking interaction hypothesized above. In crystals grown from DMSO **1b** exists as a monomer with no intermolecular H-bonding interactions between receptors (Chapter IV, Figure 12). Crystals grown from MeCN, however, take the same general conformation but incorporate H_2O into the cavities. The hydrogen bonds in the network of H_2O molecules and urea groups in each of the cavities sew together the interdigitated infinite columns (Figure 14).

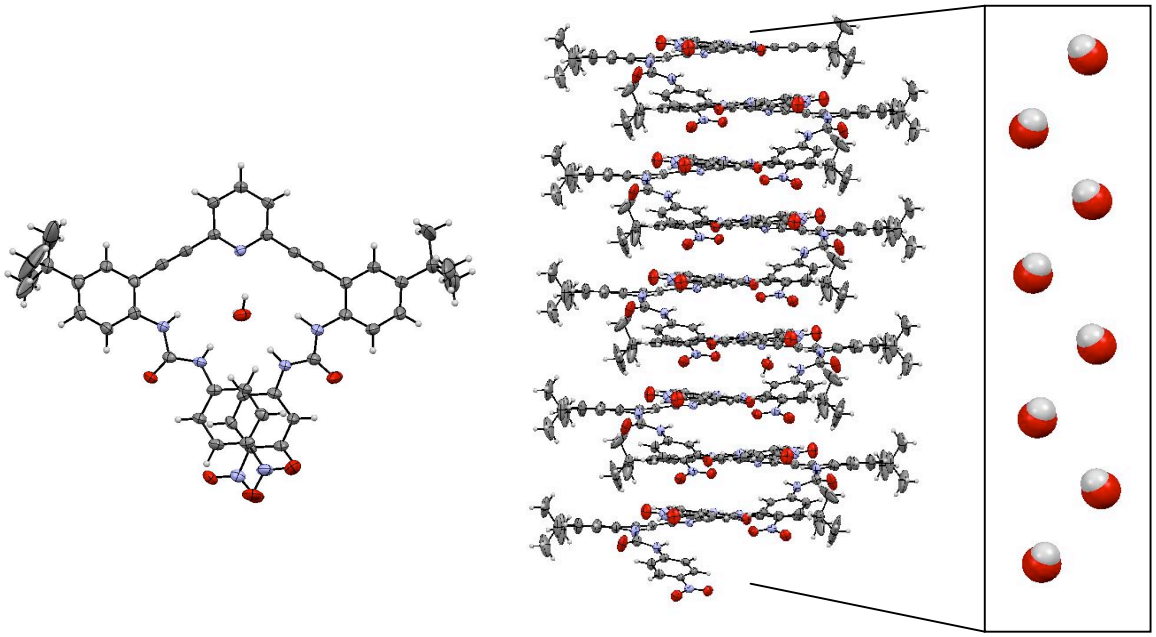

Figure 14. ORTEP representation (thermal ellipsoids at the 50% probability level) of the crystal structure of **1b** grown from MeCN. (Left) the conformation of each monomeric receptor; (middle) the infinite columnar stack of interdigitated receptors; (right) space-filling model of the structure of the two strings of H_2O that sew the columnar structure together.

The distance between each receptor is 3.37-4.01 Å, with pyridine N•••HOH hydrogen bond distance of 2.90 Å, NH•••OH_2 distances of 2.89-3.80 Å and C=O•••HOH bond distance of 2.86 Å. The two receptors in each stack are brick-and-mortar offset by

4.05 Å, about the distance of the ethynyl linkages between the pyridine and each arm. While crystal structure of the protonated **1b** complexes have yet to be solved, it can be imagined that the electrostatic interactions between the pyridinium rings and their Cl^- guests would offer an additional source of stabilization energy to stacks such as these. Additionally, one could envision the larger trifluoroacetate anion's $-CF_3$ moieties acting as caps to the dimers, limiting the growth of the stacks in each direction. This would result in the smaller, dimeric aggregates that would give rise to the globular structures seen in Figure 9, while replacement with Cl^- would allow the receptor complexes to aggregate more closely, thus forming the wire-like structures seen in Figure 11. This anion-induced aggregation phenomenon led us to begin investigation of whether or not there was evidence of the formation of ordered aggregates or stacks in solution prior to precipitation.

Circular Dichroism. We turned to circular dichroism spectroscopy to investigate the aggregation phenomenon in dilute solution. Chiral analogs of the urea receptors were synthesized: a simple model urea **4**, and analogs of **1a** and **1b** (Scheme 1). The first chiral receptor **4,** an analog of the alkyl urea receptors previously reported, was synthesized by treatment of **3** with commercially available (R)-(+)-α-methylbenzyl isocyanate in toluene.

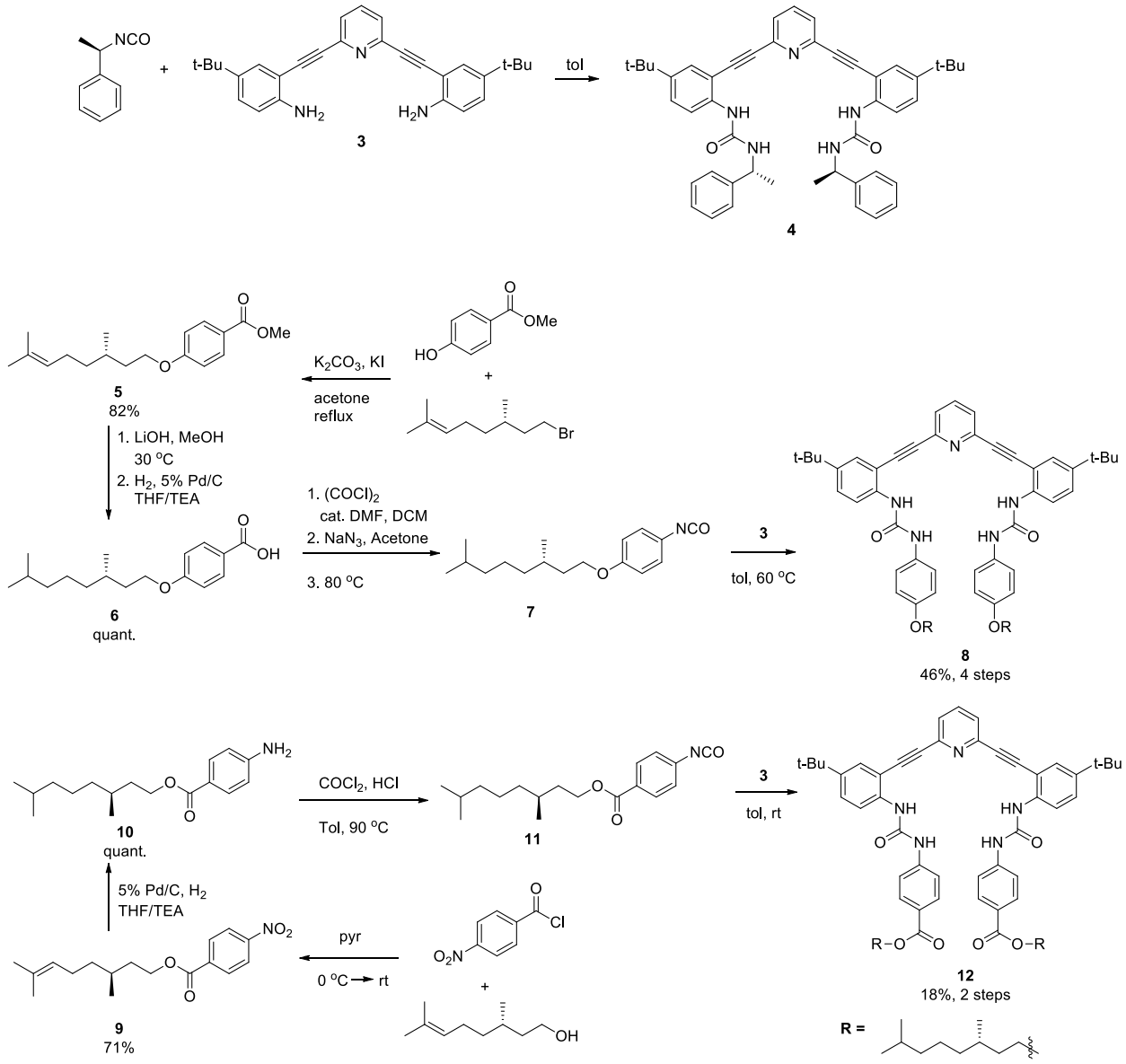

Scheme 1. Synthesis of chiral urea compounds **4, 8** and **12**.

Chiral **1a** analog **8** was synthesized first by treatment of methylparaben with commercially available citronellyl bromide under basic conditions. The chiral ester **5** was subsequently saponified with lithium hydroxide in methanol at 30 °C, followed by

hydrogenation in THF to yield **6** in quantitative yield over the two steps. Carboxylic acid **6** was treated with oxalyl chloride in dichloromethane in the presence of catalytic DMF. The crude acid chloride was carried on to the acyl azide without purification by treatment with sodium azide in acetone. The crude acyl azide was then converted to the isocyanate by Curtius rearrangement at 80 ^{o}C in toluene. Treatment of the isocyanate with dianiline **3** yielded **8,** the analog of **1a** in 46% yield over the 4 steps.

Lastly, chiral **1b** analog **12** was synthesized first by treatment of citronellol with *p*-nitrobenzoyl chloride in pyridine, yielding the nitrophenyl ester **9** in moderate yield. Hydrogenation of this compound yielded the chiral aniline **10** in quantitative yield, which was carried on to the isocyanate by treatment with phosgene in slightly acidic toluene. Isocyanate **11** was carried on to the final product without purification by treatment of **3** in toluene with **11**, yielding the product in 18% isolated yield.

The optoelectronic spectra of **4**, **8** and **12** in $CHCl_3$ conform to the trends observed in each of these classes: alkyl analog **4** is fluorescent as the freebase, quenched when protonated with TFA, and recovers but red shifts in its emission upon exposure to Cl^-; and electron-poor **12** is OFF-ON in its response (Appendix D).

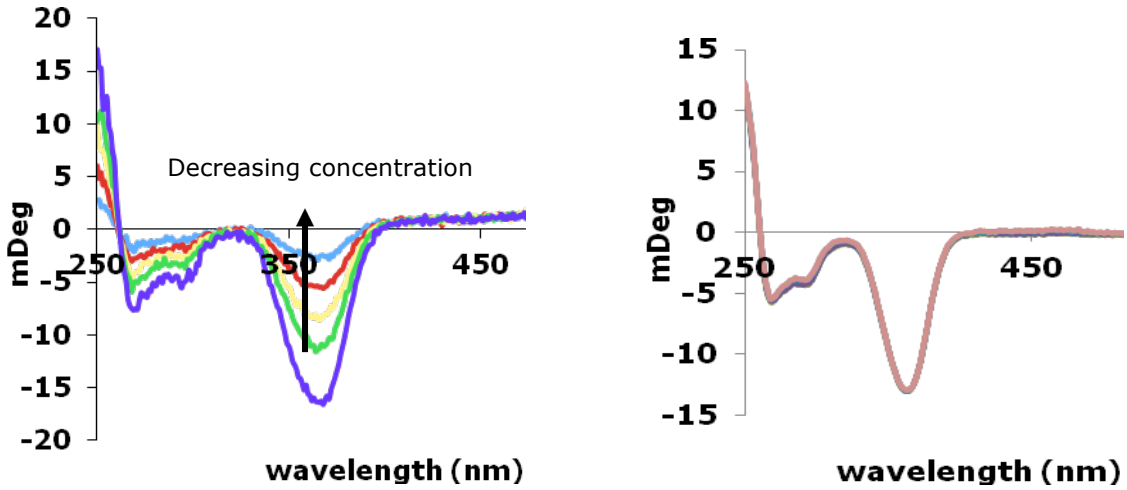

Figure 15. (Left) CD spectra of **4** with decreasing concentration (start: 7 µM final: 0.5 µM); (right) CD spectra of **4** with increasing TBACl concentration (7 µM **4** from 0 to 6.8 equiv TBACl).

Circular dichroism spectra of **4** were collected in $CHCl_3$, and resemble typical random coil spectra at shorter wavelengths (Figure 15).[16] During dilution experiments it was apparent from 7 µM to 0.5 µM that the linear change in intensity of the CD spectrum with decreasing concentration was consistent with simply a decrease in the presence of **4**. The attribution of this CD response to absorbance by the arylethynyl scaffold was confirmed by CD spectra of control solutions of the chiral benzyl moiety alone, which exhibited no CD response in the 300-375 nm portion of the spectrum. CD spectra match the absorbance bands seen in UV-Vis experiments and are visible out to 375 nm, indicating structural influence from the chiral positions on the absorbing ethynylpyridine backbone. This influence is most likely through intermolecular interaction due to the lack of conjugation between the pendant phenyl rings and the scaffold and our previous assertions about the dimeric nature of the neutral ureas in

solution. Supporting this hypothesis is the DFT-calculated lowest energy "W" conformation of the freebase form of the urea receptors, which would not result in chiral transfer from the benzyl groups to the scaffold in monomers of **4** in this conformation due to the distance between the arms in this conformation (Chapter IV). Treatment of neutral **4** with tetrabutylammonium chloride at 7 μM yielded no change in the CD spectrum, signaling either no Cl^- binding or a lack of influence of Cl^- binding on the structure of the neutral receptor in solution (Figure 15).

Titration with trifluoroacetic acid was more enlightening (Figure 16). The splitting observed in the CD spectrum at the π-π* transition band at 330 nm during titration with TFA can be assigned to positive exciton coupling between chromophores, and to a right-handed twist to the interacting π-systems.[16] Since the absorbing species in the non-conjugated (R)-(+)-methylbenzyl rings is not in conjugation with the scaffold, for CD activity to be seen in the low energy end of the spectrum the chiral information must be transferred to the arylethynylpyridine moiety. This can happen either by static conformational influence in the monomer or through the shape of the intermolecular aggregates.

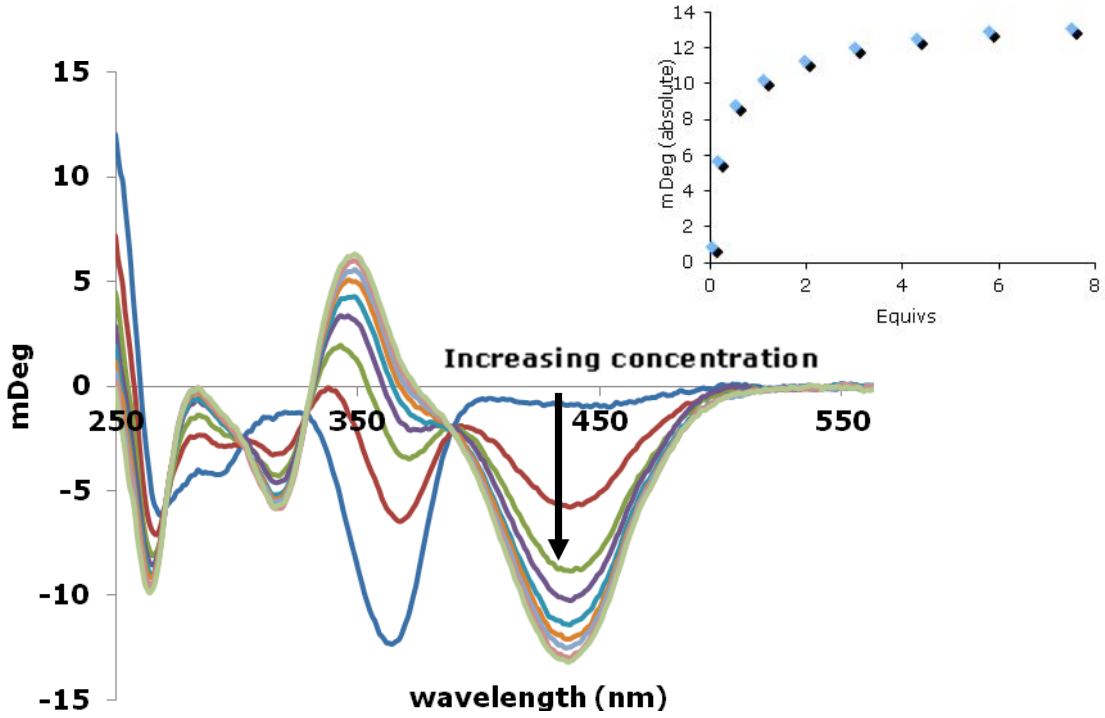

Figure 16. CD spectra of **4** during titration of TFA in $CHCl_3$ at 7 µM receptor (0 – 28 µM TFA). (Inset) Isotherm of the change in mDeg (absolute) during the titration at 445 nm shows that this change in the spectra is a function of the protonation of the pyridine, as the isotherm levels after 1 equiv.

Since the intensity of exciton coupling of this type is dependent upon the distance between chromophores it can be assumed that this bisignate Cotton effect at the π-π* band in the protonated receptor arises either from tightly associated aggregates or enforced chirality in the arene scaffold due to the conformation of the arms of the receptor around the anionic guest (Figure 17). [16]

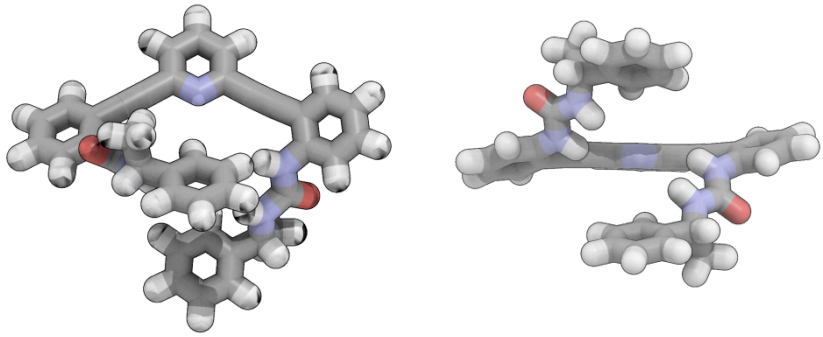

Figure 17. Illustrative MM3 minimized model of the simplest chiral conformation of the arylethynyl pyridine scaffold in **4.** (Left) Top view of a model representation of **4** and (right) side view illustrating the right-handed helical twist in the backbone that could give rise to a CD response in the low energy region of the spectra of monomers of **4·TFA**; however, the data support a more complex intermolecular arene-arene interaction.

Treatment of the end point of the TFA-**4** titrations with tetrabutylammonium chloride intensifies and shifts the absorbance bands. While there is no further change in the bisignate nature of the CD spectrum, these further changes in the spectra indicate a slight difference in conformation in solution between the two complexes, indicative of incorporation of Cl^- into the structure (Figure 18). The decrease in the absorbance bands at 330 – 360 nm is consistent with a decrease in the electronic dipole moment that could be attributed to a closer pyridinium NH•••X distance than that found with trifluoroacetate. This red-shifting of the entire spectrum is also indicative of closer arene-arene interactions, lending credence to the argument for aggregate formation.[16]

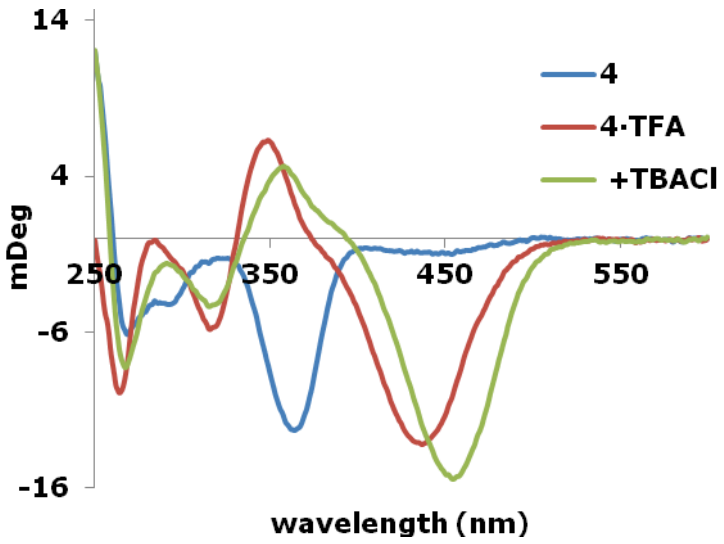

Figure 18. Comparison of **4**, **4·TFA** and **4·TFA** with a slight excess of TBACl.

Circular dichroism studies with the chiral analogs of **1a** and **1b**, and treatment of the protonated receptors with $TBANO_3$ are underway and have thus far not provided any stronger evidence of stacking than those with **4** presented above. While the data presented in this section are incomplete, even the weak evidence of ordered stacking observed thus far in these experiments is supportive of the general behavior of the achiral receptors in both solution and the solid-state. Future work on this project will focus on elucidating the structures of these receptors in concentrated solution, and relate these structural features to the optoelectronic responses observed in this family of compounds.

Conclusions

This chapter focused on both the application of urea-functionalized phenylethynyl scaffolds to *in vitro* imaging, fluorescent sensing of NO_3^- anion in organic

media by aggregation induced emission, and the self-assembled aggregates of these receptors around appropriately sized anionic guests to form topographically distinct nanostructures.

In summary, the fluorescence behavior and discrete, selective responses to target analytes exhibited by urea-functionalized anilinoethynyl pyridine structures augers well for their application as cellular probes for anions and as building blocks of well-defined nanoscale architectures. The columnar stacking observed in the solid-state is tentatively supported in even dilute solution, and seems to be dependent upon the anion involved. Anion-mediated self-assembly into well-defined structures is a lively field of research now, making these results exciting for the prospects of arylethynylpyridine-based research. Future work applying the design principles learned from this first generation of fluorionophores should lead to more effective and differentially selective materials suitable for application in advanced bioimaging and high-performance supramolecular materials.

Experimental

General Details. ^{1}H and ^{13}C NMR spectra were obtained on a Varian 300 MHz spectrometer (^{1}H 299.95 Hz, ^{13}C 75.43 Hz) or Inova 500 MHz spectrometer (^{1}H 500.10 MHz, ^{13}C 125.75 MHz) or Varian Inova 600 (^{1}H 599.98 MHz, ^{13}C 150.86 MHz) spectrometer. Chemical shifts (ð) are expressed in ppm downfield from tetramethylsilane (TMS) using non-deuterated solvent present in the bulk deuterated solvent ($CDCl_3$: ^{1}H 7.26 ppm, ^{13}C 77.0 ppm; CD_2Cl_2: ^{1}H 5.32 ppm ^{13}C 54.0 ppm). Unless

otherwise specified, solvents were obtained from distillation using published literature procedures directly before use.

Mass spectra were acquired on a Thermo Finnigan LCQ Deca XP Plus electrospray ionization spectrometer in positive mode in MeOH solvent.

UV-Vis spectra were acquired with a Hewlett-Packard 8453 UV-Visible spectrophotometer equipped with a 250 nm cutoff filter.

Fluorescence data were acquired with a Horiba Jobin-Yvon FluoroMax-4 fluorescence spectrophotometer equipped with an integrating sphere. All spectra were uncorrected for lamp response unless otherwise specified. All slit widths (ex/em) were held constant at 5 nm/5 nm, and quantifiable data was obtained by correction of the spectra to lamp response and/or integrating sphere reflectivity.

Circular dichroism spectra were acquired on a Jasco J-815 CD Spectropolarimeter in standard sensitivity mode (50-100 nm/min scan rate) at 20 ^{o}C.

Experimental conditions for fluorescence measurements, excitation spectra, vesicle preparation and ^{1}H-NMR data can be found in Appendix D.

Methylbenzyl urea 4. All glassware was flame-dried before use. Dianiline **3** (800 mg, 1.9 mmol) was reacted with (R)-(+)-α-methylbenzyl isocyanate (3 equiv) in 25 mL toluene with stirring for 3 h under N_2. Following concentration *in vacuo*, the crude product was filtered through a short silica plug (2:1 hexanes/$CHCl_3$). Trituration with Et_2O afforded **4** (82%) as an amorphous white solid. ^{1}H-NMR (600 MHz, $CDCl_3$): δ 8.01 (d, *J* = 8.9 Hz, 2H), 7.51 (t, *J* = 7.8 Hz, 1H), 7.44 (br s, 2H), 7.41 (d,

J = 2.4 Hz, 2H), 7.35 (d, *J* = 7.8 Hz, 2H), 7.32-7.28 (m, 6H), 7.21 (t, *J* = 7.8 Hz, 4H), 7.13 (t, *J* = 7.2 Hz, 2H), 6.26 (br s, 2H), 4.94 (pentet, *J* = 7.2 Hz, 2H), 1.41 (d, *J* = 7.2 Hz, 6H), 1.28 (s, 18H); ^{13}C-NMR (600 MHz, $CDCl_3$): δ 154.76, 144.91, 144.19, 142.87, 138.89, 128.45, 126.06, 119.39, 109.84, 92.97, 87.64, 34.18, 31.25, 31.19.

Methylester 5. To a 10 mL round bottomed flask equipped a stir bar, reflux condensor and N_2 inlet was added methyl paraben (100 mg, 0.657 mmol), citronellyl bromide (152 mg, 0.696 mmol), potassium carbonate (93 mg, 0.670 mmol) in 5 mL acetone. The mixture was refluxed 20 h. Upon completion, the reaction was concentrated *in vacuo*, taken up in 15 mL EtOAc and washed thrice with water. After drying over $MgSO_4$, the crude material was concentrated *in vacuo* and purified by column chromatography (10% EtOAc/hexanes) to yield a colorless oil (82%). ^{1}H-NMR (300 MHz, $CDCl_3$): δ 7.98 (d, *J* = 8.7 Hz, 2H), 6.90 (d, *J* = 8.7 Hz, 2H), 5.10 (unresolved tt, *J* = 1.5, 4.2 Hz, 1H), 4.03 (m, 2H), 2.00 (pentet, *J* = 7.5 Hz, 2H), 1.84 (m, 1H), 1.64-1.53 (m, 8H), 1.40-1.20 (m, 2H), 0.96 (d, *J* =6.3 Hz, 3H).

Carboxylic acid 6. To a 25 mL round bottomed flask containing LiOH (72 mg, 1.72 mmol) in 2:1 MeOH/H_2O (12 mL) was added the ester **5** (100 mg, 0.344 mmol) as a solution in MeOH (4 mL) such that the final ratio was 3:1 MeOH/H_2O. The resulting mixture was stirred at 35 ^{o}C for 24 h and cooled to rt. A dilute NH_4Cl solution was added until the pH reached 8. This solution was then treated dropwise with dilute aqueous acetic acid until the pH reached 5. This was acidified with aqueous HCl until white precipitate was formed (pH 4). The precipitate was collected by suction filtration and dried with EtOH. This white precipitate was taken up in 15

mL THF/TEA (5:1) in a Parr flask, to which was added 5% Pd/C (50 mg) and the suspension was shaken with H_2 at 45 psi for 45 minutes. Upon completion the reaction was acidified with 10% aqueous HCl, filtered and dried over $MgSO_4$ to yield **7** quantitatively. ^{1}H-NMR (300 MHz, $CDCl_3$): δ 8.09 (d, *J* = 4.8 Hz, 2H), 6.96 (d, *J* =4.8 Hz, 2H), 5.12 (unresolved tt, *J* = 1.8, 5.4 Hz, 1H), 4.08 (m, 2H), 2.03 (septet, *J* = 7.5 Hz, 2H), 1.85 (pentet, 4.8 Hz, 1H), 1.69 (m, 8H), 1.43-1.21 (m, 3H), 0.97 (d, *J* = 6.3 Hz, 3H).

Alkoxyphenyl urea 8. In a flame-dried 50 mL round bottomed flask was added **7** (100 mg, 0.342 mmol) in 20 mL dichloromethane under argon. Oxalyl chloride (56.4 mg, 0.444 mmol) was added followed by 2 drops DMF. This solution was allowed to stir to completion (until bubbles stopped forming, 2 h) whereupon it was evaporated to dryness, forming a glass on the walls fo the flask. To this was added 3 mL acetone and cooled to 0 ^{o}C in an ice bath. Sodium azide (26.5 mg, 0.408 mmol) was added as a solution in water (1 mL) and this was allowed to reach rt over 3 h. Upon completion the solution was evaporated to dryness *in vacuo* and rediluted in 10 mL freshly distilled toluene and evaporated again *in vacuo*. This was repeated thrice, whereupon a an additional 10 mL dry toluene was added and the solution was brought to 90 ^{o}C. Once bubbling stopped (~3 h), dianiline **3** (60 mg, 0.142 mmol) was added and the solution allowed to stir 3 h. Upon completion, the reaction was concentrated *in vacuo* and purified by column chromatography (15-50% EtOAc/hexanes, 5% TEA) to yield a semi-pure product. This was subsequently taken up in 1 mL $CHCl_3$ and purified by GPC (retention time 46 min at 3 mL/min) to yield

the product (88 mg, 46%) as a colorless solid. ^{1}H-NMR (300 MHz, $CDCl_3$): δ 8.15 (d, *J* = 8.7 Hz, 4H), 7.72 (s, 2H), 7.33 (m, 13H), 6.72 (d, *J* = 8.7 Hz, 4H), 3.86 (t, *J* = 7.2 Hz, 4H), 1.80-1.5 (m, 8H), 1.36-1.10 (m, 38H), 0.96 (d, *J* = 4.5 Hz, 6H), 0.90 (d, *J* = 6.6 Hz, 12H). ^{13}C-NMR (300 MHz, $CDCl_3$): δ 202.69, 161.10, 154.06, 152.43, 150.21, 146.31, 144.41, 138.60, 136.31, 135.78, 130.06, 122.40, 116.99, 95.26, 74.11, 46.86, 44.96, 43.88, 41.81, 38.87, 37.46, 35.58, 32.28, 30.33, 27.26.

Nitrobenzene 9. In a flame-dried 50 mL round bottomed flask was combined nitrobenzoyl chloride (1.06 g, 5.73 mmol) and pyridine (20 mL). The flask was cooled to 0 ^{o}C in an ice bath and to this was added citronellol (1 mL, 5.46 mmol) dropwise. The reaction was allowed to reach rt, whereupon it was concentrated *in vacuo* and taken up in EtOAc. This was washed thrice with saturated $NaHCO_3$ followed by brine and dried over $MgSO_4$. Concentration yielded the product as a yellowish oil (182 mg, 71%). ^{1}H-NMR (300 MHz, $CDCl_3$): δ 8.30 (d, *J* =8.7 Hz, 2H), 8.20 (d, *J* = 8.7 Hz, 2H), 5.09 (unresolved tt, 1H), 4.40 (t, *J* =6.9 Hz, 2H), 2.01 (pentet, *J* = 7.8 Hz, 2H), 1.82 (m, 2H), 1.67-1.59 (m, 9H), 1.46-1.34 (m, 1H), 1.25 (pentet, *J* = 7.5 Hz, 2H), 0.982 (d, *J* = 6.3 Hz, 3H).

Alkylbenzoate aniline 10. In a Parr flask was combined in 15 mL THF/TEA (5:1) **9** (1.00g, 3.27 mmol) and 30% Pd/C (55 mg). The flask was pressurized with H_2 (45 psi) and allowed to shake for 3h. Upon completion the mixture filtered through Celite and concentrated *in vacuo* to yield a yellowish oil (900 mg, 99%). ^{1}H-NMR (300 MHz, $CDCl_3$): δ 7.86 (d, *J* = 8.4 Hz, 2H), 6.67 (d, *J* = 8.4 Hz, 2H), 4.29 (t, *J* = 6.9 Hz, 2H),

1.99 (pentet, *J* = 7.5 Hz, 1H), 1.76 (m, 1H), 1.67-1.52 (m, 8H), 1.32-1.13 (m, 7H), 0.87 (d, *J* = 8.6 Hz, 3H), 0.85 (d, *J* = 7.5 Hz, 6H).

Alkylbenzoate urea 12. To a flame-dried 50 mL three-neck round bottomed flask equipped with a stirbar, reflux condensor, N_2 bubbler and addition funnel (25 mL) was added 20% phosgene in toluene (9g, 18.03 mmol). A salt suspension was formed by bubbling anhydrous HCl through **10** (500 mg, 1.80 mmol) in toluene (20 mL) and this was added to the addition funnel. The reaction flask was heated to 90 ^{o}C and dropwise addition of the aniline salt was carried out overnight. The reaction solution was then evaporated to ½ its volume whereupon **3** was added (250 mg, 0.60 mmol) and the reaction was stirred to completion by TLC (10% EtOAc/hexanes). Upon completion, the reaction was concentrated *in vacuo* and taken back up in $CHCl_3$. The organics were washed thrice with saturated $NaHCO_3$ and brine and dried over $MgSO_4$. Purification by GPC (retention time 49 min at 3 mL/min) yielded the pure product (88 mg) as an orange solid. ^{1}H-NMR (300 MHz, $CHCl_3$): δ 8.81 (br s, 2H), 8.20 (br s, 2H), 8.00 (d, *J* = 8.7 Hz, 2H), 7.918 (t, *J* = 8.8 Hz, 1H), 7.81 (d, *J* = 8.1 Hz, 4H), 7.48 (m, *J* = 8.4 Hz, 4H), 7.39-7.29 (m, 8H), 4.28 (t, *J* = 7.2 Hz, 4H), 1.77 (pentet, 4H), 1.66-1.47 (m, 5H), 1.37-1.14 (m, 28H), 0.94 (d, *J* = 6.3 Hz, 6H), 0.86 (d, *J* = 6.6 Hz, 12H). ^{13}C-NMR (600 MHz, DMSO-d_6): δ 166.27, 152.64, 145.61, 142.84, 137.56, 130.63, 128.97, 128.16, 126.35, 124.59, 119.16, 118.24, 109.88, 92.83, 87.64, 63.42, 39.19, 37.16, 35.58, 34.22, 31.17, 30.01, 27.92, 24.61, 22.68, 22.59, 19.62.

CHAPTER VI

CONCLUDING SUMMARY

The work presented herein represents two main focal areas of my doctoral research: the design and synthesis of fluorescent receptors and the study of their self-assembled complexes with anions. This project had its genesis in both the metal cation self-assembly and anion-π research of the Darren W. Johnson lab and the metallated arylethynyl scaffolds and optoelectronic materials being investigated in the Michael M. Haley lab at the time. The course of research that led from these two seemingly disparate fields to a sensor for anions, and ultimately a fluorescent probe for chloride that functioned *in vitro,* led me to focus much of my efforts on the mechanisms of photoluminescence in these molecules.

Research started with a survey of the synthetic ionophore and sensor literature to identify ideal targets and design strategies, which was partially summarized in the introductory chapter of this dissertation. The incorporation of rigid phenylacetylenic linkers was found to lend tenability both to the optoelectronic responses and the solution-phase shape-persistence of the sensor, and is a key structural feature in this class of receptors. Additionally, these easily functionalizable moieties allow for facile expansion or contraction of the conjugation in the fluorophore, thereby lending us a simple pathway to binding site size and bite-angle modification while eschewing the typical fluorophore-spacer-receptor motif of many synthetic probes.

The proof-of-principle work outlined in Chapter II convinced us that our design strategy was viable. The well documented binding behavior of metal cations was used to test the hypothesis that perturbation of the electronic system in our receptor scaffold would result in easily observable changes in the receptor's optoelectronic output upon binding. The confirmation of this behavior in our system allowed us to begin tuning our probe design towards anionic targets.

The results of our halide binding studies in both solution and the solid state were outlined in Chapter III. Binding studies focused on the urea-functionalized receptors due to the complex speciation apparent in solutions of sulfonamide-functionalized compounds and the apparent [1 + 1] binding stoichiometry in the protonated ureas. While the neutral receptors showed a preference for the smaller halides, this trend was reversed upon protonation and the strength of the binding interaction was increased by at least an order of magnitude.

Chapter IV focused on the fluorescence responses of the receptor. In electron-rich receptors containing a pendant phenyl ring the fluorescence emission observable in the neutral state was effectively quenched upon protonation. This trend was reversed in solutions of the electron-poor receptors. In those functionalized without a direct urea NH-phenyl linkage on the pendant moiety the fluorescence emission could be recovered upon treatment with chloride. These results were promising for the use of functionalized arylethynylpyridine scaffolds as probes in both binary (ON-OFF or OFF-ON) or tertiary (ON-OFF-ON) modes. The mechanisms behind this fluorescence were found to be governed by excimeric interactions in the case of OFF-ON receptors,

whereas the ON-OFF response appeared to be due to mundane pyridinium electron transfer quenching. The excimer-like behavior observed in the OFF-ON responsive receptors is attributable to ground-state complexes, rather than excited-state interactions in solution.

In vitro assays yielded surprising preliminary results, which were outlined in Chapter V. Unexpectedly, the ON-OFF response in the methoxyphenyl-functionalized urea receptor was inverted, and this receptor functioned as an OFF-ON responsive probe for Cl^- in cellular matrices. The mechanism governing this newly observed fluorescence is unclear, but seems to be due to aggregation induced emission in poor solvents such as water. Restricted intermolecular rotation in the aggregated sensor gives rise to some of the emission, while close-contact intermolecular interactions in Cl^- induced assemblies of this receptor gives rise to excimer-like green fluorescence, even in competitive hydrogen-bonding media. This anion-induced effect was the key to signaling for Cl^-, and seems to be exploitable in the nitrophenyl urea functionalized receptors as well. Preliminary results from TEM studies of the nanoscale self-assembly observed upon evaporation of acetonitrile from this receptor were also reported. These results underscore the need for more investigation of the aggregate structure and the self-assembly process, and are the obvious direction to take this research in the future.

APPENDIX A

SUPPORTING INFORMATION FOR CHAPTER II:

SYNTHESIS OF FIRST GENERATION DERIVATIVES AND PROOF OF PRINCIPLE

Titration Data

In all titrations care was taken to keep the receptor concentration constant during the titration. A stock solution of receptor was prepared and the guest serial dilution was prepared with the stock receptor solution. Receptor concentration was thus kept constant while titrating in the guest solution to avoid concentration effects and to provide clean isosbestic points in the UV spectra. All additions were done through septa with a Hamilton gas-tight syringe. Titrations were carried out in triplicate. Representative data are provided for each set.

$Zn(NO_3)_2$ Titration. A 3.07 mM solution of $Zn(NO_3)_2$ and a 3.07 μM solution of **13** were prepared. Starting vol in cuvet of 1 mL.

anion stock added (ml)	mol anion total	[X-] M
0	0	0
0.01	3.42532E-08	1.71265E-05
0.01	6.85065E-08	3.42529E-05
0.01	1.0276E-07	5.13791E-05
0.01	1.37013E-07	6.85051E-05
0.01	1.71266E-07	8.56309E-05
0.01	2.05519E-07	0.000102757
0.01	2.39773E-07	0.000119882
0.01	2.74026E-07	0.000137007
0.01	3.08279E-07	0.000154133
0.01	3.42532E-07	0.000171258
0.02	4.11039E-07	0.000205507

0.02	4.79545E-07	0.000239756
0.02	5.48052E-07	0.000274004
0.02	6.16558E-07	0.000308251
0.02	6.85065E-07	0.000342498
0.02	7.53571E-07	0.000376744
0.02	8.22078E-07	0.000410989
0.02	8.90584E-07	0.000445234
0.02	9.59091E-07	0.000479478
0.02	1.0276E-06	0.000513721
0.04	1.16461E-06	0.000582206
0.04	1.30162E-06	0.000650688
0.04	1.43864E-06	0.000719167
0.04	1.57565E-06	0.000787643
0.04	1.71266E-06	0.000856117
0.08	1.98669E-06	0.000993056
0.08	2.26071E-06	0.001129984
0.08	2.53474E-06	0.001266901
0.08	2.80877E-06	0.001403807
0.08	3.08279E-06	0.001540702
0.16	3.63084E-06	0.00181446
0.32	4.72695E-06	0.002361843
0.32	5.82305E-06	0.002909052

Table 1. Representative titration conditions for **13** and Zn(II).

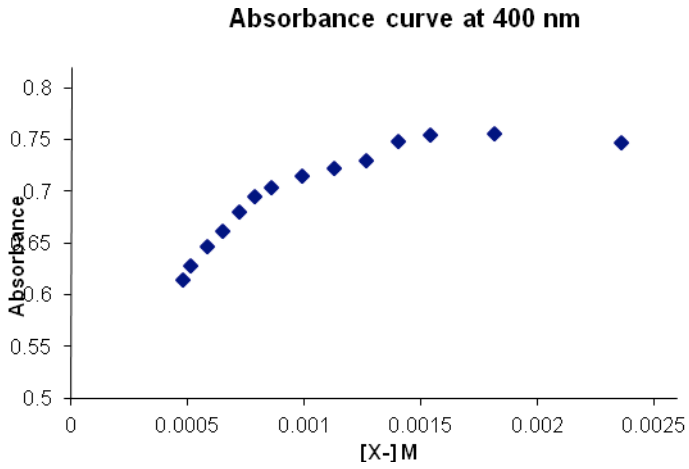

Figure 1. Isotherm plotted by following the absorbance at 400 nm of **13** during Zn(II) titration.

APPENDIX B

SUPPORTING INFORMATION FOR CHAPTER III:

ANION BINDING: SELECTIVITY EFFECTS AND SOLID-STATE CONFORMATION

Titration Details

In all titrations care was taken to keep the receptor concentration constant during the titration. A stock solution of receptor was prepared and the guest serial dilution was prepared with the stock receptor solution. Receptor concentration was thus kept constant while titrating in the guest solution to avoid concentration effects on the urea N–H proton chemical shifts and provide clean isosbestic points in the UV spectra. All additions were done through septa with a Hamilton gas-tight syringe. Titrations were carried out in triplicate and the reported binding constants represent the average of the fits from three titrations. Representative data are provided for each set.

NMR Titration Conditions. ^{1}H NMR titrations were carried out on an Inova 500 MHz spectrometer (^{1}H 500.10 MHz). Chemical shifts (δ) are expressed in ppm downfield from tetramethylsilane (TMS) using non-deuterated solvent present in the bulk deuterated solvent ($CDCl_3$: ^{1}H 7.26 ppm). $CDCl_3$ was passed over activated alumina and saturated with deionized water (1:1 v/v $CDCl_3$ and water were mixed in a separatory funnel and the organic layer was collected). Tetrabutylammonium salts were used as purchased from TCI America.

Tetrabutylammonium chloride. A 10 mL stock solution of **2a** (12.60 mg, [R]=1.60 mM) in $CDCl_3$ was prepared and used in the dilution of TBACl guest solution (9.11 mg, [G]=16.40 mM). Starting volume of 700 µL.

Addition (uL)	Volume of Anion (uL)	[TBACl]	Equivalents	s	s
0	0	0.00E+000	0	8.073	7.806
5	5	1.16E-004	0.07254619	8.184	7.854
5	10	2.31E-004	0.144070602	8.282	7.897
5	15	3.43E-004	0.214594673	8.374	7.938
5	20	4.55E-004	0.284139243	8.461	7.976
5	25	5.65E-004	0.352724577	8.541	8.011
5	30	6.73E-004	0.420370387	8.610	8.041
5	35	7.80E-004	0.487095845	8.681	8.072
5	40	8.85E-004	0.552919608	8.745	8.101
5	45	9.89E-004	0.61785983	8.803	8.126
5	50	1.09E-003	0.681934183	8.855	8.150
5	55	1.19E-003	0.745159869	8.907	8.171
5	60	1.29E-003	0.807553638	8.953	8.193
5	65	1.39E-003	0.869131802	8.996	8.211
5	70	1.49E-003	0.92991025	9.034	8.228
5	75	1.58E-003	0.989904459	9.075	8.246
5	80	1.68E-003	1.049129512	9.111	8.262

Table 1. Representative titration table for TBACl titration with **2a**.

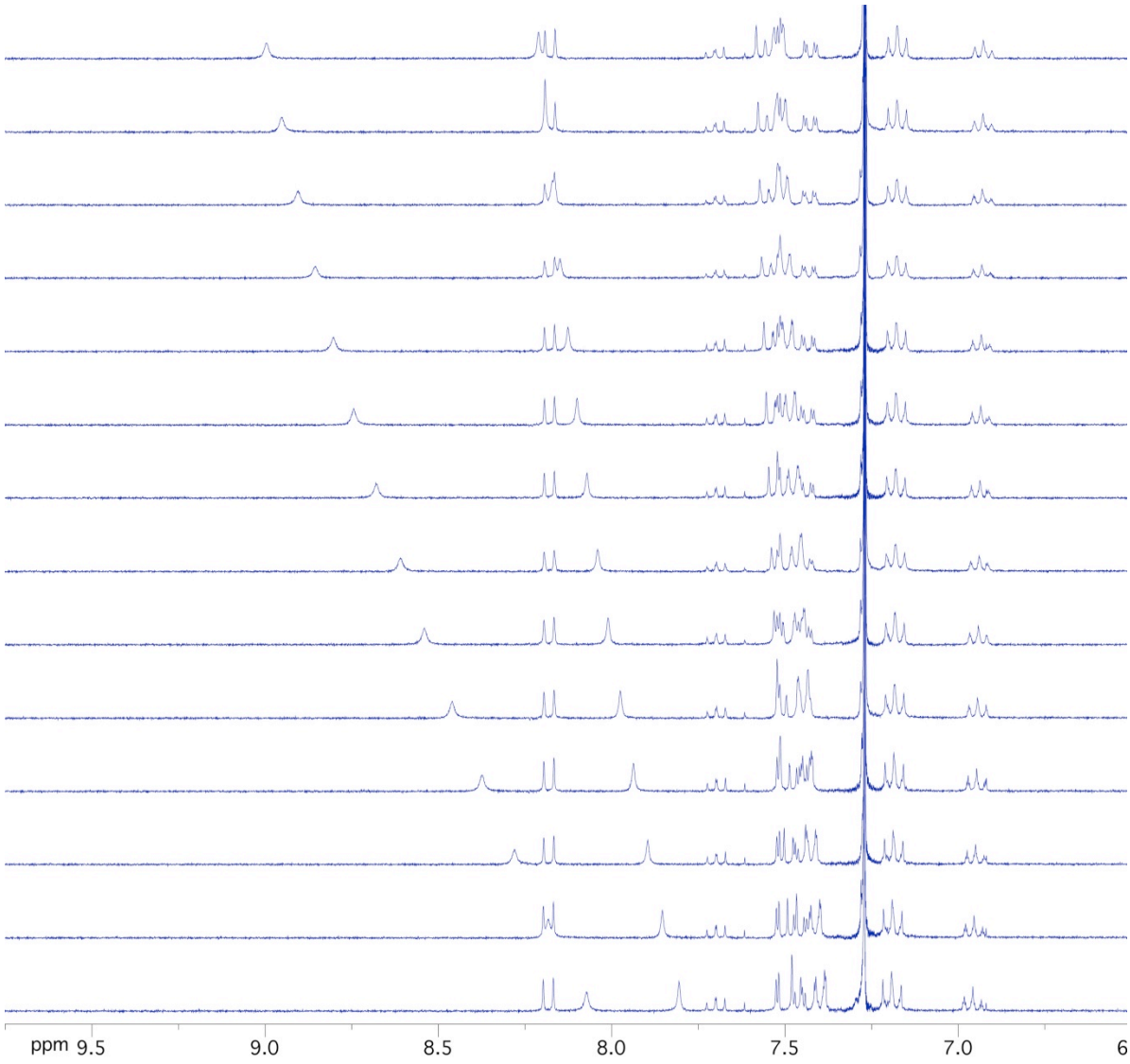

Figure 1. Representative ^{1}H-NMR spectra during the titration of **2a** with TBACl.

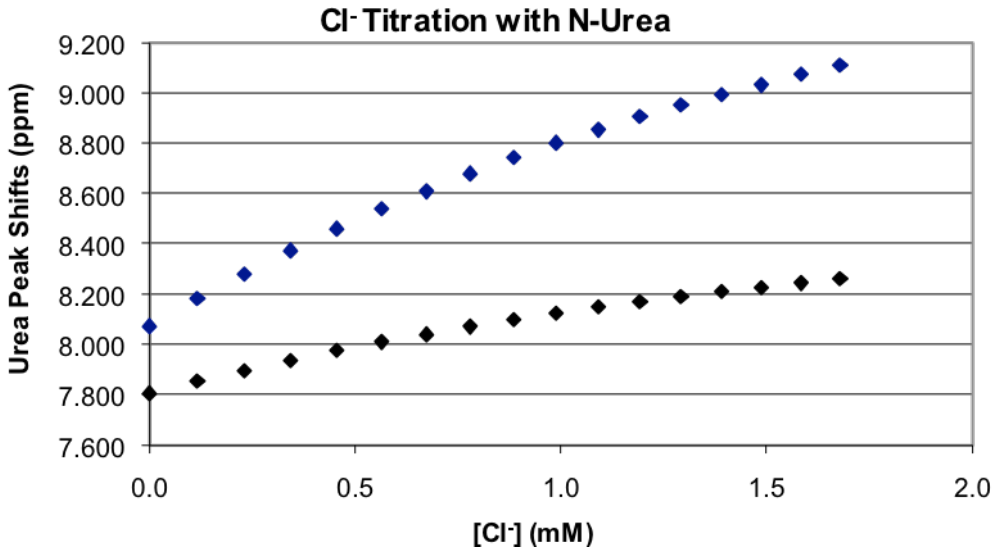

Figure 2. Isotherms formed from plotting the urea chemical shifts during **2a** titration with TBACl in $CDCl_3$.

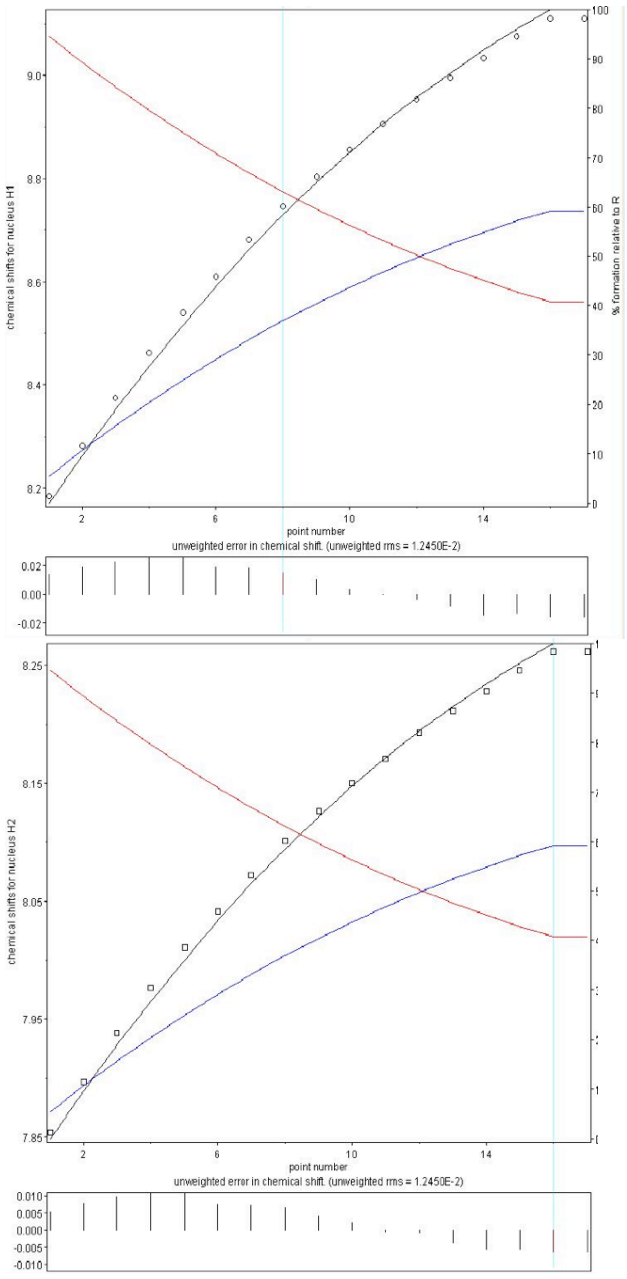

Figure 3. Non-linear regressional fits of the chemical shifts of the urea protons with RMS residuals.

Tetrabutylammonium bromide. A 10 mL stock solution of **2a** (10.90 mg, [R]=1.38 mM) in $CDCl_3$ was prepared and used in the dilution of TBABr guest solution (34.8 mg, [G]=54.00 mM). Starting volume of 700 µL.

Addition (uL)	Volume of Anion (uL)	[TBABr]	Equivalents	s	s
0	0	0.00E+000	0.000	8.086	7.810
2	2	1.54E-004	0.111	8.160	7.843
2	4	3.07E-004	0.221	8.214	7.867
2	6	4.59E-004	0.331	8.270	7.890
2	8	6.10E-004	0.440	8.316	7.912
2	10	7.60E-004	0.549	8.364	7.932
2	12	9.10E-004	0.657	8.407	7.951
2	14	1.06E-003	0.764	8.445	7.969
2	16	1.21E-003	0.871	8.484	7.986
2	18	1.35E-003	0.977	8.522	8.001
2	20	1.50E-003	1.083	8.557	8.017
2	22	1.64E-003	1.188	8.591	8.032
2	24	1.79E-003	1.292	8.624	8.046
2	26	1.93E-003	1.396	8.652	8.059
2	28	2.08E-003	1.499	8.681	8.071
2	30	2.22E-003	1.602	8.708	8.082
5	35	2.57E-003	1.856	8.773	8.112
5	40	2.92E-003	2.107	8.828	8.136
5	45	3.26E-003	2.354	8.879	8.159
5	50	3.60E-003	2.598	8.927	8.184
5	55	3.93E-003	2.839	8.967	8.197
5	60	4.26E-003	3.077	9.007	8.214
10	70	4.91E-003	3.543	9.072	8.243
10	80	5.53E-003	3.997	9.131	8.268
10	90	6.15E-003	4.440	9.179	8.289
10	100	6.75E-003	4.872	9.222	8.308

Table 2. Representative titration table for the titration fo **2a** with TBABr in $CDCl_3$.

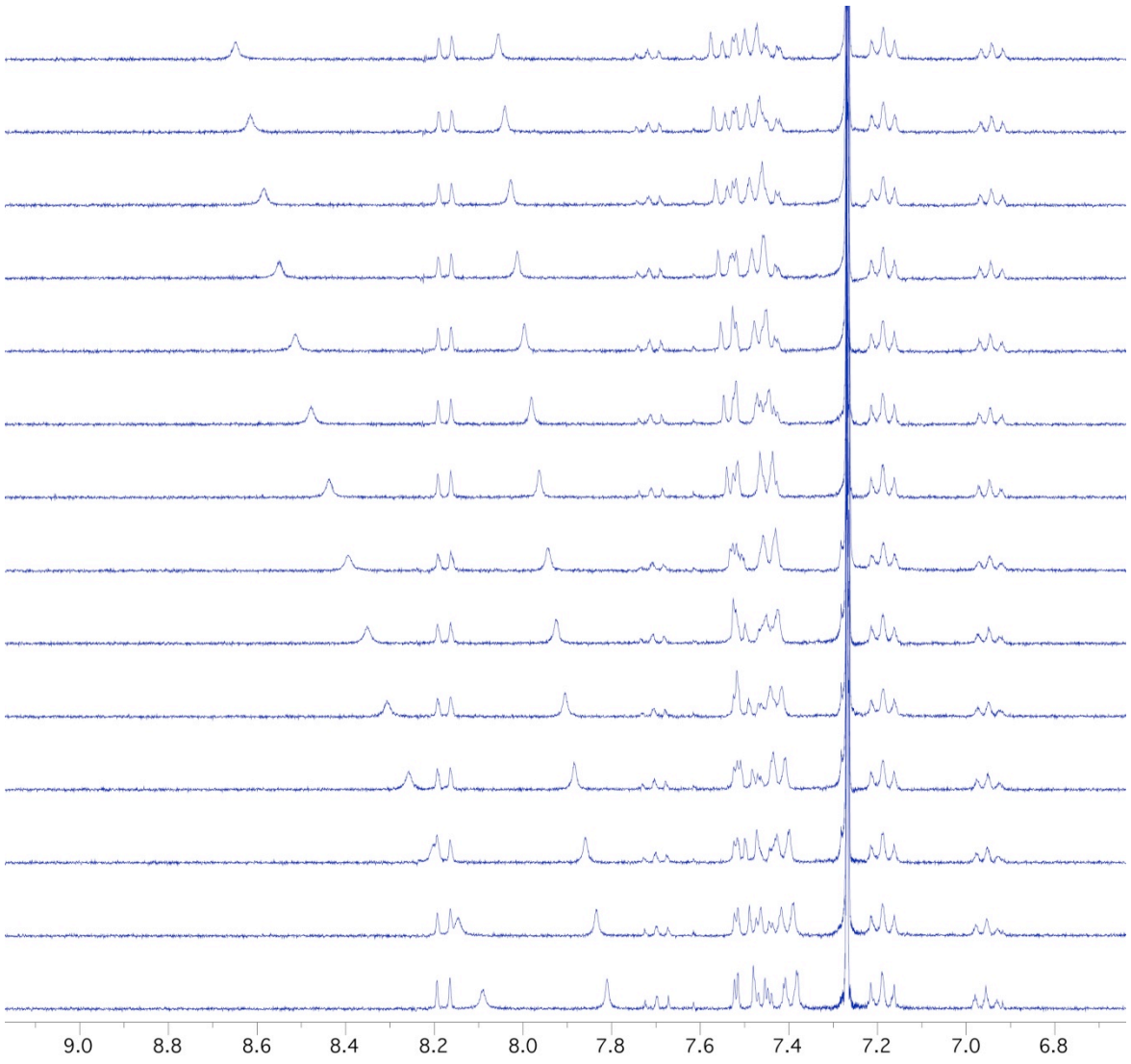

Figure 4. ^{1}H-NMR spectra of the titration of **2a** with TBABr in $CDCl_3$.

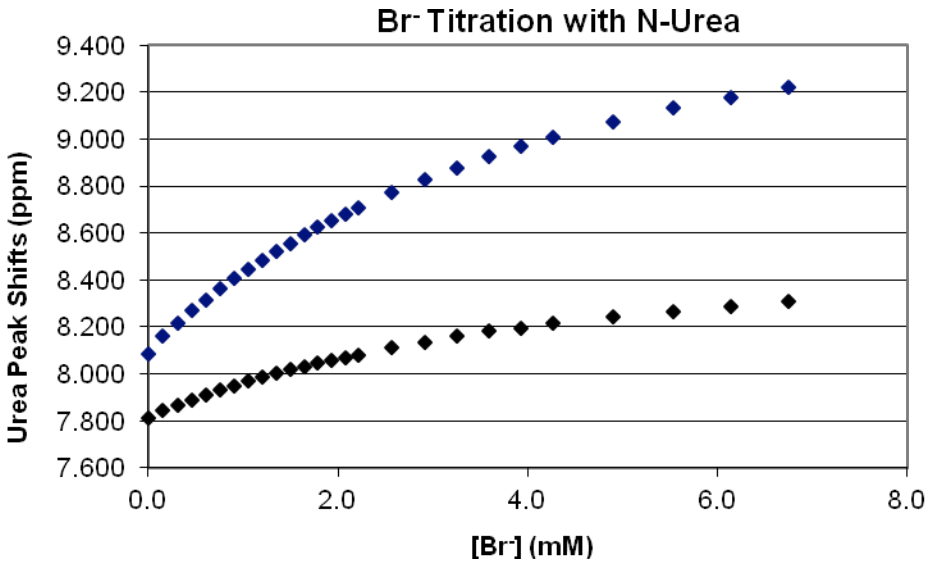

Figure 5. Isotherms formed from plotting the chemical shifts of the urea protons of **2a** during titration with TBABr.

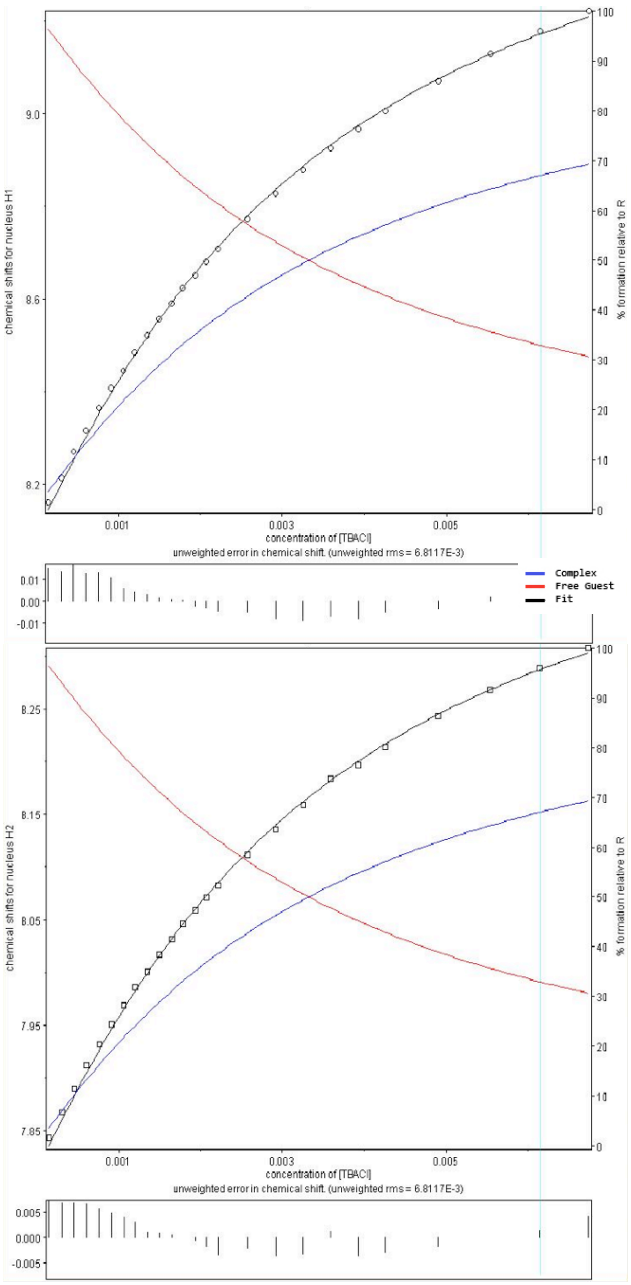

Figure 6. Non-linear regressional fits of the isotherms in Figure 5.

Tetrabutylammonium iodide. A 10 mL stock solution of **2a** (11.60 mg, [R]=1.47 mM) in $CDCl_3$ was prepared and used in the dilution of TBAI guest solution (36.3 mg, [G]=54.00 mM). Starting volume of 700 µL. Titration to 2 equiv with 5 µL aliquots

showed no shift in the N-H protons from the initial spectrum. Plotting N-H chemical shifts vs [TBAI] yielded flat isotherms. No binding was measurable.

UV-Vis Titration Conditions

UV-Vis titrations held the receptor concentration constant as in the ^{1}H NMR titrations. Spectroscopically pure CH_3CN was passed over basic alumina, dried over 4 Å molecular sieves, and used immediately. Tetrabutylammonium salts were purchased from TCI America and purified by recrystallization and heating above the melting point *in vacuo* or by sublimation.

Tetrabutylammonium chloride. A 10 mL stock solution of **2a•TFA** (6.01 mg, 7.77 µmol) in CH_3CN was prepared and used in the dilution of TBACl guest solution (5.02 mg, 18.00 µmol). Serial dilution to [Host]= 6.00 x 10^{-5} ; [Guest]= 4.00 x 10^{-4}. Host starting volume of 2 mL.

Additions	Total TBACl (mL)	mol Cl- Delivered	[Cl] Cuvett
0	0	0	0
1	0.01	4.00E-06	2.00E-06
2	0.02	8.00E-06	4.00E-06
3	0.03	1.20E-05	6.00E-06
4	0.04	1.60E-05	8.00E-06
5	0.05	2.00E-05	1.00E-05
6	0.06	2.40E-05	1.20E-05
7	0.07	2.80E-05	1.40E-05
8	0.08	3.20E-05	1.60E-05
9	0.09	3.60E-05	1.80E-05
10	0.1	4.00E-05	2.00E-05
11	0.11	4.40E-05	2.20E-05
12	0.12	4.80E-05	2.40E-05
13	0.13	5.20E-05	2.60E-05
14	0.14	5.60E-05	2.80E-05
15	0.15	6.00E-05	3.00E-05
16	0.3	1.20E-04	6.00E-05
17	0.45	1.80E-04	9.00E-05
18	0.6	2.40E-04	1.20E-04
19	0.75	3.00E-04	1.50E-04
20	0.9	3.60E-04	1.80E-04
21	1.05	4.20E-04	2.10E-04
22	1.2	4.80E-04	2.40E-04
23	1.35	5.40E-04	2.70E-04
24	1.5	6.00E-04	3.00E-04
25	1.65	6.60E-04	3.30E-04

Table 3. Representative titration table for titration of **2a·TFA** with TBACl.

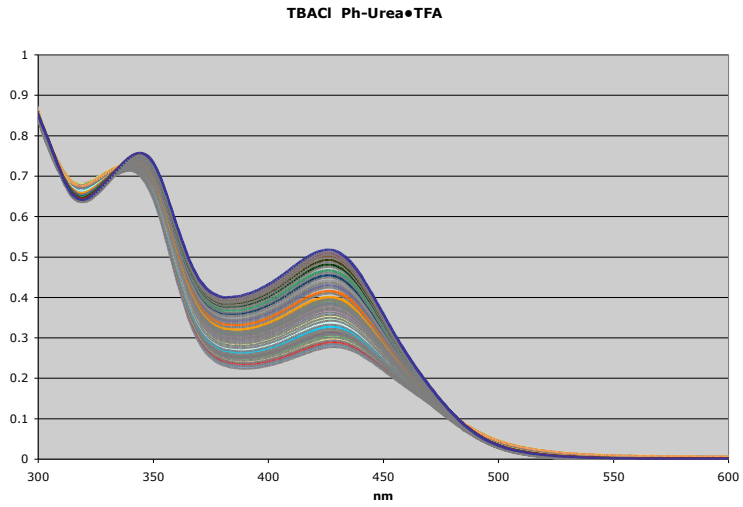

Figure 7. UV-Vis spectra illustrating the change in absorbance during titration of **2a·TFA** with TBACl.

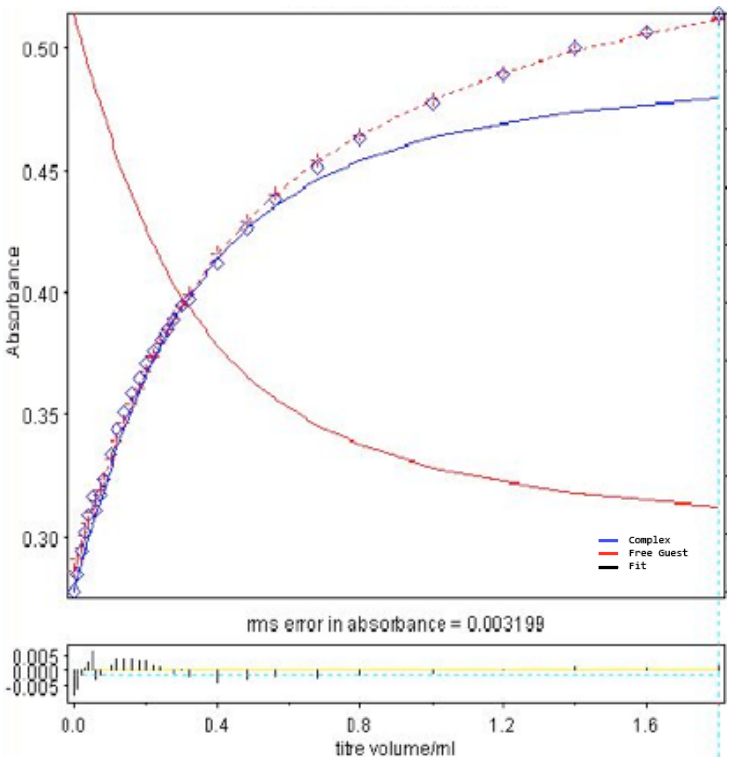

Figure 8. Non-linear regressional fit of the change in absorbance during titration of **2a·TFA** with TBACl.

Tetrabutylammonium bromide. A 10 mL stock solution of **2a•TFA** (6.01 mg, 7.77 µmol) in CH_3CN was prepared and used in the dilution of TBABr guest solution (12.26 mg, 38.03 µmol). [Host]= 8.20 x 10^{-5} ; [Guest]= 1.82 x 10^{-3}. Host starting volume of 2.00 mL.

Additions	Total TBABr (mL)	mol Br-	[Br-] Cuvett
0	0	0	0
1	0.01	1.82E-05	9.10E-06
2	0.02	3.64E-05	1.82E-05
3	0.03	5.46E-05	2.73E-05
4	0.04	7.28E-05	3.64E-05
5	0.05	9.10E-05	4.55E-05
6	0.06	1.09E-04	5.46E-05
7	0.07	1.27E-04	6.37E-05

8	0.08	1.46E-04	7.28E-05
9	0.09	1.64E-04	8.19E-05
10	0.1	1.82E-04	9.10E-05
11	0.15	2.73E-04	1.37E-04
12	0.2	3.64E-04	1.82E-04
13	0.25	4.55E-04	2.28E-04
14	0.3	5.46E-04	2.73E-04
15	0.35	6.37E-04	3.19E-04

Table 4. Representative titration table for **2a·TFA** titration with TBABr.

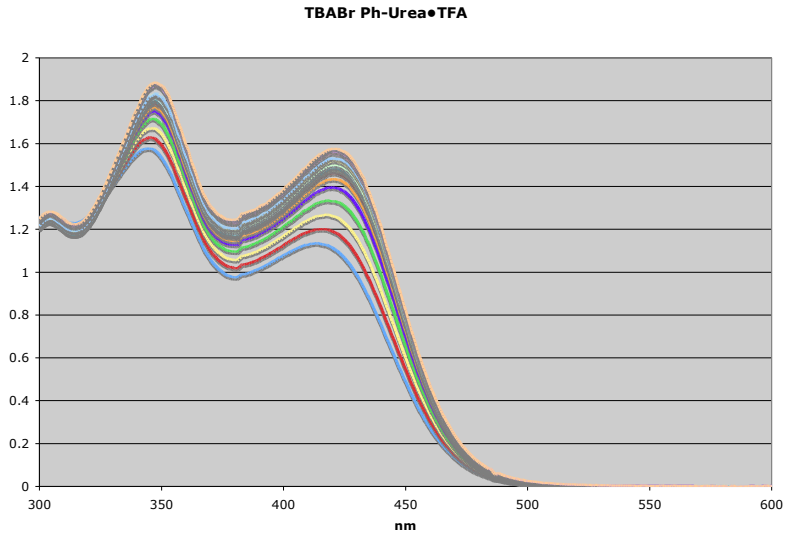

Figure 9. UV-Vis spectra illustrating the change in absorbance during titration of **2a·TFA** with TBABr.

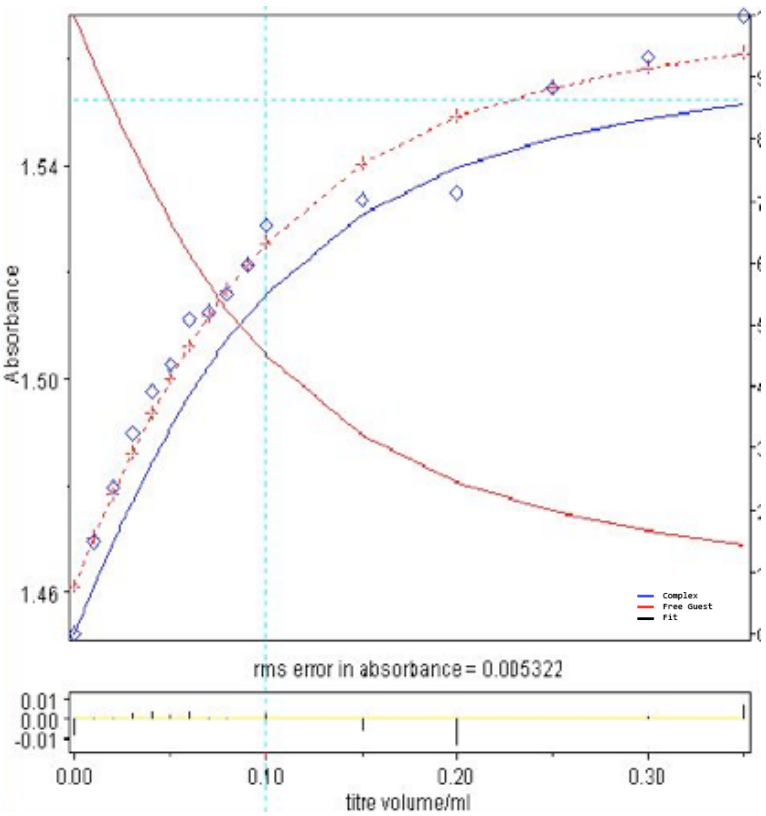

Figure 10. Non-linear regressional fit of the change in absorbance with TBABr concentration during titration into **2a·TFA**.

Tetrabutylammonium iodide A 10 mL stock solution of **2a•TFA** (3.95 mg, 5.11 µmol) was prepared and used in the dilution of TBAI guest solution (10.65 mg, 1.98 µmol). [Host]= 2.60 x 10^{-5} ; [Guest]= 1.39 x 10^{-3}. Host starting volume of 2.00 mL.

Additions	Total X (mL)	mol X Delivered	[X] Cuvett
0	0	0	0
1	0.005	6.95E-06	3.48E-06
2	0.01	1.39E-05	6.95E-06
3	0.015	2.09E-05	1.04E-05
4	0.02	2.78E-05	1.39E-05
5	0.025	3.48E-05	1.74E-05
6	0.035	4.87E-05	2.43E-05
7	0.045	6.26E-05	3.13E-05
8	0.055	7.65E-05	3.82E-05
9	0.065	9.04E-05	4.52E-05
10	0.075	1.04E-04	5.21E-05

11	0.085	1.18E-04	5.91E-05
12	0.095	1.32E-04	6.60E-05
13	0.105	1.46E-04	7.30E-05
14	0.115	1.60E-04	7.99E-05
15	0.125	1.74E-04	8.69E-05
16	0.155	2.15E-04	1.08E-04
17	0.185	2.57E-04	1.29E-04
18	0.215	2.99E-04	1.49E-04
19	0.245	3.41E-04	1.70E-04
20	0.275	3.82E-04	1.91E-04
21	0.325	4.52E-04	2.26E-04
22	0.375	5.21E-04	2.61E-04
23	0.425	5.91E-04	2.95E-04
24	0.475	6.60E-04	3.30E-04
25	0.525	7.30E-04	3.65E-04
26	0.675	9.38E-04	4.69E-04
27	0.825	1.15E-03	5.73E-04

Table 5 . Representative titration table for **2a·TFA** with TBAI.

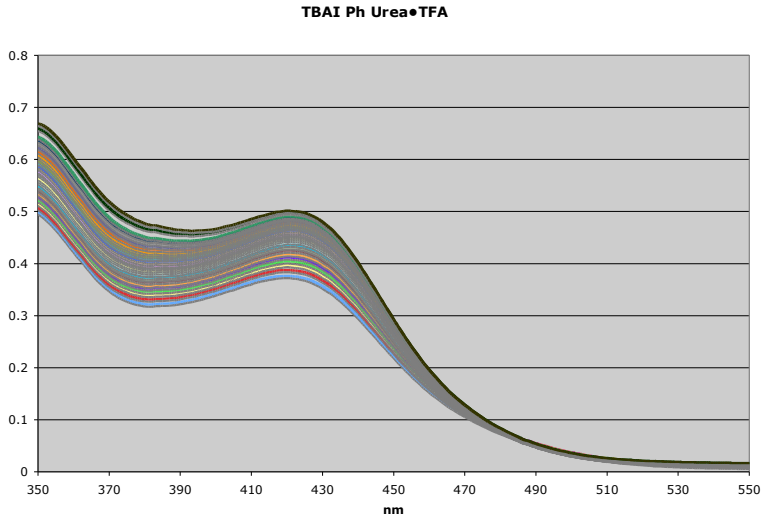

Figure 11. UV-Vis spectra of the change in absorbance during titration of **2a·TFA** with TBAI.

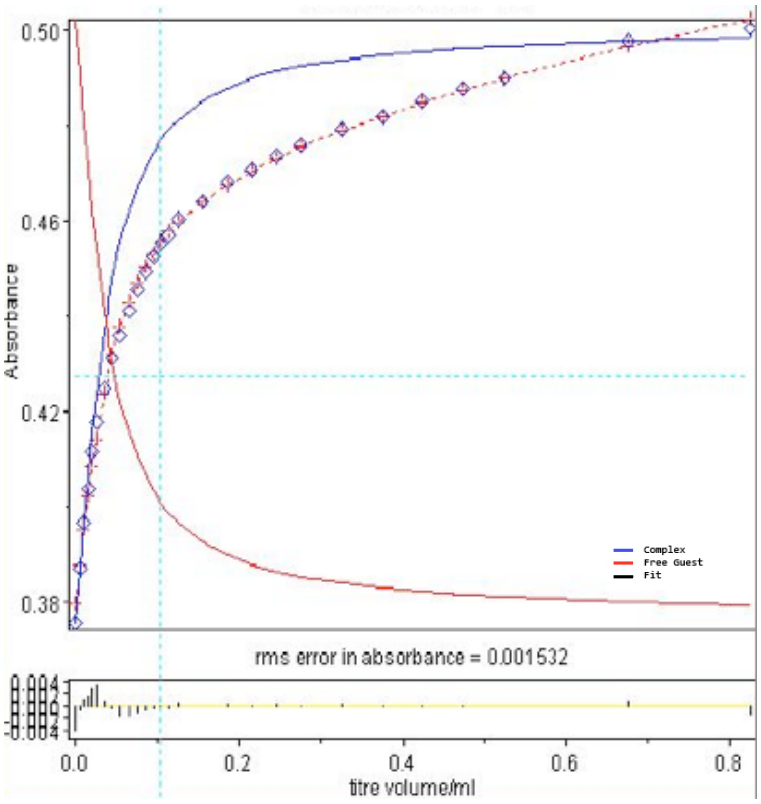

Figure 12. Non-linear regressional fit of the isotherm formed from plotting the change in absorbance during titration of **2a·TFA** with TBAI.

DFT Details

B3LYP/6-31G = -2299.19660605 au
B3LYP/6-31G Zero Point Corrected Energy = -2298.626895 au
NIMAG = 0

C	0.35263200	0.60728600	5.12140200
C	0.33553500	0.69053800	3.71895000
N	-0.71221500	0.11757500	3.04393000
C	-1.73773900	-0.55234600	3.66829700
C	-1.71217000	-0.66162900	5.07047700
C	-0.66972200	-0.07436400	5.78621900
C	1.35943000	1.32442700	2.98609000
C	-2.77565400	-1.06595700	2.87306100
C	2.31329700	1.86008000	2.43895000
C	-3.70952600	-1.45302000	2.18267500
C	3.43451600	2.48056000	1.83347800
C	-4.79245400	-1.80392500	1.34758000
C	3.83157600	3.76120100	2.28914100
C	4.94661400	4.39301400	1.75656200
C	5.68876800	3.73792600	0.76070200
C	5.32520800	2.47739600	0.29396700
C	4.18834400	1.82090200	0.81198000
C	-4.95390600	-1.15541300	0.07934100
C	-6.10078500	-1.45277100	-0.68456400
C	-7.03364300	-2.37663300	-0.21944200
C	-6.86716400	-3.03527300	1.01138200
C	-5.75512500	-2.74441800	1.78802200
N	3.76966900	0.56361900	0.37209800
N	-3.96681800	-0.26255800	-0.33407500
C	4.54856000	-0.36386300	-0.34521400
C	-4.09896800	0.73676100	-1.31238200
N	-2.94553800	1.47734100	-1.44378100
O	-5.15476900	0.92654100	-1.95755000
C	-2.71700800	2.57542600	-2.30684300
O	5.75511200	-0.16802600	-0.62097700
N	3.83706300	-1.49226500	-0.68354800
C	4.33310200	-2.66411700	-1.30434100
C	3.40521900	-3.69784300	-1.54216900
C	3.81438600	-4.89157200	-2.13642200
C	5.15294300	-5.07932800	-2.50199800

C	6.07197700	-4.05157700	-2.26671200	H	6.56550600	4.21825000	0.33820900
C	5.67900700	-2.84702100	-1.67399100	H	5.91541700	1.97308200	-0.45531800
C	-1.41817800	3.12071800	-2.30918800	H	-6.24207200	-0.94282000	-1.62530300
C	-1.11210400	4.21388500	-3.11925900	H	-7.90356900	-2.59312700	-0.83110400
C	-2.09368700	4.78222600	-3.94034800	H	-7.60029800	-3.75722300	1.35271700
C	-3.38204000	4.23751100	-3.93839600	H	-5.60703200	-3.22680100	2.74811200
C	-3.70635200	3.14188000	-3.13148400	H	2.83271400	0.26353500	0.63494700
H	-0.73893700	0.17049900	1.98455100	H	-3.05672100	-0.33965200	0.11370600
C	-0.27060800	-1.06002400	-1.64027800	H	-2.14979900	1.18875200	-0.87974900
F	0.68308000	-1.94645400	-2.10469400	H	2.83881400	-1.48644100	-0.47831100
F	-1.50486700	-1.68892000	-1.72433800	H	2.36460600	-3.55440500	-1.27153100
F	-0.29471100	0.02599500	-2.50996400	H	3.08385400	-5.67466100	-2.31501800
C	0.02228000	-0.58473900	-0.20661000	H	5.47131500	-6.00797600	-2.96446300
O	-0.95769700	0.03667700	0.36431500	H	7.11280700	-4.18100700	-2.54794900
O	1.16843200	-0.80257300	0.26987300	H	6.39044600	-2.05399100	-1.50012300
H	1.17481300	1.05900900	5.65900500	H	-0.64939100	2.67395500	-1.68619900
H	-2.51449500	-1.18997600	5.56696000	H	-0.10455900	4.61783700	-3.11090900
H	-0.65036400	-0.14962100	6.86767000	H	-1.85620400	5.63174100	-4.57225000
H	3.24175100	4.23945100	3.06374300	H	-4.15203900	4.66648700	-4.57242400
H	5.23951600	5.37589000	2.10807500	H	-4.70075000	2.72127100	-3.13554500

APPENDIX C

SUPPORTING INFORMATION FOR CHAPTER IV:

ANION-DEPENDENT, SWITCHABLE ON-OFF AND OFF-ON FLUORESCENCE EMISSION IN BIS(ANILINOETHYNYL)PYRIDINE DERIVATIVES

UV-visible and fluorescence excitation spectra

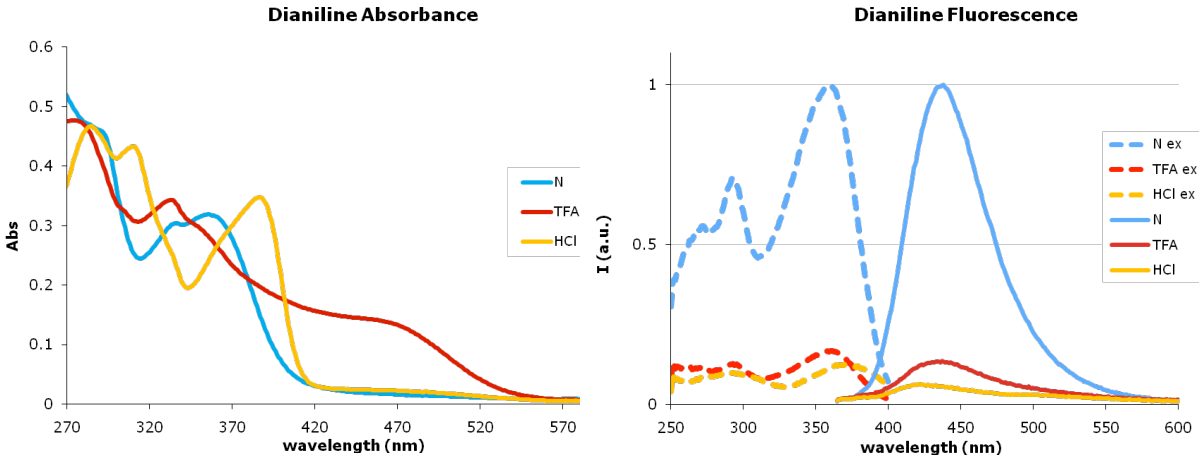

Figure 1 UV-visible and fluorescence spectra for **1**, **1•TFA** and **1•HCl**

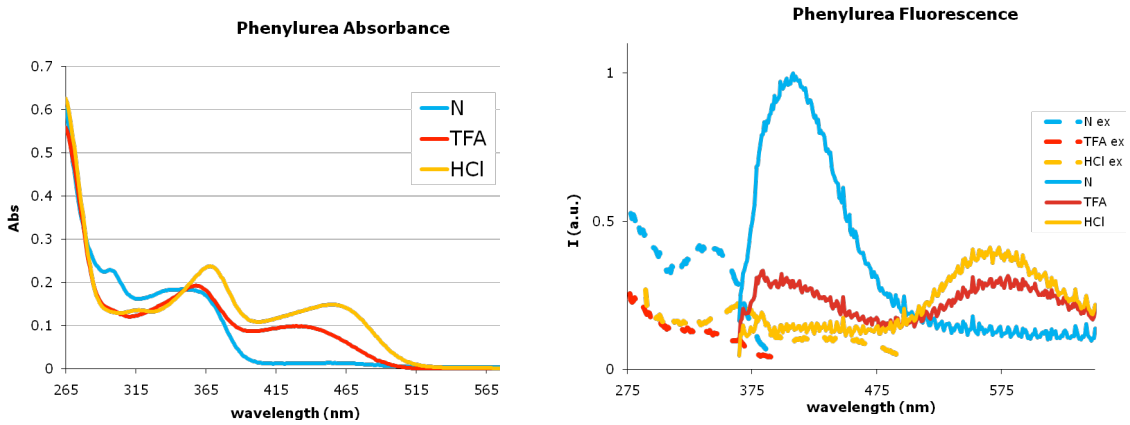

Figure 2 UV-visible and fluorescence spectra for **2**, **2•TFA** and **2•HCl**

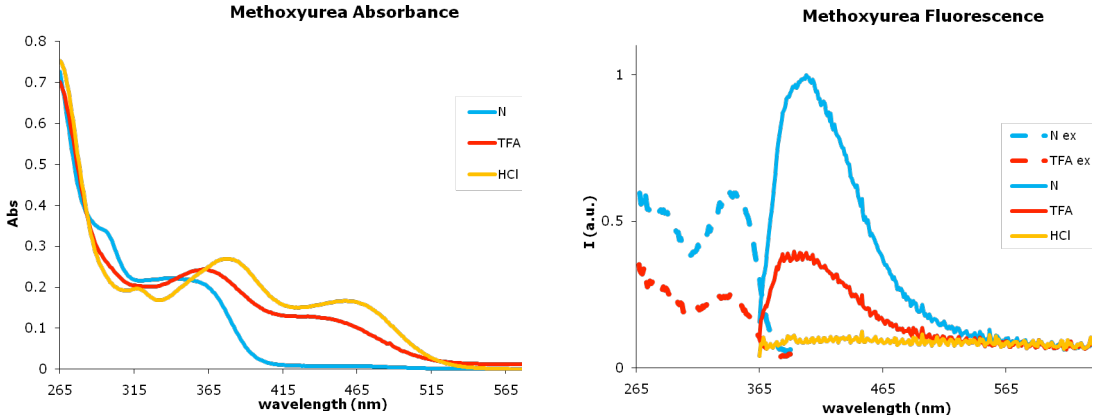

Figure 3 UV-visible and fluorescence spectra for **3a**, **3a•TFA** and **3a•HCl.** HCl protonation results in a fully non-fluorescent species at any of the absorbing wavelengths, thus no excitation spectrum was recorded.

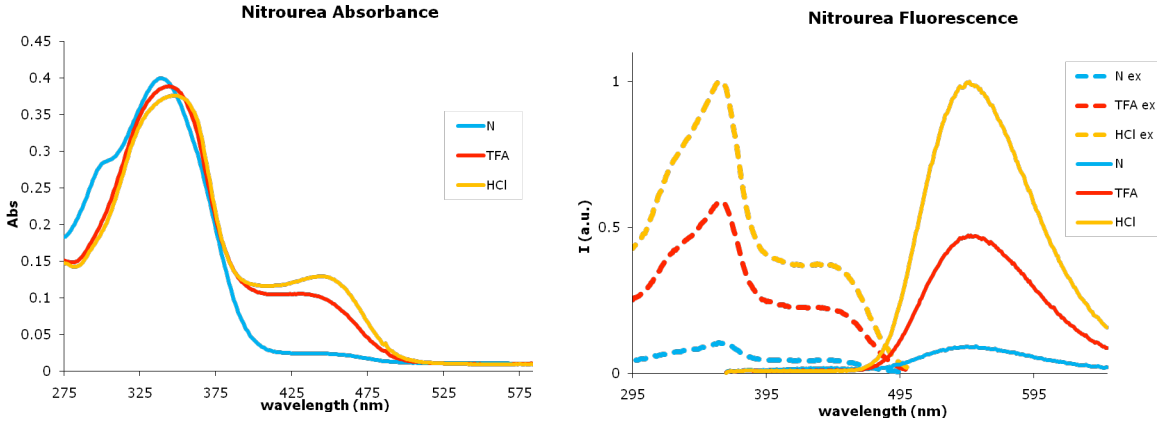

Figure 4. UV-visible and fluorescence spectra for **3b**, **3b•TFA** and **3b•HCl**

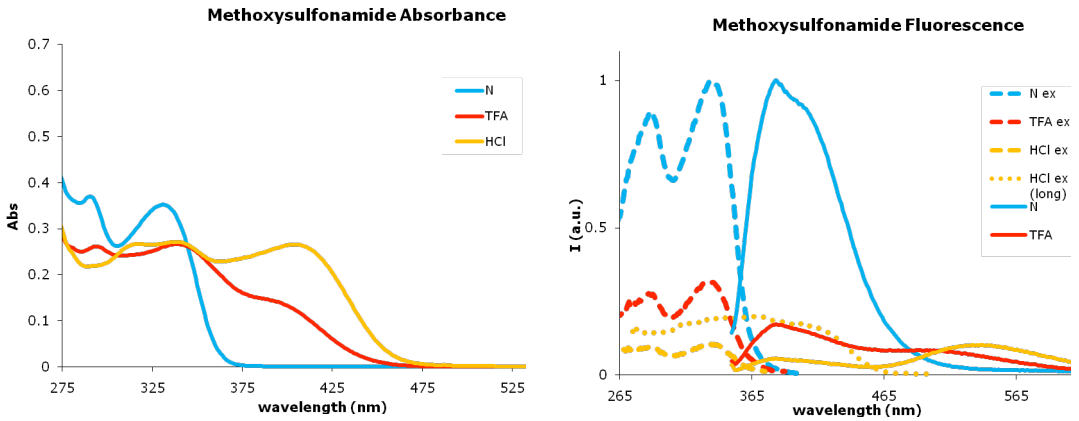

Figure 5. UV-visible and fluorescence spectra for **4a**, **4a•TFA** and **4a•HCl**. The dotted "HCl ex (long)" trace is the excitation spectrum when monitoring emission at 535 nm.

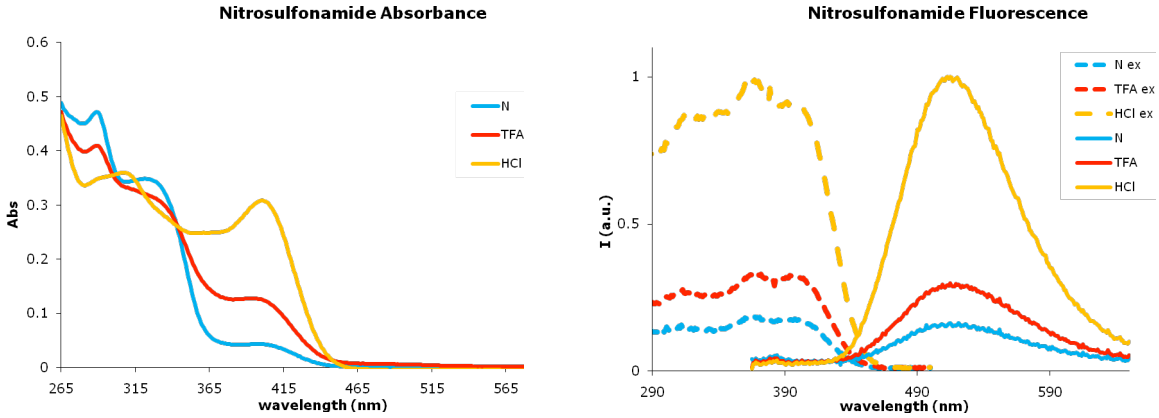

Figure 6. UV-visible and fluorescence spectra for **4b**, **4b•TFA** and **4b•HCl**

HBr protonated fluorescence emission

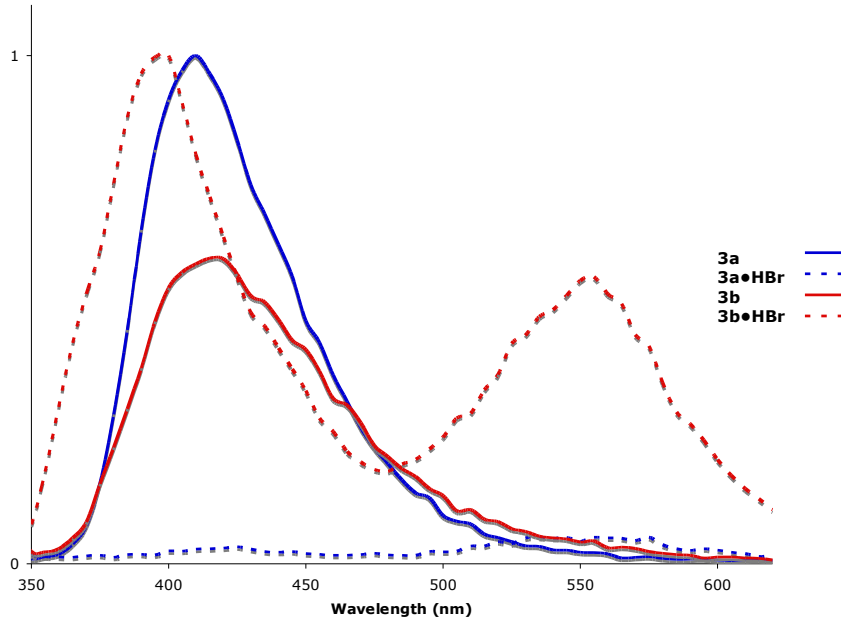

Figure 7. Fluorescence emission in $CHCl_3$ of **3a** and **3b** with HBr. The dual emission in **3b•HBr** is possibly from incomplete protonation of the receptor, although treatment with an excess of HBr exhibited no further change in the spectra.

Self-Association of 3a. Self-association dilution experiments for **3a** were carried out in $CDCl_3$ from stock solutions of **3a** near the limit of its solubility (2.75 mM). Titrations started with 600 µL of solution.

Addition	[H]v	Dilution	[H]t
0	600	0	2.75E-03
1	600	50	2.54E-03
2	600	100	2.36E-03
3	600	200	2.06E-03
4	600	300	1.83E-03
5	600	500	1.50E-03
6	600	700	1.27E-03
7	600	900	1.10E-03
8	600	1,100	9.70E-04
9	600	1,500	7.86E-04

10	600	1,900	6.60E-04
11	600	2,300	5.69E-04
12	600	2,300	5.69E-04

Table 1. Representative dilution data for **3a** dilution experiments

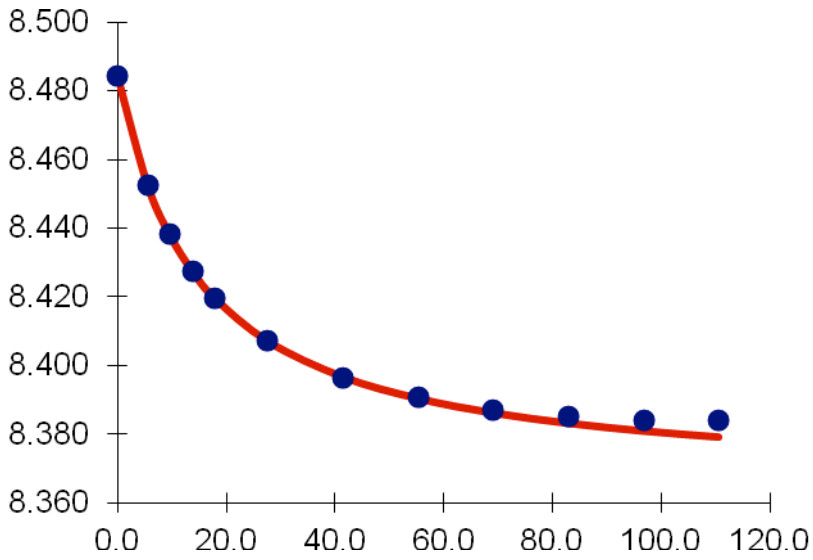

Figure 8. Plot of urea ^{1}H chemical shifts in **3a** the dilution experiment in Table 1. The values are estimated and irreproducible due to the significant broadening of the spectra.

3a 2-D ROESY. 2-D ROESY spectra of **3a** in water saturated chloroform were collected at 3.4 mM. These spectra lacked the single cross-peak indicative of intermolecular interactions under these conditions.

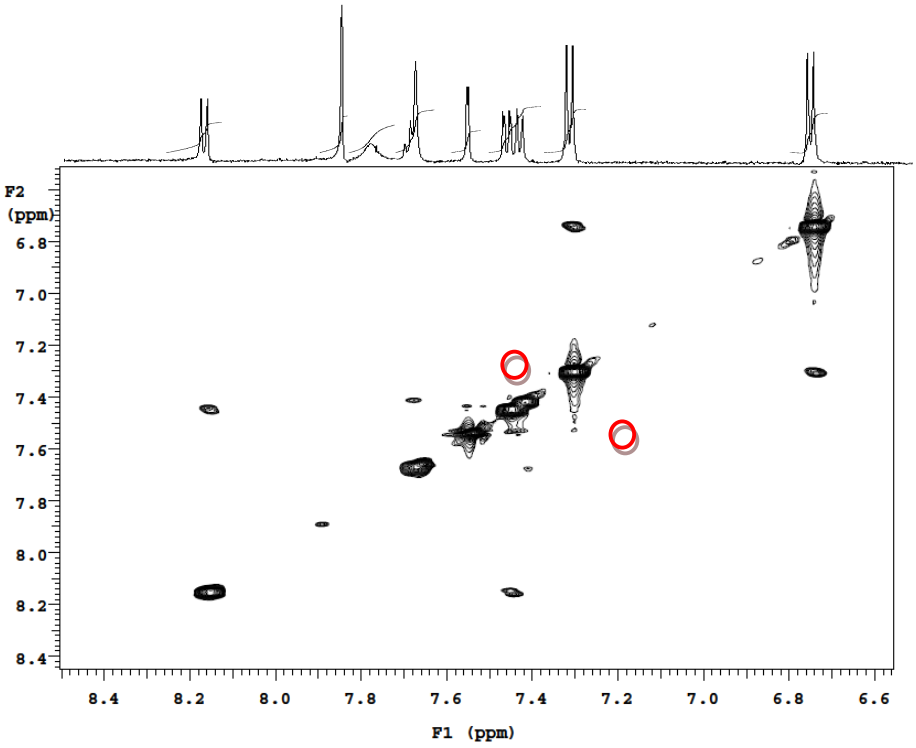

Figure 9. 2-D ROESY spectrum of **3a** in water-saturated $CDCl_3$. Red circles indicate where the cross-peaks should have appeared.

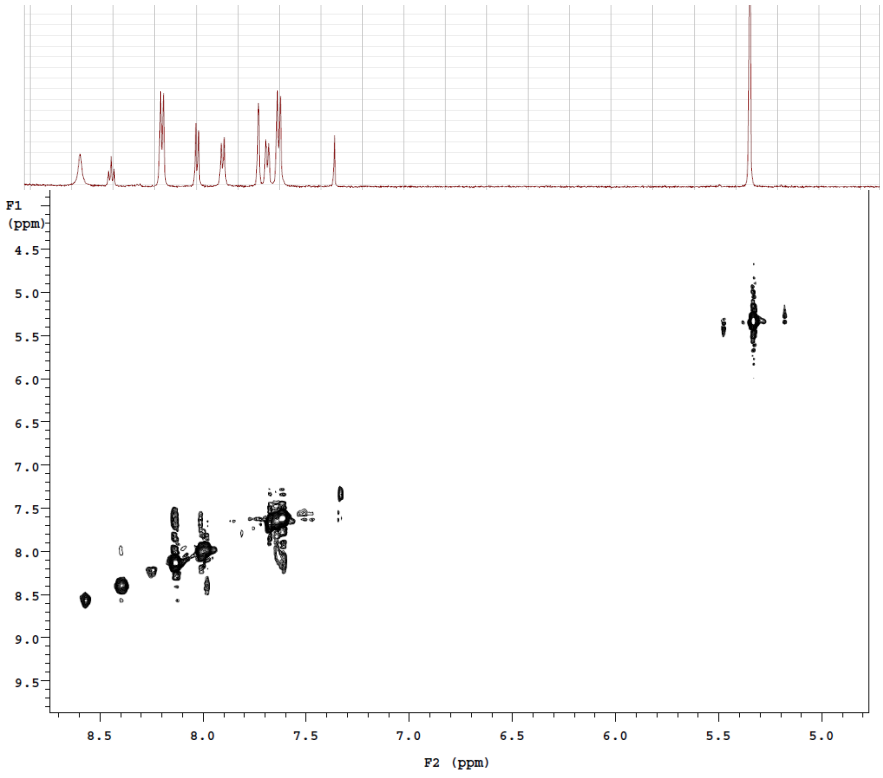

Figure 10. 2-D ROESY spectrum of **3b** in water-saturated $CDCl_3$ with no observable intermolecular NOE cross-peaks.

Positive mode ESI-mass spectral data. Positive mode mass spectral data were acquired under the same conditions as those found in the text.

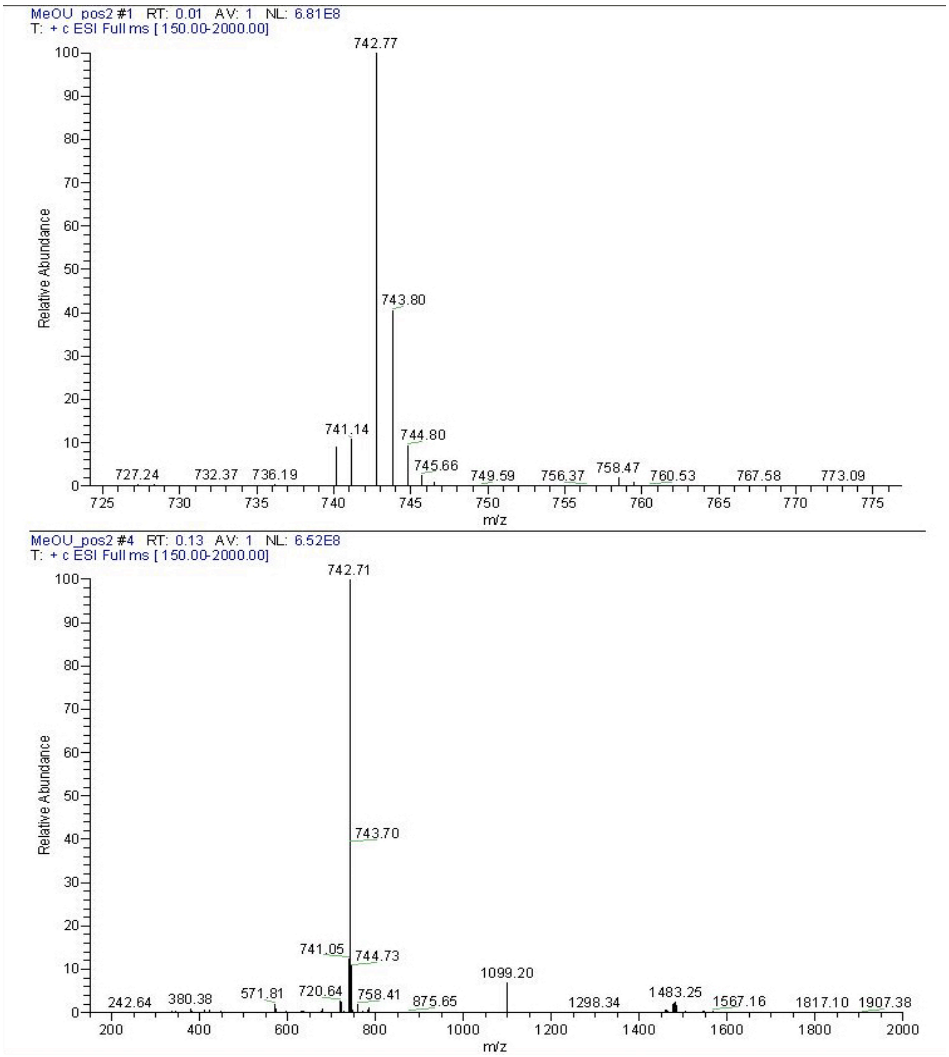

Figure 11. ESI pos mode spectrum of **3a·TFA**

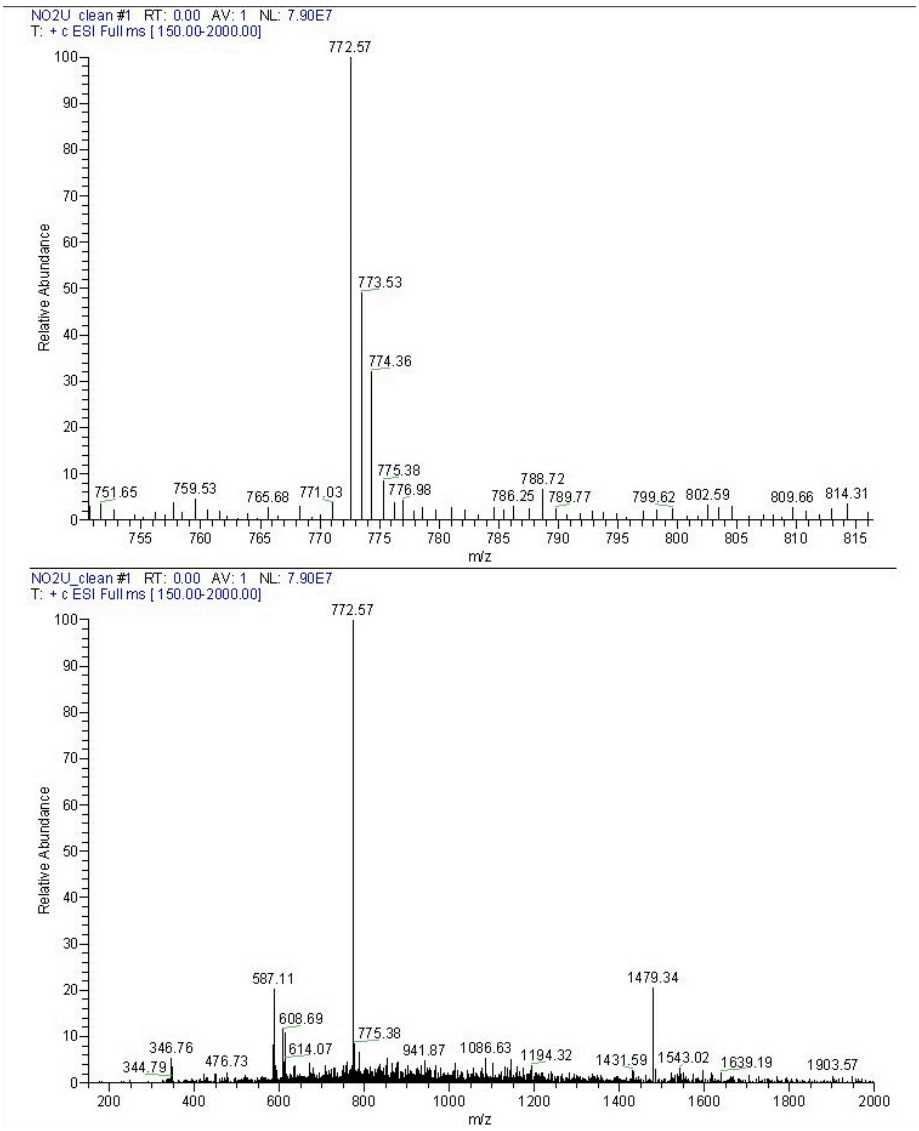

Figure 12. ESI pos mode spectrum of **3b·TFA**

Crystal Data for Nitrophenylurea 3b. Empirical formula C48 H55 N7 O9 S2. Formula weight 938.11. Temperature 173(2) K. Wavelength 0.71073 Å. Crystal system: Triclinic. Space group P-1. Unit cell dimensions a = 13.037(8) Å a= 112.755(10)°; b = 14.106(9) Å b= 103.142(10)°; c = 14.707(9) Å g = 92.983(11)°. Volume 2399(3) $Å^3$. Density (calculated) 1.299 Mg/m^3. Absorption coefficient 0.173 mm^{-1}. Crystal size 0.38 x 0.22 x 0.05 mm^3. Theta range for data collection 1.58 to 24.00°. Index ranges -14<=h<=14, -16<=k<=16, -16<=l<=16. Reflections collected 20819. Independent reflections 7533 [R(int) = 0.0580]. Completeness to theta = 24.00° 99.9 %. Absorption correction Semi-empirical from equivalents. Max. and min. transmission 0.9914 and 0.9370. Refinement

method Full-matrix least-squares on F^2. Data / restraints / parameters 7533 / 6 / 666. Goodness-of-fit on F^2 1.032. Final R indices [I>2sigma(I)] R1 = 0.0867, wR2 = 0.2233. R indices (all data) R1 = 0.1382, wR2 = 0.2502. Largest diff. peak and hole 0.609 and -0.759 e.$Å^{-3}$

APPENDIX D

SUPPORTING INFORMATION FOR CHAPTER V:

FUNCTIONALIZED ANILINOETHYNYLPYRIDINE UREAS: *IN VITRO* IMAGING AND ANION-MEDIATED SELF-ASSEMBLY

Cell assays. NIH3T3 murine fibroblast cells were cultured on sterile 18mm glass cover slips in DME Media containing 9% FCS for 4 days until near confluent. Cover slips were transferred to 12 well plates for treatment. The media was aspirated, and the cells were incubated with a Cl^- ion containing buffer solution (120 mM KCl, 20 mM NaCl, 1 mM $MgCl_2$, 1 mM $CaCl_2$) for 20 minutes. The buffer was then aspirated and cells incubated with DMEM (no serum) containing 50uM of either **1a** or **1a·TFA** in DMSO (Diluted into media 1:10) for 45 minutes. Cover slips were transferred to microscope slides by inversion using silicone rubber o-rings (17 mm) to provide wells on slides containing DI H_20, viewed and photographed with a Nikon epifluorescence microscope with EX 450-490nm/EM 515nm. All photos were at 500X magnification.

^{1}H-NMR titration data. Solutions of **1a** in $CDCl_3$ were prepared at stock concentration (5.52 mM) and used to dilute the guest solutions such that both [Host] and [Guest] are equimolar in [**1a**]. The titrations started with 600 µL of [Host] in the tube.

Addition	[H]v µL	[Cl]v µL	[H]t	[Cl]t
1	650	0	2.76E-03	0.00E+00
2	650	25	2.76E-03	4.27E-04
3	650	50	2.76E-03	8.23E-04
4	650	75	2.76E-03	1.19E-03
5	650	100	2.76E-03	1.54E-03
6	650	150	2.76E-03	2.16E-03
7	650	200	2.76E-03	2.71E-03
8	650	300	2.76E-03	3.64E-03
9	650	400	2.76E-03	4.39E-03
10	650	500	2.76E-03	5.01E-03
11	650	600	2.76E-03	5.53E-03
12	650	900	2.76E-03	6.69E-03
13	650	1,200	2.76E-03	7.47E-03
14	650	1,500	2.76E-03	8.04E-03
15	650	1,800	2.76E-03	8.47E-03

Table 1. Representative titration table of **1a** with TBACl.

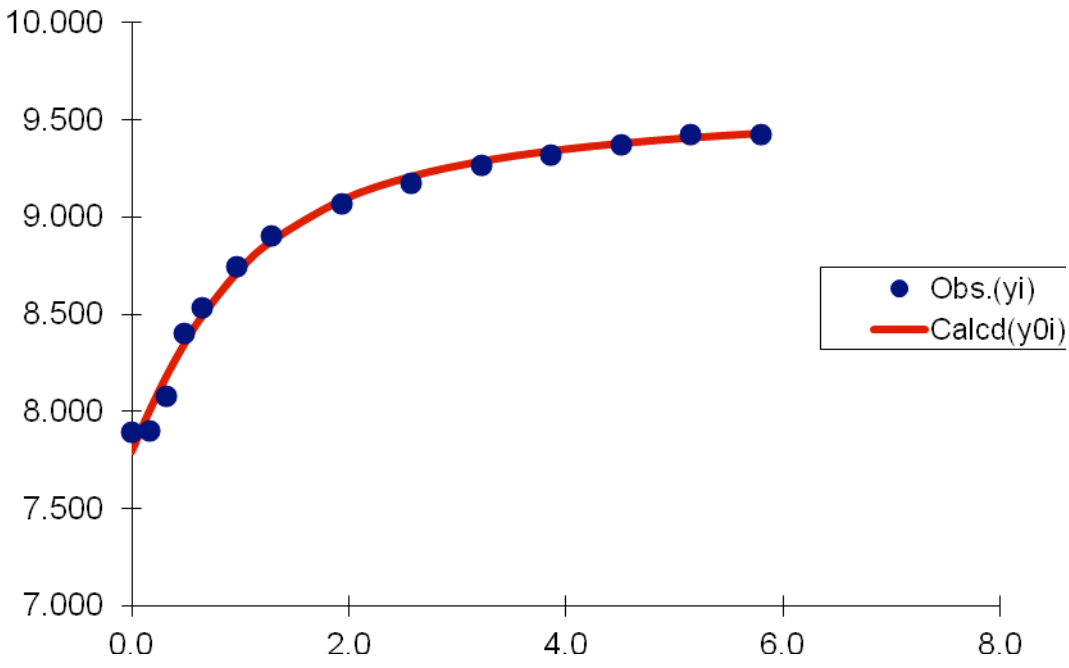

Figure 1. Non-linear regressional fit to the observed chemical shifts during **1a** and TBACl titration

Addition	[H]v µL	[NO_3]v µL	Buffer	[H]t	[NO_3]t
0	600	0	0	2.75E-03	0.00E+00
1	600	50	0	2.54E-03	6.98E-04
2	600	100	0	2.36E-03	1.30E-03
3	600	200	0	2.06E-03	2.27E-03
4	600	300	0	1.83E-03	3.02E-03
5	600	150	0	2.20E-03	1.81E-03
6	600	200	0	2.06E-03	2.27E-03
7	600	250	0	1.94E-03	2.67E-03
8	600	300	0	1.83E-03	3.02E-03
9	600	350	0	1.74E-03	3.34E-03
10	600	400	0	1.65E-03	3.63E-03

Table 2. Representative titration table for **1a** and $TBANO_3$.

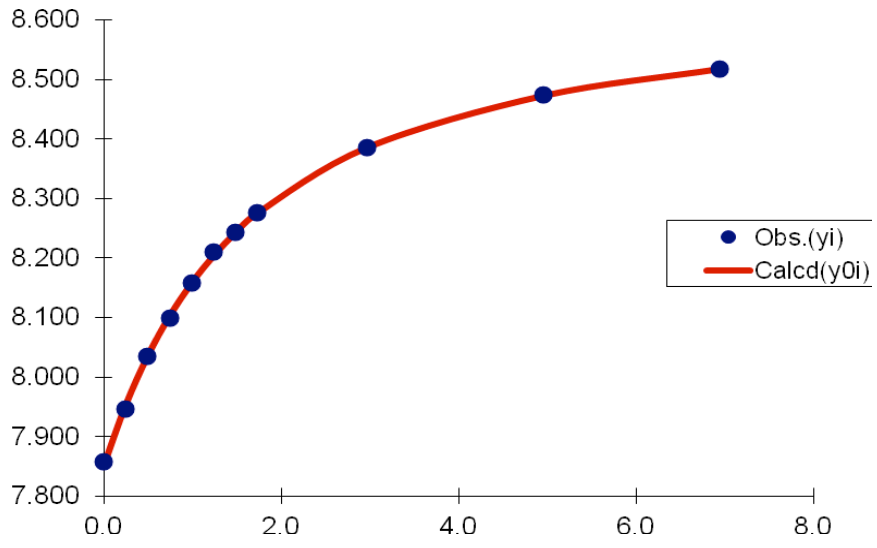

Figure 2. Non-linear regressional fit to the observed chemical shifts during **1a** and $TBANO_3$ titration

UV-Vis titration data. Titrations were carried out in the same manner as ^{1}H-NMR titrations. Fitting was done both by HyperQuad minimization and Rose-Drago fitting. Stock concentration: 0.319 mM.

Running index	[H]v µL	[Cl]v µL	[H]t	[Cl]t
1	250	0	3.19E-05	0.00E+00
2	250	50	3.19E-05	4.55E-06
3	250	100	3.19E-05	9.10E-06
4	250	150	3.19E-05	1.36E-05
5	250	250	3.19E-05	2.27E-05
6	250	350	3.19E-05	3.18E-05
7	250	500	3.19E-05	4.55E-05
8	250	650	3.19E-05	5.91E-05
9	250	800	3.19E-05	7.28E-05
10	250	1,000	3.19E-05	9.10E-05
11	250	1,200	3.19E-05	1.09E-04
12	250	1,400	3.19E-05	1.27E-04
13	250	1,600	3.19E-05	1.46E-04
14	250	1,800	3.19E-05	1.64E-04

Table 3. Representative titration table for **1a·TFA** and TBACl titration.

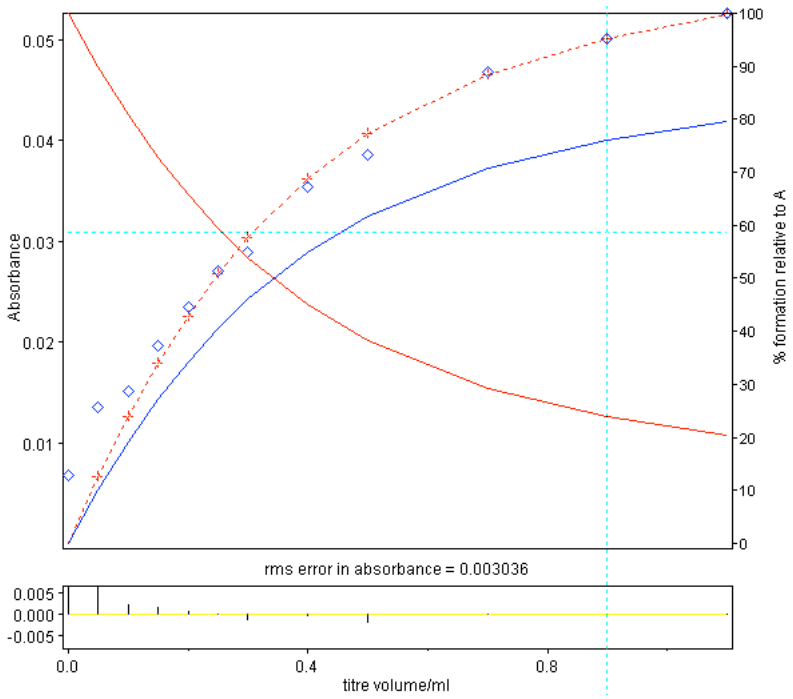

Figure 3. Non-linear regressional fit to the observed chemical shifts during **1a·TFA** and TBACl titration.

	[H]v µL	[G]v µL	An
n=1	3.20E-05	6.67E-06	0.2709
n=2	3.20E-05	2.00E-05	0.3252
n=3	3.20E-05	4.00E-05	0.3461
n=4	3.20E-05	9.34E-05	0.3803
n=5	3.20E-05	1.47E-04	0.3911

Table 4. Representative titration table for Rose-Drago fitting of **1a·TFA** and TBACl.

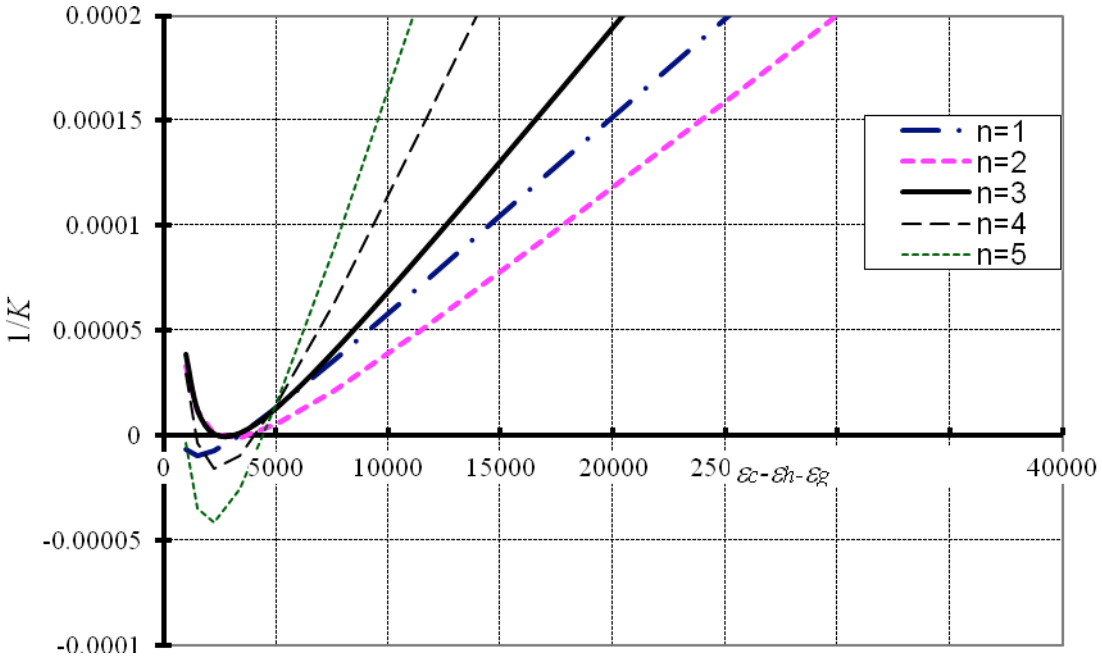

Figure 4. Rose-Drago plot for determining the molar absorptivity of the complex **1a·HNO$_3$.** Use of this method corroborates non-linear regressional methods by experimentally verifying the calculated ε values.

Vesicle fluorescence. 1a·TFA in vesicles containing high Cl^- buffer in external low Cl^- buffer were heated at 50 ^oC for 15 minutes and 12 h in order to probe the stability of

the fluorescing complex in solution. The 530 nm emission band indicative of Cl^- concentration remains intact after short periods of heating. Extended periods of time at high temperatures fully recovered only the high energy emission associated with the receptor in solution and lacks the band indicative of **1a·Cl** complex.

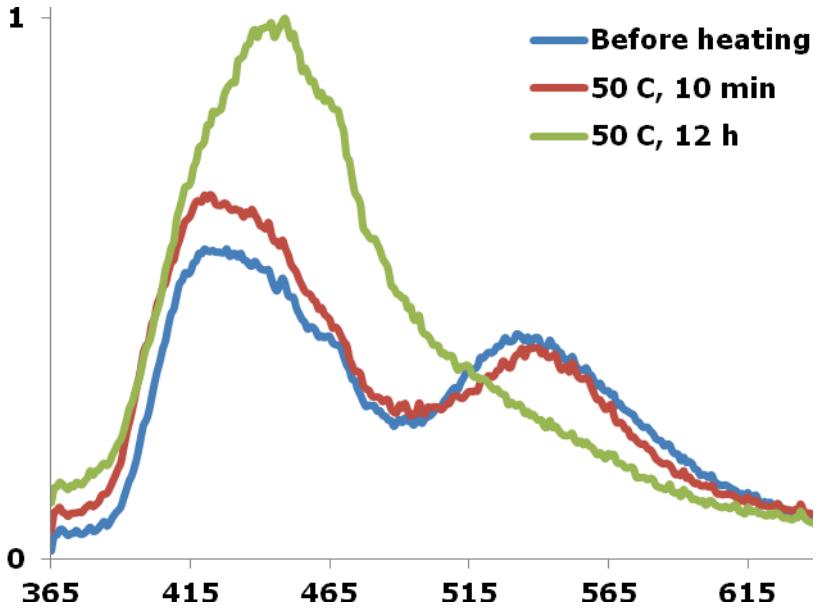

Figure 5. Fluorescence emission of a solution of high Cl^- content vesicles in buffered water with **1a·TFA** in DMSO (10% DMSO in solution) before, during, and after heating at 50 ^oC.

Aggregation induced emission with other anion solutions. Both $LiClO_4$ and pure water were also used to induce AIE fluorescence in **1a·TFA** solutions in DMSO. These spectra were acquired with the same solutions as those found in the text (1.96 mM solutions diluted with varying amounts of aqueous media).

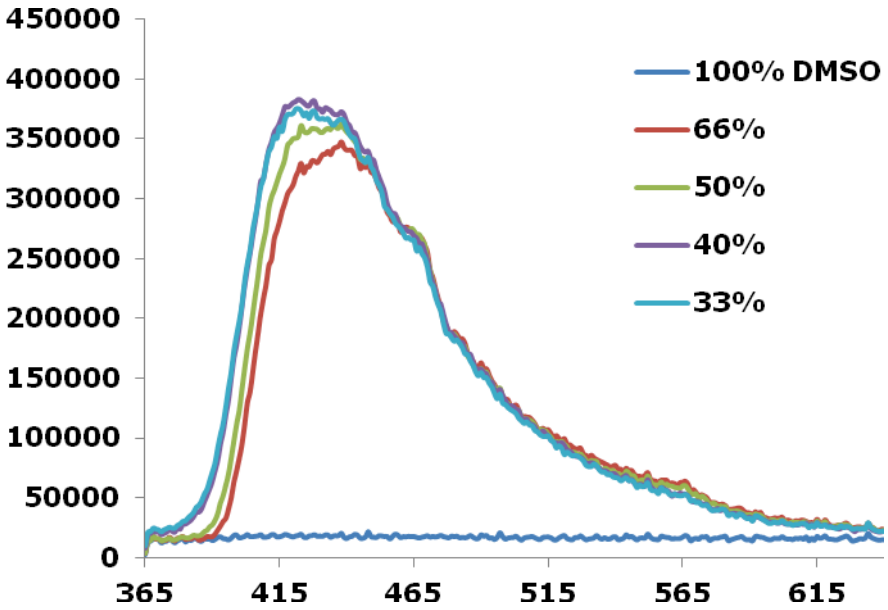

Figure 6. Fluorescence emission upon introduction of $LiClO_4$-containing water to DMSO solution of **1a·TFA**. Perchlorate addition results in almost immediate aggregate formation.

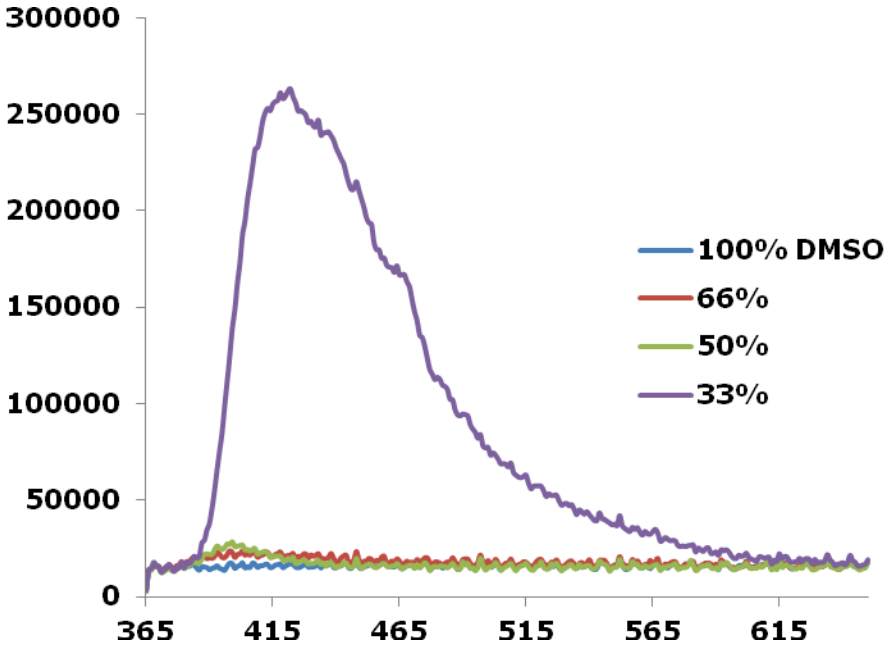

Figure 7. Fluorescence emission upon introduction of deionized water to DMSO solution of **1a·TFA**. No fluorescence is observed until the solution is greater than 50% H_2O in DMSO.

TEM microscopy. Control images were taken with only the tetrabutylammonium salts in order to verify the formation of structures consisting of **1b**.

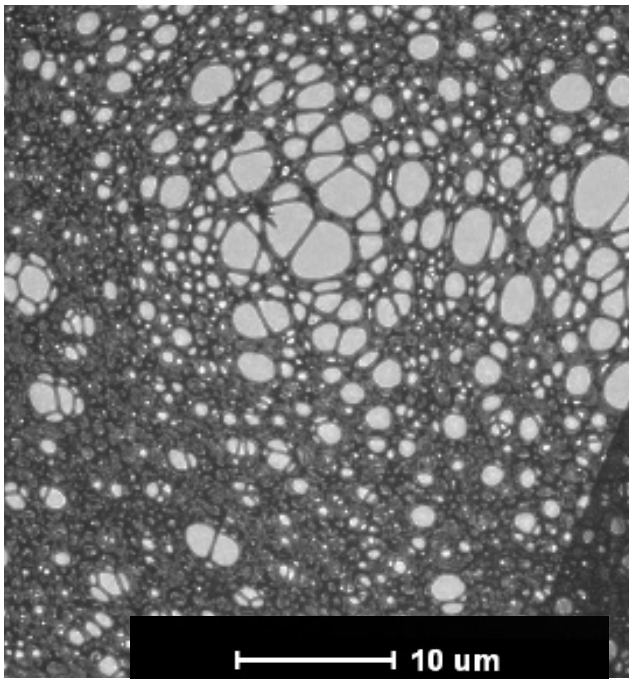

Figure 8. TEM image of $TBANO_3$ blank prepared by floating the grid on the MeCN solution of $TBANO_3$ that was added to **1b·HBF$_4$** solution for the images found in the text.

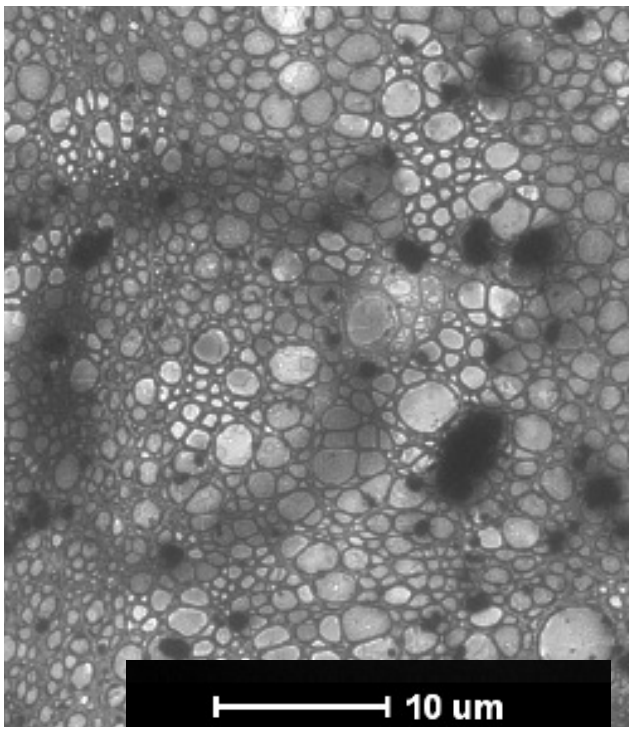

Figure 9. TEM image of TBACl blank prepared by floating the grid on the MeCN solution of TBACl that was added to **1b·HBF$_4$** solution for the images found in the text.

Crystal data for Nitrophenylurea 1b. Empirical formula C44 H42 Cl3 N7 O7. Formula weight 887.20. Temperature 173(2) K. Wavelength 0.71073 Å. Crystal system Monoclinic. Space group P2(1)/c. Unit cell dimensions a = 9.5229(13) Å a= 90°; b = 39.529(5) Å b= 98.282(3)°; c = 11.6647(16) Å g = 90°. Volume 4345.2(10) Å^3. Z 4 Density (calculated) 1.356 Mg/m^3. Absorption coefficient 0.270 mm^{-1}. F(000) 1848. Crystal size 0.21 x 0.14 x 0.02 mm^3. Theta range for data collection 1.03 to 25.00°. Index ranges -11<=h<=11, -46<=k<=46, -13<=l<=13. Reflections collected 41736. Independent reflections 7661 [R(int) = 0.0927]. Completeness to theta = 25.00° 100.0 %. Absorption correction Semi-empirical from equivalents. Max. and min. transmission 0.9946 and 0.9455. Refinement method Full-matrix least-squares on F^2. Data / restraints / parameters 7661 / 0 / 538. Goodness-of-fit on F^2 0.996. Final R indices [I>2sigma(I)] R1 = 0.0808, wR2 = 0.1968. R indices (all data) R1 = 0.1361, wR2 = 0.2255. Largest diff. peak and hole 0.418 and -0.316 e.Å^{-3}

REFERENCES CITED

Chapter I

1. J. L. Sessler, P. A. Gale, and W.-S. Cho, *Anion Receptor Chemistry*, Royal Society of Chemistry, Cambridge, 2006.

2. W. -S. Cho, J. L. Sessler, *Functional Synthetic Receptors*, ed. T. Schrader, A. D. Hamilton, Wiley-VCH, Weinheim, 2005, 165-256.

3. *Supramolecular Chemistry of Anions*, ed. A. Bianchi, K. Bowman-James and E. Garcia-España, Wiley-VCH, New York, 1997.

4. A. Houssain, *Curr. Org. Chem.*, 2008, **12**, 1231-1256.

5. K. Campbell, R. R. Tykwinski, *Carbon-rich Compounds: From Molecules to Materials,* ed. M. M. Haley, R. R. Tykwinski, Wiley-VCH, New York, 2006, 229-294.

6. R. Welti and F. Diederich, *Helv. Chim. Acta*, 2003, **86**, 494.

7. C. -Y. Huang, L. A. Cabell and E. V. Anslyn, *J. Am. Chem. Soc.*, 1994, **116**, 2778.

8. J. L. Sessler, A. E. Vivian, D. Seidel, A. K. Burrell, M. Hoehner, T. D. Mody, A. Gebauer, S. J. Weghorn and V. Lynch, *Coord. Chem. Rev.*, 2000, **216-217**, 411-434.

9. A. Jasat and D. Dolphin, *Chem. Rev.*, 1997, **97**, 2267-2340.

10. P. A. Gale, P. Anzenbacher, Jr. and J. L. Sessler, *Coord. Chem. Rev.*, 2001, **222**, 57-102.

11. P. Anzenbacher, Jr., R. Nishiyabu and M. A. Palacios, *Coord. Chem. Rev.*, 2006, **250**, 2929-2938.

12. J. L. Atwood, K. T. Holman and J. W. Steed, *J. Chem. Soc., Chem. Commun.*, 1996, 1401-1407

13. J. L. Sessler, B. L. Rubin, S. Camiolo, W. -S. Cho, G. D. Pantos and V. M. Lynch, *Supramolecular Chem.*, 2006, **18**, 103-109.
14. P. A. Gale, *Chem. Commun.*, 2005, 3761-3772.

15. T. Evan-Salem, I. Baruch, L. Avram, Y. Cohen, L. C. Palmer and J. Rebek, Jr., *Proc. Nat. Acad. Sci.*, 2006, **103**, 12296-12300.

16. S. Leininger, B. Olenyuk and P. J. Stang, *Chem. Rev.*, 2000, **100**, 853-908.

17. H. L. Anderson and J. K. M. Sanders, *Chem. Commun.,* 1996, 946-947.

18. J. D. Ferrara, C. Tessier-Youngs and W. J. Youngs, *Organometallics,* 1987, **6**, 676-678.

19. M. Iyoda, S. Sirinintasak, Y. Nishiyama, A. Vorasingha, F. Sultana, K. Nakao, Y. Kuwatani, H. Matsuyama, M. Yoshida and Y. Miyake, *Synthesis*, 2004, 1527-1531.

20. J. D. Ferrara, A. A. Tanaka, C. Fierro, C. Tessier-Youngs and W. J. Youngs, *Organometallics*, 1989, **8**, 2089-2098.

21. J. D. Ferrara, A. Djebli, C. Tessier-Youngs and W. J. Youngs, *J. Am. Chem. Soc.*, 1988, **110**, 647-649.

22. J. D. Ferrara, C. Tessier-Youngs and W. J. Youngs, *J. Am. Chem. Soc.*, 1985, **107**, 6719.

23. P. N. W. Baxter, *Chem. Eur. J.*, 2003, **9**, 2531-2541.

24. P. N. W. Baxter, *Chem. Eur. J.*, 2002, **8**, 5250-5264.

25. P. N. W. Baxter and R. Dali-Youcef, *J. Org. Chem.,* 2005, **70**, 4935-4953.

26. S. Samori, S. Tojo, M. Fujitsuka, E. L. Spitler, M. M. Haley and T. Majima, *J. Org. Chem.,* 2007*,* **72**, 2785-2793.

27. E. L. Spitler, S. P. McClintock and M. M. Haley, *J. Org. Chem.,* 2007, **72**, 6692-6699.

28. H. Zhang, X. Wan, X. Xue, Y. Li, A. Yu and Y. Chen, *Eur. J. Org. Chem.*, 2010, 1681-1687.

29. E. L. Spitler and M. M. Haley, *Tetrahedron*, 2008*,* **64**, 11469-11474.

30. J. -H. Liao, C.-T. Chen, H.-C. Chou, C.-C. Cheng, P.-T. Chou, J.-M. Fang, Z. Slanina and T. J. Chow, *Org. Lett.,* 2002, **4**, 3107-3110.

31. J. M. Fang, S. Selvi, J. H. Liao, Z. Slanina, C. T. Chen and P. T. Chou, *J. Am. Chem. Soc.*, 2004, **126**, 3559.

32. (a) M. Inouye, T. Miyake, M. Furusyo and H. Nakazumi, *J. Am. Chem. Soc.*, 1995, **117**, 12416; (b) M. Inouye, J. Chiba, H. Nakazumi, *J. Org. Chem.*, 1999, **64**, 8170-8176.

33. S. Anderson, U. Neidlein, V. Gramlich, and F. Diederich, *Angew. Chem. Int. Ed. Engl.*, 1995, **34**, 1596.

34. U. Neidlein and F. Diederich, *Chem. Commun.*, 1996, 1493.

35. A. S. Droz, U. Neidlein, S. Anderson, P. Seiler and F. Diederich, *Helv. Chim. Acta*, 2001, **84**, 2243.

36. M. Inouye, M. Waki, and H. Abe, *J. Am. Chem. Soc.*, 2004, **126**, 2022.

37. R. Martínez-Máñez and F. Sancenón, *Chem. Rev.*, 2003, **103**, 4419-4476.

38. E. Anslyn, *J. Org. Chem.*, 2006, **72**, 687-699.

39. T. Gunnlaugsson, M. Glynn, G. M. Tocci, P. E. Kruger and F. M. Pfeffer, *Coord. Chem. Rev*., 2006, **250**, 3094-3117.

40. A. Metzger and E. V. Anslyn, *Angew. Chem. Int. Ed.*, 1998, **37**, 649-651.

41. S. A. Malashikhin, K. K. Baldridge and N. S. Finney, *Org. Lett.*, 2010, **12**, 940-943.

42. S. Kondo and M. Sato, *Tetrahedron*, 2006, **62**, 4844.

43. J. E. Anthony, S. I. Khan and Y. Rubin, *Tetrahedron*, 1997, **38**, 3499-3502.

44. M. Taniguchi, D. L. Cramer, A. D. Bhise, H. L. Kee, D. F. Bocian, D. Holten and J. S. Lindsey, *New. J. Chem.*, 2008, **32**, 947-958.

45. A. S. Droz, F. Diederich, *J. Chem. Soc., Perkin Trans. 1,* 2000, 4224-4226.

46. J. K. Young and J. S. Moore, *Modern Acetylene Chemistry*, ed. P. J. Stang and F. Diederich, Wiley-VCH, New York, 1995, 415-442.

47. S. Beer, C. G. Hrib, P. G. Jones, K. Brandhorst, J. Grunenberg and M. Tamm, *Angew. Chem. Int. Ed.,* 2007, **46**, 8890-8894.

48. W. Zhang and J. S. Moore, *Adv. Syn. Catal.*, 2007, **349**, 93-120.

49. K. G. Scrimgeour, *Chemistry and Control of Enzymatic Reactions,* Academic Press, Inc., New York, 1977.

50. J. A. Schetz and D. R. Sibley, *J. Pharmacol Exp. Ther.,* 2001, **296**, 359.

51. (a) M. -V. Martinez-Diaz, N. Spencer and F. Stoddart, *Angew. Chem. Int. Ed. Engl.*, 1997, **36**, 1904. (b) Y.-L. Huang, W.-C. Hung, C.-C. Lai, Y.-H. Liu, S. M. Peng and S.-H. Chiu, *Angew. Chem., Int. Ed.,* 2007, **46**, 6629-6633.

52. M. H. Al-Sayah and N. R. Branda, *Org. Lett.*, 2002, **4**, 881.

53. M. H. Al-Sayah and N. R. Branda, *Angew. Chem., Int. Ed. Engl.,* 2000, **39**, 945.

54. M. H. Filby, S. J. Dickson, N. Zaccheroni, L. Prodi, S. Bonacchi, M. Montalti, M. J. Paterson, T. D. Humphries, C. Chiorboli and J. W. Steed, *J. Am. Chem. Soc.,* 2008, **130**, 4105-4113.

55. C. Bucher, C. H. Devillers, J. -C. Moutet, G. Royal and E. Saint-Aman, *New J. Chem.,* 2004, **28**, 1584-1589.

56. H. Miyaji, G. Gasser, S. J. Green, Y. Molard, S. M. Strawbridge and J. H. R. Tucker, *Chem. Commun.*, 2005, 5355-5357.

57. M. Inouye, K. Takahashi and H. Nakazumi, *J. Am. Chem. Soc.*, 1999, **121**, 341.

58. S. Rashadan, M. E. Light and J. D. Kilburn, *Chem. Commun.*, 2006, 4578-4580.

59. J. W. Steed, *Chem. Soc. Rev.*, 2008, **38**, 506-519.

60. V. Amendola, M. Bonizzoni, D. Esteban-Goméz, L. Fabrizzi, M. Licchelli, F. Sancenón and A. Taglietti, *Coord. Chem. Rev.,* 2006, **250**, 1451-1470.

61. *Cercla Priority List of Hazardous Substances*, 2007, http://www.atsdr.cdc.gov/cercla.

62. *US EPA Case Study – Arsenic Treatment Technologies, Tucson, Arizona*, 2003, http://www.epa.gov/safewater/arsenic/publications.html.

63. C.-Q. Liu, S.-L. Li, Y.-C. Lang and H.-Y. Xiao, *Env. Sci. Technol.*, 2006, **40**, 6928.

64. E. A. Katayev, G. V. Kolesnikov and J. L. Sessler, *Chem. Soc. Rev.*, 2009, **38**, 1572-1586.

65. N. P. Cherimisinoff, *Pollution Engineering*, 2001, **33**, 38.

66. S. K. Maji, A. Pal and T. Pal, *J. Haz. Mat.*, 2008, **151**, 811-820.

67 (a) B. Gu, G. M. Brown, P. V. Bonnesen, L. Liang, B. A. Moyer, R. Ober and S. D. Alexandratos, *Env. Sci. Technol.,* 2000, **34**, 1075; (b) W. Chuoyyok, R. J. Wiacek, K. Pattamakomsan, T. Sangvanich, R. M. Grudzien, G. E. Fryxell and W. Yantasee, *Env. Sci. Technol.*, 2010, **44**, 3073.

68. R. Dutzler, E. B. Campbell, M. Cadene, B. T. Chait and R. Mackinnon, *Nature*, 2002, **415**, 287.

69. G. Y. Rychkov, M. Pusch, M. L. Roberts, T. J. Jentsch and A. H. Bretag, *J. Gen. Physiol.,* 2001, **530**, 379-393.

70. P. Cudic, M. Zinic, V. Tomisic, V. Simeon, J.-P. Vigneron and J.-M. Lehn, *J. Chem. Soc., Chem. Commun.,* 1995, 1073.

71. K.-J. Chang, D. Moon, M. S. Lah and K.-S. Jeong, *Angew. Chem., Int. Ed.,* 2005, **44**, 7926.

72. N.-K. Kim, K.-J. Chang, D. Moon, M. S. Lah and K.-S. Jeong, *Chem. Commun.,* 2007, 3401-3403.

73. K.-J. Chang, M. K. Chae, C. Lee, J.-Y. Lee and K.-S. Jeong, *Tetrahedron Lett.*, 2006, **47**, 6385.

74. T. H. Kwon and K.-S. Jeong, *Tetrahedron Lett.,* 2006, **47**, 8539.

75. A. T. Wright, Z. Zhong and E. V. Anslyn, *Angew. Chem. Int Ed.*, 2005, **44**, 5679-5682.

76. Z. Zhong, E. V. Anslyn, *J. Am. Chem. Soc.,* 2002, **124**, 9014-9015.

77. A. N. Swinburne, M. J. Paterson, A. Beeby and J. W. Steed, *Org. Biomol. Chem.*, 2010, **8**, 1010-1016.

78. A. N. Swinburne, M. J. Paterson, A. Beeby and J. W. Steed, *Chem. Eur. J.,* 2010, **16**, 2714-2718.

79. O. Hirata, M. Takeuchi and S. Shinkai, *Chem. Commun.*, 2005, 3805-3807.

80. C. B. Black, B. Andrioletti, A. C. Try, C. Ruiperez and J. L. Sessler, *J. Am. Chem. Soc.*, 1999, **121**, 10438-10439.

81. C.-Y. Wu, M.-S. Chen, C.-A. Lin, S.-C. Lin and S.-S. Sun, *Chem. Eur. J.*, 2006, **12**, 2263-2269.

82. N. Pucher, A. Rosspeinter, V. Satzinger, V. Schmidt, G. Gescheidt, J. Stampfl and R. Liska, *Macromolecules*, 2009, **42**, 6519-6528.

83. L. Porres, M. Charlot, C. D. Entwistle, A. Beeby, T. B. Marder and M. Blanchard-Desce, *Proc. SPIE*, 2005, **5943**, 559340F.

84. R. Y. Tsien, *Nature*, 1981, **290**, 527.

85. D. S. Bush and R. L. Jones, *Plant Physiol.*, 1990, **93**, 841.

86. T. H. Steinberg, A. S. Newman, J. A. Swanson and S. C. Silverstein, *J. Biol. Chem.,* 1987, **262**, 8884.

87. B. Pilas and G. Durack, *Cytometry*, 1997, **28**, 316.

88. A. D. Doyle and J. Lee, *Biotechniques*, 2002, **33**, 358.

89. R. Martínez-Zaguilán, G. Parnami and R. M. Lynch, *Cell Calcium*, 1996, **19**, 337.

90. H. E. Katerinopoulos, *Curr. Pharm. Design*, 2004, **10**, 3835.

91. F. A. Lattanzio, *Biochem. Biophys. Res. Commun.*, 1991, **177**, 184.

92. F. Di Virgilio, T. H. Steinberg and S. C. Silverstein, *Cell Calcium*, 1990, **11**, 57.

93. H. A. Clark, R. Kopelman, R. Tjalkens and M. A. Philbert, *Anal. Chem.*, 1999, **71**, 4837.

94. R. B. Silver, *Methods Cell Biol.*, 1998, **56**, 237.

95. G. R. Bright, G. W. Fisher, J. Rogowska and D. L. Taylor, *Methods Cell Biol.*, 1989, **30**, 157.

96. R. D. Carpenter and A. S. Verkman, *Org. Lett.*, 2010, **12**, 1160.

97. J. Biwersi, N. Farah, Y.X. Wang, R. Ketchum and A. S. Verkman, *Am. J. Physiol.*, 1992, **262-1**, C242.

98. G. Grynkiewicz, M. Poenie and R. Y. Tsien, *J. Biol. Chem.*, 1985, **260**, 3440.

99. N. D. Sonawane, J. R. Thiagarajah and A. S. Verkman, *J. Biol. Chem.,* 2002, **277**, 5506.

100. J. I. Schroeder, *Plant Mol. Biol.*, 1995, **28**, 353.

101. K. Renkawek and G. J. Bosman, *NeuroReport*, 1995, **6**, 929.

102. M. P. Anderson, R. J. Gregory, S. Thompson, D. W. Souza, S. Paul, R. C. Mulligan, A. E. Smith and M. J. Welsh, *Science*, 1991, **253**, 202.

103. U. Kornak, D. Kasper, M. R.Bosl, E. Kaiser, M. Schweizer, A. Schulz, W. Friederich, G. Delling and T.J. Jentsch, *Cell*, 2001, **104**, 205.

104. R. S. Kaplan, *J. Membr. Biol.*, 2001, **179**, 165.

105. R. J. Thompson, H. C. S. R. Akana, C. Finnigan, K. E. Howell and J. H. Caldwell, *Am. J. Physiol. Cell Physiol.*, 2006, **290**, C499.

106. S. F. Okada, W. K. O'Neal, P. Huang, R. A. Nicholas, L. E. Ostrowski, W. J. Craigen, E. R. Lazarowski and R. C. Boucher, *J. Gen. Phys.*, 2004, **124**, 513.

107. S. Zhang, A. Finkelstein and R. J. Collier, *Proc. Natl. Acad. Sci,* 2004, **101**, 16756.

108. M. Hara-Chikuma, B. Yang, N.D. Sonawane, S. Sasaki, S. Uchida and A. S. Verkman, *J. Biol. Chem.,* 2005, **280**, 1241.

109. F. Gasparini, K. Lingenhöhl, N. Stoehr, P. J. Flor, M. Heinrich, I. Vranesic, M. Biollaz, H. Allgeier, R. Heckendorn, S. Urwyler, M.A. Varney, E. C. Johnson, S. D. Hess, S. P. Rao, A. I. Sacaan, E. M. Santori, G. Veliçelebi and R. Kuhn, *Neuropharmacology*, 1999, **38**, 1493.

110. F. Gasparini, H. Andres, P. J. Flor, M. Heinrich, W. Inderbitzin, K. Lingenhöhl, H. Müller, V. C. Munk, K. Omilusik, C. Stierlin, N. Stoehr, I. Vranesic and R. Kuhn, *Bioorg. Med. Chem. Lett.,* 2002, **12**, 407.

111. M. Yu, W. Tueckmantel, X. Wang, A. Zhu, A. P. Kozikowski and A.-L. Brownell, *Nucl. Med. Biol.*, 2005, **32**, 631.

112. J. M. Nores, B. Biacabe and P. Bonfils, *Ann. Med. Interne (Paris)*, 2000, **151**, 97.

113. W. Qu, S.-R. Choi, C. Hou, Z. Zhuang, S. Oya, W. Zhang, M.-P. Kung, R. Manchandra, D. M. Skovronsky and H. F. Kung, *Bioorg. Med. Chem. Lett.,* 2008, **18**, 4823.

114. J. Dash, P. S. Shirude, S.-T. D. Hsu and S. Balasubramanian, *J. Am. Chem. Soc.*, 2008, **130**, 15950.

Chapter II

1. C. A. Johnson II, B. A. Baker, O. B. Berryman, L. N. Zakharov, M. J. O'Connor and M. M. Haley, *Organomet. Chem.*, 2006, **691**, 413-421.

2. C. N. Carroll, O. B. Berryman, C. A. Johnson, L. N. Zakharov, M. M. Haley and D. W. Johnson, *Chem. Commun.*, 2009, 2520.

3. W. B. Wan and M. M. Haley, *J. Org. Chem.,* 2001, **66**, 3893-3901.

4. K. Sonogashira in *Metal-Catalyzed Cross-Coupling Reactions*, P. J. Stang and F. Diederich, Eds., Wiley-VCH: Weinheim, 1997, 203-229.

5. J. A. Marsden and M. M. Haley in *Metal Catalyzed Cross-Coupling Reactions, 2nd ed.*, A. de Meijere and F. Diederich, Eds., Wiley-VCH: Weinheim, 2004, 317-394.

6. J. M. Heemstra and J. S. Moore, *Org. Lett.*, 2004, **6**, 659-662.

7. T. L. Davis and K. C. Blanchard, *Organic Syntheses*, 1941, **1**, 453; 1923, **3**, 95.

8. M. L. Gross, D. H. Blank and W. M. Welch, *J. Org. Chem.,* 1993, **58**, 2104-2109.

9. J. Yan, J. Li and D. Cheng, *Synlett*, 2007, 2442-2444.

10. S.-Y. Han and Y.-A. Kim, *Tetrahedron*, 2004, **60**, 2447-2467.

11. C. A. Johnson II, *Synthesis, Characterization and Materials Properties of Benzocyclynes and Metallobenzocyclynes*, Doctoral Dissertation, University of Oregon, 2007.

12. C. A. Johnson II, O. B. Berryman, A. C. Sather, L. N. Zakharov, M. M. Haley and D. W. Johnson, *Cryst. Growth Des.,* 2009, **9**, 4247-4249.

13. W. J. Vickaryous, E. Rather-Healey, O. B. Berryman and D. W. Johnson, *Inorg. Chem.*, 2005, **44**, 9247-9252.

14. T. G. Carter, W. J. Vickaryous, V. M. Cangelosi and D. W. Johnson, *Comm. Inorg. Chem.*, 2007, **28**, 97-122.

15. K. J. C. vam Bommel, M. R. de Jong, G. A. Metselaar, W. Verboom, J. Huskens, R. Hulst, H. Kooijman, A. L. Spek and D. N. Reinhoudt, *Chem. Eur. J*, 2001, **7**, 3603-3615.

16. W. Konigsberg, *Methods Enzymol.*, 1972, **25**, 185-188.

17. M. Sridhar, S. K. Vadivel and U. T. Bhalerao, *Synth. Commun.*, 1997, **27**, 1347-1350.

18. J. Lukkari, M. Meretoja, I. Kartio, K. Laajalehto, M. Rajamaki, M. Lindstrom and J. Kankare, *Langmuir*, 1999, **15**, 3529-3537.

19. J. L. Kice, *J. Org. Chem.*, 1963, **28**, 957-961.

20. J. Houk and G. M. Whitesides, *J. Am. Chem. Soc.*, 1987, **109**, 6825-6836.

21. J. Wu, W. Liu, J. Ge, H. Zhang and P. Wang, *Chem. Soc. Rev.*, 2011, **40**, 3483-3495.

22. B. Valeur in *Molecular Fluorescence,* Wiley-VCH: Weinheim, 2002, 72-123.

Chapter III

1. (*a*) B. Dietrich, *Pure Appl. Chem.*, 1993, **65**, 1457; (*b*) A. Bianchi, K. Bowman-James, E. Garcia-España, *Supramolecular Chemistry of Anions*, Wiley: New York, 1997; (*c*) P. D. Beer, P. A. Gale, *Angew. Chem. Int. Ed.* 2001, **40**, 486; (*d*) J. L. Sessler, P. A. Gale, W.-S. Cho, *Anion Receptor Chemistry*, The Royal Society of Chemistry: Cambridge, UK, 2006.

2. (*a*) J. Friedman, Y. T. Meharenna, A. Wilks, T. L. Poulos, *J. Biol. Chem.*, 2006, **282***,* 1066; (*b*) C. E. MacBeth, A. P. Golombek, V. G. Young, Jr., C. Yang, K. Kuezera, M. P. Hendrich, A. S. Borovik, *Science*, 2000*,* **289***,* 938; (*c*) For a recent review of anions in supramolecular chemistry, see: P. A. Gale, S. E. Garcia-Garrido, J. Garric, *Chem. Soc. Rev.*, 2008, **37**, 151.

3. (*a*) S. Leininger, B. Olenyuk, P. J. Stang *Chem. Rev.* 2000, **100**, 853; (*b*) F. Romero, R. Ziessel, A. Dupont-Gervais, A. van Dorsselaer *Chem. Commun.* 1996, **4**, 551.

4. (*a*) A. J. Zucchero, J. N. Wilson, U. H. F. Bunz *J. Am. Chem. Soc.* 2006, **128**, 11872; (*b*) J. D. Lewis, J. N. Moore *Phys. Chem. Chem. Phys.* 2004, **6**, 4595; (*c*) J. Tolosa, A. J. Zucchero, U. H. F. Bunz *J. Am. Chem. Soc.* 2008, **130**, 6498.

5. (*a*) P. A. Gale, Amide and Urea based Anion Receptors. In The Encyclopedia of Supramolecular Chemistry, J. Atwood, J. W. Steed Eds.; Dekker: New York, 2004; pp 31-41; (*b*) V. A. Amendola, D. Esteban-Gómez, L. Fabbrizzi, M. Licchelli *Acc. Chem. Res.* 2006, **39**, 343; (*c*) E. Quinlan, S. E. Matthews, T. Gunnlaugsson, *J. Org. Chem.*, 2007, **72***,* 7497.

6. (*a*) M.-V. Martinez-Diaz, N. Spencer, J. F. Stoddart, *Angew. Chem. Int. Ed. Engl.*, 1997, **36**, 1904; (*b*) M. H. Al-Sayah, N. R. Branda, *Org. Lett.*, 2002, **4**, 881; (*c*) S. Rashdan, M. E. Light, J. D. Kilburn, *Chem. Commun.*, 2006, 4578; (*d*) E. Cordova, R. A. Bissell, N. Spencer, P. Ashton, J. F. Stoddart, A. E. Kaifer, *J. Org. Chem.*, 1993, **58**, 6550.

7. (a) C. A. Johnson II, *Synthesis, Characterization and Materials Properties of Benzocyclynes and Metallobenzocyclynes*, Doctoral Dissertation, University of Oregon, 2007. (b) O. B. Berryman, C. A. Johnson, L. N. Zakharov, M. M. Haley, D. W. Johnson, *Angew. Chem. Int. Ed.*, 2008, **47**, 117.

8. G. Blotny, *Tet. Lett.,* 2003, **44**, 1499-1501.

9. W. B. Wan, M. M. Haley, *J. Org. Chem.*, 2001, **66**, 3893.

10. N. E. Kelly, S.-O. Lee, K. D. Harris, *J. Am. Chem. Soc.*, 2001, **123**, 12682.

11. M. J. Frisch, G. W. Trucks, H. B. Schlegel, G. E. Scuseria, M. A. Robb, J. R. Cheeseman, J. A. Montgomery, Jr., T. Vreven, K. N. Kudin, J. C. Burant, J. M. Millam, S. S. Iyengar, J. Tomasi, V. Barone, B. Mennucci, M. Cossi, G. Scalmani, N. Rega, G. A. Petersson, H. Nakatsuji, M. Hada, M. Ehara, K. Toyota, R. Fukuda, J. Hasegawa, M. Ishida, T. Nakajima, Y. Honda, O. Kitao, H. Nakai, M. Klene, X. Li, J. E. Knox, H. P. Hratchian, J. B. Cross, C. Adamo, J. Jaramillo, R. Gomperts, R. E. Stratmann, O. Yazyev, A. J. Austin, R. Cammi, C. Pomelli, J. W. Ochterski, P. Y. Ayala, K. Morokuma, G. A. Voth, P. Salvador, J. J. Dannenberg, V. G. Zakrzewski, S. Dapprich, A. D. Daniels, M. C. Strain, O. Farkas, D. K. Malick, A. D. Rabuck, K. Raghavachari, J. B. Foresman, J. V. Ortiz, Q. Cui, A. G. Baboul, S. Clifford, J. Cioslowski, B. B. Stefanov, G. Liu, A. Liashenko, P. Piskorz, I. Komaromi, R. L. Martin, D. J. Fox, T. Keith, M. A. Al-Laham, C. Y. Peng, A. Nanayakkara, M. Challacombe, P. M. W. Gill, B. Johnson, W. Chen, M. W. Wong, C. Gonzalez, J. A. Pople, *Gaussian 03*, Revision B.04, Gaussian, Inc. Pittsburgh PA, 2003.

Chapter IV

1. (a) K. Kikuchi, Chem. Soc. Rev., 2010, 39, 2048-2053.; C. N. Carroll, Chem. Soc. Rev., 2010, 39, 3875-3888.; (b) For reviews of molecular logic see: C.A. Mirkin and M. A. Ratner, Molecular Electronics Annual Reviews, Inc.; 1992, 43.; B. L. Feringa, Molecular Switches, Wiley-VCH GmbH, Weinheim, Germany, 2001. (c) A. G. Montalban, S. M. Baum, A. G. M. Barrett and B. M. Hoffman, Dalton. Trans., 2003, 2093-2102.; O.- J. Norum, P. K. Selbo, A. Weyergang, K.- E. Giercksky and K. Berg, J. Photochem. Photobiol. B, 2009, 96, 83-92.

2. (a) P. A. Gale and T. Gunnlaugsson, Chem. Soc. Rev., 2010, 39, 3595-3596. (b) B. Valeur, Molecular Fluorescence, Wiley-VCH Verlag GmbH, Weinheim, Germany, 2002, 273-350.

3. (a) L. Fabbrizzi, F. Gatti, P. Pallavicini, and L. Parodi, New J. Chem., 1998, 1403. (b) H. Shizuka, and S. Tobita, J. Am. Chem. Soc., 1982, 104, 6919. (c) J. H. Clements, S. E. Webber, Macromolecules, 2004, 37, 1531. (d) A. P. de Silva, H. Q. Nimal Gunaratne, C. P. McCoy, Chem. Commun., 1996, 21, 2399.

4. (a) G. De Santis, L. Fabrizzi, M. Licchelli, A. Poggi, and A. Taglietti, Angew. Chem. Int. Ed. Engl., 1996, 35, 202. (b) T. Gunnlaugsson, A. P. Davis, J. E. O'Brien, and M. Glynn, Org. Biomol. Chem., 2005, 3, 48. (c) S. E. Garcîa-Garrido, C. Caltagirone, M. E. Light, P. A. Gale, Chem. Commun., 2007, 1450.
5. (a) S. J. Dickson, A. N. Swinburne, M. J. Paterson, G. O. Lloyd, A. Beeby and J. W. Steed, Eur. J. Inorg. Chem., 2009, 3879-3882. (b) A. Roque, F. Pina, S. Alves, R. Ballardini, M. Maestri and V. Balzani, J. Mater. Chem., 1999, 9, 2265.

6. C. N. Carroll, O. B. Berryman, C. A. Johnson II, M. M. Haley, and D. W. Johnson, Chem. Commun., 2009, 2520.

7. J. M. Heemstra and J. S. Moore, Org. Lett., 2004, 6, 659-662.

8. M. J. Frisch, et al. Gaussian 03, Revision B.04, Gaussian, Inc. Pittsburgh PA, 2003. Full reference in ESI.; Spartan 08, Wavefunction, Inc., Irvine, CA, USA.

9. (a) B. Valeur in *Molecular Fluorescence,* Wiley-VCH: Weinheim, 2002, 72-123. (b) J. R. Lakowicz in *Principles of Fluorescence Spectroscopy*, Springer, 2006.

10. (a) J. H. Clements and S. E. Webber, *Macromolecules*, 2004, **37**, 1531-1536. (b) J. Duhamel, *Macromolecules,* 2004, **37**, 1987-1989.

11. (a) K. W. Allen, E. S. Cockburn, R. S. Davidson, K. S. Tranter and H. S. Zhang, *Pure & Appl. Chem.*, 1992, **64**, 1225-1230. (b) T. Handa, Y. Utena and H. Yajima, *J. Phys. Chem.*, 1984, **88**, 5150-5154.

12. (a) C. A. Crutchfield and D. J. Harris, *J. Magnetic Resonance*, 2007, **185**, 179-182. (b) Y. Cohen, L. Avram and L. Frish, *Angew. Chem. Int. Ed.,* 2005, **44**, 520-554.

13. (a) A. A. Marti, X. Li, S. Jockusch, Z. Li, B. Raveendra, S. Kalachikov, J. J. Russo, I. Morozova, S. V. Puthanveettil, J. Ju and N. J. Turro, *Nucl. Acids Res.*, 2006, **34**, 3161-3168. (b) J. B. Birks, D. J. Dyson and I. H. Munro, *Proc. Royal Soc. London A,* 1963, **275**, 575-588.

Chapter V

1. (a) J. T. Davis, O. Okunola and R. Quesada, *Chem. Soc. Rev.*, 2010, **39**, 3843-3862. (b) R. G. Deeley, C. Westlake and S. P. C. Cole, *Physiol. Rev.*, 2006, **86**, 849-899. (c) J. Mareda and S. Matile, *Chem. Eur. J.*, 2008, **15**, 28-37.

2. (a) K. Renkawek and G. J. Bosman, *NeuroReport*, 1995, **6**, 929. (b) M. P. Anderson, R. J. Gregory, S. Thompson, D. W. Souza, S. Paul, R. C. Mulligan, A. E. Smith and M. J. Welsh, *Science*, 1991, **253**, 202.

3. (a) C. E. Johanson, S. M. Sweeney, J. T. Parmelee and M. H. Epstein, Am. J. Physiol. *Cell Physiol.*, 1990, **258**, C211-C256. (b) R. D. Egleton, C. C. Campos, J. D. Huber, R. C. Brown and T. P. Davis, *Diabetes*, 2003, **52**, 1496-1501.

4. (a) T. J. Jentsch, V. Stein, F. Weinreich and A. A. Zdebik, *Physiol. Rev.*, 2002, **82**, 503-568. (b) C. Kubisch, T. Schmidt-Rose, B. Fontaine, A. H. Bretag and T. J. Jentsch, *Hum. Mol. Genet.,* 1998, **7**, 1753-1760.

5. J. O. Lundberg *et al*., *Nature Chem. Biol.*, 2009, **5**, 865-869.

6. (a) N. S. Bryan *et al*., *Proc. Natl. Acad. Sci.,* 2007, **104**, 19144-19149. (b) U. Hink *et al.*, *Circulation Research*, 2001, **88**, e14-e22.

7. C. Chang, *Nature ,*2007*,* **448**, 654-655 and references therein.

8. J. A. Prescher and C. R. Bertozzi, *Nature Chem. Biol.,* 2005, **1**, 13-21.

9. I. Chen and A. Y. Ting, *Curr. Opin. Biotechnol.*, 2005, **16**, 35-40.

10. (a) S. L. R. Barker, B. A Thorsrud and R. Kopelman, *Anal. Chem.*, 1998, **70**, 100-104. (b) M. Hara-Chikuma, B. Yang, N.D. Sonawane, S. Sasaki, S. Uchida and A. S. Verkman, *J. Biol. Chem.,* 2005, **280**, 1241. (c) E. B. Veale, D. O. Frimannsson, M. Lawler and T. Gunnlaugsson, *Org. Lett.*, 2009, **11**, 4040.

11. C. E. J. Haynes and P. A. Gale, *Chem. Commun.*, 2011, **47**, 8203-8209.

12. H. Matsumura, M. Iwamoto and K. Furusawa, *Bull. Chem. Soc. Jpn.*, 1986, **59**, 1533-1537.

13. (a) Y. Hong, J. W. Y. Lam and B. Z. Tang, *Chem. Commun.,* 2009, 4332-4353. (b) Y. Hong, J. W. Y. Lam and B. Z. Tang, *Chem. Soc. Rev..,* DOI: 10.1039/CICSI5113D. (c) C. Zhu, S. Pang, J. Xu, L. Jia, F. Xu, J. Mei, A. Qin, J. Sun, J. Ji and B. Tang, *Analyst*, 2011, **136**, 3343.

14. J. B. Birks in *Photophysics of Aromatic Molecules,* Wiley-VCH: London, 1970.

15. S. Doose, H. Neuweiler and M. Sauer, *Chem. Phys. Chem.*, 2009, **10**, 1389-1398.

16. (a) N. J. Greenfield, *Anal. Biochem.*, 1996, **235**, 1-10. (b) P. Jonkheijm, F. J. M. Hoeben, R. Kleppinger, J. van Herrikhuyzen, A. P. H. J. Schenning and E. W. Meijer, *J. Am. Chem. Soc.*, 2003, **125**, 15941-15949.